Loughborough University

This item was submitted to Loughborough's Research Repository by the author.
Items in Figshare are protected by copyright, with all rights reserved, unless otherwise indicated.

Iterative learning control of crystallisation systems

PLEASE CITE THE PUBLISHED VERSION

PUBLISHER

© Nahid Sanzida

LICENCE

CC BY-NC-ND 4.0

REPOSITORY RECORD

Sanzida, Nahid. 2014. “Iterative Learning Control of Crystallisation Systems”. figshare.
https://hdl.handle.net/2134/14981.

Loughborough University

This item was submitted to Loughborough University as a PhD thesis by the author and is made available in the Institutional Repository (https://dspace.lboro.ac.uk/) under the following Creative Commons Licence conditions.

creative commons

COMMONS DEED

Attribution-NonCommercial-NoDerivs 2.5

You are free:

- to copy, distribute, display, and perform the work

Under the following conditions:

Attribution. You must attribute the work in the manner specified by the author or licensor.

Noncommercial. You may not use this work for commercial purposes.

No Derivative Works. You may not alter, transform, or build upon this work.

- For any reuse or distribution, you must make clear to others the license terms of this work.
- Any of these conditions can be waived if you get permission from the copyright holder.

Your fair use and other rights are in no way affected by the above.

This is a human-readable summary of the Legal Code (the full license).

Disclaimer

For the full text of this licence, please go to:
http://creativecommons.org/licenses/by-nc-nd/2.5/

Loughborough University

Iterative Learning Control of Crystallisation Systems

by

Nahid Sanzida

A Doctoral Thesis

Submitted in partial fulfillment of the requirements for the award of the degree of Doctor of Philosophy in Chemical Engineering

December 2013

© by Nahid Sanzida (2013)

Abstract

Under the increasing pressure of issues like reducing the time to market, managing lower production costs, and improving the flexibility of operation, batch process industries thrive towards the production of high value added commodity, i.e. specialty chemicals, pharmaceuticals, agricultural, and biotechnology enabled products. For better design, consistent operation and improved control of batch chemical processes one cannot ignore the sensing and computational blessings provided by modern sensors, computers, algorithms, and software. In addition, there is a growing demand for modelling and control tools based on process operating data. This study is focused on developing process operation data-based iterative learning control (ILC) strategies for batch processes, more specifically for batch crystallisation systems.

In order to proceed, the research took a step backward to explore the existing control strategies, fundamentals, mechanisms, and various process analytical technology (PAT) tools used in batch crystallisation control. From the basics of the background study, an operating data-driven ILC approach was developed to improve the product quality from batch-to-batch. The concept of ILC is to exploit the repetitive nature of batch processes to automate recipe updating using process knowledge obtained from previous runs. The methodology stated here was based on the linear time varying (LTV) perturbation model in an ILC framework to provide a convergent batch-to-batch improvement of the process performance indicator. In an attempt to create uniqueness in the research, a novel hierarchical ILC (HILC) scheme was proposed for the systematic design of the supersaturation control (SSC) of a seeded batch cooling crystalliser. This model free control approach is implemented in a hierarchical structure by assigning data-driven supersaturation controller on the upper level and a simple temperature controller in the lower level.

In order to familiarise with other data based control of crystallisation processes, the study rehearsed the existing direct nucleation control (DNC) approach. However, this part was more committed to perform a detailed strategic investigation of different possible structures of DNC and to compare the results with that of a first principle

model based optimisation for the very first time. The DNC results in fact outperformed the model based optimisation approach and established an ultimate guideline to select the preferable DNC structure.

Batch chemical processes are distributed as well as nonlinear in nature which need to be operated over a wide range of operating conditions and often near the boundary of the admissible region. As the linear lumped model predictive controllers (MPCs) often subject to severe performance limitations, there is a growing demand of simple data driven nonlinear control strategy to control batch crystallisers that will consider the spatio-temporal aspects. In this study, an operating data-driven polynomial chaos expansion (PCE) based nonlinear surrogate modelling and optimisation strategy was presented for batch crystallisation processes. Model validation and optimisation results confirmed this approach as a promise to nonlinear control.

The evaluations of the proposed data based methodologies were carried out by simulation case studies, laboratory experiments and industrial pilot plant experiments. For all the simulation case studies a detailed mathematical models covering reaction kinetics and heat mass balances were developed for a batch cooling crystallisation system of Paracetamol in water. Based on these models, rigorous simulation programs were developed in MATLAB®, which was then treated as the real batch cooling crystallisation system. The laboratory experimental works were carried out using a lab scale system of Paracetamol and iso-Propyl alcohol (IPA). All the experimental works including the qualitative and quantitative monitoring of the crystallisation experiments and products demonstrated an inclusive application of various in situ process analytical technology (PAT) tools, such as focused beam reflectance measurement (FBRM), UV/Vis spectroscopy and particle vision measurement (PVM) as well. The industrial pilot scale study was carried out in GlaxoSmithKline Bangladesh Limited, Bangladesh, and the system of experiments was Paracetamol and other powdered excipients used to make paracetamol tablets.

The methodologies presented in this thesis provide a comprehensive framework for data-based dynamic optimisation and control of crystallisation processes. All the simulation and experimental evaluations of the proposed approaches emphasised the potential of the data-driven techniques to provide considerable advances in the current state-of-the-art in crystallisation control.

Table of Contents

ABSTRACT *i*

LIST OF FIGURES *vi*

LIST OF TABLES *x*

LIST OF ACRONYMS *xi*

NOMENCLATURE *xiv*

ACKNOWLEDGEMENT *xvi*

CHAPTER 1 INTRODUCTION **1**

1.1 Motivation 1

1.2 Research Aim and Objectives 6

1.3 Scope of the Research 7

1.4 Research Contribution 8

1.5 Thesis Structure 10

CHAPTER 2 LITERATURE REVIEW **12**

2.1 Overview 12

2.2 Distributed Parameter Systems 12

2.3 Control of DPSs 14

2.3.1 Model Based Control 15

2.3.2 Data Based Control 19

2.4 Iterative Learning Control (ILC) 22

2.4.1 Generic Description of ILC/ Technical Overview 22

2.4.2 ILC in Batch Chemical Processing 23

2.5 Polynomial Chaos Expansion (PCE) Based Control 38

2.6 Theory and Practices in Crystallisation Process 41

2.6.1 Fundamentals and Mechanisms of Crystallisation Processes 42

2.6.2 Measurement Techniques for State Variables 46

2.6.3 Crystallisation Operation and Control 49

2.6.4 Process Analytical Technology (PAT) in Crystallisation Operation 53

2.7 Conclusions 59

CHAPTER 3 DEVELOPMENT OF LINEAR TIME VARYING (LTV) PERTURBATION MODEL BASED ITERATIVE LEARNING CONTROL (ILC) **60**

3.1 Overview 60

3.2 Methodology Development 60

3.3 Results and Discussions 64

3.3.1 Case Study 1: Typical Batch Reactor 64
3.3.2 Case Study 2: Batch Cooling Crystallisation System 67
3.3.3 Case Study 3: Batch Cooling Crystallisation System with Model-Plant Mismatch 71
3.3.4 Case Study 4: Determination of Drying Temperature to Obtain a Desired Moisture Content in Paracetamol Granules at the End of the Batch 74
3.4 Conclusions 81
CHAPTER 4 DESIGN OF SUPER SATURATION CONTROL (SSC) OF A SEEDED BATCH COOLING CRYSTALLISER BASED ON ILC **82**
4.1 Overview 82
4.2 Theory of SSC for Controlling Crystallisation Process 82
4.3 Development of Hierarchical ILC (HILC) for Systematic Design of SSC of a Seeded Batch Cooling Crystalliser 84
4.4 Results and Discussions 85
4.4.1 Seeded Batch Cooling Crystallisation System 85
4.4.2 Seeded Batch Cooling Crystallisation System with Kinetic Parameter Perturbation 90
4.5 Conclusions 92
CHAPTER 5 EXPERIMENTAL EVALUATION OF THE HIERARCHICAL ILC (HILC) APPROACH FOR SUPERSATURATION CONTROL (SSC) OF A SEEDED BATCH COOLING CRYSTALLISER **93**
5.1 Overview 93
5.2 Experimental Evaluation of HILC 93
5.3 Experiment Design 95
5.3.1 Experimental Set-up 95
5.3.2 Materials 96
5.3.3 Seed Preparation 97
5.3.4 Concentration Measurement 98
5.4 Results and Discussions 99
5.4.1 Results from ILC1 99
5.4.2 Results from ILC2 101
5.5 Conclusions 110
CHAPTER 6 DIRECT NUCLEATION CONTROL (DNC) APPROACH FOR CONTROLLING BATCH CRYSTALLISATION PROCESSES **111**
6.1 Overview 111
6.2 Direct Nucleation Control (DNC) Approaches 111
6.2.1 Simple DNC Approach 112
6.2.2 Predictive DNC Approach 113

6.2.3 Reverse DNC Approach 113
6.2.4 Basic DNC Approach 114
6.3 Experimental Set-up and Materials 116
6.4 Results and Discussions 116
6.4.1 Simulation Case Studies 116
6.4.2 DNC Experiments 129
6.4.3 Comparative Analysis of Different Simulated and Experimental DNC Results 131
6.5 Conclusions 133
CHAPTER 7 POLYNOMIAL CHAOS EXPANSION (PCE) BASED MODELING AND OPTIMISATION OF BATCH CRYSTALLISATION PROCESSES **134**
7.1 Overview 134
7.2 Introduction 134
7.3 Methodology Development 136
7.4 Results and Discussions 139
7.4.1 Surrogate Model Identification and Validation 139
7.4.2 Optimisation of the Surrogate Model 143
7.5 Conclusions 150
CHAPTER 8 CONCLUSIONS AND FUTURE WORKS **154**
8.1 Conclusions 151
8.2 Recommendations for Future Works 154
REFERENCES 155
APPENDICES 171
LIST OF PUBLICATIONS 181

LIST OF FIGURES

Figure 2.1: Steps for modelling known and unknown DPSs. 14

Figure 2.2: Classification of advanced control techniques (Agachi et al., 2006). 16

Figure 2.3: Basic structure of model predictive control (MPC). 17

Figure 2.4: Basic framework of iterative learning control (ILC). 22

Figure 2.5: Basic structure of ILC for output PDF shaping (Wang et al., 2005). 28

Figure 2.6: Concept of geometric analysis (Zheng et al., 2009). 34

Figure 2.7: Supersaturation in crystallisation processes. 43

Figure 2.8: Types of nucleation. 44

Figure 2.9: Typical profiles of natural, linear, and programmed cooling operations. 50

Figure 2.10: Scheme of process analytical technology (PAT) (Valero, 2013). 53

Figure 3.1: Algorithm of the LTV perturbation models based on ILC scheme. 63

Figure 3.2: Simulated ILC profiles of different batches (a) concentration profiles (b) temperature profiles. 66

Figure 3.3: The SSE values for the batches. 66

Figure 3.4: Historical data sets (a) mean crystal length trajectories (b) temperature trajectories. 69

Figure 3.5: Trajectories of (a) mean crystal size (b) temperature. 70

Figure 3.6: The SSE values for the batches. 71

Figure 3.7: Trajectories of (a) mean crystal size (b) temperature. 73

Figure 3.8: Tracking performance of ILC. 73

Figure 3.9: Mighty Mixer Granulator. 76

Figure 3.10: Sapphire Fluid Bed Dryer (a) with wet granules loaded (b) during operation. 76

Figure 3.11: MJ33 Moisture Analyser (a) sieved granules loaded (b) during operation. 77

Figure 3.12: Process block diagram. 78

Figure 3.13: Trajectories of moisture content. 80

Figure 3.14: Final moisture content vs. temperature plot. 80

Figure 3.15: Tracking performance of ILC. 81

Figure 4.1: Operating curve for supersaturation control of a seeded batch cooling crystalliser. 83

Figure 4.2: Architecture of proposed HILC for SSC of a seeded batch cooling crystalliser. 85

Figure 4.3: Steps followed in the case study of SSC of a seeded batch cooling crystalliser by HILC. 87

Figure 4.4: Tracking performance of ILC1. 88

Figure 4.5: Profiles from simulated batch to batch (a) SSC profiles (b) input temperature trajectories. 89

Figure 4.6: Tracking performance of ILC2. 90

Figure 4.7: Mean length profile for the final temperature trajectory. 90

Figure 4.8: Tracking performance of ILC2 when a -5% error was introduced to the system after 10th batch for kinetic parameter perturbation test. 91

Figure 5.1: A schematic representation of the experimental set-up. 96

Figure 5.2: Microscopic image of seeds. 97

Figure 5.3: Variation in SWMCL at the end of the batch with increasing supersaturation. 99

Figure 5.4: Variation in CLD at the end of the batch with increasing supersaturation. 100

Figure 5.5: Variation in SWMCL over the batch with increasing supersaturation. 100

Figure 5.6: Trajectories of historical batches (a) SS trajectories (b) temperature trajectories. 102

Figure 5.7: Plots for concentration profiles in the phase diagram for different experimental batches (a) Batch 1 (b) Batch 2 (c) Batch 3 (d) Batch 4 (e) Batch 5 (f) Batch 6. 103

Figure 5.8: Plot for SSE for different experimental batches. 104

Figure 5.9: Plot for SWMCL vs. no of experimental batches for Case 1. 104

Figure 5.10: Microscopic images of crystals (a) Batch 1 (b) Batch 2 (c) Batch 3 (d) Batch (e) Batch 5 (f) Batch 6 (g) Batch 7. 105

Figure 5.11: Phase diagrams for (a) Batch 1 (b) Batch 2 (c) Batch 3 (d) Batch 4 (e) Batch 5 (f) Batch 6 (g) Batch 7. 107

Figure 5.12: Plot for SSE for different experimental batches. 108

Figure 5.13: Plot for SWMCL vs. no of experimental batches for Case 2. 108

Figure 5.14: Microscopic images of crystals (a) Batch 1 (b) Batch 2 (c) Batch 3 (d) Batch (e) Batch 5 (f) Batch 6 (g) Batch 7. 109

Figure 6.1: Conventional DNC operating profile in the phase diagram. 112

Figure 6.2: Algorithms of different DNC approach (a) Simple DNC (b) Predictive DNC (c) Reverse DNC (d) Basic DNC. 114

Figure 6.3: Primary and secondary nucleation rates. 118

Figure 6.4: Simulated optimum profiles (a) temperature profile and change in mean length (b) concentration profile with simulated metastable limit (c) number of counts/s and total length (d) super saturation profile. 119

Figure 6.5: Counts/s and temperature profiles for simple DNC when the target is (a) optimal counts/s (b) doubled optimal counts/s (c) optimal counts/s is reduced by 50%. 121

Figure 6.6: Cooling-heating cycles in simple DNC approach when the target is (a) optimal counts/s (b) doubled optimal counts/s (c) optimal counts/s is reduced by 50%. 122

Figure 6.7: Predictive DNC (a) counts/s (b) mean length (c) temperature profile when optimal counts/s is the target. 123

Figure 6.8: Predictive DNC (a) counts/s (b) mean length (c) temperature profile when optimal counts/s is doubled and set as the target. 123

Figure 6.9: Predictive DNC (a) counts/s (b) mean length (c) temperature profile when optimal counts/s is reduced by 50% and set as the target. 123

Figure 6.10: Cooling-heating cycles in Predictive DNC approach with target limits (a) optimal counts ±500 (b) optimal counts ±1000 (c) optimal counts ±100 (d) double of optimal counts ±500 (e) double of optimal counts ±1000 (f) double of optimal counts ±100 (g) half of optimal counts ±500 (h) half of optimal counts ±100. 124

Figure 6.11: Reverse DNC (a) counts/s (b) mean length (c) temperature profile when optimal counts/s is the target. 125

Figure 6.12: Reverse DNC (a) counts/s (b) mean length (c) temperature profile when optimal counts/s is doubled and set as the target. 125

Figure 6.13: Cooling-heating cycles in Reverse DNC approach (a) optimal counts/s ±500 (b) optimal counts/s ±100 (c) doubled optimal counts/s ±500 (d) 126

doubled optimal counts/s ±100.

Figure 6.14: Basic DNC (a) counts/s (b) mean length (c) temperature profile when optimal counts/s is the target. 127

Figure 6.15: Basic DNC (a) counts/s (b) mean length (c) temperature profile when optimal counts/s is doubled and set as the target. 127

Figure 6.16: Basic DNC (a) counts/s (b) mean length (c) temperature profile when optimal counts/s is reduced by 50% and set as the target. 128

Figure 6.17: Cooling-heating cycles in Basic DNC approach with target limits (a) optimal counts ±500 (b) optimal counts ±1000 (c) optimal counts ±100 (d) double of optimal counts ±500 (e) double of optimal counts ±1000 (f) double of optimal counts ±100 (g) half of optimal counts ±500 (h) half of optimal counts ±100. 128

Figure 6.18: Temperature and counts/s profile for the Basic DNC. 129

Figure 6.19: Temperature and counts/s profile for the Simple DNC. 129

Figure 6.20: SWMCL over the entire batch time of the crystals produced by Basic DNC and Simple DNC experiments. 130

Figure 6.21: SWCLD at the end of the batches. 131

Figure 6.22: PVM images of (a) Basic DNC (b) Simple DNC. 131

Figure 7.1: The flowchart summarising the PCE based surrogate modelling and model optimisation steps. 138

Figure 7.2: Prediction of the second order PCE (a) for 30 training batches and 10 validation batches (b) comparison of PCE prediction with nonlinear model. 141

Figure 7.3: Prediction of the third order PCE (a) for 30 training batches and 10 validation batches (b) comparison of PCE prediction with nonlinear model. 142

Figure 7.4: Optimum temperature profile and the corresponding *Ln* trajectory by first principle model based optimisation 144

Figure 7.5: Optimum profiles for Case 1a (a) temperature (b) Ln (c) concentration (d) μ_o. 145

Figure 7.6: Optimum profiles for Case 1b (a) temperature (b) Ln (c) concentration (d) μ_o. 146

Figure 7.7: Optimum profiles for Case 2a (a) temperature (b) Ln (c) concentration (d) μ_o. 147

Figure 7.8: Optimum profiles for Case 2b (a) temperature (b) Ln (c) concentration (d) μ_o. 148

LIST OF TABLES

Table 2.1: Examples of Distributed Parameter Systems (DPSs) (Gay and Ray, 1995; Shang et al., 2004; Li and Qi, 2010) 13

Table 2.2: Distributed Control Problems and Applications (Christofides, 2001) 15

Table 2.3: ILC Methodologies for the Control of Batch Chemical Processes 24

Table 3.1: Parameter Values for the Batch Reactor (Ray, 1981) 64

Table 3.2: Parameters of the Crystallisation Model 67

Table 3.3: Ingredients of Parapyrol Tablet 74

Table 3.4: Historical Data 79

Table 3.5: Nominal Data 79

Table 3.6: Desired Moisture Content (%) 79

Table 3.7: Experimental ILC Data 79

Table 6.1: Parameters of the Crystallisation Model 117

Table 7.1: Most Common Distributions of Random Parameters with Corresponding Polynomial Bases (Nagy and Braatz, 2010) 135

Table 7.2: Hermite Polynomials for the Second-Order-Ten-Dimensional PCE 140

LIST OF ACRONYMS

2D-FM	Two Dimensional Fornasini-Marchsini
AC	Adaptive Control
ADNC	Automated Direct Nucleation Control
AI	Active Ingradients
ANN	Artificial Neural Networks
ARMAX	Auto Regressive Moving Average Models with eXogenous
ATR	Attenuated Total Reflection
BMPC	Batch Model Predictive Control
CBMPC	Characteristic Based Model Predictive Control
CDPS	Control of Distributed Parameter Systems
CLD	Chord Length Distributions
CryPRINS	Crystallisation Process Informatics System
CSD	Crystal Size Distribution
CSS	Constant Supersaturation
DNC	Direct Nucleation Control
DPS	Distributed Parameter Systems
D-RTO	Dynamic Real-Time Optimisation
ESC	Expert Systems Based Control
FBD	Fluid-Bed Dryer
FBRM	Focused Beam Reflectance Measurement
HILC	Hierarchical ILC
ILC	Iterative Learning Control
ILRC	Iterative Learning Reliable Control
IPA	isoPropyl Alcohol
KL	Karhunen-Loéve
LMIs	Linear Matrix Inequalities
LOD	Loss on Drying

LP	Linear Program
LPS	Lumped Parameter Systems
LSM	Least Square Minimisation
LTV	Linear Time Varying
MIMO	Multiple Input Multiple Output
MOCH	Method of Characteristics
MPC	Model Predicted Control
MSZ	Metastable Zone
MSZW	Metastable Zone Width
NMPC	Nonlinear Model Predictive Control
NIR	Near Infrared
NN	Neural Network
OC	Operating Curve
ODE	Ordinary Differential Equation
OLE	Object Linking and Embedding
OPC	Object Linking and Embedding for Process Control
PAT	Process Analytical Technology
PCM	Probabilistic Collocation Method
PDEs	Partial Differential Equations
PDF	Population Density Function
PHBP	Polyhydroxybenzophenone
PID	Proportional Integral Derivative
PML	Product Managed Locally
PTFE	Polytetrafluoroethylene
PVM®	Particle Vision Measurement
QBMPC	Quality Control-Combined Batch Model Predictive Control
Q-ILC	Quadratic Criterion Based ILC
QMOM	Quadratic Method of Moments
RNN	Recurrent Neural Network

RPM	Rotation Per Minute
SC	Solubility Curve
SEM	Scanning Electron Microscope
SHMPC	Shrinking Horizon Model Predictive Control
SISO	Single Input Single Output
SNARMAX	Spatial Nonlinear Autoregressive Moving Average Exogenous
SQP	Sequential Quadratic Programming
SSC	Supersaturation Control
SVD	Singular Value Decomposition
SWCLD	Square Weighted Chord Length Distribution
SWMCL	Square Weighted Mean Chord Length
UV/Vis	Ultra-violet/Visible

NOMENCLATURE

$\boldsymbol{\Omega}$	Historical data sets
$\boldsymbol{\Phi}$	Coefficient matrix
$\boldsymbol{\Gamma}$	Coefficient matrix
$\mathbf{Y}$	Coefficient matrix
$\boldsymbol{\Psi}$	Nonlinear static function
α	The bias correction parameter in Equation 2.3
β	Forgetting factor
$\boldsymbol{\varepsilon}$	Model prediction
η	Discrete linear systems models
Δ	Change
μ_0	Zeroth moment (total number of crystals)
μ_1	First moment (total length of crystals)
μ_2	Second moment (total area of crystals)
μ_3	Third moment (total volume of crystals)
$\mathbf{A}$, $\mathbf{B}$, $\mathbf{C}$	Coefficient matrices in Equation 2.11
B	Nucleation rate
C	Concentration
C_S	Solubility
DT	Performance index in Equation 2.4
$F(.)$	Nonlinear function in a matrix form
G	Growth rate
$\mathbf{H}$	Learning gain matrix
$\mathbf{K}$	Controller gain
L	Nonlinear learning gain in Equation 2.9
Ln	Mean crystal size
$\mathbf{L}_s$	LTV perturbation model

M	Midpoint of an individual FBRM channel
N	Number of observations
$\mathbf{O}$, $\mathbf{P}$	Weighting matrices
S	Supersaturation
T	Temperature
b_o , b_1 , b_2 , b_3	Regression coefficients
d	Derivative of absorbance
e	Error between desired output and actual output
k	Batch index
$\mathbf{m}$	Sequence of model errors
$\mathbf{n}$	Vector of measurement noice
m	Control horizon
n	Model horizon
p	Model prediction horizon
r_0	Size of the nuclei
t	Time
x	Input to the batch process
y	Output from the batch process
y_d	Desired output from the process
z	State variable

ACKNOWLEDGEMENT

First, I would like to pay my gratitude to Almighty Allah for His loving care and guidance throughout my life.

Then my heartfelt gratitude goes to my supervisor, Professor Zoltan K. Nagy for his wonderful guidance, encouragement, and support from the beginning to the end of the thesis. I have thoroughly enjoyed our work together and consider myself very fortunate to have been under his supervision. Our interaction had always been an invaluable learning experience.

Very special thanks go to my colleague Dr. Ali Saleemi whose comments and help from time to time are appreciated.

I would like to thank the technical staffs Sean, Graham, Monika, and Tony for there technical support.

I am grateful to Mr. Abdul Quader, Mr. Pradip Kumar Hore and Mr. Nasir Uddin for their support and cooperation to perform experimental works in the laboratories of GlaxoSmithKline Bangladesh Limited, Bangladesh.

Most importantly, I would like to thank my husband and my daughter for being the enormous source of inspiration for my work. Through all the ups and downs of my research career they were there for me.

Last, but not the least, I want to thank my parents for their love, support, encouragement, and prayer.

Chapter 1

Introduction

1.1 Motivation

In recent years there has been a growing emphasis on the control of complex distributed parameter chemical systems due to the boost of computing power, significant evolution in sensor and actuator, and the development of modern optimisation and model reduction algorithms (Roman et al., 2009; Araujo et al., 2007). Typically batch processes are distributed in nature that are widely applied in many sectors of the chemical industries including pharmaceuticals, polymers, food products, biotechnology, and electronic chemicals (Nagy and Braatz, 2003). These days, batch reactors have become an important feature of chemical industries. Batch chemical reactor operation throws up many challenging issues which engineers must endeavour to understand, model, and control (Ekpo, 2006). A few of these are time varying characteristics, strongly nonlinear behaviour and the presence of disturbances.

However, in batch process industries there is a common practice of overlooking those features and usually batch processes are designed using conventional methods approximating lumped models. Hence linear feedback control has developed a long history of research and diverse applications (Qin and Badgwell, 2000; Kayihan, 1997). From single-input-single-output proportional-integral-derivative (SISO PID) controllers to plantwide Model Predictive Control (MPC) systems (Qin and Badgwell, 2003), there are an abundance of feedback control systems, which implicitly or explicitly assume that process dynamics are either inherently linear or almost linear owing to process operation close to a steady state.

Because of the inherent nonlinearity of batch processes, the linear models are often not sufficient to describe the process dynamics adequately. This inadequacy of linear models is principal motivations for the increasing interest in Nonlinear Model Predictive Control (NMPC). Moreover, the spatio temporal coupled nature of DPSs demands more difficult infinite dimensional modelling as compared to the modelling

of lumped parameter systems (LPSs) (Gay and Ray, 1995). However, while the industrial application of NMPC is growing rapidly, a few of the NMPC algorithms provided by vendors includes stability constraints as required by control theory for nominal stability; usually the available techniques rely implicitly upon setting the prediction horizon long enough to effectively approximate an infinite horizon (Allgower et al., 2004). Moreover, nonlinear control usually poses substantially higher data, design, implementation, and maintenance demands than linear control (Nikolaou and Misra, 2003). Therefore, it is still a quandary to decide whether a nonlinear control strategy will offer a significant improvement over linear control alternatives because of the time and effort required to develop a nonlinear model (Seborg, 1999). The common feature of both linear and nonlinear MPC is that both of these are first principle model based approaches hence not their development is complicated, time-consuming and also expensive.

Since the model based controllers are subjected to several limitations, i.e. development of first principle model is a complicated process which is time consuming and expensive while existing models are often poor and incomplete (Bonvin, 2013). Therefore due to the limited availability of robust on-line sensors, often only off-line quality measurements are widely available for batch processes. As a result, there is a growing demand of simple data driven and computationally efficient control strategies for the robust optimal control of these processes.

Researchers also have to confront the challenge of controlling operating conditions in such a way to improve the final product quality from batch-to-batch (Xiong and Zhang, 2004). This batch-to-batch control approach exploits the repetitive nature of batch processes to update the process operating trajectories using process knowledge obtained from previous batch runs. This policy undoubtedly drags the concept of Iterative Learning Control (ILC) in the terrain of batch process control. ILC is a general technique for improving transient tracking performance of a system that executes the same operation repeatedly over a fixed time interval (Lee and Lee, 2007). It has been successfully applied to industrial robots (Arimoto et al., 1984; Norrlof, 2002), computer numerical control (CNC) machine tools (Kim and Kim, 1996), wafer stage motion systems (de Roover and Bosgra, 2000), cold rolling mills

(Garimella and Srinivasan, 1998), induction motors (Saab, 2004), chain conveyor systems (Barton et al., 2000), camless engine valves (Hoffmann et al., 2003), autonomous vehicles (Chen and Moore, 2002), antilock braking (Mi et al., 2005). However, still it is a newer concept in chemical process control after its introduction at late 1990's. Today, the control practitioners have started to take advantage of the repetitive nature of chemical processes by introducing the idea of ILC in almost every sector like chemical process, chemical reactor, thermal processing (Yang et al., 2003), water heating system, laser cutting, industrial extruder plant, moving problem of liquid container, injection moulding machines (Gao et al., 2001), packaging and assembly, and tracking control of product quality in agile batch manufacturing processes.

ILC is more advantageous than traditional feedback and feedforward controller. A feedback controller reacts to inputs and disturbances and, hence, always lags in tracking. For accurately known or measurable signals, a feedforward controller can eliminate this lag but still insufficient for unknown disturbances. On contrary, ILC being anticipatory can compensate for exogenous signals, such as persistent disturbances, in advance by learning from previous iterations. ILC also provides opportunities for advanced filtering and signal processing. Since it generates open-loop control through practice (feedback in the iteration domain), this high-performance control is also highly robust to system uncertainties. Above all, ILC has the potency to be designed as an operating data based control strategy for batch processes.

Another approach that can be used to develop a nonlinear data based control strategies for batch chemical processes is polynomial chaos expansion (PCE) based system identification and optimisation techniques. The PCE is well suited to robust design and control when the objectives are strongly dependent on the shape or tails of the distributions of product quality or economic objectives (Nagy and Braatz, 2007). PCE is convergent in the mean-square sense (Ghanem and Spanos, 1991), so the coefficients in the PCE can be calculated using least-squares minimisation considering sample input/output pairs from the model, to achieve the best fit between the PCE and nonlinear model (or experimental data). After the introduction of PCE by

Wiener in late thirties for turbulence modeling (Wiener, 1938) only relatively recently it is being widely used in different disciplines (Nagy and Braatz, 2010) and has been applied mostly for uncertainty analysis in chemical processes (Nagy and Braatz, 2007). In this study, PCE based surrogate modelling and optimisation was developed for batch crystallisation processes.

Crystallisation is a widely used solid-liquid separation process mostly carried out in batches. It has a wide range of applications in different industries such as food, fine chemical, pharmaceutical, and in the petrochemical industry. Batch crystallisation offers manufacturing of products that are able to meet certain specific regulatory requirements and specifications, such as toxicity, viscosity, and hygiene standards in food industry, or specific bio-performance and dissolution properties of active pharmaceutical ingredients (API). Batch crystallisers are simple and have the flexibility of reusing the same processing equipment for different chemical substances hence it is the best available option for multi product manufacturing (Barker and Rawtani, 2004).

Although batch crystallisation is one of the oldest unit operations there are still a number of unresolved issues associated with its control. It poses a complex process dynamics and also significant uncertainties are related to the exact mechanisms of the governing phenomena (Aamir, 2010). The control objectives of batch crystallisation processes are defined in terms of product purity, crystal habit or morphology, average particle size, crystal size distribution (CSD), bulk density, product filterability, and dry solids flow properties (Worlitschek and Mazzotti, 2004). The main difficulty in batch crystallisation is to produce a uniform and reproducible CSD which is crucial for efficient downstream operations (i.e. filtration, drying, and formulation) and better product performance (i.e. dissolution rates, bioavailability and shelf life). Many scientists and researchers have worked in the development of batch crystallisation processes for the production of crystalline compounds (Hounslow and Reynolds, 2006) with consistent physical properties i.e. purity, morphology, size distribution and polymorphic form. The suggestions for improving the control of CSD came in the form of either supersaturation control (SSC) (Aamir et al., 2009; Braatz, 2002;

Fujiwara et al., 2005; Yu et al., 2006) or direct nucleation control (DNC) (Abu Bakar et al., 2009; Woo et al., 2009).

After the Food and Drug Administration's (FDA's) process analytical technology (PAT) initiative (FDA, 2004) of encouraging more quality-by-design (QbD) approaches rather than the conventional quality-by-testing (QbT) techniques, there is a growing emphasis on active control schemes that changes process conditions based on in situ measurements. Several PAT technologies (ATR-FTIR; ATR-UV/vis) are reported to be used in pharmaceutical industry but mainly for monitoring and control concentration during batch cooling and antisolvent crystallisation, for dissolving fines, and for supersaturation control (Saleemi et al., 2012a). There are several sensors available for in situ monitoring of solid phase during crystallisation process. Ultrasound probe has been used for in situ solid and liquid phase monitoring mostly for inorganic systems. Focused beam reflectance measurement (FBRM) is used to provide both real time qualitative and quantitative information about nucleation and growth. It is often used as a complementary tool alongside other PAT tools (e.g. ATR-UV/Vis, BVI) for monitoring purpose or to trigger the switching between different predetermined operating conditions (Saleemi et al., 2012b). Other direct observation based methods like bulk video imaging (BVI), particle vision measurement (PVM) and image analysis has also been used for nucleation detection and real-time in situ particle system characterisation.

In this verge of increased sensing and computational capabilities afforded by modern sensors, computers, algorithms, and software it is more convenient to adopt operating data based operation and control strategies for batch chemical processes. The major focus of this research is to develop data driven control approaches that are able to predict and control the desired end point properties in batch chemical processes, e.g. batch crystallisation. It is expected that the ultimate contribution of this research work will reduce the gap between academic and industrial developments thereby opening the ways towards novel product manufacturing and integrated process design.

1.2 Research Aim and Objectives

The aim of this research project is to develop and apply operating data based robust optimal control approaches for batch chemical processes to achieve desired end point properties. The work will consider batch cooling crystallisation process as an example case for study.

The major objectives to achieve the overall aim of the research will be as follows:

a. To gain knowledge and understanding about the distributed parameter batch processes, e.g. batch crystallisation systems' fundamentals and behaviour through a comprehensive literature review and a hands-on in situ monitoring of the crystallisation processes.
b. Development of operating data based process models with good prediction quality based on linear time varying (LTV) perturbation model.
c. Development of an LTV perturbation model based robust iterative learning control (ILC) algorithm for monitoring and control of batch processes.
d. Development of a novel hierarchical ILC (HILC) for the systematic design of supersaturation control (SSC) of seeded batch cooling crystallisation system. Evaluation of the developed method through simulation and laboratory scale experiments.
e. Strategic investigation of different structures of an alternative operating data based control strategy, the direct nucleation control (DNC) structures via computer simulations and experiments.
f. Development of an operating data driven and polynomial chaos expansion (PCE) based nonlinear surrogate modeling and optimisation strategy for batch chemical processes.
g. Application of PAT based tools like ATR-UV/Vis spectroscopy, FBRM and PVM probes for monitoring and data based control.

1.3 Scope of the Research

The present work, given the time and resource constraints, focuses mainly on end point (i.e. mean length, total number of counts) control of batch crystallisation systems by three different data based control approaches. As a means to reduce batch to batch variations the application of iterative learning control (ILC) was proposed. Iterative learning control is relatively a new concept in the field of batch chemical processes and there are a few algorithms developed so far. These algorithms can be first principle model based or data based, based on a linear model or a nonlinear model. The exploration of all the existing ILC methodologies is somewhat outside the scope of the research. This work was focused on a linear time varying perturbation model based ILC strategy for batch crystallisation systems. Later this LTV model based ILC was extended to a hierarchical ILC (HILC) concept for supersaturation control of a seeded batch cooling crystalliser. Since the research was aimed at the development of direct design tools for batch crystallisation system operation and control. Another data based approach called direct nucleation control (DNC) was evaluated under four different structure and three different end target limits. In order to incorporate the effect of process nonlinearity in batch crystallisation control, a polynomial chaos expansion (PCE) derived nonlinear model based control approach was developed and validated for its performance. However, this research did not conduct any comparative performance analysis among all these three different control strategies but recommends this as a basis for further researches to carry out in this sector.

All the proposed methodologies were evaluated through simulation case studies, laboratory scale experiments and one industrial pilot scale experiment. The simulation case studies were performed using MATLAB® version 2008a. The experimental works were aided by process analytical technology (PAT) tools (e.g. UV/Vis spectrophotometer, FBRM, PVM) to extract operating data from the system. Since the scope of this research was limited to temperature control only strategies and recommendations of this research are based on the system's response to different temperature profiles and corresponding concentration profiles. However, the effect of other variables, e.g. pressure, density, viscosity, purity of solid was not considered in

this study. The problems considered here are all single input single output systems (SISO) problems. It is expected that the research would be used as a basis for further research to investigate the performance of proposed data based methodologies for controlling other multiple input multiple output (MIMO) batch chemical processes.

1.4 Research Contribution

The main contributions of the work presented in the thesis can be summarised as follows:

1. This research provides a comprehensive literature survey of the existing modeling and control strategies of batch chemical processes. Reviews of the fundamentals and mechanisms of crystallisation processes and various PAT tools used in batch crystallisation control are presented as well.
2. Development of an operating data-driven approach to improve the product quality from batch-to-batch by exploiting the repetitive nature of batch processes to automate recipe updating using process knowledge obtained from previous runs. The data based methodology introduced is based on using the LTV perturbation model in an ILC framework to provide a convergent batch-to-batch improvement of the process performance indicator.
3. The major contribution of this research work is the development of a novel hierarchical ILC (HILC) scheme for the systematic design of the supersaturation control (SSC) of a seeded batch cooling crystalliser. This model free control approach is implemented in a hierarchical structure. On the upper level, a data-driven supersaturation controller determines the extent of optimal supersaturation needed to produce the desired end-point property of crystals. On the lower level, the corresponding temperature trajectory is determined by time domain experiments to generate necessary supersaturation. The proposed approach is evaluated in the case of a simulated seeded batch cooling crystallisation system of Paracetamol in water and also in a laboratory scale crystallisation system of Paracetamol and iso-Propyl alcohol (IPA) system.

4. This research also includes a detailed systematic evaluation of different structures of direct nucleation control (DNC) approaches of controlling batch cooling crystallisation systems. DNC is another model free approach that is adaptive in nature and requires no prior knowledge on nucleation or growth kinetics of the system. The performance and robustness of proposed DNC approaches were examined through computer simulations and laboratory experiment. Computer simulations were done in two phases. In the first phase, detailed mathematical models covering reaction kinetics and heat mass balances were developed for a batch cooling crystallisation system of Paracetamol in water. Based on these models, rigorous simulation programs were developed in MATLAB®. This mechanistic model was used to solve an open loop optimal control problem of maximizing the mean crystal length within a fixed batch time. The successive quadratic programming solution provides the optimal temperature trajectory, corresponding number of counts and the total length. In the second phase, treating the MATLAB® model as the real processes, the performance of DNC was evaluated in comparison to the model based optimal control. Later the simulated results were justified through laboratory experiments using a system of Paracetamol and iso-Propyl alcohol (IPA).
5. Development of PCE based surrogate modelling and optimisation for batch crystallisation processes. The MatLab model of paracetamol in water system was used to generate historical data and the system was then re-identified under the nonlinear PCE scheme using those. The developed model was then validated to see how the PCE is able to predict final size, using other input profiles, which were not used in the parameter identification. Later the nonlinear model was used to optimise the temperature profile needed to obtain a desired mean length of crystals at the end of the batch.
6. All the experimental works including the qualitative and quantitative monitoring of the crystallisation experiments and products demonstrated an inclusive application of various in situ process analytical technology (PAT) tools, such as focused beam reflectance measurement (FBRM), UV/Vis spectroscopy and particle vision measurement (PVM) as well.

7. Evaluation of the proposed LTV perturbation model based ILC was carried out in an industrial pilot scale laboratory in GlaxoSmithKline Bangladesh Limited, Chittagong, Bangladesh. The method was applied to determine the required drying temperature of Paracetamol granules to obtain desired moisture content at the end of the batch.

1.5 Thesis Structure

A brief description of each chapter of the thesis is as follows:

Chapter 1 introduces the subject area with a background to the research problem. The research objective and methodology is identified in this chapter.

Chapter 2 provides an overview of the literary works pertaining to the subject area. The chapter is divided in three main parts. The first part provides an overview of batch chemical processes and the different control problems associated with these. It also reviews past works and the present trends to control such systems. The second part provides a brief analysis of the ILC approaches used for batch chemical processes and pinpoints the limitations associated with those technique. The last part provides a brief review of the fundamentals and mechanism of crystallisation processes along with the optimisation and control strategies used. In addition it also discusses in short the role of process analytical technologies in crystallisation processes.

Chapter 3 introduces the methodology for batch-to-batch control. Two Simulated systems were studied for the assessment of the proposed methodology.

Chapter 4 presents the development of a systematic approach for supersaturation control (SSC) of a seeded batch crystallisation systems. Based on the experimental data a novel hierarchical ILC (HILC) approach has been developed, in which the constant supersaturation trajectories in the phase diagram can be defined in terms of temperature trajectories, in the time domain, to produce desired crystal properties at the end of the batch. In the later part of this chapter, the proposed mythology has been evaluated for a simulated seeded batch crystallisation system of Paracetamol in water. In addition, the simulation results have been presented and discussed in detail.

Chapter 5 presents laboratory scale experimental works to evaluate the proposed HILC (described in Chapter 4) for systematic design of SSC for batch cooling crystallisers. Details of materials, seed preparation, experimental set-up, experimental conditions and experimental results are provided.

Chapter 6 presents a systematic evaluation of different direct nucleation control (DNC) approaches for controlling batch crystallisation systems. In order to examine the performance and robustness of proposed DNC approaches computer simulations were done in two phases and a novel twofold systematic evaluation of the proposed DNC approaches has been described. In the last part laboratory scale experimental results have also been included and discussed to justify the results of simulation case studies.

Chapter 7 presents the development of polynomial chaos expansion (PCE) based surrogate modelling and optimisation for batch crystallisation processes. The chapter starts with a brief review of the theoretical aspects of PCE. The results obtained by simulations case studies have also been included and discussed in detail.

Chapter 8 presents the industrial field work carried out in GlaxoSmithKline (GSK). The plan of work and experimental works performed in a pilot plant system have been described and the results have been presented and discussed.

Chapter 9 concludes the thesis by summarising all the simulation and experimental results. The conclusions of the research along with proposals for future work are also presented.

Chapter 2

Literature Review

2.1 Overview

Batch chemical processes hold a significant portion of the chemical process industry. Now a day it has captured almost 40-50% of the total empire (Wang et al., 2006). Batch or semi-batch processes are essential for the production of high value added commodity such as specialty chemicals and pharmaceuticals. Due to their time space varying nature, batch processes are generally modelled as distributed parameter systems (DPSs). The knowledge of stochastic DPSs is highly important in chemical industries for the purpose of fault detection, measurement device placing, and control (Hangos and Virág, 1986). This chapter provides an overview of the past works for modelling and control of DPSs. As an example of distributed parameter batch processes, batch crystallisation has been studied throughout the research work. The later part of this chapter includes theories and common practices for the control of batch crystallisation processes.

2.2 Distributed Parameter Systems

Distributed parameter systems (DPSs) are processes with spatially varying states, controls, and parameters (Miller and Rawlings, 1994). Almost all natural and industrial processes are distributed in nature (Gay and Ray, 1995). Chemical processes show some spatial variations due to imperfect mixing (Lee, 2008). Table 2.1 gives examples of some industrial processes whose noticeably nonuniform spatial profiles have created great interest between process and control engineering practitioner.

A proper mathematical model of the system is crucial for applications like system identification, numerical simulation, control design, and optimisation. Since the DPSs have time-space coupled characteristic, to adequately describe this distributed feature one needs to use partial differential equation (PDE) models with mixed or

homogeneous boundary constraints (Curtain, 2003). Generally, DPSs are described by first and second order PDEs that are commonly classified into three categories (Hanczyc and Palazoglu, 1995) as 1) hyperbolic, 2) parabolic, and 3) elliptic. All single first-order PDEs are considered hyperbolic. Higher order PDEs may be any one or a combination of the three. To predict the nonlinear and distributed dynamic nature accurately, these infinite-dimensional PDE models are useful.

Table 2.1: Examples of Distributed Parameter Systems (DPSs) (Gay and Ray, 1995; Shang et al., 2004; Li and Qi, 2010)

System	Example
Thermal process	- Heat conduction through a plate - Drying or curing operations - Metallurgical heating - Sheet-coating processes
Fluid process	- Counter-current heat exchanger - Absorption columns - Fluidised beds
Convection-diffusion-reaction process	- Polymer-extrusion - Plug-flow reactor or packed-tube reactor - Fixed-bed-reactor - Crystallisers
Flexible beam	-Flexible magnetic bearing system (Zhou et al., 1992) -Non-linear power generator system (United States Patent 7732994)

However, in practice there are a limited number of actuators and sensors for sensing and control and limited computing privilege for execution. Due to the infinite dimensional nature of the models, it is not possible to use them directly for the design of nonlinear controllers that can be readily put into action in real-time with available computing power.

Therefore, for engineering applications such infinite dimensional systems need to be approximated by finite dimensional systems. Then modelling and control design is generally based on different lumping techniques. Conventional trends to discretise the

nonlinear DPS involve transforming the PDEs and boundary conditions using finite-difference/finite-element methods that lead to an approximate system of thousands of ordinary differential equations. However, these solutions are also unrealistic for controller synthesis and real-time controller implementation due to the inadequacy of sensors and actuators for measuring and implementing the solution (Zheng and Hoo, 2002). Thus, further order reduction (Bonvin and Mellichamp, 1982) may be necessary to develop controllers that can be readily implemented in real time with available computing power. Moreover, it is not always possible to have a mathematical model of the system. Whether there is an exact model of the system or not, model reduction is necessary. In case an exact mode is unavailable, a nominal model of the system is conventionally used as a design platform. Figure 2.1 illustrates the steps for modelling both known and unknown DPSs for control design and development purposes.

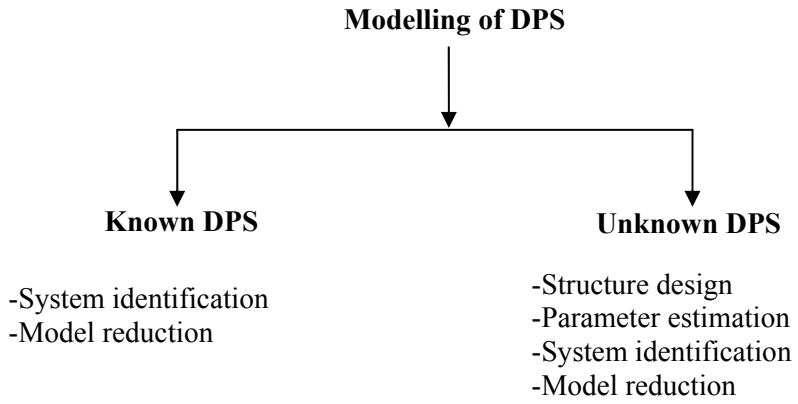


Figure 2.1: Steps for modelling known and unknown DPSs.

2.3 Control of DPSs

The diverse applications in the fields of aeronautics, biotechnology, nanotechnology, semiconductor manufacturing, and material engineering as well as in chemical processes have highly motivated the research on control of DPS. However, the spatio temporal coupling and infinite dimensionality of the DPS's still make them very complicated for analysis, modelling, and control (Wang et al., 2010). Table 2.2 summarises the industrially important control problems associated with DPS in different fields.

The general objectives behind the control of DPSs are more or less the same as those for lumped parameter systems (LPS); these are stability, optimality, robustness, etc. However, the spatially distributed characteristic requires an infinite-dimensional modelling, which is more difficult and complicated than modelling of lumped parameter systems. In addition to that, it poses certain unique challenges like satisfying the spatial boundary conditions, non-collocated, collocated control design (assuring separate locations for controllers and actuators) (Padhi and Ali, 2009).

Table 2.2: Distributed Control Problems and Applications (Christofides, 2001)

DPS Control Problem	Area of Application
Control of spatial profiles	CVD, Etching, Crystal growth, Packed-bed reactors.
Control of size distributions	Aerosol production, Crystallisation, Emulsion polymerisation, Cell cultures.
Control of fluid flows	Fluid mixing, Wave suppression, Drag reduction, Separation delay.
Control of material microstructure	Thin film growth, Nano-structured coatings processing.

The following sub-section provides an overview of the existing practices for controlling DPSs. Since this particular study is based on data based control, the overview is mainly focused on different data based control strategies.

2.3.1 Model Based Control

At present, there are several important advanced control techniques. The classification of these techniques is shown in Figure 2.2. Advanced control techniques are primarily classified in four conceptually different categories. However, a common feature of all these algorithms is that all are based on a process model. The most important approach, the model predictive control (MPC), can be classified further, for example, according to different model types used for prediction in the controller (Agachi et al., 2006). MPC is a form of control in which the current control action is obtained by solving on-line, at each sampling instant, a finite horizon open-loop optimal control problem (Orukpe, 2005).

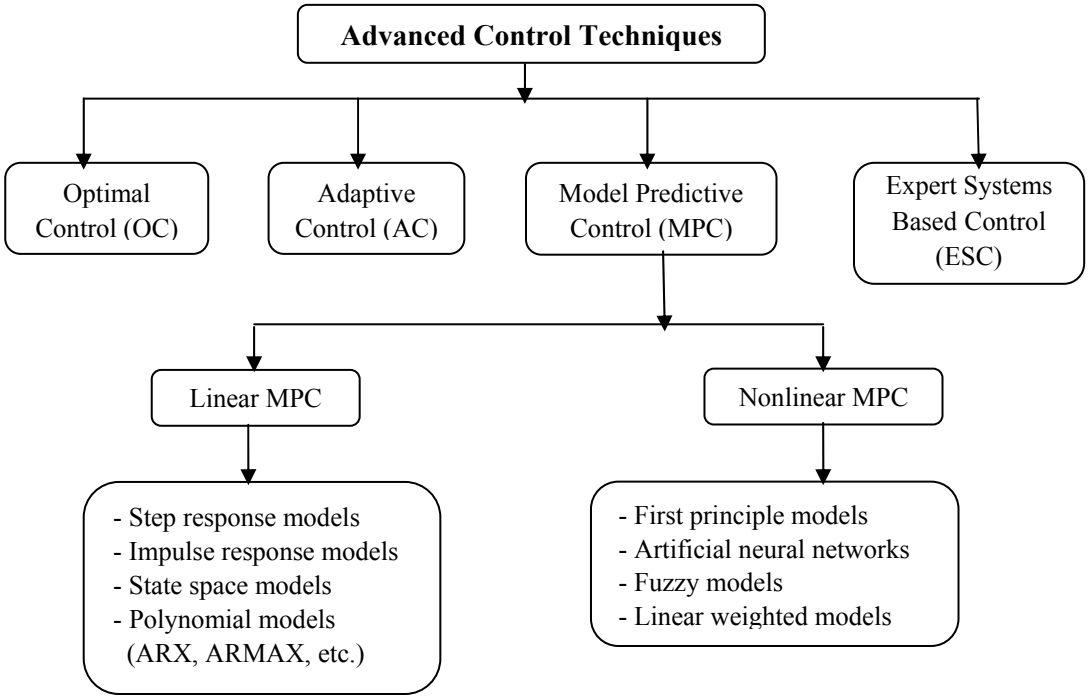


Figure 2.2: Classification of advanced control techniques (Agachi et al., 2006).

For a linear model, the objective function is a quadratic cost function. Using the current state of the plant as the initial state, the tracking error, which is the difference between the predicted output and the desired reference, is minimised over a future horizon, possibly subject to constraints on the manipulated inputs and outputs (Bemporad and Morari, 1999). The result of the optimisation is applied according to a receding horizon philosophy; at time t only the first input of the optimal command sequence is actually applied to the plant. The remaining optimal inputs are discarded, and a new optimal control problem is solved at time $t+1$. The prediction horizon keeps being shifted forward, for this reason MPC is also called receding horizon control. This idea is illustrated in Figure 2.3.

With over 4500 industrial installations across a wide range from chemicals to aerospace industries, MPC is currently the most widely implemented advanced process control technology for chemical process plants (Qin and Badgewell, 2003). MPC is suitable for almost any kind of control problem, however, it displays its main strength when applied to problems with a large number of manipulated and controlled variables, constraints imposed on both the manipulated and controlled variables,

changing control objectives and/or equipment failure and time delays (Seborg et al., 2004).

-

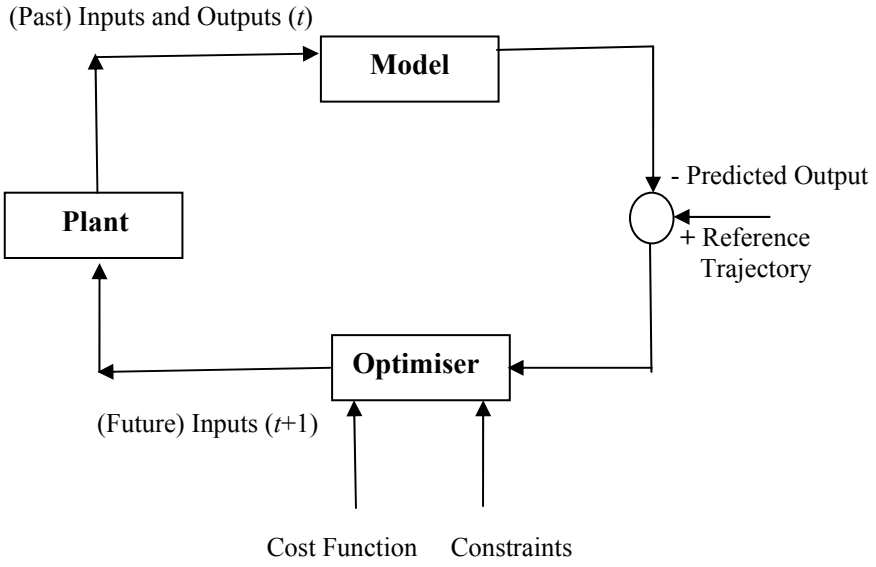


Figure 2.3: Basic structure of model predictive control (MPC).

As discussed earlier, MPC is further classified as linear and nonlinear. Linear MPC refers to a family of MPC schemes in which linear models are used to predict the system dynamics and considers linear constraints on the states and inputs and a quadratic cost function. Linear feedback control of chemical processes has a long history of research and diverse industrial applications (Qin and Badgwell, 2000; Kayihan, 1997). Whether it is a SISO-PID controllers or plantwide MPC systems there are versatile applications of feedback controllers, which implicitly or explicitly assume that process dynamics are either inherently linear or almost linear owing to process operation close to a steady state (Qin and Badgwell, 2003).

However, this is not always the right practice; even if the system is linear, the closed-loop dynamics are in general nonlinear due to the presence of constraints. There is pronounced nonlinear nature of several chemical processes such as, biochemical production of chemicals, systems operating near constraints (e.g. petroleum refining, natural gas processing), non-routine operation situations (e.g. start-ups, shut-downs, change-overs, flares, relief valve emissions), nonlinear distributed parameter systems such as control of spatial profiles (Christofides, 2001), control of size distributions (Chiu and Christofides, 1999), crystallisation, emulsion, polymerisation, cell cultures,

control of fluid flows, control of material microstructure (Nikolaou and Misra, 2003), etc. This inherent nonlinearity of batch chemical processes, along with higher product quality specifications and rising productivity demands, tighter environmental regulations and challenging economic considerations force the process dynamics to be described by nonlinear models to capture the nonlinear aspects and to adopt nonlinear model predictive control for betterment.

Nonlinear model predictive control (NMPC) refers to MPC schemes that are based on nonlinear models and/or consider non-quadratic cost-functional and general nonlinear constraints on the states and inputs (Findeisen et al., 2003). In NMPC, the process nonlinearities and constraints are explicitly considered in the controller (Allgower et al., 2004). As a result, from 1990s, there is a steadily increasing attention from control theoretists as well as control practitioners in the area of NMPC. Over 125 NMPC applications have been reported in chemical industries in the past decade (Nagy and Allgower et al., 2004) and the industrial processes are now pushed to nonlinear operation windows. Although the potential advantages of nonlinear model-based control strategies are readily apparent, there are still a number of major unresolved issues (Seborg, 1999). Nonlinear control systems usually pose substantially higher data, design, implementation, and maintenance demands than linear control systems (Nikolaou and Misra, 2003). Therefore, it is still a quandary to decide whether a nonlinear control strategy will offer a significant improvement over linear control alternatives because of the time and effort required to develop a nonlinear model (Seborg, 1999). Before developing and implementing a nonlinear control system, one must carefully examine the potential advantages of such a system in comparison to a linear one. While the existing schemes increase the general understanding, a few robust NMPC formulations exist and are computationally difficult to be applied in practice (Allgower et al., 2004). Theoretical analysis of closed-loop performance properties (e.g. stability and robustness) are very complex, especially if inequality constraints are present. Additional problems in NMPC are to ensure stability of closed-loop systems with unknown disturbances and model plant mismatch. While nominal stability and feasibility have been extensively addressed in the past decades (Limon et al., 2009), NMPC with asymptotic stability does not guarantee robust stability and large unmeasured disturbances can lead to poor performance for dynamic

real-time optimisation (D-RTO). Considering these issues, robust design strategies are necessary to account for uncertainties, explicitly in the controller formulation (Huang et al., 2009). A well-known strategy to guarantee the robust stability is the min-max NMPC formulation, which computes the best control policy based on the worst expected realisation of the uncertainties. However, this formulation dramatically increases the computational cost of the on-line NMPC problem, despite some recent remedies (Diehl et al., 2008). As the control action is based on the worst case, the performance is compromised (e.g. output variables present large offset). Therefore, more research is required for effective application of the NMPC strategy especially in batch chemical processes that are distributed in nature.

2.3.2 Data Based Control

Batch processes retain the characteristics of operating in the absence of steady state, in the presence of constraints and are repetitive in nature. The challenge of batch process control is the control of product quality, which is only at run end while the batch traverses through a wide range of operating conditions. The most appreciable approach for quality improvement is to use precise first-principle models and adopt MPC as described in the previous section. However, the available models are often poor and incomplete (Bonvin, 2013) and models are not available for most newly developed processes. Modelling of a complex industrial process is very difficult, time-consuming, and expensive. Usually modelling costs account for over 75% of the expenditures in the design of an advanced control project (Hussain, 1999). Moreover, it is difficult to build precise first-principle models that can explain why defects appear in products (Kano and Nakagawa, 2008).

In this scenario, the monitoring and control of batch processes are obviously diverted towards the use of abundant operation data. Industrial processing plants are usually equipped with a large number of sensors primarily to deliver data for process monitoring and control. It has been only two decades since the researchers started to use this operating data for building predictive models of the related process based on this data (Kadlec et al., 2009). These data based predictive models are called none other than the Soft Sensors in the context of process industry.

Soft Sensors can be either model-driven or data-driven. The model driven Soft Sensors are typically based on First Principle Models (FPM), extended Kalman filter or adaptive observer (Kadlec et al., 2009 and the references cited therein). First Principle Models describe the physical and chemical background of the process. However, the data-driven Soft Sensors gained more popularity in the process industry for being based on the data measured within the processing plants. These soft sensors describe the real process conditions in a better way. Various modelling techniques applied to data-driven Soft Sensors are the Principle Component Analysis (PCA) (Jolliffe, 2002) in a combination with a regression model for monitoring the process plan, Partial Least Squares (PLS) (Wold et al., 2001), Artificial Neural Networks (Principe et al., 2000; Hastie et al., 2001), Neuro-Fuzzy Systems (Jang et al., 1997; Lin and Lee, 1996), Data Driven Quality Improvement (DDQI) (Kano and Nakagawa, 2008) and Support Vector Machines (SVMs). In the next subsection, the more commonly used data based control techniques have been briefly discussed.

2.3.2.1 Artificial Neural Network

Artificial neural networks (ANN) designed on the concept of animal brain function (McCulloch and Pitts, 1943) are networks of simple processing elements (called 'neurons') operating on their local data and communicating with other elements. It has been extensively studied. Although there exist many different types of neural networks (Haykin, 1994) the basic principles are very similar. Each neuron in the network is able to receive input signals for processing and to send an output (Svozil et al., 1997).

While dealing with a chemical process with severe/unknown non-linearities neural networks offer a simpler and efficient alternative to extract information from plant in an efficient manner with normal availability of rich data (Kano and Nakagawa, 2008). As a data-driven modeling method, ANN possesses the ability to approximate any complex nonlinear relationships to any desired degree of accuracy with less a prior knowledge (Liu et al., 2011; Xiong and Zhang, 2005). As a result there has been substantial interest and fast development in soft sensor modeling based on ANN within batch process industry (Bo et al., 2003). However, it is still very difficult to obtain satisfying Soft Sensor model in the absence of construction theory. It is

important to establish a strict construction theory of Soft Sensor model based on artificial neural network SS-ANN and improve its performance for the on-line estimation of the key immeasurable variables (Liu et al., 2011).

Xiong and Zhang (2005) divided the neural networks for nonlinear process modelling broadly into two categories, e.g. static networks, including multi layer feed forward neural networks and radical basis function networks and dynamic networks which include globally and locally recurrent neural networks and dynamic filter networks, etc. Neural networks can also be classified according to its incorporation in three major categories of control, i.e. predictive, adaptive and inverse-model based control techniques in both simulation and online applications. For an extensive review of various neural networks based works please see Hussain (1999).

2.3.2.2 Iterative Learning Control (ILC)

Iterative Learning Control (ILC) is a general technique for improving transient tracking performance of a system that executes the same operation repeatedly over a fixed time interval (Lee and Lee, 2007). The supplementary requirements are that, the reference trajectories (to be followed by the outputs) remain the same from run to run and the process starts from the same state during each operation. ILC had been developed and studied primarily in the context of training and controlling robots and other mechanical systems under repetitive operations (Moore, 1998). In practice there are many processes repeating the same task in a finite interval, ranging from a welding robot in a VLSI production line, to a batch reactor in pharmaceutical industry. Recently the control practitioners in the field of chemical engineering have started to take advantage of this similarity of repetitiveness to introduce the idea of ILC for controlling batch chemical processes (Lee et al., 1994).

The focus of this research is to develop operating data based ILC for batch chemical processes. The following section provides a detailed review of the ILC including its structure, applications in chemical batch processes and critical analysis of the existing ILC strategies developed by researchers.

2.4 Iterative Learning Control (ILC)

2.4.1 Generic Description of ILC/ Technical overview

ILC differs from most existing control methods in the sense that, it exploits every possibility to incorporate past control information like the past tracking error signals and in particular the past control input signals, into the construction of the present control action (Xu and Tan, 2003). The basic idea of ILC is illustrated in Figure 2.4.

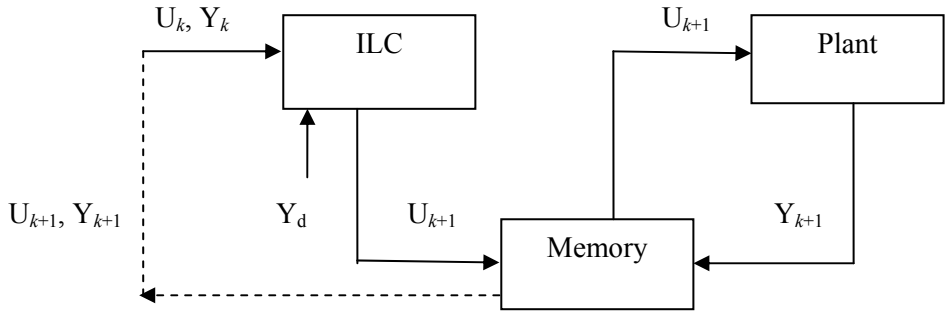


Figure 2.4: Basic framework of iterative learning control (ILC).

All the signals shown are defined on a finite interval $t \in [0, t_f]$, the subscript k denotes the run number. The key objective is to find an input profile for a new batch run based on the information gathered from previous batches such that (Lee and Lee, 2003), $\|e_k\| \to 0$ as $k \to \infty$, where, $e_k(t) = y_d(t) - y_k(t)$, is the difference between the desired output y_d and the actual output y_k during k^{th} batch. The key concept is, during the k^{th} trial an input $u_k(t)$ is applied to the system, producing the output $y_k(t)$. Based on the output error the ILC algorithm computes a modified input signal $u_{k+1}(t)$ that will be stored in memory until the next time the system operates, at which time this new input signal is applied to the system. A first-order learning algorithm is used to update the input profile as shown in Equation 2.1.

$$u_k = u_{k-1} + \mathbf{H} e_{k-1} \tag{2.1}$$

Here, $\mathbf{H}$ is called the diagonal learning gain matrix. With the above form of the learning algorithm, ILC design problem is reduced to the design of the learning gain.

2.4.2 ILC in Batch Chemical Processing

Traditionally batch process industries have managed to run quite stably by following a recipe leading to consistent and successful products. Usually the recipe is arrived at over a long period through a continuous, iterative improvement based on some analysis of products. Although such a recipe is usually adjusted based on perception and heuristics instead of a rigorous model and optimisation, such a practice can indeed be interpreted as feedback control or feedback optimisation. The repetitive nature of typical batch operations enables feedback of the results of previous batches on the recipe to improve the operation (Lee and Lee, 2003). Nonetheless, whatever the control is or however they do this, it sounds more like the basic concept of ILC. Now a day batch chemical processing and ILC is closely intertwined to each other. The repetitive nature of batch processing undoubtedly demands the application of ILC to reduce batch-to-batch variations.

The dynamic nature of operation of batch processes differs considerably from that of continuous processes. In batch processes variables swing over large ranges during operation and displays nonlinear behaviour. This makes a linear controller ineffective that is used over whole batch duration and demands manual operation over some periods. This is one of the reasons the researchers prefer to associate the problem of batch process control primarily with that of nonlinear control (Berber, 1996). However, due to the time consuming nature and economic constraints nonlinear modelling as well as nonlinear control techniques had failed to attract much attention from batch process industries (Lee and Lee, 2003) for a long time. Recently this scenario is changing; in the world of process control, the new challenge is to incorporate ILC and nonlinear control together for the betterment of the industry. Table 2.3 summarises the recent trends in ILC for batch process control.

From the literature study, it is evident that although ILC was introduced and practiced in the world of control since early 70's, this is a new concept in batch chemical process industries. However, today ILC applications have increased significantly after its introduction in late 90's. Lee and Lee, (1999) first presented a paper on model based ILC framework in AIChE Meeting, Chicago (1996) which was later published in *Automatica* in 1999. Among the researchers who are working in this field two

groups have attained significant position for their continual contribution in this sector. The first group is led by Lee and Lee whilst the second group is led by Xiong and Zhang. The following subsection gives a brief discussion on the methods tabulated in Table 2.3.

Table 2.3: ILC Methodologies for the Control of Batch Chemical Processes

Method	**Example Case Studies/ Application**	**Literature Cited**
Q-ILC	Numerical example	Lee et al. (1996, 2000)
Batch-MPC (BMPC)	Simulation of an experimental batch reactor system involving a highly exothermic reaction, Unseeded crystallisation of poly (hydroxyl-benzophenone) (PHBP)	Lee et al. (1999) Kim et al. (2009)
QBMPC (Quality Control-Combined Batch MPC)	Numerical illustration for control of a semi-batch reactor	Lee and Lee (2003)
ILC Based on Time-Varying Perturbation Models	Simulated batch reactor, Simulated batch polymerisation process, Simulated batch crystallisation process	Zhang et al. (2009a) Xiong and Zhang (2003)
ILC of Output PDF Shaping in Stochastic Systems	For stochastic systems	Wang et al. (2005)
Combined Batch-to-Batch ILC with On-line Shrinking Horizon MPC (SHMPC)	Simulated batch polymerisation reactor	Xiong et al. (2005)
Recurrent Neural Network (RNN) Models	Simulated batch polymerisation reactor	Xiong and Zhang (2005)
Auto Regressive Moving Average Models with eXogenous Inputs (ARMAX) Model	Simulation of an industrial pilot plant fermentation Simulated east fermentation	Bonne (2005)
Iterative Learning Reliable Control (ILRC)	Simulation of injection modelling, i.e. injection velocity control	Wang et al. (2006)
ILC of DPSs based on Geometric Analysis	ILC problem of distributed parameter system	Zheng et al. (2009)
Neural Network (NN) based ILC	Simulated batch reactor	Xiong et al. (2010)
ILC for Spatio-Temporal Dynamics using nD Discrete Linear Systems Models	Systems described by PDEs	Cichy et al. (2011)

Quadratic Criterion Based ILC (Q-ILC)

Lee et al. (2000) developed a general and comprehensive framework for Quadratic criterion based ILC (Q-ILC) especially for the application in chemical processes where excessive input movements are undesirable and many process variables are subject to hard constraints. In fact, it was a tailored version of their Q-ILC algorithm (Lee et al., 1996) proposed to be implemented as an output feedback algorithm to improve robustness. This quadratic performance criteria based algorithms were designed to consider the issues relevant to process control, such as disturbances, noises, nonlinearities, constraints, and model errors. They evaluated their proposed methodology using numerical examples.

In the algorithm, they first introduced an error transition model that represents the transition of tracking error trajectories between two adjacent batches. They also discussed the integration of the effects of various types of disturbances into the transition model. Based on this model, one-batch-ahead quadratic optimal control algorithms were derived for both the unconstrained and constrained cases. In addition, they proposed a robust ILC algorithm that minimises the worst-case tracking error for the next batch. They also investigated the relevant mathematical properties like convergence, robustness, and noise sensitivity for each algorithm.

Limitations

A potential problem in implementing the algorithm was that the large dimensionality of the system could lead to numerical difficulties in computing the optimal learning gain matrix.

Batch-MPC (BMPC)

Lee et al. (1999) introduced the concept of Batch-MPC (BMPC). It was based on a time-varying MIMO linear model, i.e. representing a nonlinear system along a fixed trajectory. The technique was developed by integrating the concept of iterative learning into the conventional MPC technique. They evaluated the performance of BMPC for tracking a pre-specified reaction temperature trajectory in an experimental batch reactor system involving a highly exothermic reaction. The process was

identified as a linear time-varying model by combining two linear time-invariant models with time-dependent weighting functions. They showed that BMPC is not only capable of eliminating persisting errors from previous runs but also removes new disturbances as they occur during a run.

Limitations of the BMPC Technique

Although more approachable the BMPC technique suffers from the inadequacy of fitting into every existing batch process control problem. It is not possible to manipulate the time windows within the BMPC formulation so that one can consider inputs and outputs that are active for a particular period only. Therefore, the operating trajectories cannot be contracted or dilated by reducing or expanding various phases. As they used a linearised model the operating trajectories from run-to-run did not differ so much. It requires a fundamental model to be available to re-linearise that model for updating the dynamic matrix after each batch run.

In this paper, Lee et al. (1999) evaluated the technique by using a temperature tracking problem. However, in a chemical process industry the final product quality is affected by many other factors as well the temperature trajectory. It is necessary to develop a single control framework to handle the issues of both quality control and temperature tracking.

QBMPC (Quality Control-Combined Batch Model Predictive Control)

Lee and Lee (2003) developed QBMPC (Quality Control-Combined Batch Model Predictive Control) as a batch process control technique based on a series of previous research works. As discussed earlier the first contribution of this group was Q-ILC (Lee et al., 1996) and batch MPC technique (BMPC) (Lee et al., 1999; Kim et al., 2009). QBMPC is a subsequent extension of BMPC with the added capability to perform inferential control of end-product variables. It was a fusion of Q-ILC, real-time feedback MPC, and end-product regression model to build an integrated end-product and transient profile control technique for industrial chemical batch processes.

Limitations

This ILC type approach may not be straight forwardly applied to product quality control in all batch processes.

ILC Based on Time Varying Perturbation Models

While most of the earlier works on optimal batch process control generally utilise nonlinear models such as mechanistic models, neural network models, and hybrid models (Wang et al., 2010; Shang et al., 2004; Seborg, 1999); Xiong and Zhang (2003) proposed a novel ILC strategy for tracking control of product quality in batch processes. They developed an operating data based least-squares regression method for estimating the parameters of a perturbation model linearised around the nominal trajectories. Their work was novel in the sense that they combined an updated model with modified predictions to batch-to-batch ILC by adding the model prediction errors of the previous batch run to the model predictions for the current batch run. Another perspective of this updating strategy was to handle the negative effects of unmeasured disturbances and process variations. For ensuring more weight to the recent batch runs than the previous ones, they introduced a forgetting factor. Further details of this method are discussed in Chapter 3. The convergence of tracking error under ILC was analysed. The proposed technique was successfully demonstrated on a simulated batch reactor and a simulated batch polymerisation process.

Limitations

The perturbation model proposed by Xiong and Zhang (2003), which is a linearised representation of typical nonlinear batch processes, causes offsets to occur as a result of modelling errors and unmeasured disturbances. The tracking performance is much dependent on the precision of the model. The tracking error can be decreased to a smaller value but it never becomes zero.

ILC of Output PDF Shaping in Stochastic Systems

Wang et al. (2005) developed an ILC strategy for shaping the output population density function (PDF) of stochastic systems by using a set of fixed basis functions

(Bemporad and Morari, 1999) in the B-spline approximation to the output PDFs. This concept transfers the shape control of the output PDFs into the control of the weights in the B-spline approximation. They used the traditional concept of using the tracking errors of the output PDFs with respect to the desired PDF in a batch for the iterative learning of the B-spline basis functions and the model parameters. The updated basis functions were used to design controller for the next batch. The convergence condition of the learning rate was identified. Figure 2.5 shows the basic concept of the proposed ILC law.

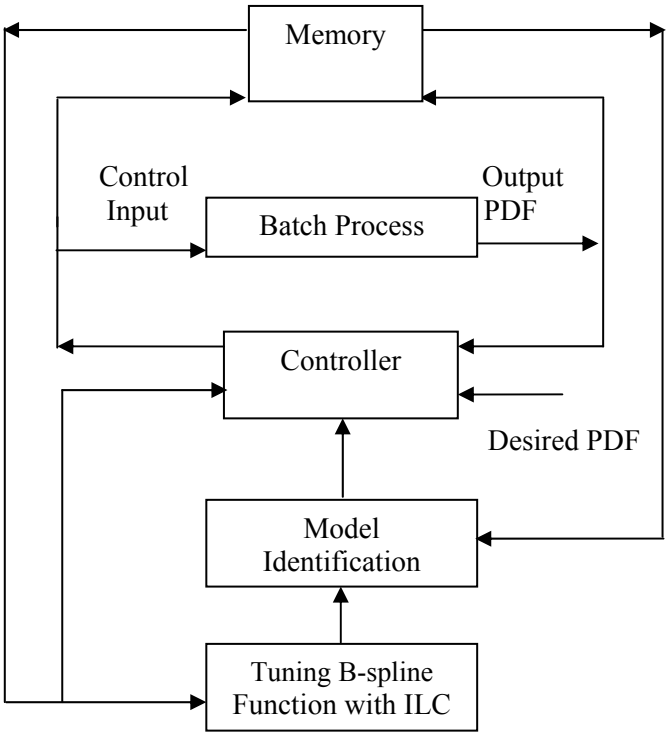


Figure 2.5: Basic structure of ILC for output PDF shaping (Wang et al., 2005).

Limitations

The proposed ILC scheme is based on complicated algorithm. The authors did not provide any rigorous proof of the convergence of the proposed ILC law. The necessary and sufficient conditions of the ILC convergence is still an open window for future research. In addition, the authors used only a simple second order tuning law of the B-spline basis functions, which is P-type learning in the ILC context.

Development of iterative tuning laws improved by using other shapes of the basis functions is still an open question.

Combined Batch-to-Batch ILC with On-line Shrinking Horizon MPC (SHMPC)

As a consequence of their endless effort to design ILC algorithms Xiong et al. (2005) proposed a combined batch-to-batch ILC and on-line shrinking horizon MPC (SHMPC) strategy for controlling product quality tracking in batch processes. They argued that though the performance of future batch runs can be improved under the conventional batch-to-batch ILC, there is no control on current batch run to improve its performance. Alternatively, on-line SHMPC within a batch, that is based on current output values and remaining input moves can reduce the effects of disturbances and improve the performance of the current batch run. However, model prediction is also modified by adding the estimated error calculated from the batch-to-batch controller. They evaluated the proposed strategy on a simulated batch polymerisation process.

In SHMPC, the optimisation problem is constantly changing during the batch because of the arrival of additional measurements and because of the decreasing length of the control vector. It means that as time progresses fewer control moves can be changed to affect the quality outcome of the batch, and prediction horizon also shrinks with time as the batch progresses (Ahn et al., 2007). Thus, the model prediction horizon p is equal to the control horizon m and they both decline as time t passes within the current batch (i.e. $m = p = n - t$). Although all of the remaining input moves are calculated at each time, only the first of these inputs is implemented, and the rest are recalculated at the next time.

Limitations

Due to the immediate response of on-line SHMPC to disturbances and correcting action of batch-to-batch ILC to correct any residual error, it is tempting to integrate both methods. However, a naive combination of the two strategies will not work rather SHMPC will ‘undo’ the ILC corrections due to conflicting predictions between the two. The idea of ILC needs to be integrated into SHMPC at the level of model

preparation. The ILC method is implemented using the batch-wise LTV perturbation model (Xiong and Zhang, 2003), for tracking trajectories, however in order to apply SHMPC on-line, a more precise model has to be developed based on the current output values and remaining control moves.

However, first principle models are usually very complicated and difficult to obtain and implement for on-line control (Xiong et al., 2010). In addition, due to the limited availability of robust on-line sensors in the industrial practice of batch process operations, typically only off-line quality measurements are available.

Recurrent Neural Network (RNN) Models

As a non-linear regression tool, properly trained and validated neural networks are increasingly used in modelling and control of chemical processes, especially for complex non-linear processes where process understanding is limited (Shang et al., 2005; Orukpe, 2005). In their paper Xiong and Zhang (2005) used Recurrent Neural Networks (RNN) to develop empirical models for providing improved long range predictions from batch process operational data.

The existence of model-plant mismatches and/or unknown disturbances is represented by the NN model prediction errors. They used the errors of the previous RNN model iteratively to modify the model predictions. Updated control policy was then calculated for each batch using the modified model predictions. As a result, modified prediction based model errors were gradually reduced as the number of batches increases. In this way, the idea of ILC was adopted in RNN scheme for improving product quality from batch-to-batch. The method is discussed below in brief. If the input and product quality sequences are defined as in Equation 2.2,

$$\mathbf{X}_k = [x_k(0), x_k(1), \ldots, x_k(N-1)]^{\mathrm{T}}, \text{ and}$$

$$\mathbf{Y}_k = [y_k(1), y_k(2), \ldots, y_k(N)]^{\mathrm{T}} \tag{2.2}$$

where, k is the batch index, $y \in R^n$ are product quality variables of batch processes, $x \in R^m$ is the input (manipulated) variable for the product qualities, and the initial

conditions (x_0, y_0) are given. The measured prediction error of the RNN model for the k^{th} batch is, $\hat{e}_k(t) = y_k(t) - \hat{y}_k(t)$. Using the averaged model prediction error to correct model predictions can reduce the effect of measurement noise and the effect of disturbances that only exist in one batch. The average model error $\bar{\hat{e}}_k(t)$, of all previous runs is calculated as in Equation 2.3.

$$\bar{\hat{e}}_k(t) = \frac{1}{k}\sum_{i=1}^{k}\hat{e}_i(t) = \frac{1}{k}\sum_{i=1}^{k} y_i(t) - \hat{y}_i(t) \tag{2.3}$$

By adding this average model error, the modified prediction $\tilde{y}_{k+1}(t)$ of RNN models is defined in Equation 2.3,

$$\tilde{y}_{k+1}(t) = \hat{y}_{k+1}(t) + \alpha\bar{\hat{e}}_k \tag{2.3}$$

Where, α is called the bias correction parameter with the range $0 < \alpha \leq 1$.

Xiong et al. (2005) successfully illustrated the RNN algorithms on a simulated MMA polymerisation reactor.

Limitations

In this algorithm the value of α cannot be set to 0. If $\alpha = 0$, the model prediction is not modified further and the same control policy is repeated in the subsequent batch run by solving the same optimisation problem. On the other hand, a larger value of α which increases the modified RNN model prediction accuracy, also causes significant changes of modified prediction in presence of considerable disturbances and/or uncertainties in the earlier batch run and the convergence of iterative optimisation is affected. Therefore, it is necessary to consider the trade-off between the convergence rate and the accuracy of the modified RNN model prediction.

The proposed algorithm considered only linear inequality constraints of the inputs and final product qualities. Although these constraints are helpful for defining the feasible region of the optimisation problem during solving it by Sequential Quadratic Programming (SQP), the lower and upper bound on the temperature may become

active and prevent the tracking error to converge to zero. Moreover, use of the SQP approach for solving the optimisation problem increase the computation cost significantly.

Auto Regressive Moving Average Models with eXogenous Inputs (ARMAX) Model

In his PhD thesis Dennis Bonne (Bonne, 2005) proposed a data driven methodology as a cost and time effective alternative to develop models. According to this method, models are developed with relatively large sets of interdependent local Auto Regressive Moving Average Models with Exogenous inputs (ARMAX). This new concept of introducing interdependency among the local ARMAX models notably decreases the sensitivity to measurement noise.

He also developed an algorithm for model quality optimisation, which includes model structure identification. For successful reduction of batch-to-batch variations and the achievement of optimal operation, he combined the concept of ILC with MPC. Initially, the proposed control methodology defines an optimal model as the solution to a Linear Program (LP) and furthermore proposes a procedure in which the learning MPC algorithm is used to iteratively bring the operation of a batch process closer to its optimal batch operational model.

The combined methodology for optimal and reproducible operation of batch chemical process proposed has been tested on several case studies including simulation of an industrial pilot plant fermentation and simulated east fermentation. Based on the results and the theory presented they claimed that the proposed methodology has demonstrated sufficient potential.

Limitations

The state of the art reproducibility proofs for ILC and Learning MPC algorithm only apply to implementations on known deterministic batch systems with perfect observations. However, as the optimisation procedure is based on local linear models it cannot be proven to achieve the optimal batch operation model.

Iterative Learning Reliable Control (ILRC)

In their paper, Wang et al. (2006) developed an iterative learning reliable control (ILRC) by combining ILC and reliable control method for batch processes with unknown disturbances and actuator faults. They transformed the batch process to a two-dimensional Fornasini-Marchsini (2D-FM) model and also introduced the relevant concepts of fault-tolerance along two-dimensional (2D) axes. Linear Matrix Inequalities (LMIs) were used to express the sufficient conditions for the proposed fault tolerance. They claimed that the closed-loop convergence is guaranteed along both time and cycle directions even in presence of unknown disturbances and actuator faults as compared to the traditional reliable control.

The proposed closed-loop system has good robust performances to unknown disturbances. They demonstrated the feasibility and effectiveness of the proposed method with the help of a simulated injection velocity control problem. To evaluate the tracking performance, they introduced the following performance index,

$$DT(k) \triangleq \sqrt{\sum_{t=1}^{200} e^2(t,k)} \tag{2.4}$$

The smaller the value of $DT(k)$ the better is the tracking performance in the k^{th} cycle.

Limitations

A linear state space model of a batch process was used to evaluate the proposed methodology. However, batch processes are nonlinear in many cases. However, they argued that the proposed method could also be used for nonlinear batch processes. Developing an iterative learning fault-tolerant control scheme for batch processes that is based on a nonlinear model is still an open problem

ILC of Distributed Parameter Systems based on Geometric Analysis

Zheng et al. (2009) proposed a new nonlinear ILC problem for DPSs based on geometric analysis. They included a complete convergence analysis of the algorithm using special norm. This algorithm could be a corner stone as the common practice of

employing ILC to DPSs are not yet so fruitful and the trend is to use linear ILC algorithms for both linear and nonlinear systems (Xie and Liu, 1998; Xie et al., 1999). Based on geometric analysis method discussed in (Xie et al., 2004; Tian et al., 2004), this group studied the ILC problem of an uncertain linear DPS and proposed a nonlinear ILC algorithm with adaptive factor. They proved the convergence of this new algorithm following the norm defined in Xie et al. (2005). The basic P-type ILC method for obtaining the control sequence $x_{k+1}(z,t)$ is,

$$x_{k+1}(z,t) = x_k(z,t) + \Gamma(t)e_k(z,t) \tag{2.5}$$

where, $e_k(z,t) = y_d(z,t) - y_k(z,t)$. The basic idea behind this method is to eventually make the norm of the vector, i.e. $\|\Gamma(t)e_k(z,t)\|$, corresponding to the sequence $x_{k+1}(z,t)$ smaller, tending to zero. Considering every term in Equation 2.5 as a vector, the following vector chart can be drawn as shown in Figure 2.6.

Limitations

Although they proposed a nonlinear ILC algorithm, they implemented it using a linear DPS example. However, most of the DPS in batch chemical processing are nonlinear in nature. Therefore, there is still a gap of employing it to a real nonlinear system. In addition, they assumed that all the states of system start with the same initial value, which is also not always realistic.

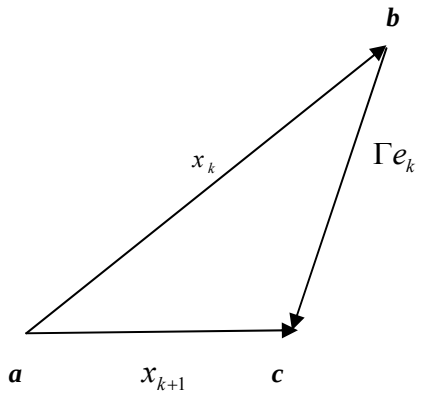


Figure 2.6: Concept of geometric analysis (Zheng et al., 2009).

Neural Network (NN) based ILC

Xiong et al. (2010) proposed a neural network based iterative learning control (NN-ILC) strategy to improve the product qualities in batch processes from batch to batch. Instead of building a model for the system dynamics, they used a single hidden-layer feed-forward neural network (FNN) as nonlinear learning gains in the ILC. As usual, tracking error profile of the previous batch is the input to the network, while the output of the network is the control change profile for the next batch. They proved that a properly trained network could make the tracking error to converge to zero with increasing batch number. Moreover, for handling model uncertainties, the neural network can be retrained during the ILC to renew the learning gain. A batch process can usually be described in the following form,

$$z_k = f(z_k, x_k),\ z_k(0) = z_{k0},$$

$$y_k = g(z_k, x_k) \tag{2.6}$$

In Equation 2.6, z, x, y and subscript k are the same as discussed in the earlier methods, $f(.)$ and $g(.)$ are two nonlinear functions. It is assumed here that the duration of batch run consists of N sampling intervals (i.e. $N = T_f/h$). A discrete-time form of Equation 2.6 using only input and output is shown in a matrix form in Equation 2.7.

$$Y_k = F(X_k) \tag{2.7}$$

here, $F(.)$ is a nonlinear function in a matrix form. For the nonlinear system in Equation 2.7 the Taylor series expansion around control trajectory and output trajectory in the k^{th} batch run is obtained as,

$$Y_{k+1} = F(X_{k+1}) = F(X_k) + \frac{\partial F(X_{k+1})}{\partial X_k}(X_{k+1} - X_k) + \frac{1}{2} \bullet \frac{\partial^2 F(X_{k+1})}{\partial X^2{}_k}(X_{k+1} - X_k)^2 + ...$$

$$= Y_k + F_{k+1}(X_{k+1} - X_k) \tag{2.8}$$

where, $F_{k+1}(.)$ is a nonlinear function of $(X_{k+1} - X_k)$. In this method, they used a nonlinear learning gain rather than using a proportional-type learning gain. Equation 2.8 is rewritten as,

$$X_{k+1} = X_k + L(e_k) \tag{2.9}$$

In Equation 2.9, $e_k = Y_d - Y_k$ is the tracking error and $L(e_k)$ denotes a nonlinear function. The nonlinear learning gains can be determined by neural networks (Ahn et al., 2007). The control policy of the $(k+1)^{th}$ batch run can be generated by the following NN-ILC law of Equation 2.10,

$$X_{k+1} = X_k + NN(Y_d - Y_k) = X_k + NN(e_k) \tag{2.10}$$

Based on the above NN-ILC law in Equation 2.9, the control profile U_{k+1} for the next batch is modified from the control profile of the previous batch U_k. Xiong et al. (2010) evaluated the proposed method successfully using a simulated batch reactor.

Limitations

Usually, abundant historical data are required to train a neural network with sufficient representation capability. However, it is not always realistic to collect a lot of process operation data for agile batch manufacturing processes as the product type changes frequently according to the changes in consumer demands. For that reason, it is highly desirable to develop neural network based methodologies that can be trained with fewer batch runs.

ILC for Spatio-Temporal Dynamics using nD Discrete Linear Systems Models

Cichy et al. (2011) developed an ILC scheme for the spatio-temporal systems described by a linear PDE. They used explicit discretisation approach to approximate the system dynamics resulting in a multidimensional, or nD, discrete linear system based on which the control law was designed. Here, n, the number of directions of information propagation is equal to the total number of indeterminates in the PDE. The resultant control laws were computed using Linear Matrix Inequalities (LMIs).

This work is an improvement over the work of Rogers et al. (2007), who applied this method to discrete linear repetitive processes.

Let us consider the following process model over the fixed time domain $R = \{(k, p) : k = 0,1,\ldots,N; p = 0,1,\ldots,\alpha\text{-}1\}$ to achieve the pre-specified output $y_k^*(p)$,

$$z_{k+1}^l(p) = \sum_{i=-\gamma}^{\gamma} \mathbf{A}(i+\gamma+1) z_k^l(p+i) + \mathbf{B}x_k^l(p),$$
$$y_k^l(p) = \mathbf{C}z_k^l(p) \tag{2.11}$$

In Equation 2.11, z is state vector, x is the vector of control inputs, y is the pass profile vector and subscript k denotes pass itself and α denotes pass length, the superscript l is used to denote the trials and $\mathbf{A}$, $\mathbf{B}$, $\mathbf{C}$ are the coefficient matrices. The tracking error $e_k^l(p)$ over R is $e_k^l(p) \hat{=} y_k^*(p) - y_k^l(p)$ and it is easy to see that,

$$e_{k+1}^{l+1}(p) = e_{k+1}^l(p) - (y_{k+1}^{l+1}(p) - y_{k+1}^l(p)) \tag{2.12}$$

The updating in p can be written as,

$$\eta_{k+1}^{l+1}(p) = \sum_{i=-\gamma}^{\gamma} A(i+\gamma+1)\eta_k^{l+1}(p+i) + B\Delta x_k^{l+1}(p) \tag{2.13}$$

Consider now the control law,

$$\Delta u_k^{l+1}(p) = \sum_{i=-\gamma}^{\gamma} K(i+\gamma+1)\eta_k^{l+1}(p+i) + K_{(2\gamma+2)} e_{k+1}^l(p) \tag{2.14}$$

applying Equation 2.14 to Equation 2.12 and 2.13 the following model is obtained for the controlled dynamics,

$$\eta_{k+1}^{l+1}(p) = \sum_{i=-\gamma}^{\gamma} \mathbf{\Phi}(i+\gamma+1)\eta_k^{l+1}(p+i) + \mathbf{\Gamma}_1 e_{k+1}^l(p),$$

$$e_{k+1}^{l+1}(p) = \sum_{i=-\gamma}^{\gamma} \mathbf{Y}(i+\gamma+1)\eta_k^{l+1}(p+i) + \mathbf{\Gamma}_2 e_{k+1}^l(p) \tag{2.15}$$

where,

$$\mathbf{\Gamma}_1 = BK_{(2\gamma+2)}, \mathbf{\Gamma}_2 = 1 - CBK_{(2\gamma+2)},$$

$$\mathbf{\Phi}_{(i+\gamma+1)} = A_{(i+\gamma+1)} + BK_{(i+\gamma+1)}, \quad \mathbf{Y}_{(i+\gamma+1)} = -C\mathbf{\Phi}_{(i+\gamma+1)} \tag{2.16}$$

for all $i = -\gamma,\ldots,0,\ldots\gamma$. Equation 2.15 represents the dynamics of a discrete 3D linear repetitive system with two non-temporal directions of information propagation p and l (space and the number of trials respectively), and one temporal (k). The subsequent ILC design algorithms can be computed using LMIs. Moreover, the resulting control law has a well defined structure which has attractions in terms of implementation architectures. They successfully evaluated their proposed mechanism using a numerical system defined by parabolic PDE.

Limitations

Obviously more research needs to be done on this method to efficiently produce a more satisfactory discrete model for design and to verify its numerical stability. They have used a numerical example to illustrate the design algorithms instead of an actual solution to a given problem. Other discretisation techniques should also be considered simultaneously with algorithms for pre-specified actuator/sensor configurations such as boundary control. In addition, it is also necessary to develop a robust control theory and supporting design algorithms for nonlinear repetitive processes.

2.5 Polynomial Chaos Expansion (PCE) Based Control

The concept of polynomial chaos was first introduced by Norbert Wiener in 1938 for turbulence modeling (please see Wiener, 1938) and later justified by Cameron and Martin (1947). Polynomial chaos expansion (PCE) can be considered as an addition to Volterra's theory of nonlinear functionals for stochastic systems (Lin et al., 2012). However, after the introduction of PCE in late thirties only relatively recently it is being widely used in different disciplines (Nagy and Braatz, 2010).

PCE have been used as a useful tool that reduced the computational effort required to simulate a stochastic system significantly (Fagiano and Khammash, 2012). Many researchers have applied PCE into various engineering applications subject to stochastic uncertainties, e.g. mechanics, heat convection, fluid dynamics or automatics (modeling and control) problems (Fisher and Bhattacharya, 2009; Thomas and C´edric, 2011). In recent years, the PCE technique has been extended to the generalised polynomial chaos (gPC) framework (Xiu and Karniadakis, 2002; Xiu 2010; Lin and Tartakovsky, 2009; Sepahvand et al., 2010). In fact gPC is the extension of PCE towards a finite number of parametric statistical distributions (e.g. Gamma, Beta, and Uniform).

Other adaptive forms of the PCE includes a multi-element generalised polynomial chaos (ME-gPC) method (Wan and Karniadakis, 2006; Prempraneerach at el., 2010) and a data-driven arbitrary polynomial chaos expansion (aPC) (Oladyshkin and Nowak, 2012). In the ME-gPC method the random space is decomposed into local elements which subsequently implements gPC locally within the individual elements. The proposed aPC offers a constructive and relatively simple tool for uncertainty quantification, global sensitivity analysis, and robust design (Oladyshkin and Nowak, 2012). In their paper Oladyshkin et al. (2011) explained how to apply PCE for robust design in presence of uncertainty with controlled failure probability. Recently, PCE decomposition based sensitivity analysis (Buzzard, 2011; Sandoval et al., 2012) has created much interest among the researchers. Sudret (2008) and Oladyshkin et al. (2012) demonstrated respectively how classical PCE and its aPC version can distribute the information essential for global sensitivity analysis at a lower computational costs.

With the increase of the polynomial's order and the number of parameters, the number of coefficients increases extensively. This makes the computation of the expansion's coefficients a crucial task. Researchers have proposed different approaches to compute coefficients. One of the methods (Xiu and Karniadakis, 2002) utilises Galerkin projection to obtain an augmented set of deterministic differential equations, which are then solved for computing the PCE coefficients. This method was originated from structural mechanics (Ghanem and Spanos, 1991) and studied for

modelling uncertainties in flow problems (Ghanem and Spanos, 1993; Matthies and Keese, 2005). This approach is affected by the limitation of being difficult and time-consuming because it requires deriving the augmented set of differential equations for complex nonlinear models. Moreover the large number of differential equations may be unfeasible to use with standard ODE solvers to produce efficient numerical solution.

For computing the coefficients of the PCE, some researchers have proposed methods that use the principle of collocation, e.g. the probabilistic collocation method (PCM) (Xiu and Hesthaven, 2005; Nagy and Braatz, 2010; 2007; Li and Zhang, 2009) and the regression method with improved sampling (RMIS) (Isukapalli et al., 1998). The basic concept is estimating the coefficients from a finite number of data, i.e. collocation points and these weighted-residual schemes differ only in the way the sampling points are chosen. These approaches can be more viable for the analysis of large-scale, complex stochastic dynamical systems. Probabilistic collocation requires a series of preliminary simulations to collect the data to be used in the coefficients' computation. However, sometimes for problems with relatively high stochastic dimensions and strong nonlinearities the number of collocation points can be very high and makes the coefficient calculations a complicated process (Fagiano and Khammash, 2012). Other proposed methods include non-intrusive sparse quadrature approach proposed by (Keese and Matthies, 2003). Fagiano and Khammash (2012) also proposed a computationally tractable technique that exploits a regularisation technique with a particular choice of weighting matrices and based on convex optimisation.

From the above survey it is clear, PCE is mostly applied for uncertainty analysis in chemical processes (Nagy and Braatz, 2007; Lin et al., 2012). In order to create a model response surface in presents of uncertain model parameters, PCE can be a good choice to represent the system in the form of a high-dimensional polynomial (Oladyshkin and Nowak, 2012). It also enables the inclusion of nonlinear effects in stochastic analysis. The chances and limitations associated with existing PCE techniques were discussed in Augustin et al. (2008). A recent wide survey of the

theoretical background including some practical results of PCE is also available in Templeton (2009).

However, in the research community it is still a new concept and not many works have been done yet. In this research work, a computationally efficient operating data based approach to identify the states and outputs of finite-time control trajectories for nonlinear systems, based on the approximate representation of the full process model via PCE was developed (please see Chapter 7 for details).

2.6 Theory and Practices in Crystallisation Process

Crystallisation is important in the pharmaceutical industry as a separation process for the intermediates and often serves as the final step in the manufacture of active pharmaceutical ingredients (APIs) (Chen et al., 2011). It is responsible for 70% of all solid materials produced by the chemical industry (Giulietti et al., 2001), more than 80% of pharmaceutical products involve at least one crystallisation step in their manufacturing process (Reutzel-Edens, 2006) whilst 90% of the Active Pharmaceutical Ingredients (API's) are found in crystalline form (Choong and Smith, 2004). The control objectives of batch crystallisation processes are defined in terms of product purity, crystal habit or morphology, average particle size, crystal size distribution (CSD), bulk density, product filterability, and dry solids flow properties (Worlitschek and Mazzotti, 2004). CSD is important for efficient downstream operations (i.e. filtration, drying, and formulation) and better product performance (i.e. dissolution rates, bioavailability, and shelf life).

This section describes the fundamentals of pharmaceutical crystallisation processes that include solubility, crystallisation mechanisms, and crystal properties. The existing techniques for characterising crystal properties are briefly reviewed. The conventional approaches for crystallisation operation and control are described. Brief reviews on process analytical technology (PAT), its tools and their application in pharmaceutical crystallisation are also included in this chapter.

2.6.1 Fundamentals and Mechanisms of Crystallisation Processes

Crystallisation is the formation of solid particles by a phase change operation like formation of solid particles from a vapour, solidification of a liquid melt, or the formation of dispersed solids from a solution. Among these, the most common approach is the production of crystals from a solution. This approach involves at least a two component system, a solute and a solvent. Hence, the concepts of solubility, supersaturation and metastable zone width (MSZW) are crucial in developing and characterising the behaviour of crystallisation system.

- *Solubility*

Solubility is the amount of a substance (solute) that can be dissolved in a given amount of solvent at a given temperature and pressure. A saturated solution is defined as the solution that is in equilibrium with excess of the solute present in the solution. Under certain circumstances, a solution can dissolve more solute than defined by the condition of saturation at a particular temperature which is referred to as a supersaturated solution.

Crystalline product properties like polymorphic form, shape and yield are dependent on solubility and supersaturation (Modarresi et al., 2008). Basically the selection of the type of crystallisation process, e.g. cooling or anti-solvent crystallisation is guided by the solubility of the component in selected solvents. The phase relationship between solute and solution helps to understand the mechanisms of solute crystallisation from a solution. A typical phase diagram for a crystallisation process is shown in Figure 2.7.

In Figure 2.7, AB represents the solubility curve that is determined by thermodynamics and is a function of temperature, solvent and impurities present in the system. A solution with composition laying on the equilibrium curve is called saturated; on the other hand, solutions with composition laying below and above the curve are termed as undersaturated and supersaturated respectively. Being in non-equilibrium system, the supersaturated solution tends to reach equilibrium and thereby it removes the solids in the form of nuclei, which then grow into crystals. The

generation of supersaturation is therefore regarded as the first step in the crystallisation process.

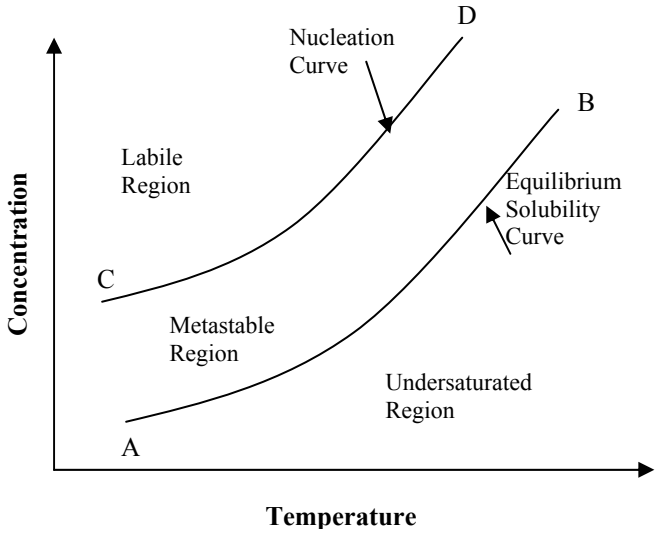


Figure 2.7: Supersaturation in crystallisation processes.

- *Supersaturation*

As mentioned earlier, supersaturation is the driving force for the crystallisation process (Mullin, 2001). It is defined as the difference between the concentration of the solute (C) and the saturation concentration at a particular temperature (C_{sat}) as given by Equation 2.17,

$$S = \Delta C = C - C_{sat} \tag{2.17}$$

with units consistent with the units of the concentrations (e.g. kg solute/kg solvent or kg solute/kg solution). It is essential to control the extent of the supersaturation during crystallisation process since the size, shape, and solid-state properties of the product crystals are decided by the supersaturation profile achieved during the crystallisation process.

- *Nucleation*

When the supersaturation moves far enough from the solubility, eventually a point is reached where the formation of nuclei occurs spontaneously. The nucleation curve is

designated as the line CD in phase diagram in Figure 2.7. The formation of nuclei is an attempt of the system to reach equilibrium. The process of forming nuclei is called nucleation that can be termed as the first step towards the formation of a solid phase (Jones, 2002). The region above the solubility curve where the nucleation starts to occur is called the metastable zone. The width of this metastable zone depends on kinetic variables, such as the rate at which supersaturation was created, the agitator speed, and the presence of impurities (Tititz-Sargut and Ulrich, 2002). Knowledge of the metastable zone width (MSZW) is important in crystallisation because it provides information on nucleation kinetics, so that the nucleation behaviour of a system can be understood (Myerson, 2002).

Nucleation is commonly classified into two types, e.g. primary nucleation and secondary nucleation. However, it can be further divided as shown in Figure 2.8. Primary nucleation is the formation of a solid phase from a clear liquid and it is more prevalent in unseeded crystallisation (Hardenberg et al., 2004). Primary nucleation is further classified as homogeneous and heterogeneous nucleation. Nucleation that occurs spontaneously from a clear pure solution is called homogeneous nucleation, whereas one stimulated by foreign particles or surfaces is called a heterogeneous nucleation (Rawlings et al., 1993).

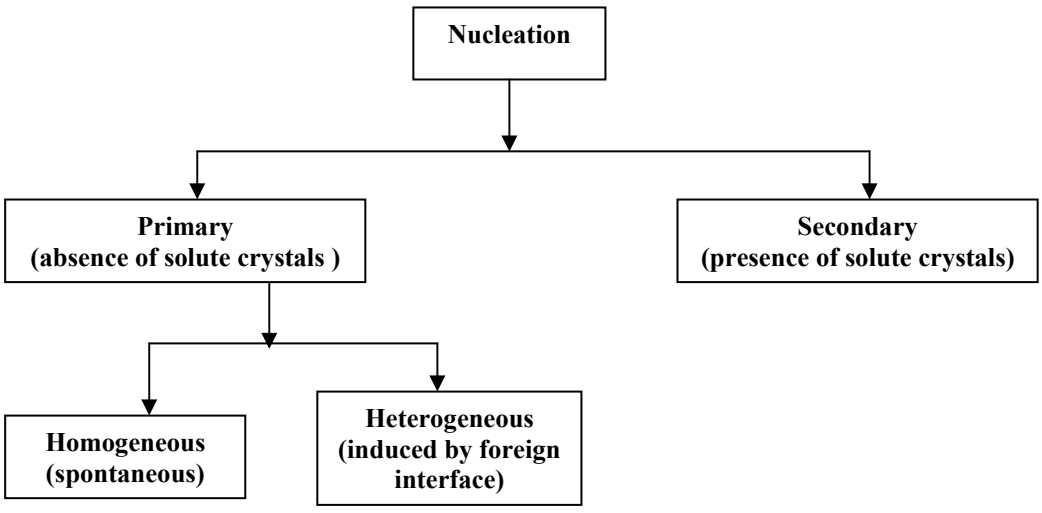


Figure 2.8: Types of nucleation.

Secondary nucleation takes place when a supersaturated solution is in contact with seed crystals of the solute. Sometimes the seeds are either deliberately added, or by

chance present in the system. These seed crystals catalyse the nucleation process and as a result, nucleation takes place at a relatively lower supersaturation than that for the primary nucleation. As a result, the secondary nucleation can be controlled more easily (Rawlings et al., 1993).

Crystal growth

After formation, nuclei grow with time by addition of solute molecules from a supersaturated solution to the crystal surface (Rodriguez-Hornedo and Murphy, 1999). Crystal growth is generally a two-step process. In the first stage, mass transfer involves the diffusion of solute molecules from the bulk liquid through the solution boundary layer adjacent to the crystal surface. In the next stage, the adsorbed solute molecules at the crystal surface are then integrated into the crystal lattice by surface reaction. However, several researchers have added heat transfer as the third step that occurs in parallel with the other two steps (Hixson and Knox, 1951).

Aggregation

The next significant phenomenon in the crystallisation process is aggregation. It is the particle size enlargement process by which fines are joined together in an assembly. Therefore, the particle characteristics obtained in the product depend on the mechanism of aggregation as well. Researchers and scientists have extensively studied and modelled the aggregation processes (Yu et al., 2005).

Dissolution

Crystal dissolution cannot be defined exactly as the reverse process of the crystal growth because dissolution does not require the surface integration step; rather it is completely controlled by the solute diffusion. Crystal dissolution rate is of first order with respect to supersaturation and the dissolution occurs at all levels of undersaturation (Mullin and Gaska, 1969). The coefficient for the dissolution rate is a function of the diffusion coefficient, crystal size, and local hydrodynamics.

Breakage and Attrition

Particle breakage initiates the formation of new smaller particles of varying sizes. The breakage occurs due to different types of collisions like particle-particle collisions, collisions of particles with the walls of the container, inserted probes, and impeller. When a crystal is fractured into two or more pieces it is called breakage, whereas attrition is the fracture of a crystal into many small fragments. Therefore, these phenomena can impose a strong impact on the CSD and the median crystal size (Qu, 2007). Breakage processes have also got significant attention by the researchers and gone through intense analysis by (Soos et al., 2006).

2.6.2 Measurement Techniques for State Variables

Generally, three types of measurement techniques are required for batch chemical processes these are,

1. *On-line measurements* to provide information during the course of the batch.
2. *In situ measurements* to get measurements made directly in the process medium.
3. *Off-line measurements* to characterise the properties based on the after batch analysis of samples taken from the process.

The common practice is to gather enough data during the experiments to provide sufficient information about the system under investigation. As crystallisation involves both solid and solution phases, information about both phases are crucial. The information about the solution phase is provided by solution temperature, concentration and supersaturation, while crystal size distribution provides information about the dispersed solid phase.

A wide variety of experimental techniques are devised for the parameter estimation of crystallisation processes. However, in most of the practical circumstances, not all variables can be reliably measured. The conventional approach is to estimate those unmeasured variables in terms of other available measurements and the model, using state estimators or observers (Motz and Gilles, 2008). The following subsection discusses in brief the different techniques for measuring the state variables.

Temperature measurement

Thermocouples are most commonly used to measure temperature. Factors that affect the selection of thermocouple are; temperature range, medium, required response time, and accuracy. Generally, the temperatures of the slurry, inlet and outlet jacket temperatures are measured using PT-100 thermocouples. These thermocouples have quick response time with accuracy within ± 0.15 °C.

Concentration/supersaturation measurement

During supersaturation control (SSC), in order to maintain the supersaturation setpoint (S_{sp}) curve in the phase diagram the controller needs to measure the concentration of the system. Some common conventional ways to measure the concentration of the solute in the continuous phase are briefly described next.

- *Conductivity*

For conducting solutions, such as salts, the solute concentration can be measured using conductivity probes. The technique has been demonstrated in the case of crystallisation of inorganic salts by Nyvlt et al. (1994).

- *Refractive index*

Since refractive index is well correlated to the concentration of many solutions (Zhou et al., 2006), this is sometimes used to measure solution concentration. However, the technique can work if there is a significant change in refractive index with change in concentration.

- *Spectroscopy*

Modern equipments like Attenuated Total Reflectance (ATR), Fourier Transform Infrared (FTIR), and ultra-violet–visible (UV-Vis) spectrometers can be used to track the changes in the concentration with time (Fujiwara et al., 2002) (see section 2.5.4 for details). In recent years, the applications of spectroscopic techniques have

increased (Liotta and Sabesan, 2004; Yu et al., 2006) especially to measure the concentration of multiple dissolved species.

- *Density*

Another way to measure the change in concentration is to measure the change in density. The technique has also been used on-line for potassium nitrate-water system (Miller and Rawlings, 1994).

Crystal size distribution (CSD) measurement

CSD provides information about the solid phase. CSD can be measured by a series of methods described as follows.

- *Sieve analysis*

Sieve analysis offers an inexpensive, simple and portable approach that is the most commonly used method for measuring particle size in the range of 10 μm to 5500 μm. However, sieving is time consuming and should be applied offline (Adi et al., 2007).

- *Laser diffraction*

The particles passing through a laser beam scatter light at an angle that is directly related to their size. As a result, large particles scatter light at narrow angles with high intensity; on the other hand, small particles scatter at wider angles with low intensity. Equipments, such as the Malvern Mastersizer and Malvern Insitic are based on this principle of laser diffraction. Malvern Mastersizer can be used both on-line and offline to measure a size range of 0.01μm to 1000 μm.

- *Laser backscattering*

Laser backscattering involves an alternative light scattering approach that is used to focus a laser beam forward through a window in a probe tip, and collect the laser light scattered back to the probe. It facilitates on-line measurement of the particle size distribution (PSD). The Lasentec Focused Beam Reflectance Measurement (FBRM)

instrument works on the laser backscattering method. The equipment is able to measure size in the range of approximately 0.5 μm to 1000 μm.

- *Image analysis*

Image analysis is the simplest direct technique to monitor the crystal size and shape in crystallisation processes that does not require any assumptions for the size or shape of the crystals. Two dimensional information are obtained in situ from the Lasentec Particle Vision Measurement (PVM) system that provides pictures of the crystals in the solution using a probe inserted directly into the dense crystal slurry (Barrett and Glennon, 2002). This video microscope can take 10-30 pictures per second and capable to measure crystals as small as 1-15 μm. PVM is more suitable for using in industrial crystallisers (Braatz, 2002);

Details of the modern tools and technologies that are used for operation, control, and measurement of crystallisation system have been discussed in subsection 2.6.4.

2.6.3 Crystallisation Operation and Control

Crystallisation can either be operated in a batch, semi-batch or continuous mode. However, batch operation is more frequently used for pharmaceutical crystallisation since their production rates are generally small and loss of the expensive materials should be kept at minimum (Myerson, 2002). In addition, the operation offers the flexibility of execution with changing recipes (Costa and Filho, 2005). Batch or semi-batch crystallisers are used to form pharmaceutical crystals by reducing the solubility of the solute in the solution and creating sufficient supersaturation. The solubility is usually reduced by different techniques depending on the properties of the material. The common methods are cooling the solution, removing the solvent (evaporation), addition of an anti-solvent (drowning out), reactive crystallisation (precipitation), and adjusting the solution pH (isoelectric precipitation). However, freeze crystallisation is also sometimes useful for those APIs that exhibit poor stability in solution (Connolly et al., 1996). The type of crystallisation operation that will be studied in this research work is cooling crystallisation.

Cooling crystallisation

The most economical means of crystallisation is cooling crystallisation, which can be applied if the temperature sensitivity of the solute is large enough (Rohani, 2010). There are several cooling policies, e.g. natural cooling, linear cooling, and controlled cooling. In natural cooling constant temperature coolant is used to cool the crystalliser contents resulting in a rapid temperature drop in the beginning of the batch run. Despite being simple, this uncontrolled cooling cannot provide good final product quality because in the early stage the supersaturation profile passes through a high peak (Tavare, 1995). In linear cooling, temperature decreases at a constant rate. The supersaturation profile shows a maximum relatively early in the batch run and hence results in copious nucleation (Jagadesh et al., 1996). This can lead to a poor quality product, with a small mean size and a wide CSD (Yang, 2005).

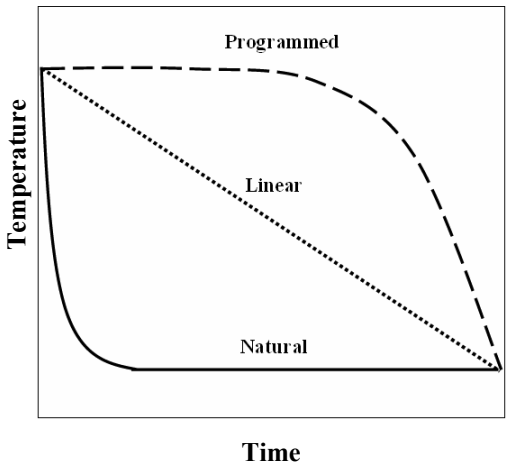


Figure 2.9: Typical profiles of natural, linear, and programmed cooling operations.

In controlled cooling, depending on the availability of accurate on-line data, either the crystalliser temperature is controlled to follow a reference trajectory or the solute concentration is controlled to follow a supersaturation profile in a feedback loop. These two approaches are known as T-control and C-control strategy respectively in literature (Fujiwara et al., 2005). T- control has the inability to reproduce results from one batch to the other since temperature is not closely related to the crystallisation dynamics. On the other hand, though supersaturation has direct influence on crystallisation process, the need for high accuracy of concentration measurement makes C-control unfeasible in industrial scale (Forgione et al., 2012). In addition, the

absence of in situ adjustments made during the process, these approaches cannot respond to unexpected disturbances (e.g. a temperature spike, mixing disturbance) resulting in a failed batch (Yu et al., 2003).

Cooling crystallisation is advantageous in the sense that it does not require additional raw material during operation which could affect the product purity and thereby increase operating and capital costs (Nagy et al., 2006). Figure 2.9 shows the difference in the profiles of the natural, linear, and the programmed cooling curves. The following section included a brief discussion about different control strategies for cooling crystallisation.

Model-based approach

The model-based approach is often referred to as the first-principle approach (Braatz, 2002) that is a theoretical prediction of the cooling profile to fulfill different control targets. The control targets can be either to maintain a constant supersaturation profile during operation, or to achieve the desired crystal properties using optimisation methods (Yang, 2005). When the control targets of the crystallisation process are defined in terms of desired properties of crystals at the end of the batch, the operating temperature profiles are usually based on a priori knowledge of nucleation and growth kinetics as a function of supersaturation. Therefore, the key of model based control is to develop an accurate kinetic model of the system in order to obtain the correct optimal cooling profile (Choong and Smith, 2004); Optimal cooling has been extensively studied by the researchers during the last four decades (Jones, 1974; Miller and Rawlings, 1994; Shen et al., 1999). Several approaches have been proposed by researchers to develop the kinetic models. Rawlings et al. (1993) proposed non-linear optimisation approaches to estimate the parameters in the kinetic models. In addition to the effects of the potential deviations from the model assumptions, Nagy and Braatz (2004) pointed out that the effects of parameter uncertainties and disturbances also have to be taken into consideration to ensure that the model-based approach produces the expected optimised product quality. From Miller and Rawlings (1994), Zhang and Rohani (2003) to Mohameed et al. (2003) are among many other research groups that used the approach to develop the cooling profiles. Although efficient, this kind of model based techniques and the resulting

performances are often susceptible to the accuracy of the model (Nagy et al., 2008b) and Chew et al. (2007a) pointed out that the substantial expertise required in process modelling and optimisation has restricted its application to small-scale laboratory studies.

Direct design approach

As mentioned above due to the complex nature of the model based approaches, now a day researchers are more prone to shift the research paradigm from an art towards a better understood scientific process. In addition the availability of PAT tools (described in Section 2.6.4) for measuring concentration and various solid state properties of crystals offers down to earth solutions of the crystallisation control approaches. These control strategies, which are also known as model-free or direct design approaches, use feedback control based on information provided by in situ sensors (Zhao et al., 2007). A major characteristic of these approaches is that no information about process kinetics is required. This is a prime advantage as multiple phenomena take place during crystallisation, for which the parameters estimation and modelling becomes very difficult. Its difference with the model-based approach is that instead of optimising a certain objective function, the direct design approach is aimed to avoid secondary nucleation to maximise crystal growth.

The direct design approach is typically based on concentration control or supersaturation control where the system follows an adaptable supersaturation setpoint within the metastable zone to obtain crystals of desired size distribution. The direct design approach has been successfully used for enhancing the crystalline product quality in many applications. Zhou et al. (2006) used this approach based on ATR-FTIR for antisolvent crystallisation of a proprietary pharmaceutical compound. They demonstrated that the approach provides rapid determination of an optimal recipe for suppressing secondary nucleation and enhancing crystal growth. Liotta and Sabesan (2004) reported significant improvement in crystal size when supersaturation control was applied for cooling crystallisation of a drug compound. Kee et al. (2009) showed how the direct design approach can be used for production of the α-form of L-glutamic acid, by using ATR-FTIR based supersaturation control.

2.6.4 Process Analytical Technology (PAT) in Crystallisation Operation

2.6.4.1 Basic concepts of PAT

In August 2002, recognising the need to eliminate the hesitancy of pharmaceutical industries to innovate, the US Food and Drug Administration (FDA) launched a new initiative entitled "Pharmaceutical CGMPs for the 21st Century: A Risk-Based Approach." This is also known as process analytical technology (PAT) initiative which is defined as, "*a system for designing, analyzing, and controlling manufacturing through timely measurements (i.e. during processing) of critical quality and performance attributes of raw and in-process materials and processes, with the goal of ensuring final product quality*" (FDA, 2004). The main goals were to promote the use of modern sensor technologies, facilitating real-time monitoring, and better control concepts to achieve reduction in process time and cost, decrease variability, improve product quality, and minimise batch failures (Yu et al., 2003). The overall PAT scheme is shown in Figure 2.10.

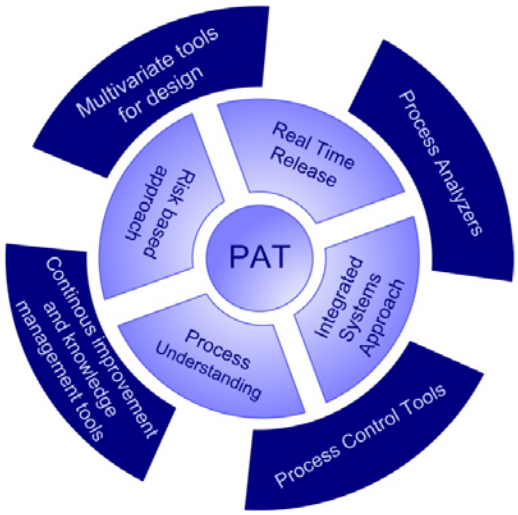


Figure 2.10: Scheme of process analytical technology (PAT) (Valero, 2013).

Conventionally, pharmaceutical industries managed to analyse the finished products' quality in the laboratory after the production. This approach is called Quality by Testing (QbT) that requires a continuous process optimisation along with higher risk of producing failed batches (Yu, 2008). Therefore, the concept of Quality by Design

(QbD) was introduced to aid the pharmaceutical industries to have a more efficient manufacturing system. The goal of PAT is harmonic with that of QbD "*quality cannot be tested into products; it should be built in by design*" (FDA, 2004). In fact, PAT can be considered as a tool or system that helps in the implementation of QbD. The word "analytical" in PAT comprises physical, chemical, microbiological, as well as statistical analysis conducted in an integrated approach (Yu et al., 2003).PAT is able to provide important information about different processes at various stages of the drug development. In crystallisation processes PAT is used to measure and monitor solubility, MSZW, supersaturation, concentration, formation of polymorphic forms, hydrates, solvates, and CSD as well as crystallisation process scale up. In the following section applications, advantages and disadvantages of the most common PAT tools have been discussed.

2.6.4.2 Overview of PAT tools and applications in crystallisation control

ATR-UV/Vis Spectroscopy

A relatively new technique for in situ analysis of measuring liquid phase concentration is the use of UV/Vis spectroscopy. The availability of UV resistant optical fibres, cheap diode array detectors, and chemometrics has facilitated its inline/online applications in many fields. However, the application of UV/Vis spectroscopy is limited as most of the compounds or functional groups are transparent in the UV/Vis spectroscopy range, i.e. 190 nm to 800 nm (Bakeev, 2005). Absorbance is correlated with the concentration of a compound according to the Beer-Lambert's law,

$$A = \log\left(\frac{I_o}{I}\right) = \varepsilon c l \tag{2.18}$$

where A is the absorbance, I_o is the incident light intensity, I is intensity of light leaving, c is the molar concentration of the solute, l is the path length in cm, and ε is the molar absorptivity. According to this law, absorbance is linearly dependent on concentration on the occasion of the molar absorptivity and path length remain constant. Absorbance depends on the temperature too. In addition, the presence of several absorbing species, interaction between solute and solvent can sometimes

cause deviations from this law. The instrumentation commonly used for UV/Vis are classified into the following four types (Cazes, 2005),

- Scanning instruments
- Diode-array instruments
- Photometers
- Fibre-optic diode array and CCD instruments

The first two are more suitable for off-line measurements and the later two are more suitable for in situ analysis.

The attenuated total reflection (ATR) probe functions by utilising the difference in refractive indices of the ATR crystal and that of the solution. Whilst ATR probes are most commonly used in conjunction with Fourier transform infrared spectroscopy (FTIR) only few studies are available that actually demonstrated the use of ATR-UV/Vis spectroscopy in crystallisation. The first application of ATR-UV/Vis spectroscopy for monitoring the crystallisation of sulfathiazole was reported by Anderson et al. (2001). Thompson et al. (2005) also used ATR-UV/Vis spectroscopy for in situ concentration measurements of a drug candidate and developed calibration model using partial least squares regression (PLSR).

ATR-Fourier Transform Infrared Spectroscopy (ATR-FTIR)

ATR-FTIR is a form of vibrational spectroscopy and probably one of the most widely used techniques in pharmaceutical crystallisation (Togkalidou et al., 2001). The IR region covers the spectral range from 4000 cm^{-1} to 400 cm^{-1} (2.5 μm to 25 μm) which is also bounded by near infrared and far infrared regions as well. The most prominent feature of using IR is the determination of the structure of the molecules. The spectrum generated is a fingerprint of a particular molecule indeed. The frequency at which IR energy is absorbed is a characteristic of a molecule, this fact can be used to identify a compound and hence the term fingerprint is used. The fact that IR absorptivities can occur in CH, OH and NH groups that are in any way prevalent in organic molecule, made IR the most extensively practiced approach in pharmaceutical crystallisation. The combination of IR spectrometers with ATR probe have facilitated

real time monitoring and control of crystallisation. Example applications include determination of metastable zone width, concentration measurement (Wang and Berglund, 2000), supersaturation control, detection of impurities, etc.

Near Infrared Spectroscopy (NIR)

Near infrared (NIR) spectroscopy represents another type of vibrational spectroscopy along with Raman and IR. NIR covers the range of 4000 cm^{-1} to 12500 cm^{-1} in the electromagnetic spectrum. The intensity of the NIR bands being weaker than the corresponding fundamental bands it eliminates the necessity of diluting the sample. Moreover, it allows the measurement of thick samples. The penetration depth of NIR beam is up to a few millimeters, which is particularly useful in the analysis of bigger sample volumes.

Raman Spectroscopy

Raman spectroscopy also belongs to the vibrational spectroscopy group along with IR and NIR. Its approximate spectral range is between 50 cm^{-1} to 4000 cm^{-1}. Raman spectrum is due to a change in the polarisability of the molecule. The key characteristic of Raman spectroscopy is that the wavelength of the scattered light changes according to the vibrational energy levels of the molecules. This fact is used to categorise the state and nature of bonds present in a molecule.

Raman spectroscopy is a powerful nondestructive technique for both qualitative and quantitative analysis. It can be applied during different stages of drug manufacturing. Being based on vibration energy changes, Raman spectroscopy is able to distinguish almost all the crystal forms. This feature is useful for characterising different forms of a pharmaceutical compound, i.e. polymorphic forms, hydrates and solvates. Raman spectroscopy requires small quantity of sample which is in favor of the pharmaceutical compounds prepared in small amounts during the early stages of development. In addition, it does not require special sample preparation hence prevents compounds from changing during sample preparation (Vergote et al., 2004).

Focused Beam Reflectance Measurement (FBRM)

FBEM provides the chord length distributions (CLD) of the crystal size. Using FBRM coupled with inverse geometric modelling the CLD can be converted into size distribution (Hukkanen and Braatz, 2003). The equipment is able to measure particle size in the range of approximately 0.5 μm to 1000 μm. FBRM is a commonly used in situ technique for obtaining information about nucleation, dissolution, metastable zone width, polymorphic transformation, growth, and size distribution in particulate systems in real time (Barthe et al., 2008; Howard et al., 2009; Abu Bakar et al., 2009). The probe is usually inserted in a crystalliser to provide real time information about the system. The laser beam used to scan a particular region is highly focused. The beam is projected through the sapphire window of the probe. This speed of the rotation of the beam is 2-6 ms^{-1} (Pons et al., 2006) and continuously scan the particles on which it is being focused. An optical receiver receives the back scattered reflected beam. The focused beam crosses the particles on a straight line between any two points on the edge of that particle. FBRM measured the CLD through 90 channels ranging from 0.8 μm to 1000 μm can be related to different phenomena, such as nucleation, growth, agglomeration, and attrition (Yu et al., 2007). The data obtained from FBRM can be interpreted in several formats from simple total number of counts per second to square weighted or length weighted mean chord length as defined in Equation 2.19 and Equation 2.20 respectively,

$$\text{Square Weighted Mean Chord Length} = \text{SWMCL} = \frac{\sum_{i=1}^{k} \mathrm{n}_i M_i^3}{\sum_{i=1}^{k} \mathrm{n}_i M_i^2} \tag{2.19}$$

$$\text{Length Weighted Mean Chord Length} = \text{LWMCL} = \frac{\sum_{i=1}^{k} \mathrm{n}_i M_i^2}{\sum_{i=1}^{k} \mathrm{n}_i M_i^1} \tag{2.20}$$

where, k is the number of channels in FBRM, n_i is the counts in an individual measurement channel and M_i is the midpoint of an individual channel. FBRM can be used for measuring solubility, detecting nucleation and MSZW determination (Barett

et al., 2002), controlling CSD, monitoring crystal growth, nucleation (Barrett et al., 2005) and agglomeration detection (Loan et al., 2002).

The above mentioned in situ techniques provide real time information about the liquid and solid phases. However, these tools are often accompanied by other off-line analysis techniques for a more complete assessment and characterisation of crystalline products (Howard et al., 2009**).** Some of the other commonly used techniques which are applied for monitoring crystallisation systems are briefly described below.

Particle vision measurement (PVM) probe provides in situ information about changes in crystal shape and morphology, and typically used as a complementary technique alongside FBRM and other spectroscopic tools. Another alternative and cheap technique is bulk video imaging (BVI), along with image analysis it also provides important information about crystallisation such as MSZW, solubility etc. Turbidimetry is another type of monitoring tool that usually measures the changes in optical properties of the solution. Turbidimetry can be used for the detection of nucleation or dissolution events during crystallisation operations.

2.6.5 Chemometrics

PAT implementation eliminates the drawbacks of traditional methods that involve excessive sampling and it also facilitates rapid testing through direct sampling without any destruction of sample. However, to adapt PAT tools successfully into pharmaceutical and biopharmaceutical environment, thorough understanding of the process is needed along with mathematical and statistical tools to analyse large multidimensional spectral data generated by PAT tools. Chemometrics is a chemical discipline which incorporates both statistical and mathematical methods to obtain and analyse relevant information from PAT tools (Challa and Potumarthi, 2013). Yu et al., (2003) defined chemometrics, as the science of relating measurements and analysis made on a system or process to the state of the system through the application of mathematical or statistical methods. It is very helpful in the interpretation of the multivariate data generated by in-situ process monitoring devices (Yu et al., 2003). Chemometrics is used for multivariate data collection and analysis protocols,

calibration, process modeling, pattern recognition and classification, signal correction and compression, and statistical process control (Workman Jr., 2005).

2.7 Conclusions

In this chapter the concept of distributed parameter systems, e.g. batch processes, the associated control objectives and challenges were addressed. The existing control practices, i.e. model predictive control and data based control were pointed out. Since the main focus of the work is to develop operating data based iterative learning control (ILC) for batch chemical processes. This chapter introduced the concept of iterative learning control (ILC) and critically analysed the available ILC strategies in the field of batch chemical processing. Details of fundamental and mechanisms of batch crystallisation, its associated control practices are also discussed in brief. Batch crystallisation will be considered as an example case for this study. Last but not the least, the advent of process analytical technology (PAT), commencement of quality by design (QBD), applications of various PAT tools in pharmaceutical crystallisation have also been discussed in brief. The next chapter describes the ILC based methodology developed to be used in simulation studies.

Chapter 3

Development of Linear Time Varying (LTV) Perturbation Model Based Iterative Learning Control (ILC)

3.1 Overview

Development of a first principle model is usually very complicated and difficult to obtain for industrial batch process (Xiong et al., 2010). In addition, due to the limited availability of robust on-line sensors in the industrial practice of batch process operations, typically only off-line quality measurements are available. Under these circumstances, it is more useful and convenient to develop and practice operating data based control strategies. In this chapter a data based control methodology is introduced based on the work of Xiong and Zhang (2003). The linear time varying (LTV) perturbation methodology developed for iterative learning control (lLC) has been evaluated through simulation case studies.

3.2 Methodology Development

In order to deal with the problem of nonlinearities in batch processes, it is a common practice to use the perturbation variables instead of using the actual process variables. Perturbation variables are deviations of variables from their nominal trajectories. Typically the input/output trajectories in batch processes are inherently nonlinear and time varying. However, the concept of subtracting the time-varying nominal trajectories from the batch operation trajectories for removing process nonlinearity is tempting which enables conventional linear modeling methods to be applied (Russell et al., 1998). So, a linear perturbation model obtained by linearising a nonlinear model along the nominal trajectories can be used in ILC scheme for tracking control of product quality.

Initially the analysis followed the methodology applied/recommended in Xiong and Zhang (2003), which is an ILC scheme based on linear time varying (LTV) perturbation models. If we consider the following nonlinear function between input $\mathbf{X}_b(t)$ and output $\mathbf{Y}_b(t)$ in the matrix form as in Equation 3.1.

$$\mathbf{Y}_b = \boldsymbol{\Psi}(\mathbf{X}_b) + \mathbf{n}_b \tag{3.1}$$

where, $\boldsymbol{\psi}(\bullet)$ is the nonlinear static function between the input and output and $\mathbf{n}_b$ is the vector of measurement noise at time t. For the system in Equation 3.1, an LTV perturbation model $\mathbf{L}_s$ is developed by linearising the nonlinear model along the nominal trajectories. At first, several sets of historical process operating data are collected and the input - output data matrices are defined as, $\boldsymbol{\Omega}_x^0 = [\mathbf{X}_1, \mathbf{X}_2, ..., \mathbf{X}_H]^T$ and $\boldsymbol{\Omega}_y^0 = [\mathbf{Y}_1, \mathbf{Y}_2, ..., \mathbf{Y}_H]^T$ respectively, here, H is the number of historical batches. From the historical data sets, the best performing trajectories are selected as the nominal trajectories $(\mathbf{X}_s, \mathbf{Y}_s)$. At any time t, the perturbation variables for b^{th} batch are calculated as $\overline{\mathbf{X}}_b = \mathbf{X}_b - \mathbf{X}_s$ and $\overline{\mathbf{Y}}_b = \mathbf{Y}_b - \mathbf{Y}_s$. Linearising the nonlinear model of Equation 3.1 around the nominal trajectories gives the following expression (Xiong and Zhang, 2003).

$$\mathbf{Y}_b = \mathbf{Y}_s + \frac{\partial \boldsymbol{\Psi}(\mathbf{X}_b)}{\partial \mathbf{X}_b}\Big|_{\mathbf{X}_s} (\mathbf{X}_b - \mathbf{X}_s) + \mathbf{m}_b + \mathbf{n}_b \tag{3.2}$$

Where, $\mathbf{m}_b = [m_b^T(1), m_b^T(2), ..., m_b^T(N)]^T$ is the sequence of model errors of N observations due to linearisation. However, the linearised time varying perturbation model and the corresponding absolute model prediction are shown in Equation 3.3a and Equation 3.3b respectively.

$$\overline{\mathbf{Y}}_b = \mathbf{L}_s \overline{\mathbf{X}}_b + \mathbf{d}_b \tag{3.3a}$$

$$\hat{\mathbf{Y}}_b = \mathbf{Y}_s + \hat{\mathbf{L}}_s \overline{\mathbf{X}}_b \tag{3.3b}$$

The tracking errors of the actual process and of the predicted perturbation model are $\mathbf{e}_b = \mathbf{Y}_d - \mathbf{Y}_b$ and $\hat{\mathbf{e}}_b = \mathbf{Y}_d - \hat{\mathbf{Y}}_b$ respectively. The transfer function $\hat{\mathbf{L}}_s$ is predicted

according to the steps of Equation 3.4 and Equation 3.5, for $i = 1,2,...,N$, number of observations per batch and $h = 1,2,...,H$, the number of historical batches,

$$\bar{y}_h(i) = y_h(i) - y_s(i),\ \bar{x}_h(i) = x_h(i) - x_s(i), \text{ and } \mathbf{u}_h(i) = [\bar{x}_1(i), \bar{x}_2(i), ..., \bar{x}_{h-1}(i), \bar{x}_h(i)]^T \tag{3.4}$$

if we define,

$$\mathbf{V}_0^i = \begin{bmatrix} \bar{y}_1^T(i) \\ \bar{y}_2^T(i) \\ \vdots \\ \bar{y}_H^T(i) \end{bmatrix} \text{ and } \mathbf{U}_0^i = \begin{bmatrix} \mathbf{u}_1^T(i) \\ \mathbf{u}_2^T(i) \\ \vdots \\ \mathbf{u}_H^T(i) \end{bmatrix} \tag{3.5}$$

then, using Equation 3.5, $\hat{l}_i$ is estimated by the least square method as, $\hat{l}_i = (\mathbf{U}_0{}^{i\mathrm{T}}\mathbf{U}_0{}^{i})^{-1}\mathbf{U}_0{}^{i\mathrm{T}}\mathbf{V}_0{}^{i}$ and $\hat{\mathbf{L}}_s$ are obtained as in Equation 3.6,

$$\hat{\mathbf{L}}_s = [\hat{l}_1, \hat{l}_2, ..., \hat{l}_N]^T \tag{3.6}$$

After the completion of the b^{th} batch, prediction errors between off-line measured or analysed product qualities and their model predictions can be calculated as, $\boldsymbol{\varepsilon}_b = \mathbf{Y}_b - \hat{\mathbf{Y}}_b$. The absolute modified model prediction is defined as, $\tilde{\mathbf{Y}}_{b+1} = \hat{\mathbf{Y}}_{b+1} + \boldsymbol{\varepsilon}_b$. The tracking error of the modified prediction of the perturbation model is defined as, $\tilde{\mathbf{e}}_b = \mathbf{Y}_d - \tilde{\mathbf{Y}}_b$. In ILC, it is desired that the learning algorithm should have the following property,

$$\lim_{b \to \infty} \|\mathbf{e}_b\|^2 \to \min_{\mathbf{X}} \|\mathbf{e}\|^2 \tag{3.8}$$

Finally, the following quadratic objective function of Equation 3.9 is formulated based on the minimisation of the predicted tracking errors,

$$J_{b+1} = \min_{\Delta \mathbf{X}_{b+1}} \frac{1}{2} [\tilde{\mathbf{e}}_{b+1}{}^{\mathrm{T}} \mathbf{O} \tilde{\mathbf{e}}_{b+1} + \Delta \bar{\mathbf{X}}_{b+1}{}^{\mathrm{T}} \mathbf{P} \Delta \bar{\mathbf{X}}_{b+1}] \tag{3.9}$$

where, $\mathbf{O}$ and $\mathbf{P}$ are weighting matrices based on output performance and input change, respectively. Since the weighting matrices influence the convergence rates they should be chosen carefully. Larger $\mathbf{P}$ imposes larger penalty on input changes implying slower convergence. The weight $\mathbf{O}$ should be chosen relative to $\mathbf{P}$ such that the performance due to input changes will not be degraded (Xiong and Zhang, 2005). This objective function of Equation 3.9 should be solved upon completion of the b^{th}

batch to update the input trajectory for the $(b+1)^{\text{th}}$ batch as, $\mathbf{X}_{b+1} = \mathbf{X}_b + \hat{\mathbf{K}}_b \mathbf{e}_b$, where, $\hat{\mathbf{K}}_b = [\hat{\mathbf{L}}_s^{\mathrm{T}} \mathbf{O} \hat{\mathbf{L}}_s + \mathbf{P}]^{-1} \hat{\mathbf{L}}_s^{\mathrm{T}} \mathbf{O}$, is the calculated control action. According to the ILC algorithm, after the completion of each iteration the new data is added to the historical data set to update $\hat{\mathbf{L}}_s$. While updating $\hat{\mathbf{L}}_s$, in order to emphasise the most recent batches, a forgetting factor $\beta \leq 1$ is multiplied with historical data in decreasing order (i.e. from β^{h+b-1} to β^1). The algorithm is shown in Figure 3.1.

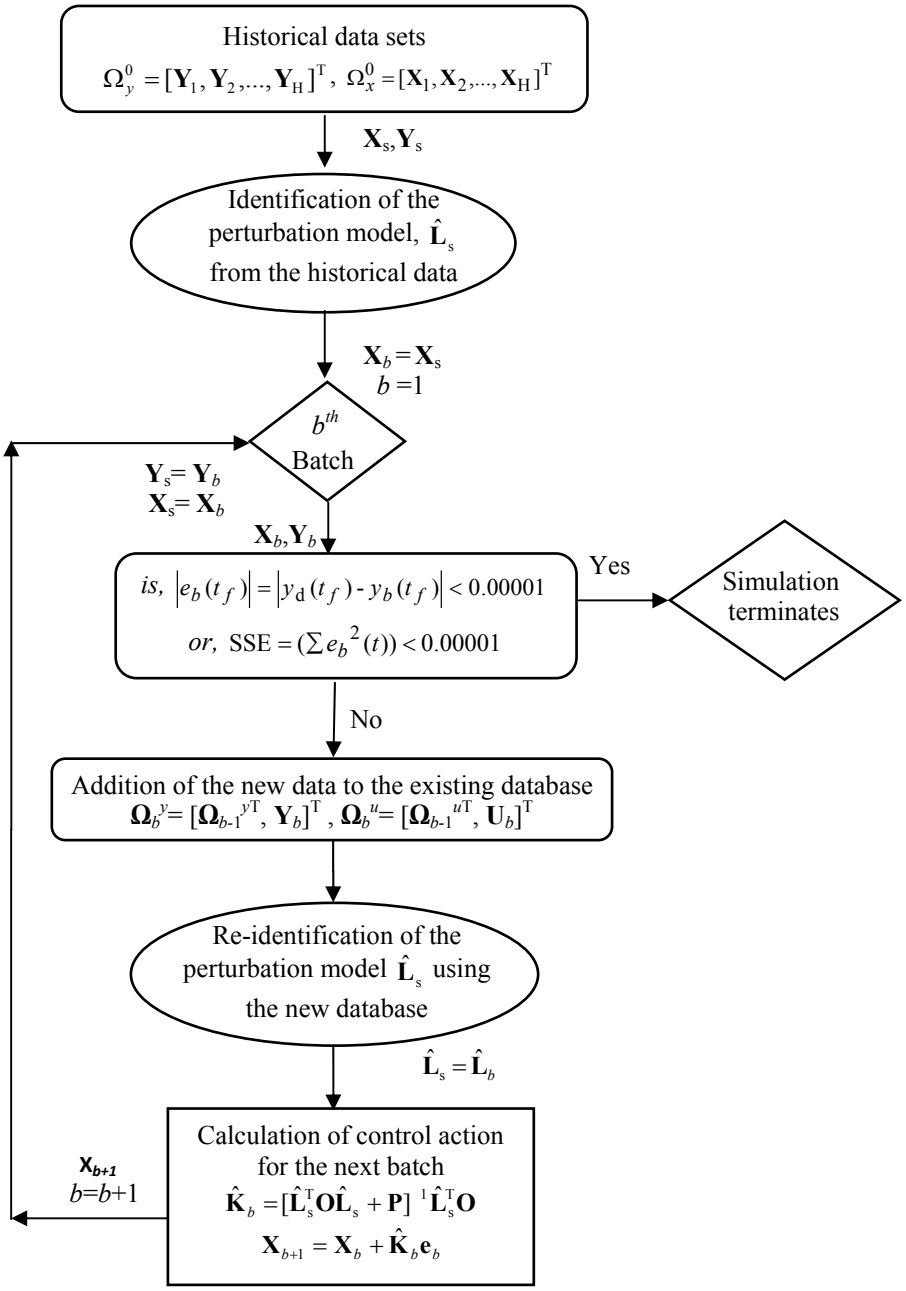


Figure 3.1: Algorithm of the LTV perturbation models based on ILC scheme.

3.3 Results and Discussions

3.3.1 Case Study 1: Typical Batch Reactor

In this case study a typical nonlinear batch reactor is considered where temperature is the control variable (Ray, 1981; Logsdon and Biegler, 1989). The objective of the control problem is to maximize the intermediate product (B) after a certain reaction time. The reaction scheme is shown in Equation 3.10.

$$\mathrm{A} \xrightarrow{k_1} \mathrm{B} \xrightarrow{k_2} \mathrm{C} \tag{3.10}$$

The rate equations describing the batch process are,

$$\frac{\mathrm{d}c_1}{\mathrm{d}t} = k_1 \exp(-E_1 / vT_{\mathrm{ref}}) c_1^2 \tag{3.11}$$

$$\frac{\mathrm{d}c_2}{\mathrm{d}t} = k_1 \exp(-E_1 / vT_{\mathrm{ref}}) c_1^2 - k_2 \exp(-E_2 / vT_{\mathrm{ref}}) c_2 \tag{3.12}$$

where, c_1 and c_2 represent the dimensionless concentrations of A and B, respectively; $v = T / T_{\mathrm{ref}}$ is the dimensionless temperature of the reactor; and T_{ref} is the reference temperature. The final time t_f is fixed to be 1 hr, and values of k_1, k_2, E_1, and E_2, are given in Table 3.1.

Table 3.1: Parameter Values for the Batch Reactor (Ray, 1981)

Parameter	Values
k_1	4.0×10^3
k_2	6.2×10^3
E_1	2.5×10^3
E_2	5.0×10^3
T_{ref}	348 K

The initial conditions are $c_1(0) = 1$ and $c_2(0) = 0$, and the reactor temperature is constrained to the interval of 298 K < T < 398 K. Based on the above information a rigorous simulation program was developed in MATLAB® and was treated as the

real process. Initially, the batch length is divided into N=10 equal stages. Eleven batches of process operations under different temperature profiles were simulated using the MATLAB® model. From these eleven data sets ten were used as the historical data sets and the data set with the best result (i.e. closest to the desired output) was used as the nominal trajectory, $\mathbf{X}_s$ and $\mathbf{Y}_s$. The existing mechanistic model was also used to generate the desired product reference trajectory, $\mathbf{Y}_d$. In the next phase it was assumed that a mechanistic model of the system is unavailable. Since the objective of the reactor is to maximize the product B, an LTV perturbation model is built to model the relationship between output $y = c_2$ and input $x = T$. Then, using these historical process data sets and the selected $\mathbf{U}_s$ and $\mathbf{Y}_s$, the parameters of $\hat{\mathbf{L}}_s$ were identified according to Equations 3.4 to Equation 3.7. The values of positive definitive matrices are set as $\mathbf{O}=10^5\times$diag (0.05,5,5,5,5,5,5,5,5,5) and $\mathbf{P} = 0.01\mathbf{I}$. The nominal case without any uncertainties (unknown disturbances) in the batch reactor was considered. According to the ILC algorithm, after $\mathbf{L}_s$ had been identified, it was then updated using new process data after the completion of each batch run.

After the termination of simulations, the final simulated input temperature profile was then applied to the mechanistic model and the corresponding concentration profile for the intermediate product (B) was obtained. This input/output data was then again included in the historical data sets and the best input temperature trajectory is again simulated using the ILC algorithm. The forgetting factor, β, selected as 0.98 was kept fixed throughout the successive batch runs. It was selected so that only the relatively recent batches are considered most. Figure 3.2 shows the tracking performance of this ILC. It can be seen from Figure 3.2 that both the concentration and temperatute profile converged to the desired trajectories as the number of batches increases. In these figures, $\mathbf{X}_{1,2,3,\ldots,12}$ and $\mathbf{Y}_{1,2,3,\ldots,12}$ are the input and ouput trajectories respectively for different batches as indicated by the subscripts. The simulation study was stopped at the end of thirteen real batches as the final result was not improving further. Figure 3.3 shows the sum squared error (SSE) values of the desired concentration trajectory and the real batch concentration trajectories.

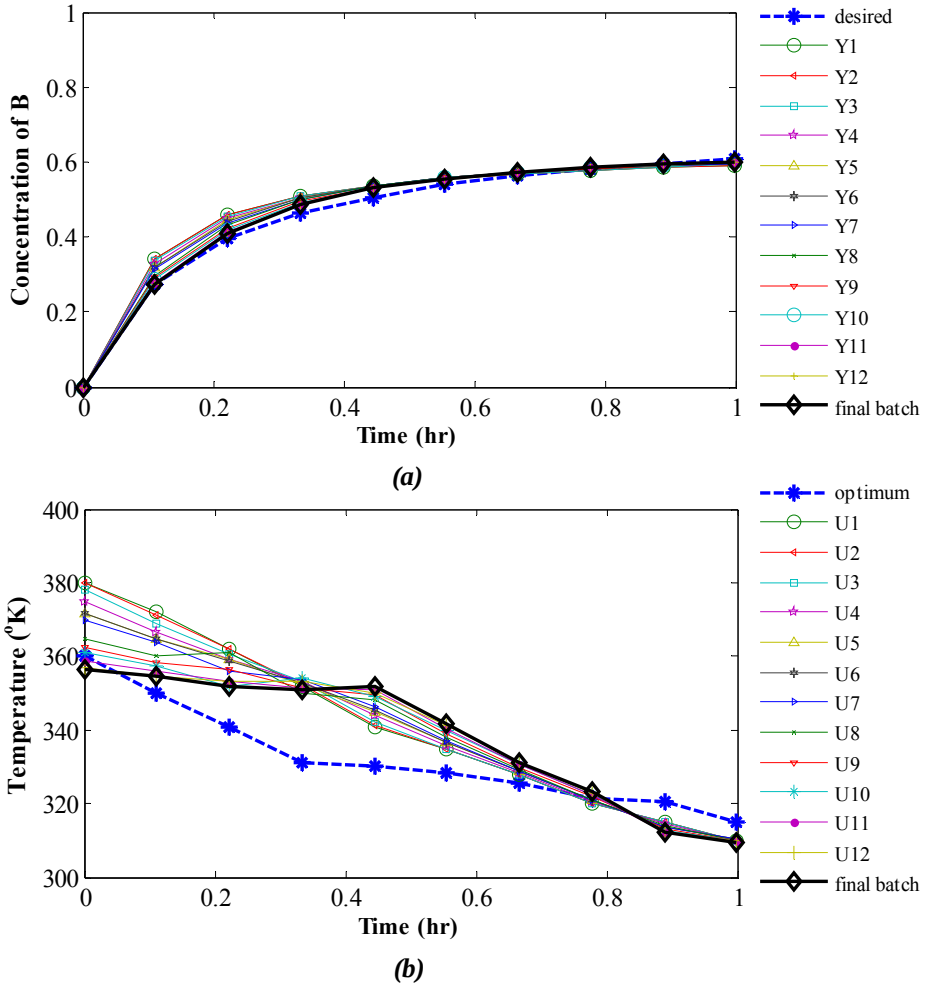


Figure 3.2: Simulated ILC profiles of different batches (a) concentration profiles (b) temperature profiles.

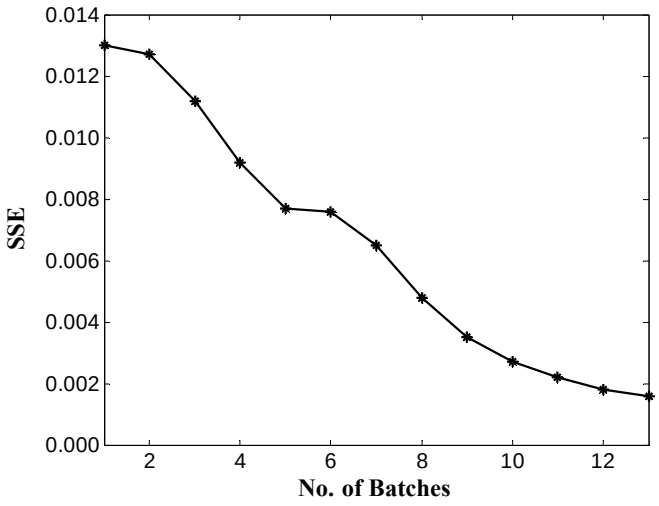


Figure 3.3: The SSE values for the batches.

3.3.2 Case Study 2: Batch Cooling Crystallisation System

In this study, an unseeded batch cooling crystalliser of Paracetamol in water was considered with a batch time of 300 minutes. The kinetics of the crystallisation system is given by the following sets of ordinary differential equations from Equation 3.13 to Equation 3.15 (Nagy et al., 2008a).

$$\mathrm{d}\mu_0/\mathrm{d}t = B \tag{3.13}$$

$$\mathrm{d}\mu_i/\mathrm{d}t = iG\mu_{i\text{-}1} + Br_0^i \qquad i = 1,2,.... \tag{3.14}$$

$$\mathrm{d}C/\mathrm{d}t = -k_v\rho(3G\mu_3 + Br_0^3) \tag{3.15}$$

where, B and G are the nucleation and growth rates respectively, $S = C - C_S(T)$ is the absolute supersaturation, C is concentration, C_S is the solubility as a function of the temperature T, μ_0, μ_1, μ_2, and μ_3 are the moments defining total number, length, area, and volume of crystals in the system respectively, r_0 is the size of the nuclei. The initial and final temperatures were 314.13K and 294.15K respectively. The physical properties are given in Table 3.2.

Table 3.2: Parameters of the Crystallisation Model

Solubility in water (T in K)	$C_S = 1.58\times10^{-5}T^2 - 9.057\times10^{-3}T + 1.31$
Growth rate	$G = \begin{cases} 1.64\times S^{1.54} & if\ \ S > 0 \\ -1.64\times S^{1.54} & if\ \ S \le 0 \end{cases}$
Nucleation rate	$B = \begin{cases} 7.8529\times10^{19}\times S^{6.23} & if\ \ S > 0 \\ -7.8529\times10^{19}\times S^{6.23} & if\ \ S \le 0 \end{cases}$
Density of crystal (g/cm^3)	ρ = 1.296
Volumetric shape factor	k_v = 0.24
Initial concentration (g/g solvent)	C_0 = 0.0254

A detailed mathematical model covering reaction kinetics and heat mass balances has been developed for the system. The details of the experimental and parameter

estimation procedures are available in literature (Nagy et al., 2008b; Fujiwara et al., 2002). Based on this model, a simulation program was developed in MATLAB® for this system to be treated as the real process. The objective of this case study was to control the crystallisation process to achieve a desired mean crystal size Ln defined in Equation 3.16 by manipulating the reactor jacket inlet temperature (T_{jin}).

$$Ln = \frac{\mu_1}{\mu_0} \tag{3.16}$$

This temperature was selected as a means to control supersaturation to restrict nucleation for obtaining appropriate sized crystals. The initial and the final temperature of the jacket were maintained at a constant value to ensure same start-up and end point condition for every batch. The batch length was divided into 10 equal stages. Eleven batches of process operations under different temperature profiles were simulated using the MATLAB® model. From these eleven data sets ten were used as the historical data sets and the data set with the best result was used as the nominal trajectory, ($\mathbf{X}_s, \mathbf{Y}_s$). Initially the existing mechanistic model was also used to generate the desired product reference trajectory $\mathbf{Y}_d$. In the next phase it was assumed that a detailed mechanistic model of the system is not available and so, the parameters of LTV perturbation model $\hat{\mathbf{L}}_s$ were re-identified using these historical process data sets and the selected nominal trajectories ($\mathbf{X}_s, \mathbf{Y}_s$). The weighting matrices were set as, $\mathbf{O} = 10^5 \times \mathrm{diag}(1,2.5,2.5,2.5,2.5,2.5,2.5,1.5,1)$ and $\mathbf{P} = 0.5\mathbf{I}$ in the light of the paper by Zhang et al. (2009b). The nominal case without any uncertainties (unknown disturbances) in the system was considered. According to the ILC algorithm, after the completion of each simulation the new input/output data is included in historical data to update $\hat{\mathbf{L}}_s$ and determine the temperature profile for the next batch until the termination conditions are satisfied. Finally, the temperature profile for the next batch as calculated by ILC scheme was applied to the real process (i.e. mechanistic model) and the corresponding mean crystal size at the end of the batch was obtained.

This input/output data was then again included in the historical data sets and the best input temperature trajectory is again simulated using the ILC algorithm as mentioned

before. The forgetting factor, β, selected as 0.8 was kept fixed throughout the successive batch runs. It was selected so that only the recent batches are considered most.

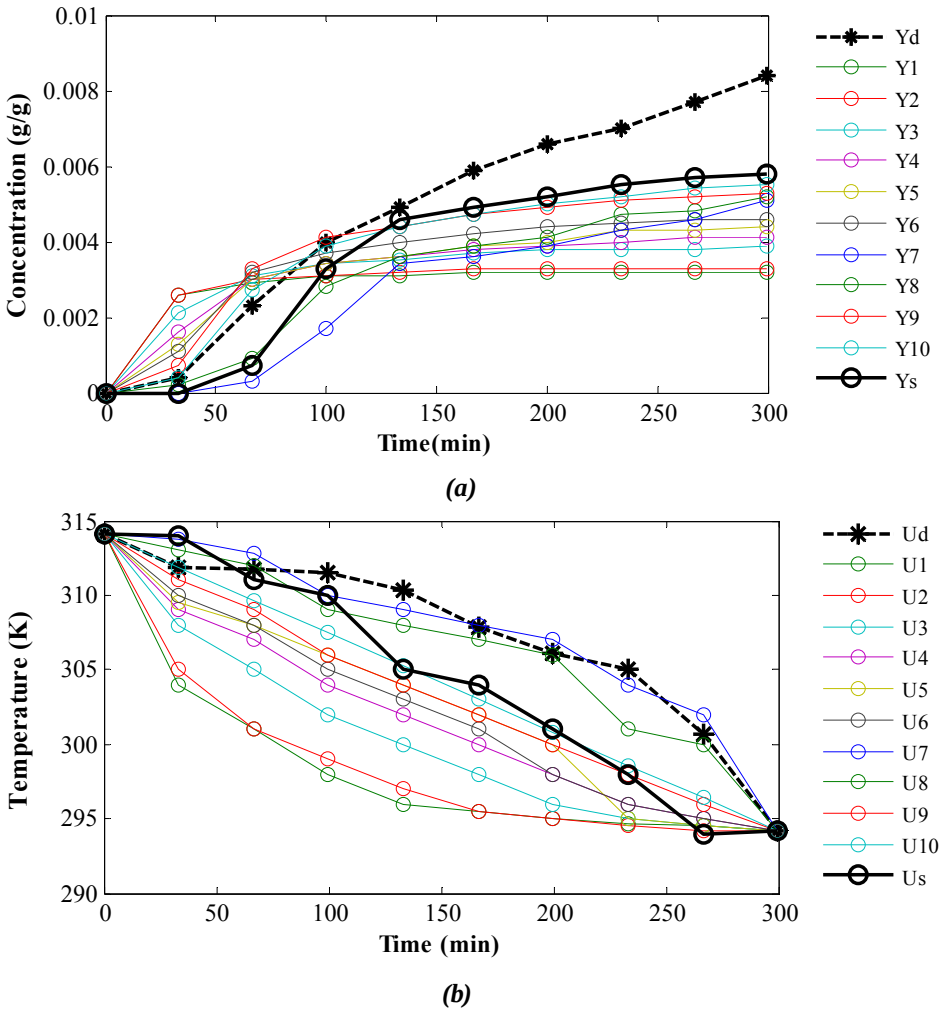
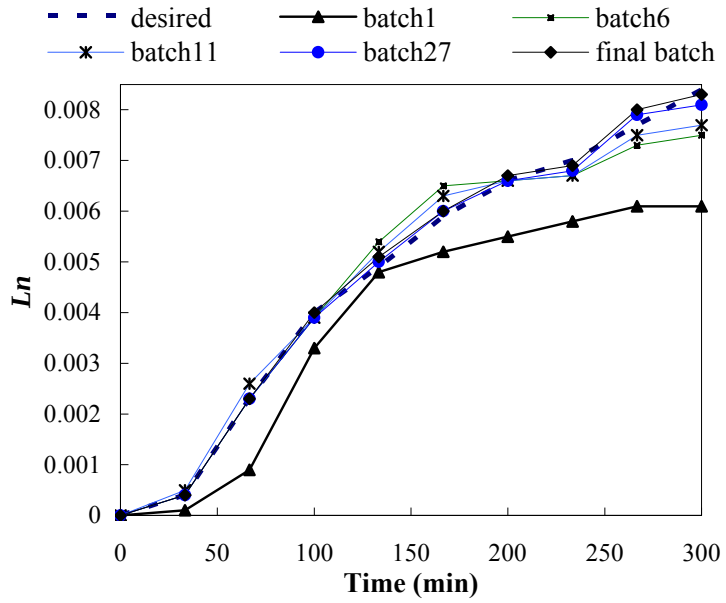


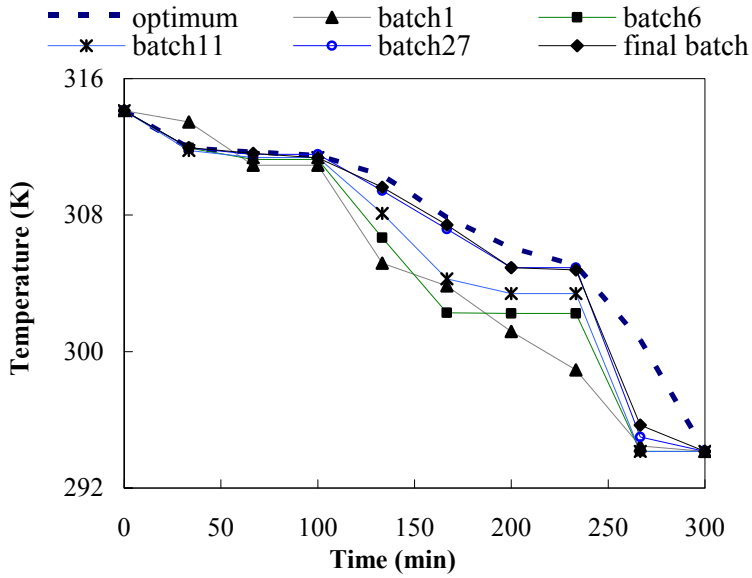
Figure 3.4: Historical data sets (a) mean crystal length trajectories (b) temperature trajectories.

Figure 3.4 (a) and Figure 3.4 (b) shows the simulated historical data sets for mean crystal length *Ln* and temperature trajectories respectively, $\mathbf{Y}_d$ is the desired mean length trajectory and $\mathbf{Y}_s$ is the selected nominal trajectory from which the simulation case study for ILC was initialised. Similarly, $\mathbf{U}_d$ is the theoretical temperature profile corresponding to $\mathbf{Y}_d$ and $\mathbf{U}_s$ is the nominal temperature trajectory. The results of the ILC approach are shown in Figure 3.5 (a) and Figure 3.5 (b). For simplicity, here only ten trajectories are shown. However, it is evident that the mean size of crystals

converged to the desired trajectory and the resulting final temperature profile was also very close to the theoretically optimum trajectory.



(a)



(b)

Figure 3.5: Trajectories of (a) mean crystal size (b) temperature.

Figure 3.6 shows the sum squared error (SSE) values of the desired and the real mean crystal size trajectories. It took about 34 batches to arrive at the final trajectories without the need of any process model. However, the results were almost converged

from the 5th batch onwards, and practically all subsequent batches after the 5th would produce crystals with very similar size to the desired target.

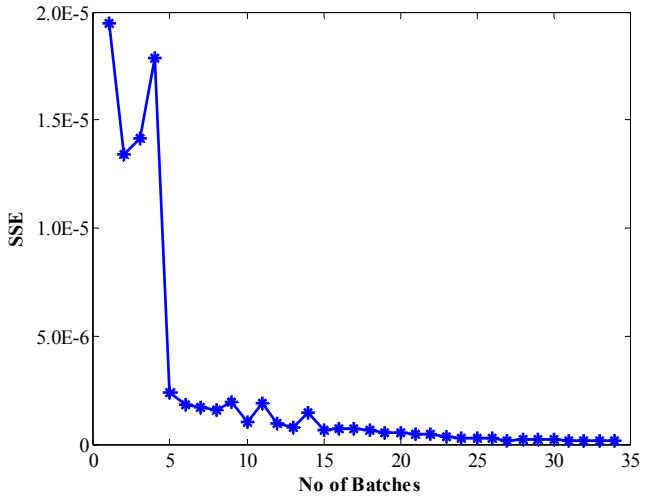


Figure 3.6: The SSE values for the batches.

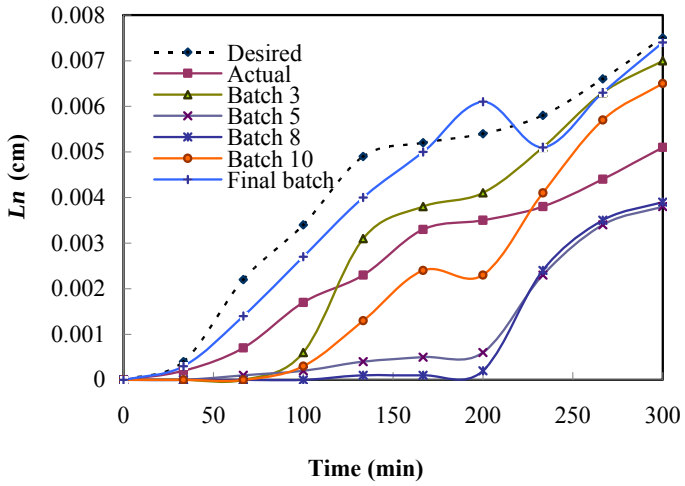
3.3.3 Case Study 3: Batch Cooling Crystallisation System with Model-Plant Mismatch

In order to assess the robustness of the proposed ILC approach, here the sensitivity of the model-based optimal control approach to errors in the model parameters is demonstrated. It was assumed that the model was identified with an error of -10% in both the growth and nucleation rate constants. In practical situation, this level of error can often occur, in particular when the scale of the crystalliser changes compared to the system used for model identification. This would often be the case when the model is identified using laboratory experiments and then the optimal operating trajectory is applied on the industrial scale. This model with error was then used for the model based optimisation to determine the optimal temperature trajectory to maximise the mean crystal size Ln. However, when this optimal temperature trajectory was applied to the real system (simulated by the same model but with the "true" parameters) it caused a 32% decrease in the actual final Ln (see Figure 3.7 (a), 'Actual' line). This simulation clearly indicates the sensitivity of model-based optimisation to uncertainties in the model parameters. This generally occurs since the optimal results of the nominal optimisation is generally on the boundary of the

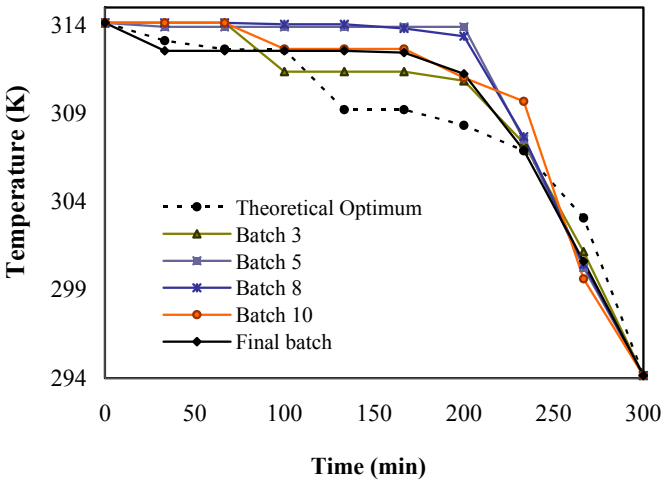
feasible operating envelope and any deviation from the nominal optimal trajectory may cause violation of constraints or significant quality degradation. One remedy to this problem is to use robust optimisation schemes that consider parameter uncertainties (Nagy and Braatz, 2004; Nagy, 2009), however these generally lead to complex and computationally intensive optimisation problems. On the other hand, the ILC control, however, is a model free approach (i.e. based on an adaptive LTV model that is re-identified after each batch based on experimental measurements).

To apply ILC to this system, the same historical input/output data and nominal trajectories were used as mentioned before in the previous sections. The optimal Ln trajectory from the model-based optimisation using the model with error was set as the desired output. The weighting matrices were set as, $\mathbf{O} = 10^5 \times \mathrm{diag}\,(1,2.5,2.5,2.5,2.5,2.5,2.5,2,1)$ and $\mathbf{P} = 0.5\mathbf{I}$. The forgetting factor was set as, $\beta = 0.8$. The rest of the test followed exactly the same steps as before.

The results of the ILC approach are shown in Figure 3.7 (a) and Figure 3.7 (b), indicating the measurement based ILC converged to the desired trajectory successfully and the resulting final temperature profile was also very close to the theoretical optimum trajectory, unlike in the case of applying the temperature trajectory resulting from the model-based optimisation using the model with parameter error. Figure 3.8 shows the sum squared error (SSE) values of the desired and the real mean crystal size trajectories. It took about 12 batches to arrive at the final trajectories without the need of any process model. The SSE values are comparatively more oscillatory than the previous case study example (see Figure 3.6) as the profiles of mean crystal size, Ln, oscillated relatively dramatically for the first few batches. However, the result was almost converged during the 12th batch and ILC simulation was terminated as both the termination conditions (i.e. $\left|e_b(t_f)\right| = \left|y_{\mathrm{d}}(t_f) - y_b(t_f)\right| < 0.00001$ or $\mathrm{SSE} = \sum e_b{}^2(t) < 0.00001$, see Figure 3.1) were fulfilled. These results indicate the increased robustness of the ILC, which can provide close to theoretically optimal results due to its adaptive nature.



(a)



(b)

Figure 3.7: Trajectories of (a) mean crystal size (b) temperature.

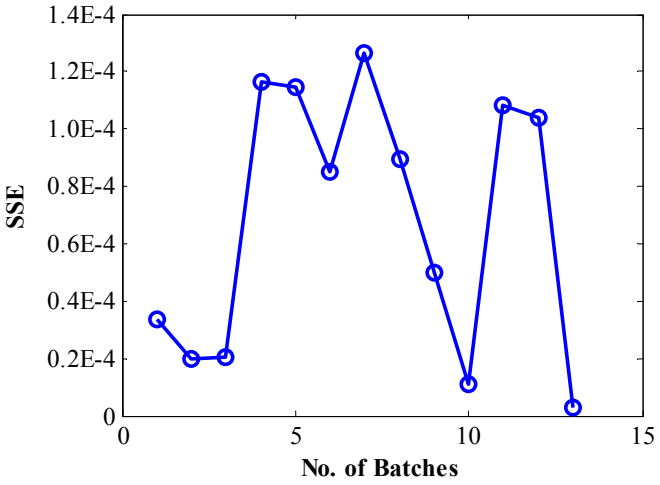


Figure 3.8: Tracking performance of ILC.

3.3.4 Case Study 4: Determination of Drying Temperature to Obtain a Desired Moisture Content in Paracetamol Granules at the End of the Batch

Paracetamol tablet is a mild analgesic and antipyretic. The main ingredients of paracetamol tablet are Acetaminophen powder along with other powdered excipients. The preparations are recommended for the treatment of most painful and febrile conditions. The Paracetamol tablet manufactured by GlaxoSmithKline Bangladesh Limited was initially marketed under generic name of 'Paracetamol Tablet' and later with trade a name from 1993 as 'Parapyrol tablets'. Parapyrol is a registered trademark product of GlaxoSmithKline Bangladesh Limited. This product is managed locally (PML). The formulation has been adopted from Speke document, UK dated 3 March 1983. Table 3.3 lists the Active Ingradient and excipients used in the formulation of Parapyrol tablets.

Table 3.3: Ingredients of Parapyrol Tablet

Active Ingredient (AI)	**Functions**
Paracetamol	Analgesic and Antipyretic
Excipients	**Functions**
Maize starch, Pregelatinised (Amigel) BP/EP/ USNF	Binder
Maize starch, BP/EP/ USNF	Diluent, Disintegration
Potassium Sorbate	Antimicrobial Preservative
Stearic acid (Powder)	Lubricant

The powder should posses good flow property to have uniformity of weight of the tablet. The flow property of powder depends upon moisture content of the powder as well as particle size, particle shape, porosity and density. Water interacts with pharmaceutical solids at virtually all stages of manufacture. Therefore, water-powder interaction is a major factor in the formulation, processing, and performance of solid dosage forms. Besides, moisture content is important for the mechanical strength of the tablet. Hence, it is important to know the optimal moisture content for the

formation of strong tablets. Within the pharmaceutical industries, it is well established that Acetaminophen with 2% moisture content gives tablet of optimum strength (Nokhodchi, 2005). Nonetheless, it is important to know the drying temperature to reach the desired moisture content after the drying process.

In the pharmaceutical industry, most products are manufactured using the wet granulation process. Wet granulation offers a wide range of capabilites for forming granules from the production of light granules to the production of very dense granules. More than 70% of the global industry's granulations are made using this method. (Tousey, 2002). When a wet-granulation technique is employed, control of the residual moisture after the drying step is important for smooth tablet compression. Too low or too high moisture contents may influence the chemical and physical stability of the final tablet (WHO, 2011).

The current practice in pharmaceutical industries for moisture content determination is based on off-line loss on drying (LOD) techniques (Bhalani, 2010). LOD techniques requires frequent stopping of the dryer during the operation to check the moisture content. This results in significantly increased cycle times. Samples collected manually are also susceptible to changes in physical conditions like humidity and segregation leading to inaccurate moisture analysis. In addition, generally there is a delay before analysis results are available to the operator that causes processing decisions, like end-point determination, to be made without optimal product moisture information.

Within the existing pharmaceutical industrial practice framework, the exact knowledge of drying temperature against a fixed time to reach the desired moisture content is important. This saves companies huge energy cost, eliminate the damage of product due to over-drying, and increase the overall efficiency of the drying process.

In this study an LTV perturbation model based ILC was applied to determine the drying temperature to obtain the desired moisture content in Paracetamol granules granulates at the end of the batch. The industrial case study was carried out in the pilot plant laboratory at GlaxoSmithKline Bangladesh Limited, Bangladesh.

3.3.4.1 Experimental Set-up

Figure 3.9 to Figure 3.11 shows the different experimental units operated in the pilot scale laboratory at GlaxoSmithKline Bangladesh Limited during this case study work.



Figure 3.9: Mighty Mixer Granulator.



(a) ***(b)***

Figure 3.10: Sapphire Fluid Bed Dryer (a) with wet granules loaded (b) during operation.



(a) ***(b)***

Figure 3.11: MJ33 Moisture Analyser (a) sieved granules loaded (b) during operation.

3.3.4.2 Batch Size and Duration

The amounts of the material required for the work have been listed below,

Paracetamol Powder 2 Kg,

Amigel 239.5 gm,

Maize Starch 80.239 gm,

Potassium Sorbate 7.98 gm,

Water 400 mL.

The batch time was 20 minutes and it was divided in 5 time steps each of 5 minutes. Sample was collected after each 5 minutes and the corresponding moisture content was measured for 10 minutes using a MJ33 Moisture analyser by Mettler Toledo.

3.3.4.3 Experimental Procedure

Moisture content was determined by loss on drying (LOD) method. Formula for calculating moisture content in percentage is as follows,

$$\%\ Moisture\ Content = \frac{(Loss\ in\ weight)}{(Initial\ weight)} \times 100$$

Figure 3.12 shows the block diagram of the complete drying and moisture content measurement procedure.

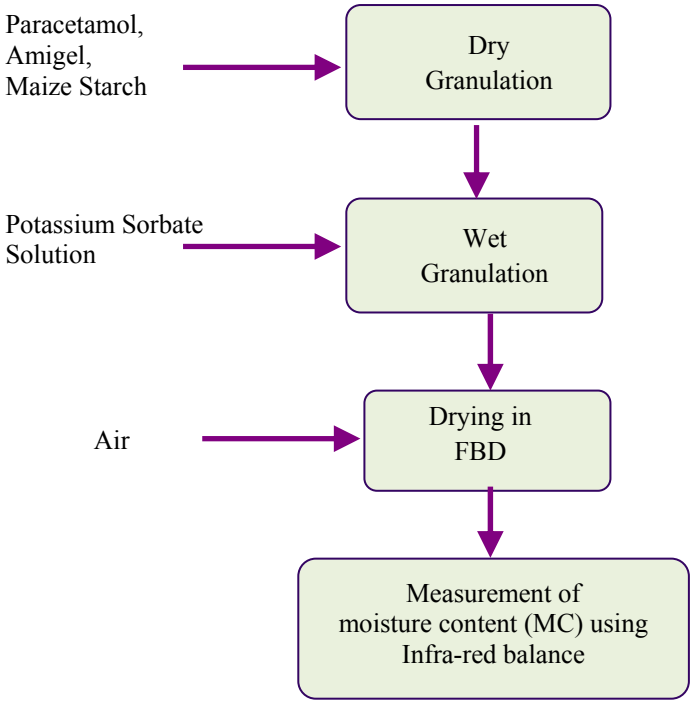


Figure 3.12: Process block diagram.

During drying sample was collected after each 5 minutes, sieved with #20 Mesh and used to measure the moisture content in a MJ33 Moisture analyser by Mettler Toledo balance at 373.16 K for 10 minutes.

3.3.4.4 Results and Discussions

The historical data sets were collected for six batches to identify the LTV perturbation model of the system. The required drying temperature was calculated using LTV model based ILC. The historical data, nominal data, desired MC and calculated ILC data are tabulated in Table 3.4 to Table 3.7 consecutively.

Table 3.4: Historical Data

Time (min)		0	5	10	15	20
Batch No.	**Drying Temp. (^{o}C)**	**Moisture Content (%)**				
1	313.16	9.96	7.55	6.79	6.59	5.95
2	315.66	9.61	7.40	6.32	6.22	5.00
3	318.16	9.90	7.25	6.59	6.20	4.91
4	320.66	9.92	6.96	6.07	6.07	4.63
5	323.16	9.89	6.85	5.91	5.61	4.59
6	325.66	9.76	6.68	5.61	5.16	4.49

Table 3.5: Nominal Data

Time (min)	0	5	10	15	20
Drying Temp. (^{o}C)	**Moisture Content (%)**				
328.16	9.85	6.77	4.85	4.71	4.46

Table 3.6: Desired Moisture Content (%)

Time (min)	0	5	10	15	20
Moisture Content (%)	9.5	5.0	4.0	3.0	2.0

Table 3.7: Experimental ILC Data

Time (min)		0	5	10	15	20
Batch No.	**Drying Temp. (^{o}C)**	**Moisture Content (%)**				
1	331.44	9.96	6.90	5.64	4.39	4.15
2	334.18	9.61	6.20	5.14	4.15	4.00
3	337.07	9.9	6.77	5.11	4.07	3.88
4	339.81	9.92	6.41	5.14	3.68	3.50
5	343.07	9.89	5.95	4.92	3.80	3.00
6	344.86	9.76	6.73	4.89	3.56	2.80
7	347.06	9.85	5.11	4.07	3.88	2.40
8	348.56	9.96	5.60	4.38	3.04	2.05

Here, drying temperature is the input and moisture content (%) is the output.

Figure 3.13 shows the moisture content trajectories for different temperatures and Figure 3.14 shows how the final moisture content decreased gradually with the increase in drying temperature. Figure 3.15 shows the sum squared error SSE values

between the desired and actual MC trajectories. It took 7 batches to drop the SSE significantly and during the 8th batch the result converged to the desired MC trajectory (See Figure 3.14 and Figure 3.15). The required temperature is 348.56 K. To confirm the drying temperature two additional batches were ran at 348.56 K and these gives slight deviations in MC trajectories within acceptable limit.

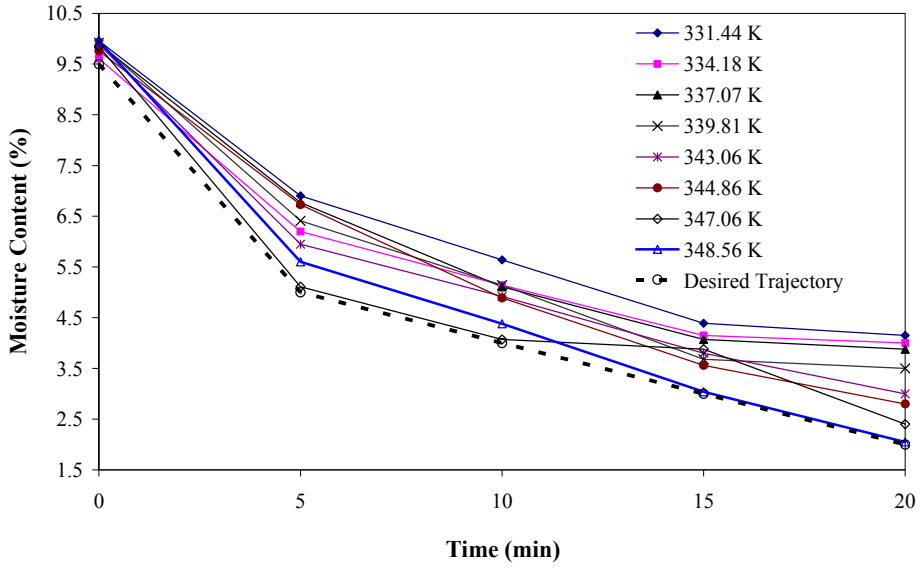


Figure 3.13: Trajectories of moisture content.

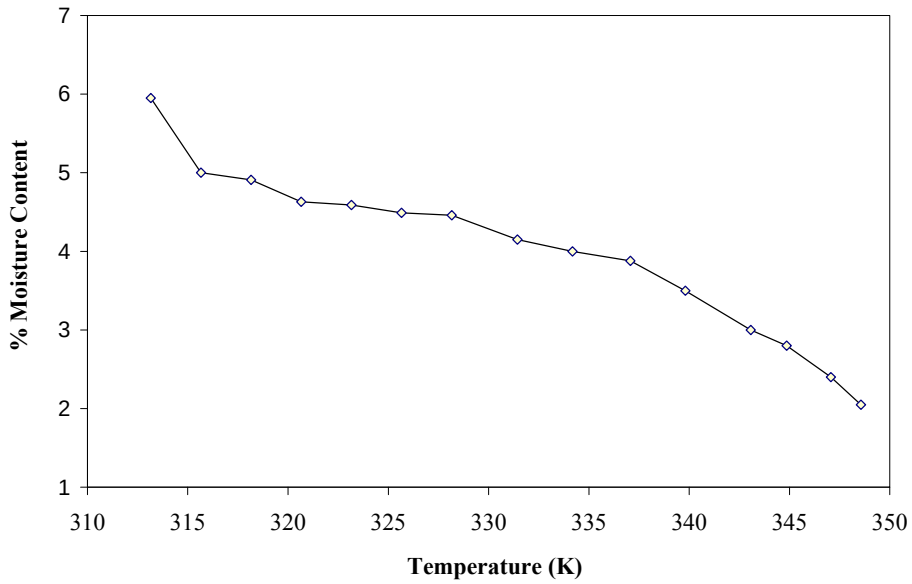


Figure 3.14: Final moisture content vs. temperature plot.

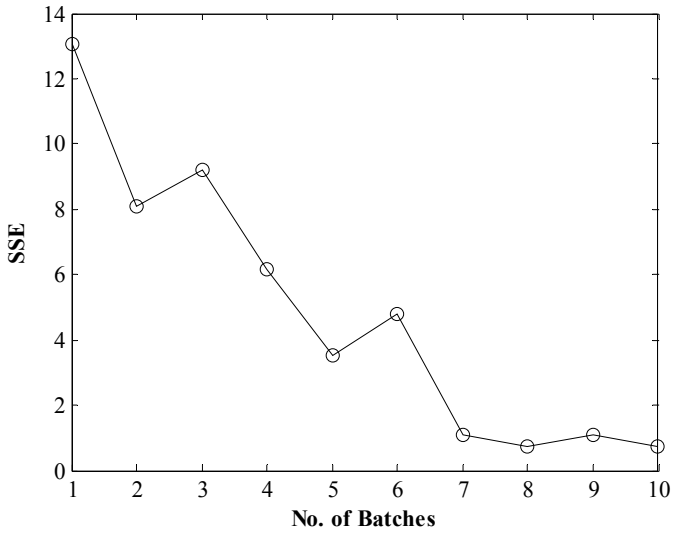


Figure 3.15: Tracking performance of ILC.

The study shows that the proposed ILC strategy can calculate the required drying temperature, eliminate the within batches measurement of moisture contents and gives the desired moisture content at the end of the batch under a fixed batch time.

3.4 Conclusions

In this Chapter a linear time varying (LTV) perturbation model based iterative lerning control (ILC) strategy was developed for batch processes which are distributed parameter systems in nature. Since this is an operating data based methodology it is capable of controlling a process in the absence of a first principle model. The proposed methodology was evaluated using three simulation case studies and one industrial pilot scale case study. The results show that this approach can track the desired set points satisfactorily even in the present of model plant mismatch. In the next chapter this LTV perturbation model based ILC strategy is used to develop a systematic supersaturation control scheme for batch crystallisation system.

Chapter 4

Design of Supersaturation Control (SSC) of a Seeded Batch Cooling Crystalliser Based on ILC

4.1 Overview

Following from Chapter 4, a novel hierarchical ILC (HILC) scheme for the systematic design of the supersaturation control (SSC) of a seeded batch cooling crystalliser was developed and introduced. The proposed HILC can be a convenient tool to select the operating profile. This model free control approach is implemented in a hierarchical structure. On the upper level, a data-driven supersaturation controller determines the extent of optimal supersaturation needed to produce the desired end-point property of crystals. On the lower level, the corresponding temperature trajectory is determined by time domain experiments to generate necessary supersaturation. In the later part of this chapter the proposed approach is evaluated in the cases of a simulated seeded batch cooling crystallisation system of Paracetamol in water.

4.2 Theory of SSC for Controlling Crystallisation Process

Supersaturation is the driving force to create crystals from the solution. It is defined as the difference between the actual dissolved concentration and the corresponding saturated concentration (or solubility) at a specific temperature (Barrett et al., 2010). Supersaturation control of batch cooling crystalliser is a popular control strategy since it does not require any first principle model of the system. The basic idea of this direct design approach is to maintain the operating profile within the metastable zone (see Figure 4.1) over the course of the batch to avoid nucleation (Fujiwara et al., 2005). Supersaturation is the fundamental parameter that affects the outcome of crystallisation processes, such as chemical purity, polymorphic content, crystal dimension and shape, and batch-to-batch consistency of the product. The main

advantage of this approach is its insensitivity to most parameter variations and process disturbances (Woo et al., 2009). However, it is crucial to have a systematic methodology for designing the supersaturation and temperature trajectories to produce products with the desired CSD. Operation close to the metastable limit (high supersaturation) results in excessive nucleation, lower purity and longer filtration times. Operation close to solubility curve (low supersaturation) leads to slow growth and long batch times. Hence, the setpoint supersaturation curve is a compromise between fast crystal growth and low nucleation rate (Aamir et al., 2008).

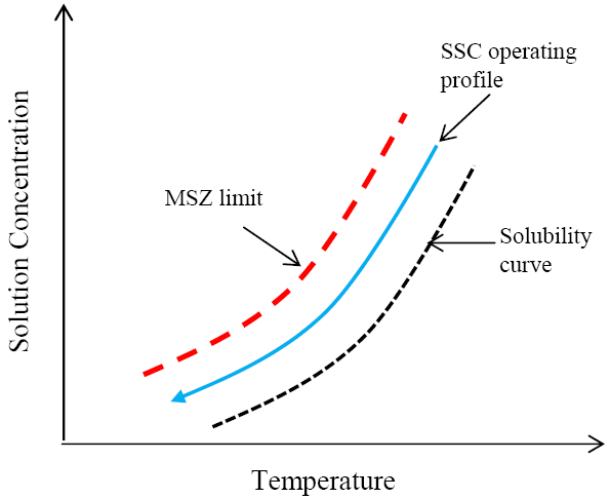


Figure 4.1: Operating curve for supersaturation control of a seeded batch cooling crystalliser.

Although applying SSC improves the quality of the product CSD, and can produce consistently high quality crystals, until now there is no systematic design approach to select the set-point operating profiles. In practice, the supersaturation profile is chosen by trial-and-error experimentation (Fujiwara et al., 2005; Aamir et al., 2008). Zhou et al. (2006) investigated an automated approach to design a nearly optimal supersaturation profile by applying different constant supersaturation (CSS) profiles and observing the related counts/sec over time. Due to unsatisfactory results, they ended up with constant relative supersaturation instead of CSS to avoid secondary nucleation. However, it was not mentioned in the paper how the specified constant relative supersaturation was selected.

Therefore, in an effort to develop a systematic approach for supersaturation control (SSC) of seeded batch cooling crystalliser a novel hierarchical ILC (HILC) scheme is introduced here.

4.3 Development of Hierarchical ILC (HILC) for Systematic Design of SSC of a Seeded Batch Cooling Crystalliser

The proposed HILC is a systematic approach to determine the setpoint supersaturation profile and corresponding temperature trajectory by two consecutive ILC strategies (ILC1 and ILC2) arranged in a hierarchical structure. ILC1 is applied at the upper level of hierarchy, aimed to determine the extent of constant supersaturation needed to produce crystals with desired end-point properties. With this end, initially a set of input-output data is generated from constant supersaturation control experiments of a seeded batch cooling crystalliser where the inputs are constant supersaturation (SS) values and the outputs are the mean length (Ln) of crystals at the end of the batch. The supersaturation is usually maintained at the desired constant value throughout the entire batch by application of properly designed control algorithms (Zhang and Rohani, 2003). This historical data is then used in ILC1 framework to identify the LTV perturbation system, $Ln = f(\text{Css})$ and optimise the extent of supersaturation (SS) needed for a desired mean length of crystals at the end of the batch. Since direct supersaturation measurement sensors are often not available for industrial scale use (Braatz, 2002; Fujiwara et al., 2005), ILC1 is developed to be implemented in pilot plant or laboratory scale.

ILC2 is applied at the lower level of hierarchy. The main objective of ILC2 is to redefine the supersaturation profile in terms of the temperature profile in time, which is designed to maintain the supersaturation at a certain setpoint. This follows the concept of direct design introduced by Fujiwara et al. (2005), whereby supersaturation control can be used to generate a temperature profile which is then applicable at industrial scale. However, instead of directly applying a temperature profile obtained at the lab scale, the HILC determines, based on historical real plant data, the required temperature profile under the real operating conditions. For ILC2, initially a set of input-output data is generated by typical temperature controlled operation of the

industrial crystalliser where the inputs are different cooling temperature profiles and the outputs are corresponding supersaturation (SS) trajectories (not necessarily constant supersaturation trajectories). This historical data is then used in ILC2 framework to identify the LTV system $\mathbf{SS} = f(\mathbf{T})$ and determine the best temperature profile needed to maintain the optimal supersaturation profile as calculated by ILC1. The hierarchical implementation of the approach, which consists of the constant supersaturation controller (SSC) at the higher level and the temperature controller at the lower level is shown in Figure 4.2.

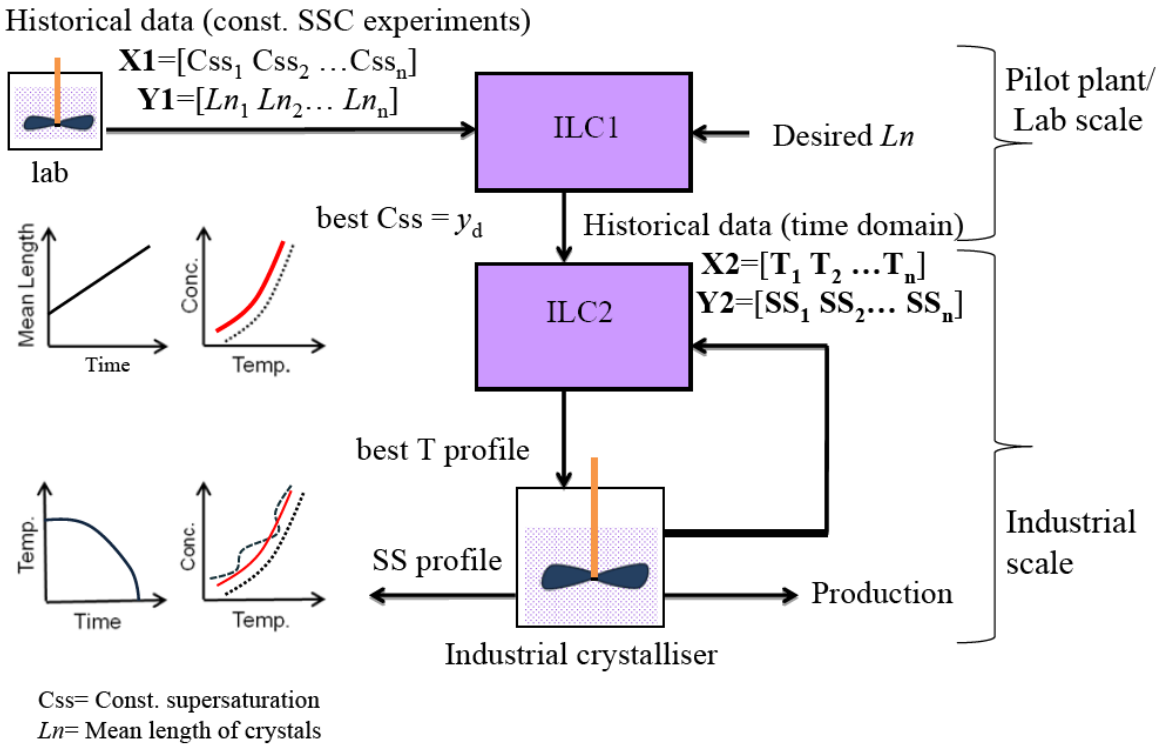


Figure 4.2: Architecture of proposed HILC for SSC of a seeded batch cooling crystalliser.

4.4 Results and Discussions

4.4.1 Seeded Batch Cooling Crystallisation System

In this case, the same system of Paracetamol in water as described in Chapter 3 was used but this time seed was introduced to the system at the beginning of the batch. The HILC was applied to design the setpoint of the SSC required to achieve a desired

Ln at the end of the batch, as well as to determine the necessary temperature trajectory in time domain that can produce the required constant supersaturation.

The ILC for the supersaturation control design – ILC1

The objective was to achieve a desired mean crystal size Ln of 0.012 cm at the end of the batch by maintaining a constant supersaturation throughout the batch. Six batches considering different supersaturation profiles were simulated using the MatLab® model that was treated as the real process. From these six data sets, five were used as the historical data and the data with the best result was selected as the nominal data set $(\mathbf{X}_s, \mathbf{Y}_s)$. Using the historical data sets and the selected nominal trajectories $(\mathbf{X}_s, \mathbf{Y}_s)$, the parameters of LTV model $\hat{\mathbf{L}}_s$ were re-identified. The weighting matrices were set as, $\mathbf{O} = 10^5 \times 2.5$ and $\mathbf{P} = 0.005\mathbf{I}$, since only the supersaturation and the corresponding mean length at the end of the batch was considered, i.e. $(\mathbf{X}_s, \mathbf{Y}_s)$ is a (1,1) matrix. The forgetting factor was, $\beta = 0.8$. In this study, ILC1 was completed in a single stage of one thousand iterations instead of applying the result again to the real system to update the historical data.

Direct design of temperature trajectory for constant supersaturation control using ILC – ILC2

The objective of this ILC scheme (ILC2) was to achieve a desired supersaturation profile (i.e. $S = 3.76 \times 10^{-4}$, as determined by ILC1) by manipulating the reactor temperature T in time domain. The batch time was divided into $N = 10$ equal stages. Eleven batches considering different temperature profiles were simulated using the model. From these eleven data sets ten were used as the historical data and the best data was selected as the nominal data $(\mathbf{X}_s, \mathbf{Y}_s)$. The LTV model $\hat{\mathbf{L}}_s$ was determined similarly as in the previous cases. The weighting matrices were set as, $\mathbf{O} = 10^5 \times \mathrm{diag}(1,2.5,2.5,2.5,2.5,2.5,2.5,2.5,1)$ and $\mathbf{P} = 0.05\mathbf{I}$. The forgetting factor was, $\beta = 0.8$. The temperature profile resulting from the ILC2 scheme was applied to the mechanistic model (i.e. real process) and the corresponding

supersaturation was obtained. Figure 4.3 illustrates the steps followed in the proposed HILC.

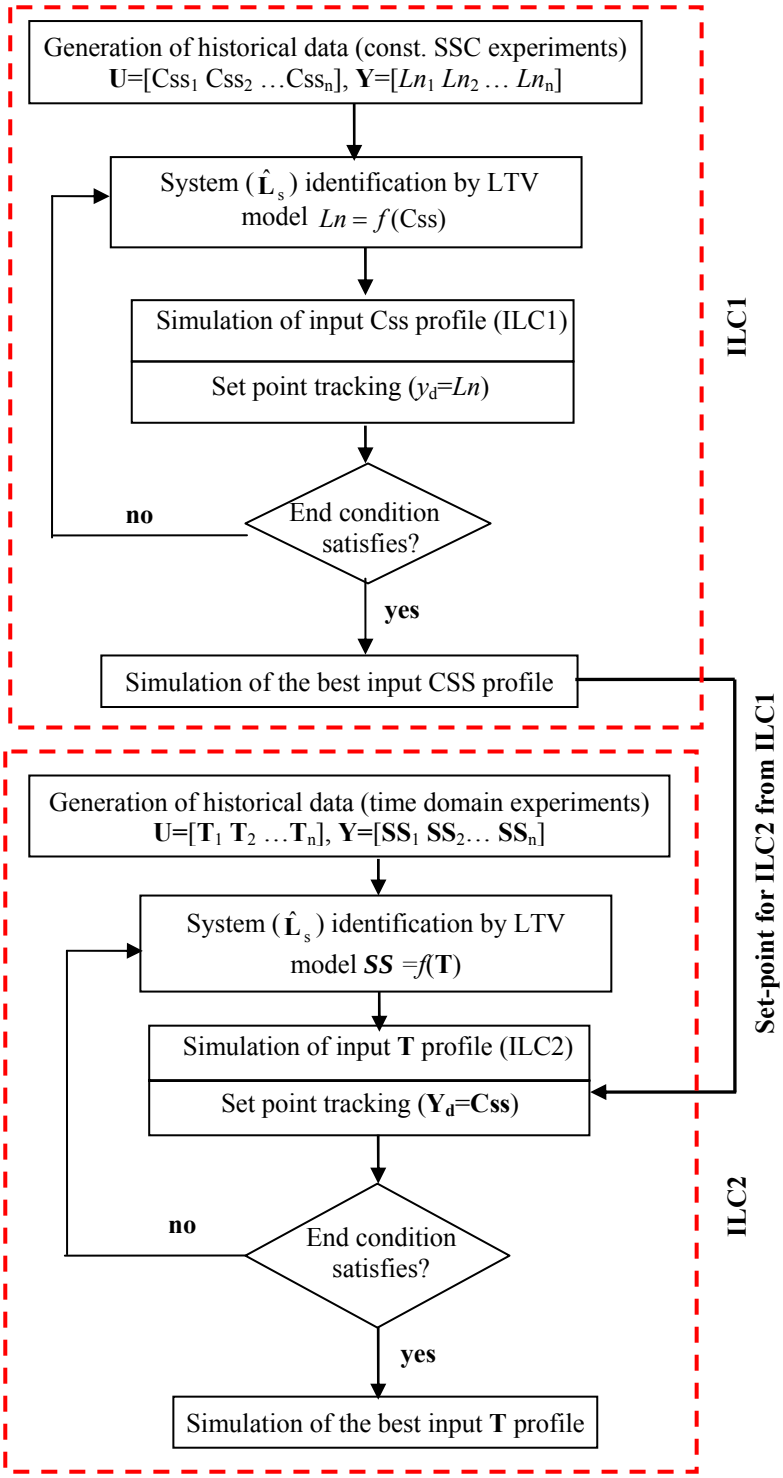


Figure 4.3: Steps followed in the case study of SSC of a seeded batch cooling crystalliser by HILC.

Figure 4.4 shows the results of the ILC1, however, these are all simulated batches where every batch corresponds to a single iteration within the LTV perturbation model based ILC algorithm. It shows the error between desired Ln and calculated Ln at the end of the batch continues to decrease from simulated batch-to-batch. The calculated input supersaturation was 3.76×10^{-4} producing $Ln = 0.0107$ cm at the end of one thousand simulated batches resulting in a 10.83 % error which was considered acceptable for this study.

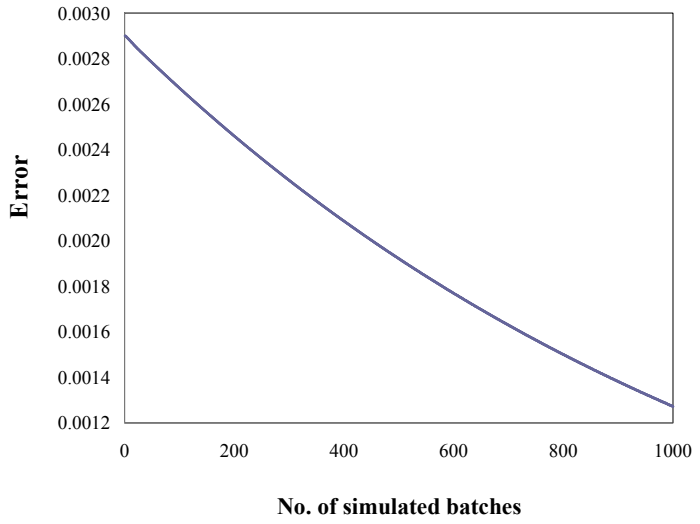
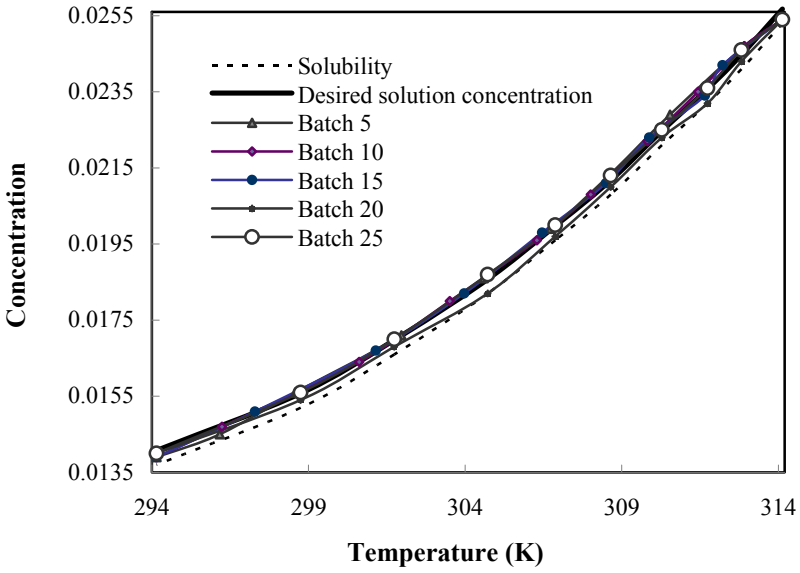


Figure 4.4: Tracking performance of ILC1.

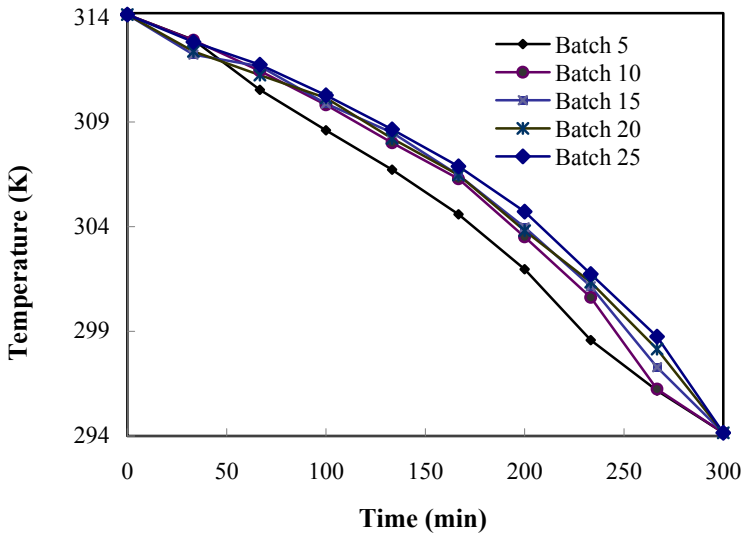
Figure 4.5 (a) and Figure 4.5 (b) show the supersaturation profiles and corresponding temperature profiles respectively from the ILC2. For simplicity only five batches have been shown. The trajectories named as 'Batch 25' in Figure 4.5 (a) and Figure 4.5 (b) represents the concentration profile that was closest to 3.76×10^{-4} target supersaturation and the corresponding temperature profile respectively.

Figure 4.6, the SSE plot for ILC2 shows that it took about 25 real batches to arrive at the final trajectories without the need of any process model and the SSE dropped significantly after the fourth batch onwards. One point to be noted that, like the previous case studies the initial and final temperatures were always maintained at 314.13 K and 214.15 K respectively. These constraints tend to limit the performance of ILC2, and the error $e_b(t) = y_{\mathrm{d}}(t) - y_b(t)$ was always higher at the beginning and end, ultimately this led to compromise the extent of desired supersaturation at these

time steps. Figure 4.7 shows that the final temperature profile from ILC2 produced an Ln profile that increased linearly over time and the final Ln was 0.0114 cm resulting in only a 5% error with the desired Ln of 0.012 cm. This 5% error can be subject to the linearisation of a nonlinear crystallisation system by LTV perturbation model. However, the overall results indicate that the proposed approach can be used to improve crystallisation processes very quickly within a small number of batches.



(a)



(b)

Figure 4.5: Profiles from simulated batch to batch (a) SSC profiles (b) input temperature trajectories.

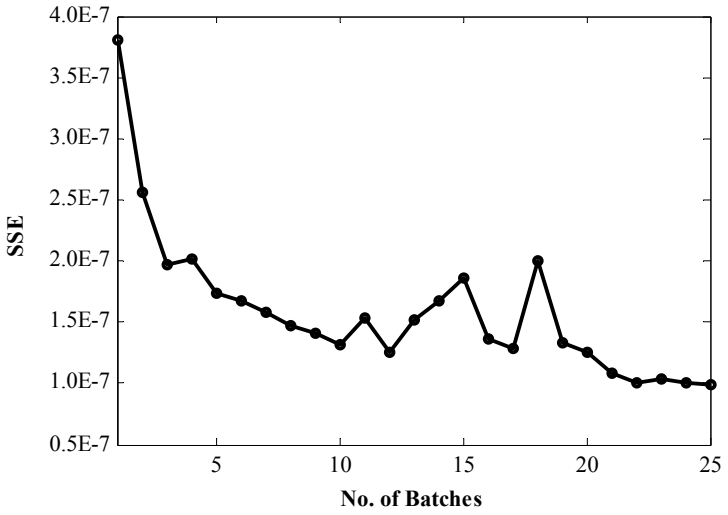


Figure 4.6: Tracking performance of ILC2.

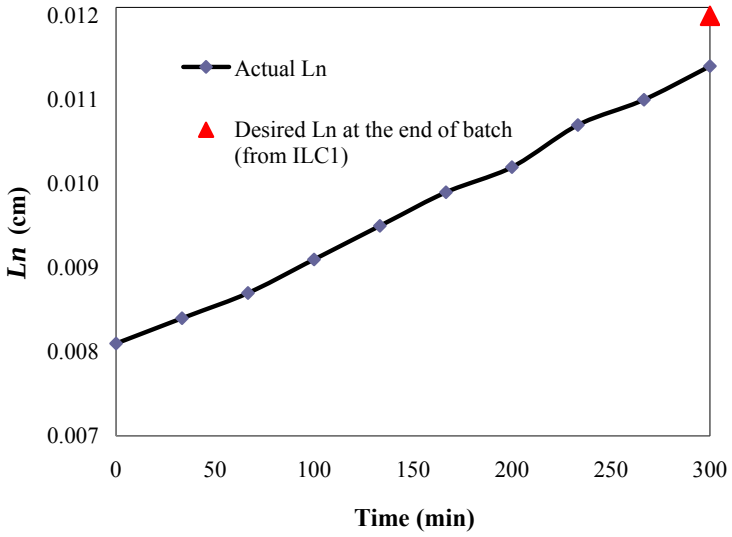


Figure 4.7: Mean length profile for the final temperature trajectory.

4.4.2 Seeded Batch Cooling Crystallisation System with Kinetic Parameter Perturbation

In order to assess the robustness of the HILC in presence of kinetic parameters perturbation, error was introduced in both the growth and nucleation rate constants during the batch-to-batch improvement in ILC2.

The objective was to achieve a desired supersaturation profile (i.e. $S = 3.76\times10^{-4}$, determined from ILC1) by manipulating the reactor temperature T in presence of

kinetic parameter perturbation. The batch time was divided into $N = 10$ equal stages. Eleven batches considering different cooling temperature profiles were simulated using the model. From these eleven data sets ten were used as the historical data and the best data was selected as the nominal data $(\mathbf{X}_s, \mathbf{Y}_s)$. The LTV model $\hat{\mathbf{L}}_s$ was determined similarly as in the previous cases. The weighting matrices were set as, $\mathbf{O} = 10^5 \times \text{diag}(1,2.5,2.5,2.5,2.5,2.5,2.5,2.5,2.5)$ and $\mathbf{P} = 0.05\mathbf{I}$. The forgetting factor was, $\beta = 0.8$. The temperature profile resulting from each step of the ILC scheme was applied to the mechanistic model (i.e. real process) and the corresponding supersaturation was obtained.

In order to assess the robustness of the HILC in presence of kinetic parameters perturbation, after the 10th real batch an error of -5% was introduced in both the growth and nucleation rate constants. Hence, from the 11th batch onwards the iterations are based on historical data from a wrong system. The SSE plot for this test is shown in Figure 4.8.

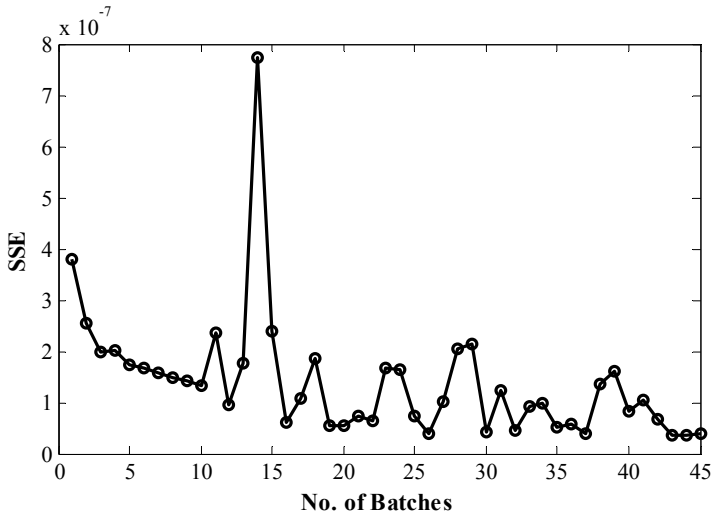


Figure 4.8: Tracking performance of ILC2 when a -5% error was introduced to the system after 10th batch for kinetic parameter perturbation test.

It shows that after the 10th batch the SSE increased suddenly and started to oscillate as the process changes. This time the controller needed more iterations until the historical data set is slowly replaced by the data from the new process (with new

kinetic parameters). From the 39th batch, ILC started to converge again. It took 45 batches to arrive at the final trajectories without the need of any process model.

4.5 Conclusions

A hierarchical ILC (HILC), is proposed for the systematic design of supersaturation controlled (SSC) seeded batch cooling crystallisation processes. This automated approach uses two ILC strategies in a hierarchical structure primarily to determine the optimal supersaturation profile to produce crystals with desired end-point properties and to generate the corresponding temperature trajectory in the time domain. The proposed method was evaluated using simulated batch cooling crystallisation process of Paracetamol in water. The results demonstrated that the approach is able to converge to the desired operating profiles even in the presence of kinetic parameter perturbations without the need of a detailed mechanistic process model. The convergence of the approach can be improved by using nonlinear data-driven models in the ILC scheme, such as artificial neural networks or polynomial chaos expansions.

Chapter 5

Experimental Evaluation of the Hierarchical ILC (HILC) Approach for Supersaturation Control (SSC) of a Seeded Batch Cooling Crystalliser

5.1 Overview

This chapter describes the experimental evaluation of the hierarchical ILC (HILC) approach for supersaturation controlled (SSC) batch cooling crystallisation processes. The methodology has been described in detail in Chapter 4. All experiments were carried out in a laboratory scale seeded batch cooling crystallisation system of Paracetamol in isoPropyl alcohol (IPA). For in situ measurement of chord length distributions (CLD) and particle counts of crystals a Lasentec FBRM probe and for in situ measurement of concentration an ATR-UV/Vis probe was used. Microscopic images of the crystals were taken at the end of the batches using a light microscope. In the later part of the chapter, the experimental results have been presented and discussed.

5.2 Experimental Evaluation of HILC

As described in the previous section, ILC1 is applied at the upper level of hierarchy, aimed to determine the extent of constant supersaturation needed to produce a certain SWMCL of crystals at the end of the batch. With this end, initially five batches of constant supersaturation control experiments of a seeded batch cooling crystalliser were run where the inputs are constant supersaturation (CSS) values and the outputs are the SWMCL of crystals at the end of the batch. These five data sets were then arranged in the order of increasing supersaturation. The first four sets were used as historical data for ILC1. The data set that produced the maximum SWMCL was used

as the nominal data set. This historical data along with the nominal data were then used in ILC1 framework to identify the LTV perturbation system, $SWMCL = f(\text{CSS})$. The LTV model was then used to optimise the extent of constant supersaturation (CSS) needed for two desired SWMCL of crystals at the end of the batch. The first desired SWMCL was set to lie within the limit of measured historical data to validate the findings of the measurements. The second SWMCL was chosen to be just outside the boundary to investigate the extrapolation characteristics of the system. During all the ILC1 experiments, the supersaturation was maintained at a desired constant value throughout the entire batch by application of a feedback controller.

ILC2 is applied at the lower level of hierarchy. The main objective of ILC2 was to redefine the constant supersaturation profile determined in ILC1 in terms of the temperature profile in time, which is designed to maintain the supersaturation at a certain setpoint. During implementing ILC2, initially eleven sets of input-output data was generated by typical temperature controlled operation of the seeded batch cooling crystalliser where the inputs are different random cooling temperature profiles and the outputs are corresponding supersaturation trajectories (not necessarily constant supersaturation trajectories). From these data sets, ten were used as historical data and the data with the best result was selected as the nominal data. These historical data and the nominal data was then used in ILC2 framework to identify the LTV system $\mathbf{SS} = f(\mathbf{T})$.

In this study, two individual sets of ILC2 experiments were performed against two different desired SWMCL as mentioned above. Using the same historical and nominal data and the LTV model in ILC2 framework, the temperature profiles were determined to maintain the desired optimal supersaturation profiles as calculated by ILC1. In all of the experiments, after the solution was cooled down to just below the saturation temperature, 5% seed was added to the system. Further details of the experiments are discussed in the results and discussions section of this chapter.

5.3 Experiment Design

As mentioned in the previous section, the experimental investigation of supersaturation control of the seeded batch cooling crystallisation for Paracetamol in IPA was carried out in two different sets of experimental work. The experimental data was obtained from a laboratory scale crystallisation system at Loughborough University. This section describes the experimental setup, materials used and seed preparation in detail.

5.3.1 Experimental Set-up

The experiments were carried out in a 500 mL jacketed glass vessel. The temperature in the vessel was controlled with a stainless steel Pt100 thermocouple connected to a thermo fluid circulator bath (Huber Variostat CC-415 VPC) via a specially designed crystallisation control interface in Labview (National Instruments). The temperature readings were recorded every 10 seconds on a PC. Snapshots of the control interface are shown in Appendix B. An overhead PTFE coated 4-pitched blade was used to agitate the system at 360 rpm. This agitation speed was chosen to be high enough to guarantee that particles are well suspended throughout the process, but low enough to avoid attrition or generation of bubbles due to vortex formation. An FBRM probe (model D600L, Lasentec) was used to measure chord length distributions. FBRM data collection and monitoring was carried out by the FBRM control interface software (version 6.7). The probe was inserted into the solution to measure chord length distributions in the range 0.8 to 1000 μm (the lower limit therefore requires nucleation plus some growth to occur before detection occurs in the FBRM) using 38 bins. The position and orientation of the probe were chosen according to the standard recommendations to avoid particles adhering to the probe and provide suitable sampling. The distributions were collected at every 10 seconds and averaged during collection. The UV/vis spectra of the solution were measured using a Hellma 661.822 ATR probe connected to a Carl Zeiss MCS621 UV/ vis spectrometer. Software written in LabVIEW (National Instruments) using libraries provided by Carl Zeiss was used for spectra collection. The absorbance was recorded at every 10 s over a wavelength range of 240 – 720 nm, and the absorbance values at selected wavelengths

were used in calibration to determine the concentration. The data collected by computers connected to FBRM and UV/vis were sent to a third computer, running the Crystallisation Process Informatics System (CryPRINS) software (in-house developed software) written in LabVIEW. This software is capable of receiving and sending data through an RS232 interface, by file sharing, or using an OPC (OLE, Object Linking and Embedding, for Process Control) server. The software enables the simultaneous monitoring of the data from various PAT tools and the implementation of the required temperature profiles in an automated way. A schematic representation of the equipment is shown in Figure 5.1.

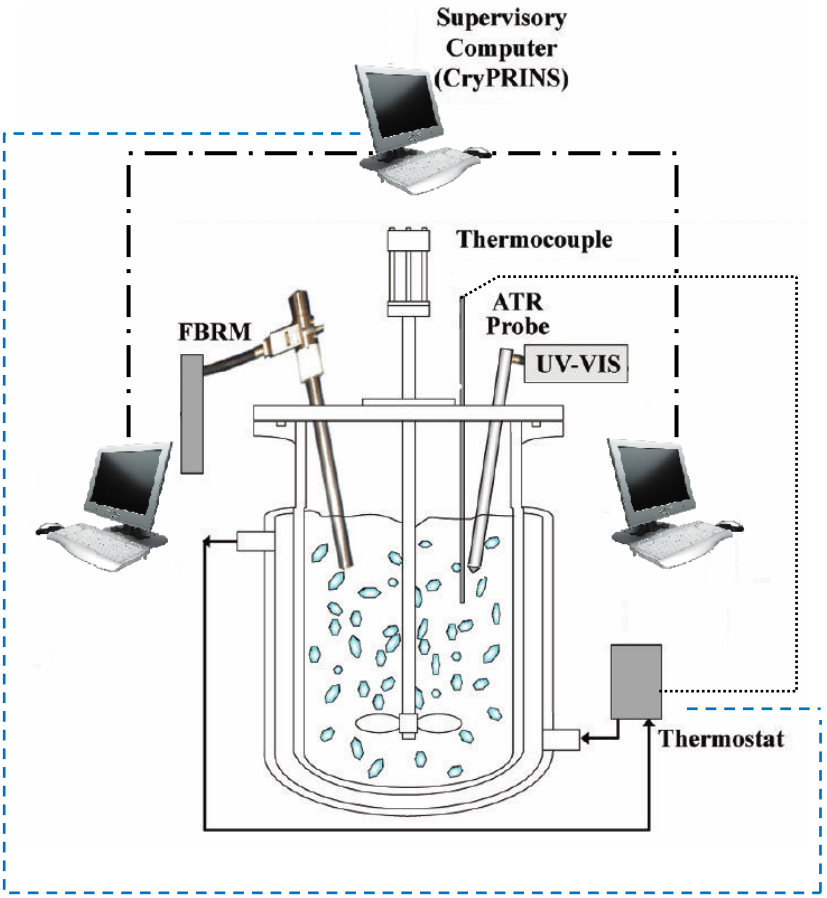


Figure 5.1: A schematic representation of the experimental set-up.

5.3.2 Materials

The experiments were carried out using pharmaceutical-grade Paracetamol (4-Acetamiphenol, 98% purity, purchased from Aldrich) and Analytical grade 2-

Propanol (isoPropanol, IPA). Based on a saturation temperature of 323.16 K, the solution was prepared by mixing 63.02 g of Paracetamol in 300 g of IPA. Crystalline seeds of 3.151 gm (5% of 63.02 gm Paracetamol) were added to the system. For the current study, Paracetamol in IPA was selected as the model system as it is a widely used compound and relevant solubility data are easily available.

5.3.3 Seed Preparation

Paracetamol and IPA solution was prepared corresponding to a solubility of 21.07 g of Paracetamol per 100 g of water at 323.16 K. Paracetamol was dissolved in IPA by heating to 333.16 K at a rate of 0.67 K/min. The solution was equilibrated at 333.16 K for 15 minutes, to ensure complete dissolution of solids, and then the temperature of the solution was reduced from 333.16 K to 283.16 K following a linear cooling profile at a rate of 0.1 K/min. The solution was left at 283.16 K for 20 min so that newly nucleated crystals could grow. The crystals obtained were filtered, dried at 323.16 K for two hours, and then sieved using laboratory scale sieves. The consecutive sieve sizes used were 125-106 μm, 106-90 μm and 90-75 μm (coarser sizes were placed on the top and finer at the bottom).

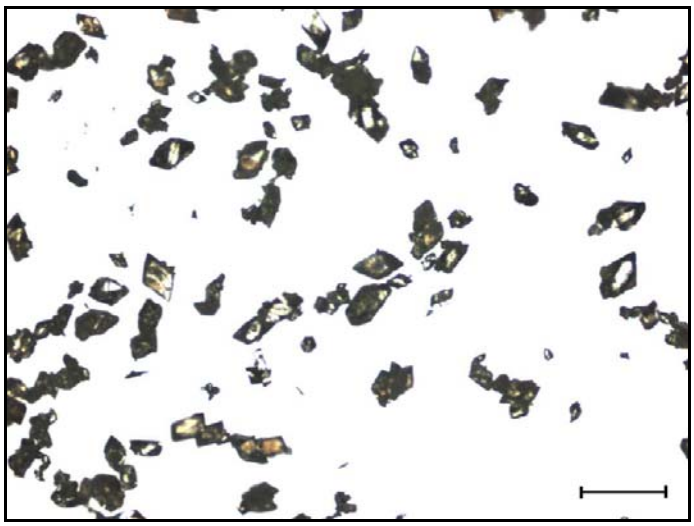


Figure 5.2: Microscopic image of seeds.

The sieving time was 120 minutes, and the shaking caused the crystals to distribute throughout the sieve stack. The product obtained between the sieve sizes of 125-75

μm was collected for seeding. The required amount of the seed mass was achieved after several batches of sieving. Microscopic images of the seeds are shown in Figure 5.2, which reveals that the crystal shape is irregular.

5.3.4 Concentration Measurement

Measurement of the solution concentration is the key to SSC of batch crystallisation systems. To maintain the operating curve along a constant supersaturation in the phase diagram the feedback controller requires continuous concentration measurement. In these experimental works an ATR-UV/Vis spectroscopy probe in conjunction with a suitable calibration model was used for concentration measurements. The applied solubility relation for Paracetamol in IPA was adopted from Hojjati and Rohani (2006). The solubility of Paracetamol in IPA is given by a second-order polynomial of Equation 5.1 (for details please see Hojjati and Rohani, 2006).

$$C_{sol}(T) = a_2 T^2 + a_1 T + a_o \tag{5.1}$$

where, a_2=0.00002742, a_1= 0.001328, and a_o = 0.072027.

The concentration is computed from the derivative of the absorbance at a characteristic wavelength of 240 – 720 nm for Paracetamol in IPA, using the calibration model of Equation 5.2 adopted from Saleemi et al. (2012b),

$$C = b_o + b_1 d + b_2 T + b_3 dT \tag{5.2}$$

where, C is the concentration in (g/g solvent), b_o, b_1, b_2 and b_3 are the regression coefficients, d is the derivative of absorbance at the selected wavelength, and T is the system temperature. The term d can either be the absorbance or the derivative of the absorbance (first or second) depending on the model selected. Since derivative absorbance can remove any baseline offset in the spectrum it was selected for this operation. A simple nonlinear term, expressed as the product of the derivative absorbance and temperature, is also included to improve the accuracy of the

calibration model (Saleemi et al., 2012b). The supersaturation is computed using the concentration measurement and the solubility information. In this study the absolute supersaturation (S) has been used, which is defined as the difference between the solution concentration and the equilibrium concentration (solubility) at a particular temperature as given by Equation 5.3,

$$S = C - C_{sol} \tag{5.3}$$

5.4 Results and Discussions

5.4.1 Results from ILC1

Figure 5.3 shows the historical data of output SWMCL values of crystals at the end of the batches against input constant supersaturation (CSS) values. The results conform to the theoretical concept of the relation between mean crystal size and increasing supersaturation (SS) for growth-dominated processes (which are controlled in a supersaturation region where nucleation is negligible), i.e. with increasing supersaturation crystal grow to larger size. However, with further increase in supersaturation crystal nucleation dominates crystal growth and the overall CSD reduces (O'Grady, 2011) as also be seen from Figure 5.3.

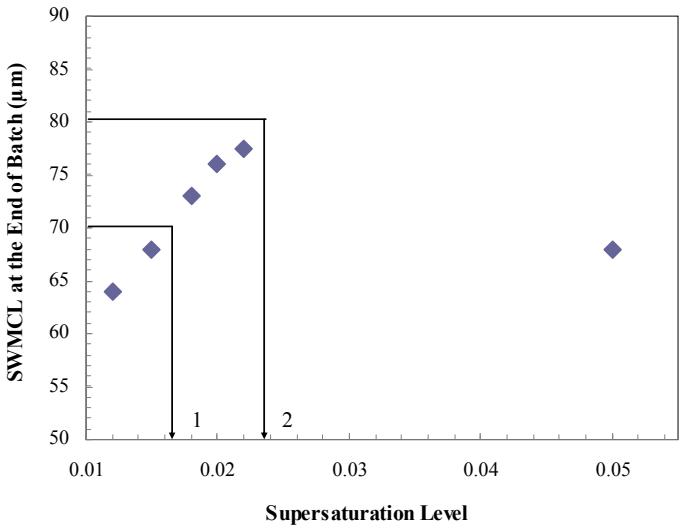


Figure 5.3: Variation in SWMCL at the end of the batch with increasing supersaturation.

Figure 5.4 shows the SWCLD at the end for the historical batches along with the SWCLD of seeds added at the beginning. The seed distribution stands at the left most side and with increasing supersaturation the SWCLD curves tend to shift to the right as they produce bigger crystals. However, the SWCLD for SS=0.05 shifted to the left again which simply confirms the drop in CSD with increasing supersaturation.

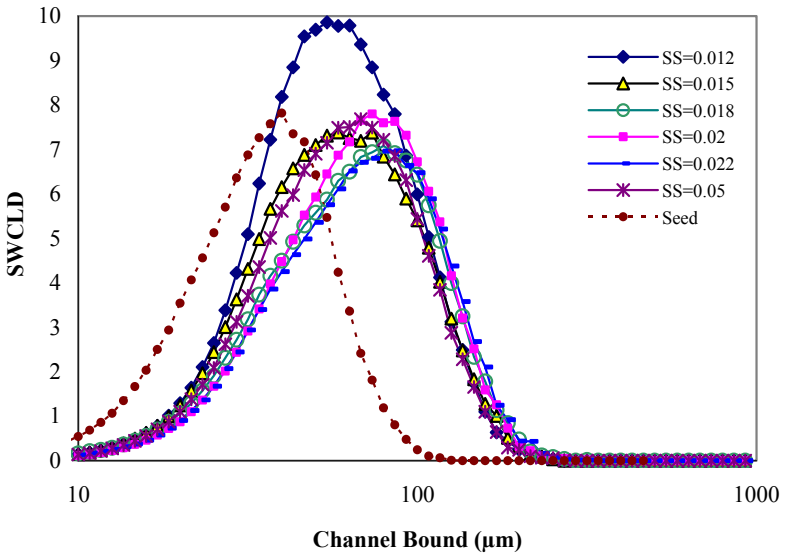


Figure 5.4: Variation in CLD at the end of the batch with increasing supersaturation.

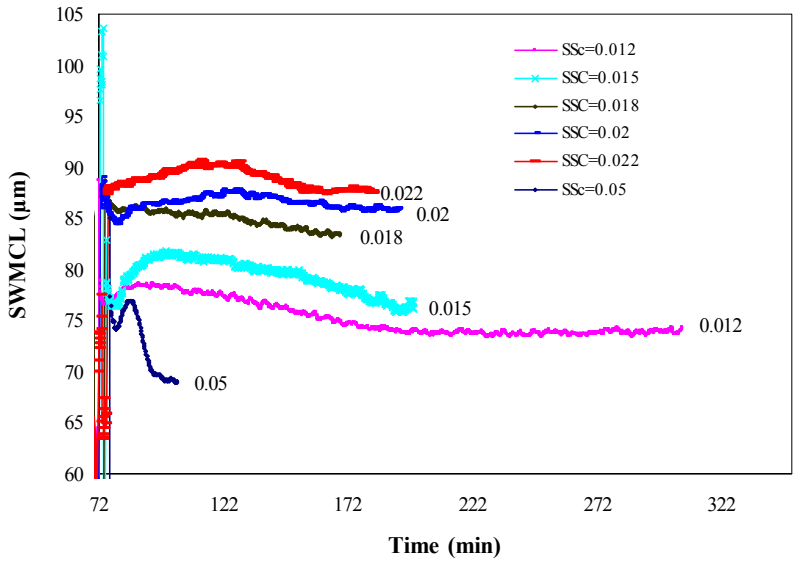


Figure 5.5: Variation in SWMCL over the batch with increasing supersaturation.

Figure 5.5 shows the SWMCL profiles for the historical batches for ILC1. This figure once again conforms to the findings in previous figures that with increasing supersaturation the SWMCL increases up to a level and then will decrease again. The nominal SWMCL was 88.5 μm and nominal CSS was 0.022. The first desired SWMCL at the end of the batch was set as 70 μm which was within the limit of these data and the second desired SWMCL was set as 80μm just outside the boundary. Based on these historical data, ILC1 calculated the desired CSS to be 0.017 for a SWMCL of 70 μm and 0.0223 for 80 μm indicated as 1 and 2 in Figure 5.3 respectively.

5.4.2 Results from ILC2

5.4.2.1 Case 1: Required SWMCL within the limit

As mentioned in Section 5.2, these experiments were performed under ILC2 framework to determine the temperature profile needed to maintain a constant supersaturation over the entire batch to produce crystal with a desired SWMCL at the end of the batch. For this particular case, the desired SWMCL was chosen to lie within the bound of historical data as indicated by Point 1 in Figure 5.3. The constant supersaturation of SS = 0.017 needed to produce a SWMCL of 70μm was determined by ILC1 experiments (see subsection 5.4.1). The objective of this case study was to evaluate the performance and robustness of the proposed HILC scheme.

Figure 5.6 (a) and Figure 5.6 (b) shows the trajectories of batches used as historical batches (HB) for ILC2 for Case 1 and Case 2, these figures include the nominal trajectories as well. All the temperature trajectories are cooling profiles and were chosen randomly (see subsection 4.4.1). The supersaturation (SS) curves were the corresponding output profiles. For all these experiments, the batch duration was 4 hr and 30 minutes and it was discretised in 9 intervals of 30 minutes to have 10 data points over the batches. For these experiments, the initial temperature was 323.16 K and the final temperature was 283.16 K, which were kept constant during all batches. A 5% (wt/wt) seed was added after the temperature reached 320.16 K in all cases.

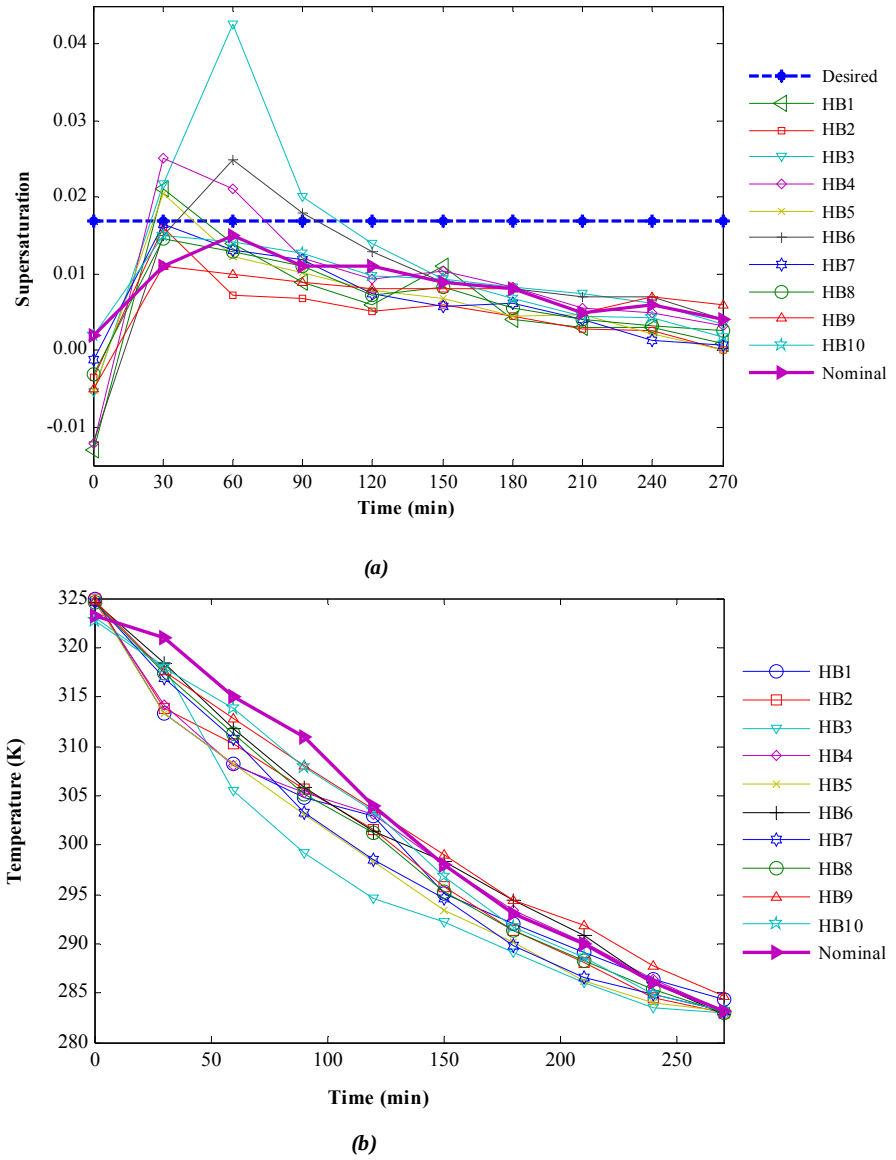


Figure 5.6: Trajectories of historical batches (a) SS trajectories (b) temperature trajectories.

Figure 5.7 (a) to Figure 5.7 (f) shows the concentration profiles in the phase diagram for these ILC2 experiments. It is evident from the figures that the concentration profiles eventually became consistent from batch-to-batch and converged to the desired SS profile at (0.017) very closely. Figure 5.8 shows the SSE plot between desired supersaturation and the actual supersaturation in the system. It also shows that the SSE eventually decreased and the experiments were terminated after the 7th batch as SSE reached a stable value for two consecutive batches.

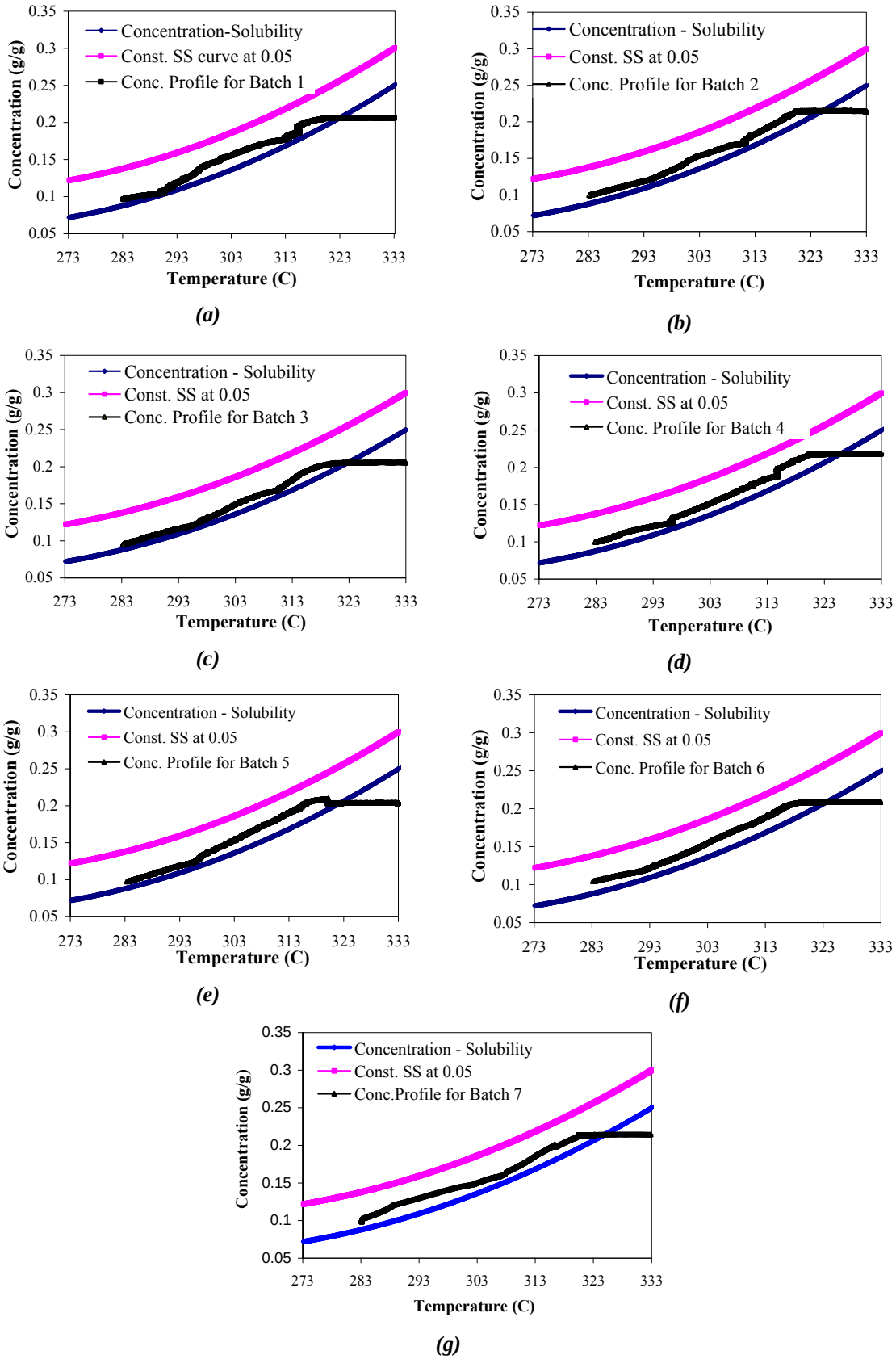


Figure 5.7: Plots for concentration profiles in the phase diagram for different experimental batches (a) Batch 1 (b) Batch 2 (c) Batch 3 (d) Batch 4 (e) Batch 5 (f) Batch 6.

Figure 5.9 shows the resulting SWMCL values for the experimental batches as obtained from FBRM data. After the 5th batch onwards the SWMCL subsided closer to the desired value of 70µm. The obtained SWMCL was 71µm after 7th batch. This error is subjected to the effect of linearising the system. Figure 5.10(a) to Figure 5.10 (g) shows the microscopic images of the crystals taken. The images reveal that from an array of irregular shaped crystals finally the crystals adopted a regular size distribution as the system approached the set-point supersaturation more closely.

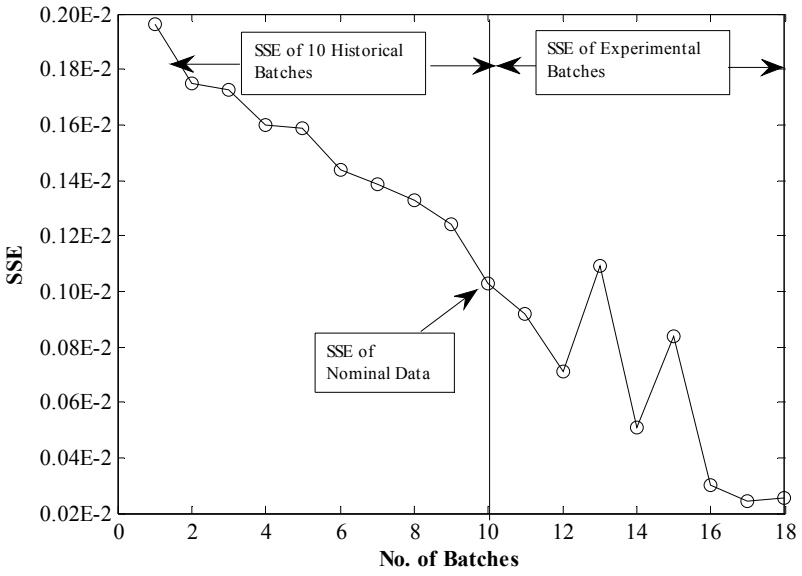


Figure 5.8: Plot for SSE for different experimental batches.

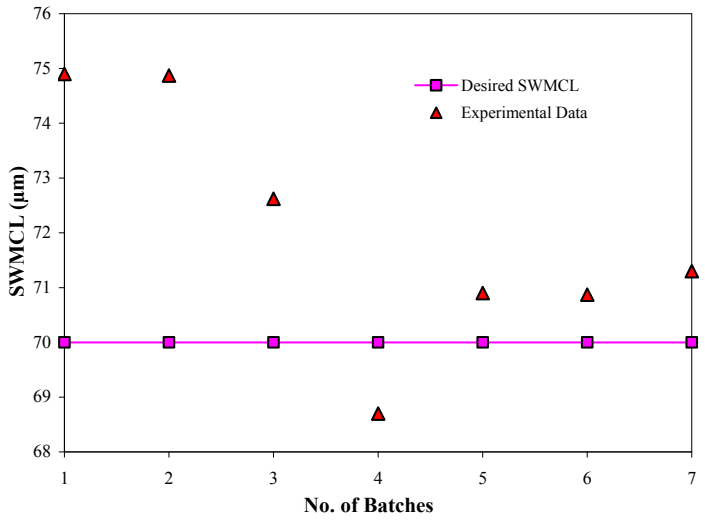


Figure 5.9: Plot for SWMCL vs. no of experimental batches for Case 1.

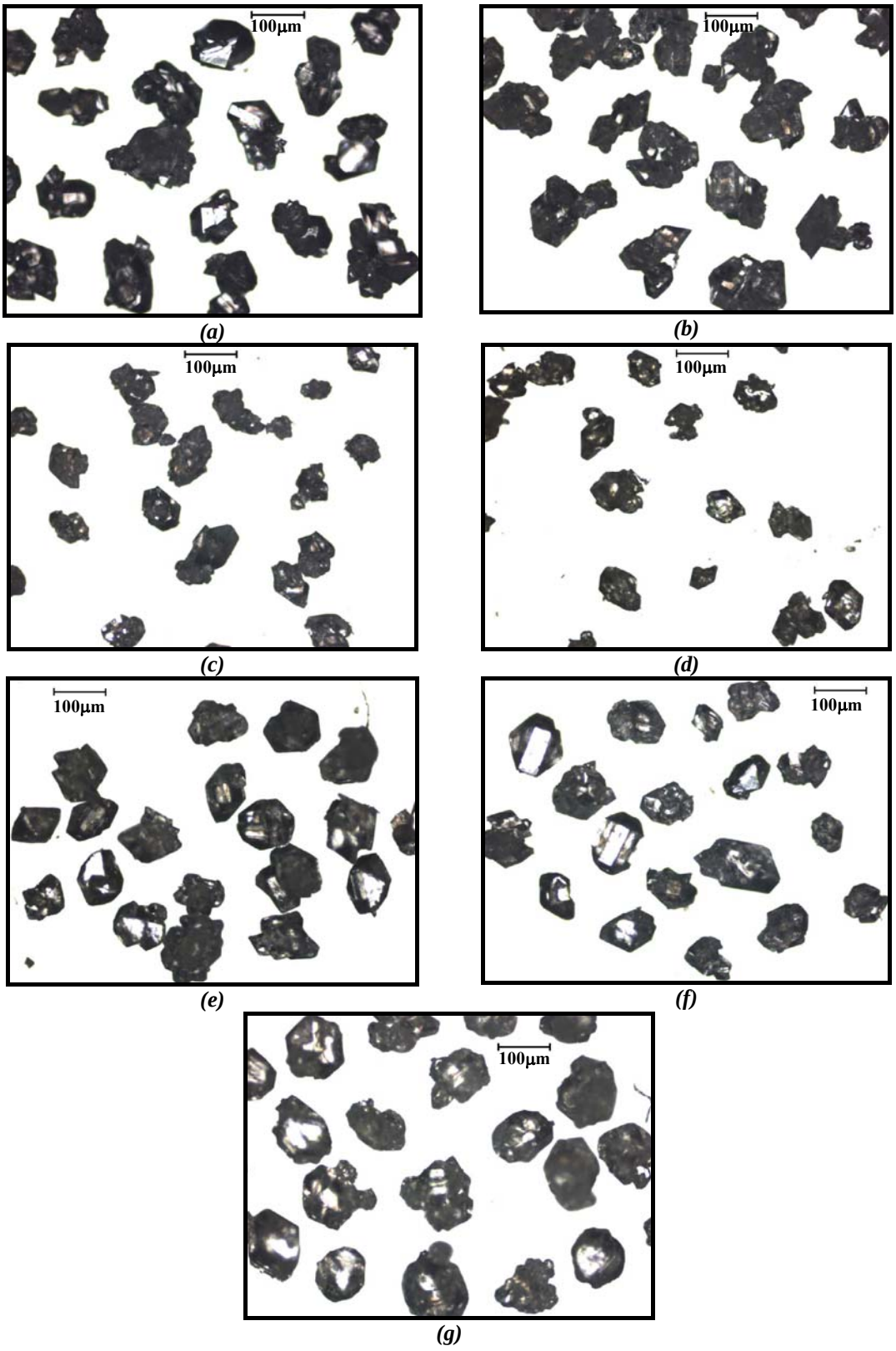


Figure 5.10: Microscopic images of crystals (a) Batch 1 (b) Batch 2 (c) Batch 3 (d) Batch (e) Batch 5 (f) Batch 6 (g) Batch 7.

5.4.2.2 Case 2: Required SWMCL outside the limit

According to Section 5.2, these case study experiments were performed under ILC2 framework to determine the temperature profile needed to maintain a constant supersaturation over the entire batch to produce crystal with a desired SWMCL at the end of the batch. For this particular case, the desired SWMCL was chosen to lie outside the bound of historical data as indicated by Point 2 in Figure 5.3. The extent of constant supersaturation required to maintain a SWMCL of 80μm was SS = 0.024 which was determined by ILC1 experiments (see subsection 5.4.1). The objective of this case study was to evaluate the extrapolation performance of the proposed HILC scheme. For Case 2 experiments, the same set of historical data was used and exactly the same procedure was followed as mention in subsection 5.4.2.1.

Figure 5.11 (a) to Figure 5.11 (g) shows the concentration profiles in the phase diagram for the ILC2 experiments. It is evident from the figures that the concentration profiles eventually became consistent from batch to batch and converged to the desired SS profile at (0.024) quite closely. This time the set-point was at a larger distance from the solubility than the previous case. Figure 5.12 shows the SSE plot between desired supersaturation and the actual supersaturation in the system. It also shows that the SSE eventually decreased and the experiments were terminated after the 7^{th} batch as SSE reached a stable value for two consecutive batches. Figure 5.13 shows the resulting SWMCL values for the experimental batches as obtained from FBRM data. It shows that SWMCL was always in the range of 78μm to 80μm, since the operating line of concentration was hovering in the same region of the phase diagram and shifting slowly to the desired set-point supersaturation. This is also indicated by Figure 5.12 which shows that the SSE was quite larger than the previous case. The obtained SWMCL was 79μm after 7^{th} batch. This error is subjected to the effect of linearising the system. However, this SWMCL is in good consistency of the findings in Figure 5.3. Figure 5.14 (a) to Figure 5.14 (g) shows the microscopic images of the crystals taken. The images reveal that from an array of irregular shaped crystals finally the crystals adopted a regular size distribution as the system approached the set-point supersaturation more closely.

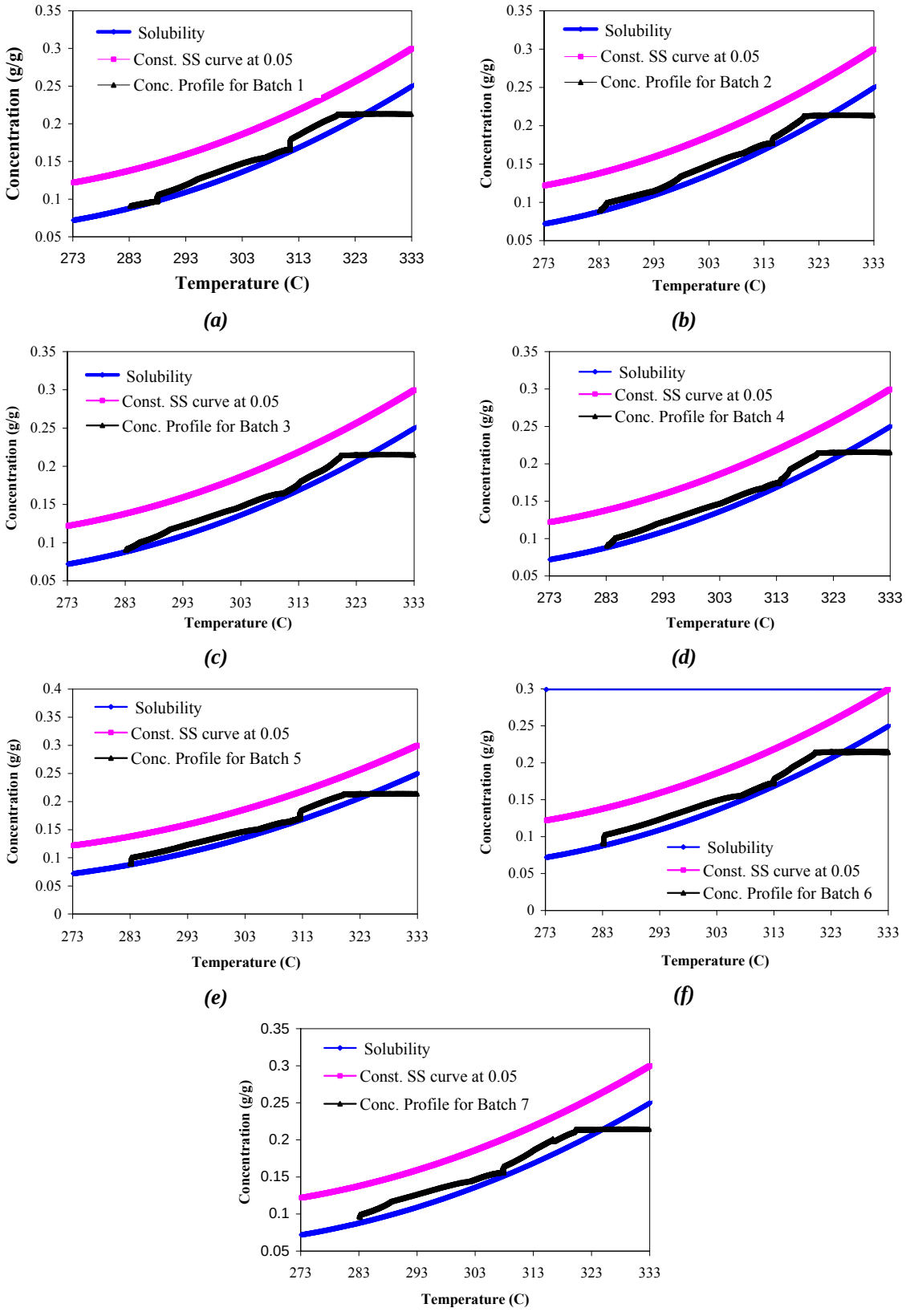


Figure 5.11: Phase diagrams for (a) Batch 1 (b) Batch 2 (c) Batch 3 (d) Batch 4 (e) Batch 5 (f) Batch 6 (g) Batch 7.

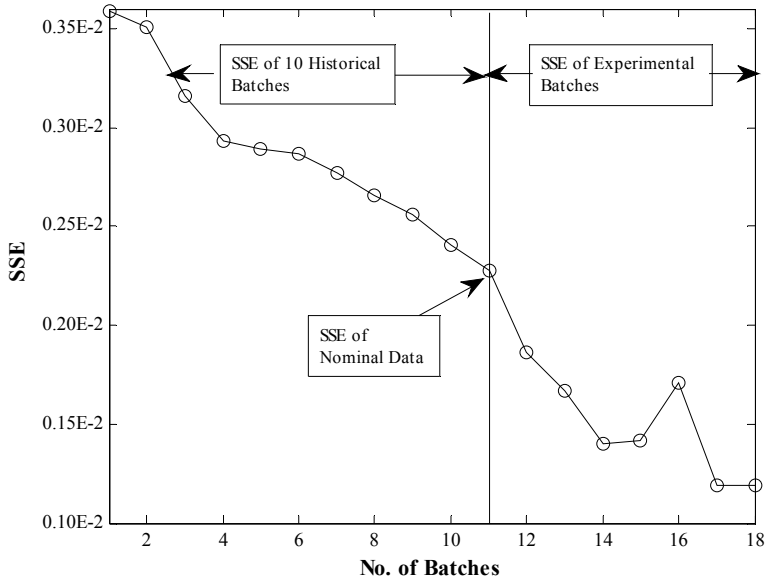


Figure 5.12: Plot for SSE for different experimental batches.

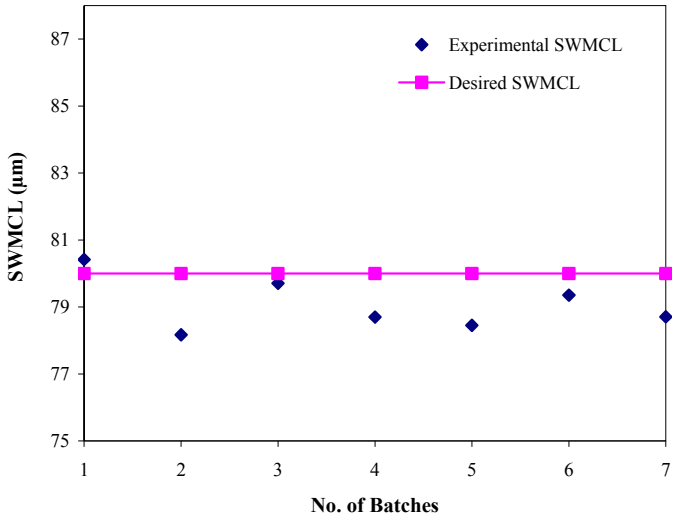


Figure 5.13: Plot for SWMCL vs. no of experimental batches for Case 2.

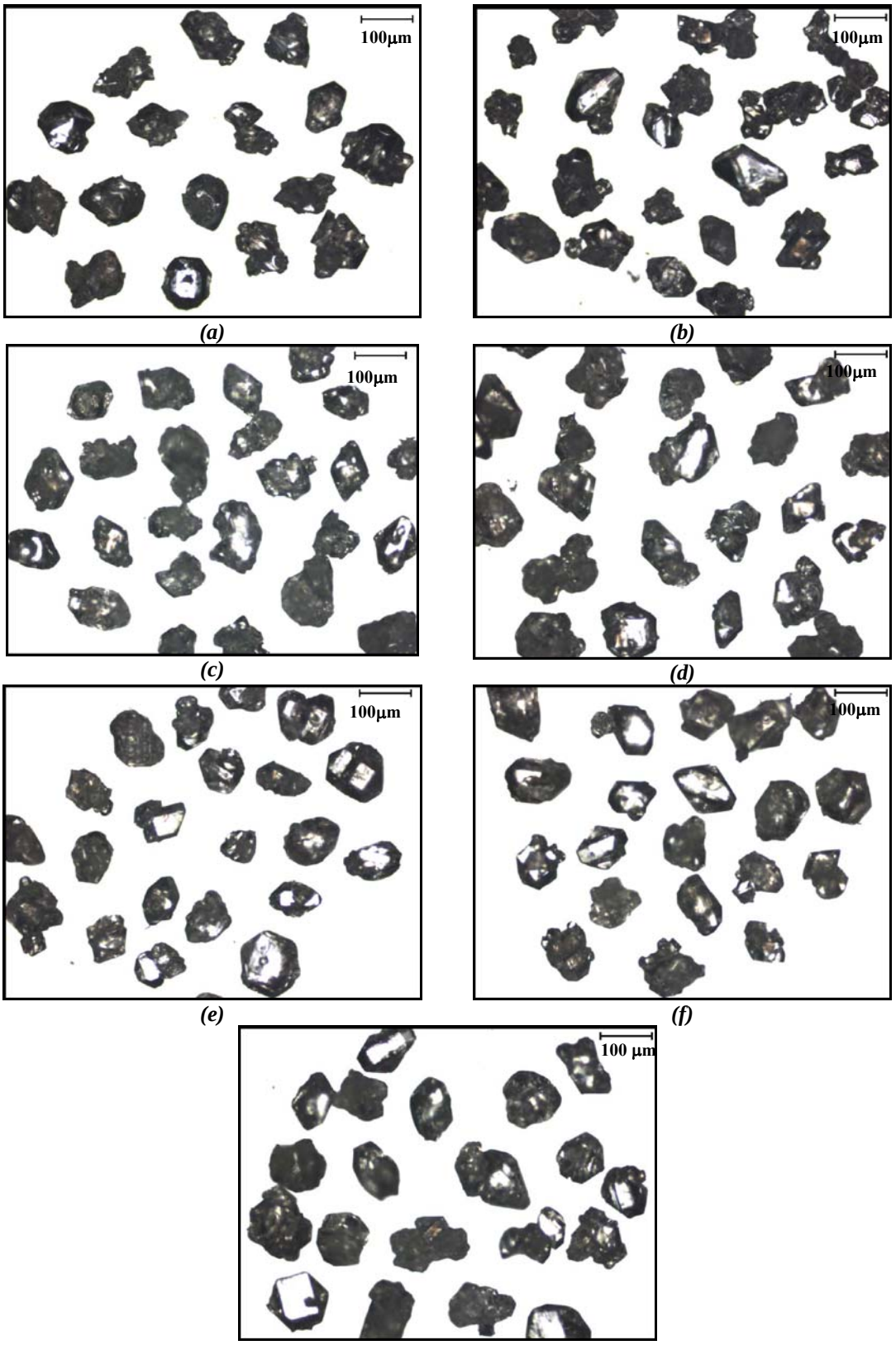


Figure 5.14: Microscopic images of crystals (a) Batch 1 (b) Batch 2 (c) Batch 3 (d) Batch (e) Batch 5 (f) Batch 6 (g) Batch 7.

5.5 Conclusions

In this chapter the proposed hierarchical ILC (HILC) for systematic design of supersaturation control of seeded batch cooling crystallisation (please see Chapter 4) was evaluated through laboratory scale experiments. The system was Paracetamol in IPA. The results from the two case studies indicate that HILC could converge to the desired set points closely. However, there is some discrepancy due to the linearisation of the system. This chapter also presents a successful application of various PAT tools (e.g. FBRM, UV/Vis probe) in robust optimal automated control of batch cooling crystallisation processes**.** Therefore, the proposed HILC can be used as a systematic design tool to select the required extent of supersaturation to produce crystals with desired end property. This is a simple data based approach hence does not require model building, extensive modelling or experimentation.

Chapter 6

Direct Nucleation Control (DNC) Approach for Controlling Batch Crystallisation Processes

6.1 Overview

This chapter presents a systematic evaluation of direct nucleation control (DNC) approach of controlling batch cooling crystallisation systems. DNC, as named is aimed to control nucleation events to achieve the desired crystal size distribution (CSD) in a model free approach that requires no prior knowledge on nucleation or growth kinetics of the system and responds immediately to any unexpected disturbances. In order to examine the performance and robustness of proposed DNC approaches computer simulations were done in two phases and a novel twofold systematic evaluation of the proposed DNC approaches has been described in this chapter. Laboratory experimental results have also been included to justify the results of simulation case studies.

6.2 Direct Nucleation Control (DNC) Approaches

In crystallisation processes, focused beam reflectance measurement (FBRM) is used to provide both real time qualitative and quantitative information about nucleation and growth. It is often used as a complementary tool alongside other PAT tools (e.g. ATR-UV/Vis, BVI) for monitoring purpose or to trigger the switching between different predetermined operating conditions (Saleemi et al., 2012a) in open loop control and rarely used as a direct control tool (Chew et al., 2007b; Woo et al., 2009). Recently, Abu Bakar et al. (2009) proposed a novel model-free real time feedback control approach, that uses FBRM measurements. This approach, called direct nucleation control (DNC), relates the chord length distributions measurements to the

number and size of the particles present in the system to maintain a desired number of FBRM counts during the entire duration of crystallisation.

The operating profile of conventional DNC in the phase diagram is represented in Figure 6.1. The main idea behind DNC approach is to automatically alter from cooling to heating cycles to generate nucleation or fines dissolution, for maintaining the number of counts/s at desired level. In the event, the number of counts/s exceeds the desired value or a certain acceptable limit, the system's temperature increases causing the excess particles to be dissolved, which drives the process close to the solubility curve until the number of counts/s decreases. This controversial idea of including heating steps in typical cooling crystallisation concept benefits the system by providing in situ fine removal and eradicating the need for external heating loop installation.

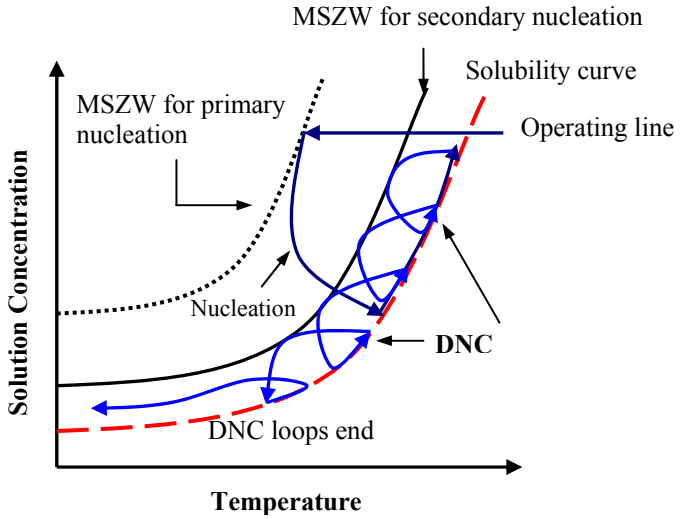


Figure 6.1: Conventional DNC operating profile in the phase diagram.

The different DNC algorithms proposed in this work is described below in brief. The minimum and maximum temperature limits were specified for the system.

6.2.1 Simple DNC Approach

Figure 6.2(a) illustrates the algorithm of simple DNC. In this approach, there are no upper and lower limits on the number of counts/s. The system simply switches

between cooling and heating as it crosses the desired target counts and continues the heating and cooling cycles until the total counts have stabilised close to the target value and the crystalliser temperature at its minimum limit.

6.2.2 Predictive DNC Approach

Figure 6.2(b) illustrates the algorithm of predictive DNC, used to maintain the total counts/s at its target value. In this method an upper and lower limits were used along with the target number of counts/s setpoint. Initially when everything is dissolved, the process starts cooling at a specified rate until the nucleation takes place and counts/s reached the lower limit. As it crosses the lower limit, the cooling rate is slowed until the upper limit is reached. After crossing the upper limit, the system adapts fast heating mode to facilitate the dissolution of fine particles and drives the number of counts/s measurements to fall below the upper limit. This turns on slow heating and keeps the system in heating mode until the counts is above the lower limit. The heating and cooling cycles continue until the total counts have stabilised in the specified range and the crystalliser temperature is at its minimum limit.

6.2.3 Reverse DNC Approach

Figure 6.2(c) illustrates the algorithm of reverse DNC. As described earlier, upper and lower limits on the number of counts/s were used. Initially when everything is dissolved, the process starts cooling at a specified rate to start nucleation and drive the counts/s to reach the lower limit. As it crosses the lower limit, the system switches to slow heating to suppress excess nucleation until the upper limit is reached. After crossing the upper limit, the system adapts fast heating mode to facilitate dissolution of fine particles and drives the number of counts/s to fall below the upper limit. This turns on slow cooling to prevent rapid dissolution of particles and keeps the system in slow cooling mode until the counts reside above the lower limit. The heating and cooling cycles continue until total counts have stabilised in the specified range and the temperature is at its minimum limit.

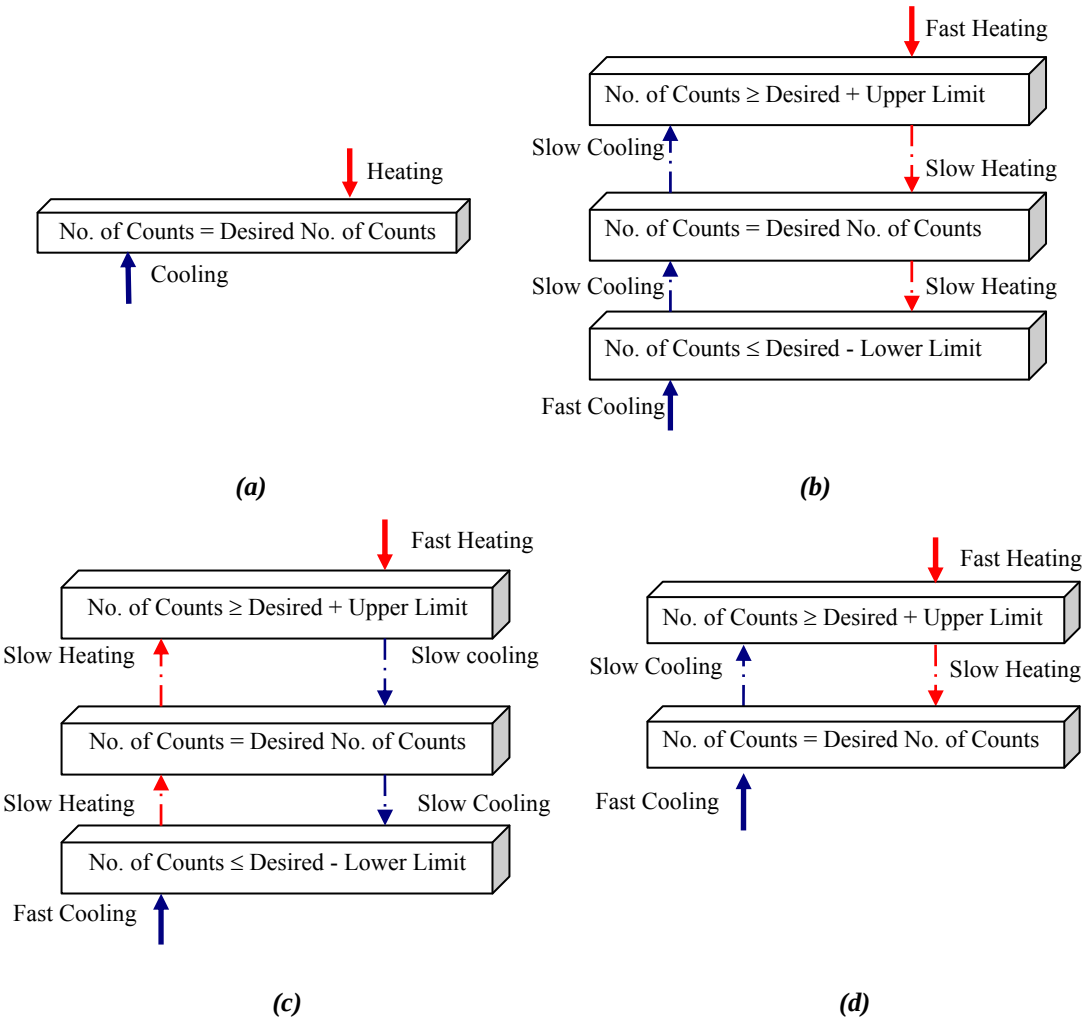


Figure 6.2: Algorithms of different DNC approach (a) Simple DNC (b) Predictive DNC (c) Reverse DNC (d) Basic DNC.

6.2.4 Basic DNC Approach

Figure 6.2(d) illustrates the algorithm of conventional DNC (Abu Bakar et al., 2009) used to maintain the total counts/s at its target value. In this method an upper limit was used along with the target setpoint. Initially when everything is dissolved, the process starts cooling at a specified rate until the nucleation takes place and counts/s reached the target. As it crosses the target, the cooling rate is slowed until the upper limit is reached. After crossing the upper limit, the system adapts fast heating mode to facilitate dissolution of fine particles and drives the number of counts/s measurements to fall below the upper limit. This turns on slow heating and keeps the system in heating mode until the counts is above the target. Once the number of counts/s falls

below the target, the system starts faster cooling again. One intelligent aspect is that, it itself can recognize whether it is in cooling or heating modes while changing from faster to slower cooling rates and vice versa. The heating and cooling cycles continue until the total counts have stabilised in the specified range and the crystalliser temperature at its minimum limit.

In practice, during crystallisation processes, FBRM provides thousands of individual cord length measurements through its channels. The summation of the number of cord lengths detected gives the total number of counts/s (#/s) in the system. In this work, imitating the real life FBRM measurements, the total number of counts/s from a simulated system of Paracetamol in water is continuously sent to the simulated nucleation controller, where the measurement is compared against the target counts/s and the vessel jacket temperature (T_{jacket}) was controlled accordingly. As the operating profile is always based on the real time detection of nucleation and dissolution events, the proposed approach is free from pre-designing a temperature profile.

In order to examine its performance and robustness of the proposed DNC approaches, a comparison study has been carried out between a first principle model based optimal control and the model-free DNC approach. Computer simulations were done using an unseeded batch cooling crystallisation system of Paracetamol in water developed in MATLAB®. In the first phase, the mechanistic model was used to solve an open loop optimal control problem where the objective was to maximise the mean crystal length within a fixed batch time. The successive quadratic programming solution provides the optimal temperature trajectory, corresponding number of counts and the total length. In the second phase, treating the MATLAB® model as the real process the performance of DNC was evaluated by setting the optimal number of counts as the control target. In addition, the DNC approach itself was evaluated by changing the algorithm of the DNC; varying the acceptable range of counts limits; increasing and decreasing the target of counts/s; and changing the heating and cooling rates for the same system. The results identified the advantages and disadvantages of different

DNC structures in terms of producing large uniform crystals, reduced number of cooling-heating loops, reduced batch time while maintaining the same yield.

6.3 Experimental Set-up and Materials

The experimental set-up was the same as described in the subsection 5.3.2 in Chapter 5. The only difference was that a PVM probe, Model V819 by Mettler Toledo was inserted in to the system to capture in situ images of the crystals. The probe was connected to a third computer to store the image sequences captured.

The laboratory experiments were carried out using pharmaceutical-grade Paracetamol (4- acetaminophenol, 98% purity, purchased from Aldrich) and Analytical grade 2-Propanol (isopropanol, IPA). The solute (paracetamol in IPA) concentration in all experiments was 0.21 g g^{-1} solvent.

Two DNC experiments, one Basic DNC and one Simple DNC were performed under similar experimental conditions using the same experimental setup. The target was 4000 counts/s with a cooling rate of -0.3 °K/min and heating rate of 0.K °C/min. For Basic DNC the acceptable range was ±200 counts/s. In both experiments, the cooling was initiated after complete dissolution and was continued until primary nucleation occurred (in situ seed generation).

6.4 Results and Discussions

6.4.1 Simulation Case Studies

Batch Cooling Crystalliser

A simulation program was developed in MATLAB® for Paracetamol in water system to treat as the real process. The kinetics of this unseeded system has been described in subsection 3.3.2. As previous case studies, the initial and final temperatures were 314.13K and 294.15K respectively. The model parameters are shown in Table 6.1.

Table 6.1: Parameters of the Crystallisation Model

Solubility in water (T in K)	$C_S = 1.58\times10^{-5}T^2 - 9.057\times10^{-3}T + 1.31$
Growth rate	$G = \begin{cases} 1.64\times S^{1.54} \; if \;\; S > 0 \\ -1.644\times S \;\; if \;\; S \le 0 \end{cases}$
Nucleation rate	$B = \begin{cases} 7.8529\times10^{19} 4\times S^{7.8} + 1.3\times10^{20} 4\times S^{5.8}\mu_3 \;\; if \;\; S > 0 \\ -7.8529\times10^{19} 4\times S^{3.8} \;\; if \;\; S \le 0 \end{cases}$
Density of crystal (g/cm^3)	ρ = 1.296
Volumetric shape factor	k_v = 0.24
Initial concentration (g/g solvent)	C_0 = 0.0254

The unseeded nucleation rate for the system is given as,

$$B = K_a S^a + K_b S^b \mu_3 \;\; and \;\; b < a \tag{6.4}$$

where, $K_a S^a$ stands for primary nucleation and $K_b S^b \mu_3$ for secondary nucleation. Figure 6.3 shows the nucleation rate, B against S. It is evident from the plot that, while only primary nucleation is considered, the rate increases very slowly for smaller supersaturation and only when the system goes far in the metastable zone (i.e. higher supesaturation) the rate increases considerably. In case of a combined primary and secondary nucleation system, initially primary nucleation dominates until the surface area of the crystals are large enough for substantial secondary nucleation to occur, which then accelerates the formation of number of counts/s even for a smaller supersaturation.

Another, important aspect of this model is the inclusion of dissolution and disappearance rates (negative G and B respectively, when $S \le 0$. These rates are as important as nucleation and growth rates in batch crystallisation, to produce a uniform and reproducible CSD (Nagy et al., 2011). During the process, different sizes of crystals are present in the system due to simultaneous nucleation and growth, attrition, breakage and agglomeration. A controlled dissolution event dissolves out small crystals (fines dissolution) and aids the production of large crystals. Hence, a combined mechanism of nucleation-growth-dissolution provides better control over batch crystallisation. For this system, since the growth rate is slower than nucleation

rate as given in Table 6.1, the system is nucleation dominated and both dissolution and disappearance rates are faster than nucleation and growth rates as expected.

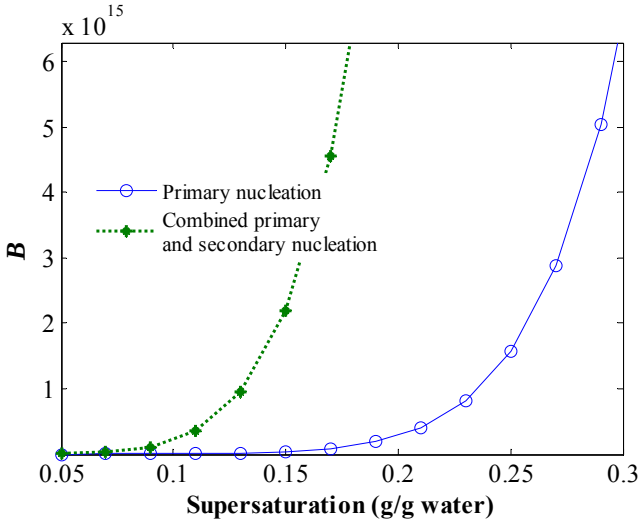


Figure 6.3: Primary and secondary nucleation rates.

6.4.1.1 Phase 1: Model Based Open Loop Optimal Control

The simulation model developed above is used to optimise its performance. In open loop optimal control of a batch process generally the time profile of the manipulated variable is determined that optimises the process performance. For a batch cooling crystalliser, the manipulated variable is reactor jacket temperature T_{jacket}. In this work, the objective function was to maximise the mean crystal size (Ln) defined in Equation 6.5, leading to the optimal control problem of Equation 6.6.

$$Ln = \frac{\mu_1}{\mu_0} \tag{6.5}$$

$$\max_{T(1),T(2),.....,T(N)} Ln \tag{6.6}$$

The system is subjected to the following constraints,

$$\begin{aligned} &T_{\min} \le T(k) \le T_{\max}, \\ &R_{\min} \le dT/dt \le R_{\max}, \text{ and} \\ &C_{final} \le C_{final,\max} \end{aligned} \tag{6.7}$$

where, $T_{\min}$, $T_{\max}$, $R_{\min}$, and $R_{\max}$ are the minimum and maximum temperatures and temperature ramp rates, respectively, during the batch. The first two inequality constraints ensure that the optimised temperature profile is implementable. The last inequality constraint is imposed to ensure minimum yield as specified by economic considerations (Miller and Rawlings, 1994; Nagy et al., 2008a). The optimisation problem is solved using a sequential quadratic programming (SQP) approach implemented in the MATLAB® function *fmincon*. Figure 6.4 (a) shows the optimal temperature trajectory. Initially the temperature drops to create nuclei by primary nucleation (Doki et al., 2002) after that secondary nucleation takes hold and temperature decreases at different rates. The mean length of crystals increase steadily (please see Figure 6.4 (a)) with the maximum value at the end of the batch equal to 0.015 cm. The $C(T)$ trajectory corresponding to the optimum temperature profile from Figure 6.4 (a) is shown in Figure 6.4 (b).

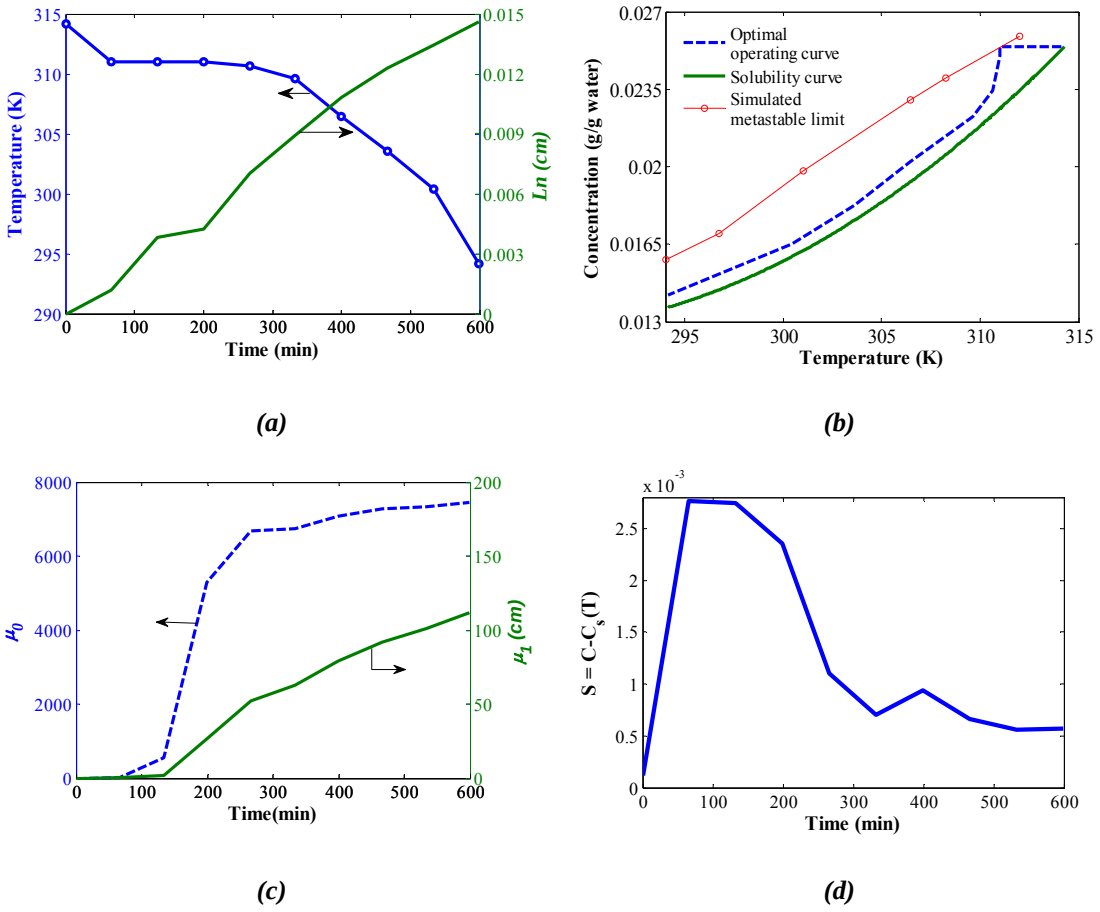


Figure 6.4: Simulated optimum profiles (a) temperature profile and change in mean length (b) concentration profile with simulated metastable limit (c) number of counts/s and total length (d) supersaturation profile.

The optimum temperature profile creates a higher supersaturation at the beginning to generate the initial nuclei, and then it keeps a nearly constant supersaturation within the metastable zone for remaining of the batch as expected for an unseeded system. In this work, the metastable limit was generated by simulating six batches of linear cooling crystallisation system for different initial temperature leading to different initial concentration. From all these simulations, the point of maximum supersaturation was noted and plotted in the concentration vs. temperature plot (see Figure 6.4 (b)). Figure 6.4 (c) shows optimal number of counts and corresponding total length with time. Figure 6.4 (d) shows the supersaturation profile; initially the high driving force for the growth of seed crystals causes the supersaturation to achieve its peak value at about 66 minute. After the initial peak at around 66 minutes to 134 minutes, the supersaturation raises again during 400 minute leading to additional nucleation events and growth.

6.4.1.2 Phase 2: Evaluation of Different DNC Algorithms

In the second phase of simulation case studies, various structures of DNC (simple, predictive, reverse and basic) were evaluated. Under each structure the target number of counts/s were changed as, i) optimal counts; ii) 100% increase in optimal counts; and iii) 50% reduction in optimal counts, and under each target various acceptable ranges (e.g. $\pm 500; \pm 1000; \text{and} \pm 100$) were tested where applicable. Equation 6.8 shows the expression of the controller that was used in the DNC algorithm to calculate the successive temperatures (T).

$$T(i+1) = T(i) \pm R \times \Delta t \tag{6.8}$$

where, $i = 1,2,3,...,N$ and N is the total number of observation at an interval (Δt) of 40 seconds throughout the batch, R is the rate of cooling and heating (i.e. $+R$ is the heating rate and $-R$ is the cooling rate).

The crucial design parameters of the DNC approach are the cooling and heating rates. Initially for a new system, it requires some trial runs to tune the cooling and heating rates to their bests. Conventionally, for a system that is nucleation dominated, lower cooling rates are preferable. It was observed that the present system was growth

dominated; hence, the determined cooling rates were higher than the heating rates in all case. Another important point to be noted that though the heating rates were almost the same for all the cases, the system was quite sensitive to the rate of cooling. A higher cooling rate (for both fast and slow cooling) is required for a larger target and vice versa. Selection of an appropriate cooling rate is a challenge because a wrong rate may take the system far away from the metastable zone resulting in excessive nucleation or render the system in overheated condition resulting in very small or no crystals at all. Finally, after several trial runs the appropriate cooling and heating rates were carefully selected so that the operating curve (OC) does not cross the solubility curve (SC) and go to the undersaturated region during the simulation case studies as discussed below.

Case 1: The Simple DNC

The Simple DNC structure was investigated to understand the impact of introducing heating steps in typical cooling crystallisation systems and to compare the approach with model based optimal control. Figure 6.4 (a-c) shows the target counts/s along with the temperature profile for different cases. In each case there is zero offset with respect to counts/s. However, the system took the longest batch time of 1000 minutes for the optimal target case. The temperature profile shows instability resulting in too many heating-cooling loops in the phase diagrams of Figure 6.6 (a-c) where OC is the operating curve and SC is the solubility curve.

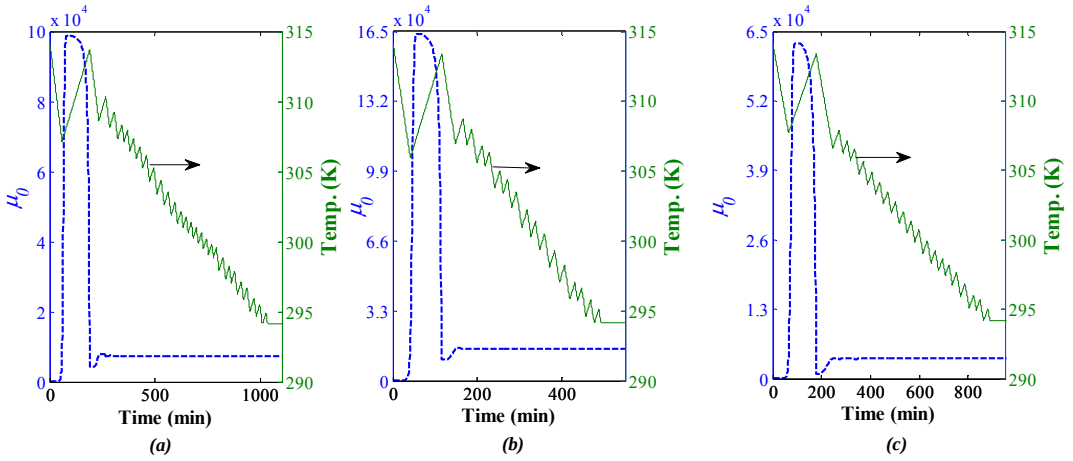


Figure 6.5: Counts/s and temperature profiles for simple DNC when the target is (a) optimal counts/s (b) doubled optimal counts/s (c) optimal counts/s is reduced by 50%.

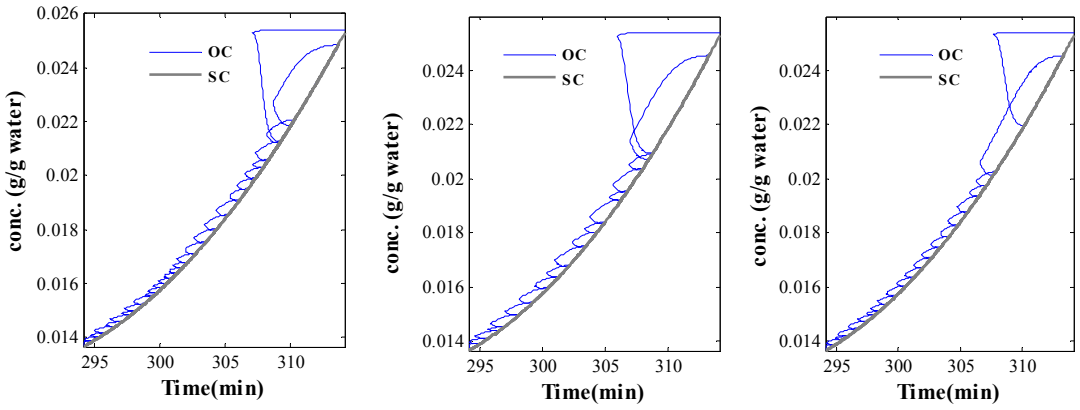


Figure 6.6: Cooling-heating cycles in simple DNC approach when the target is (a) optimal counts/s (b) doubled optimal counts/s (c) optimal counts/s is reduced by 50%.

Case 2: Applying the Predictive DNC Approach

The aim of this experiment was to understand the impact of using acceptable ranges of target counts/s, as well as, its impact on batch time and offset. Figure 6.7 (a-c) shows, how the set point target of counts/s was achieved along with the mean length and temperature profile when optimal counts/s is the target. System's responses with different acceptable ranges were plotted in the same plot to compare their effects. It is shown clearly that, with a smaller acceptable range of ± 100 counts/s, the target was achieved very closely (offset is 65.8) and for the largest range of ± 1000 counts/s, it was the maximum (offset is -744) from the target as expected. In addition, the initial overshoot was less for case; Target Counts (TC) ± 1000, as it started to slow down the cooling rate earlier and it took least time to stabilise because of its less sensitivity to the target. For all cases, the mean length of crystals were three times greater than the optimal mean length of 0.015 cm with the maximum achieved by TC ± 1000 case of 0.048 cm. This was because, in these studies the yield achieved was 3.5 % greater than the optimal case. All three simulations took 220 to 280 minutes to finish which was less than the time used in the optimal case study. All the cases started from 314 K and ended at 294.15 K. Similar results were obtained for cases, when the target was double the optimal counts/s and half the optimal counts/s as shown in Figures 6.8 (a-c) and Figure 6.9 (a-c) respectively. Figure 6.10 shows the temperature loops created by the operating curve (OC) in phase diagram.

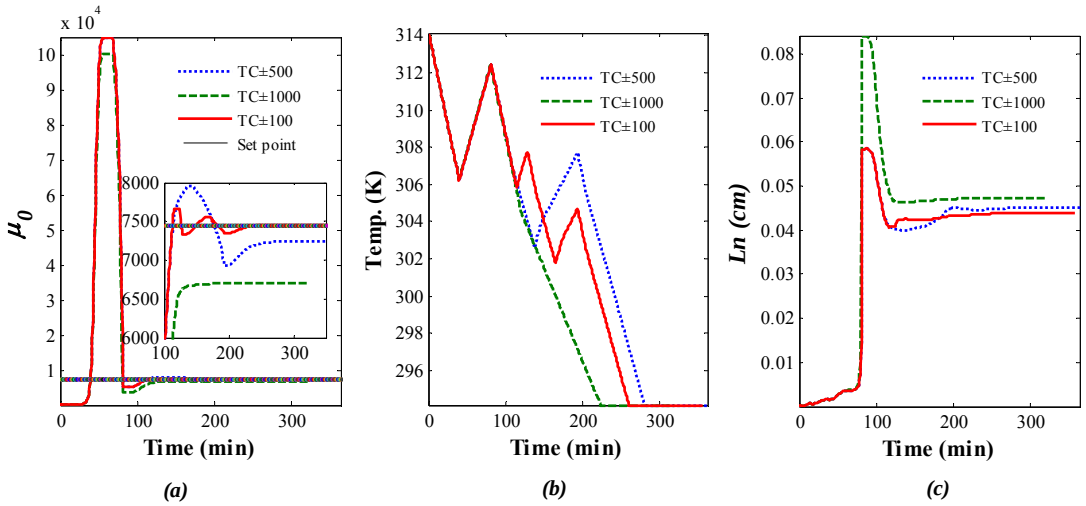


Figure 6.7: Predictive DNC (a) counts/s (b) mean length (c) temperature profile when optimal counts/s is the target.

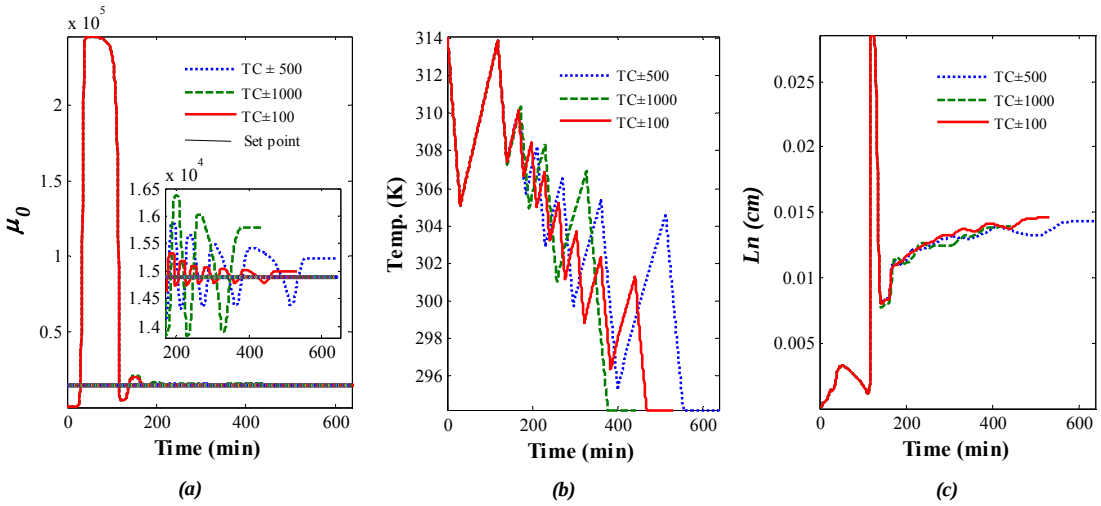


Figure 6.8: Predictive DNC (a) counts/s (b) mean length (c) temperature profile when optimal counts/s is doubled and set as the target.

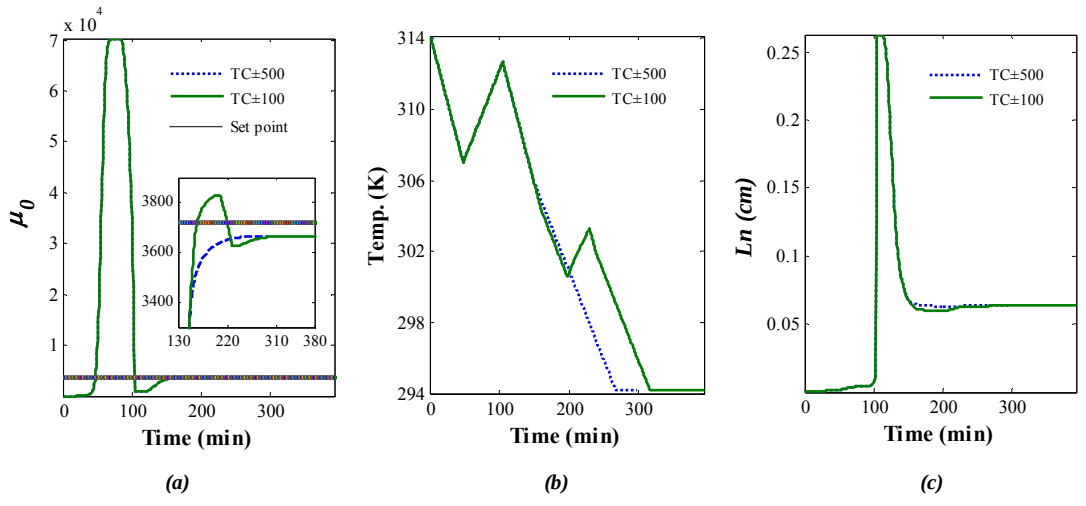


Figure 6.9: Predictive DNC a) counts/s b) mean length c) temperature profile when optimal counts/s is reduced by 50% and set as the target.

For all cases, the number of cycles increases with the decrease of acceptable ranges as the system becomes more target sensitive. In addition it took longer batch time and more temperature loops as the target counts/s was set double of the optimal counts/s.

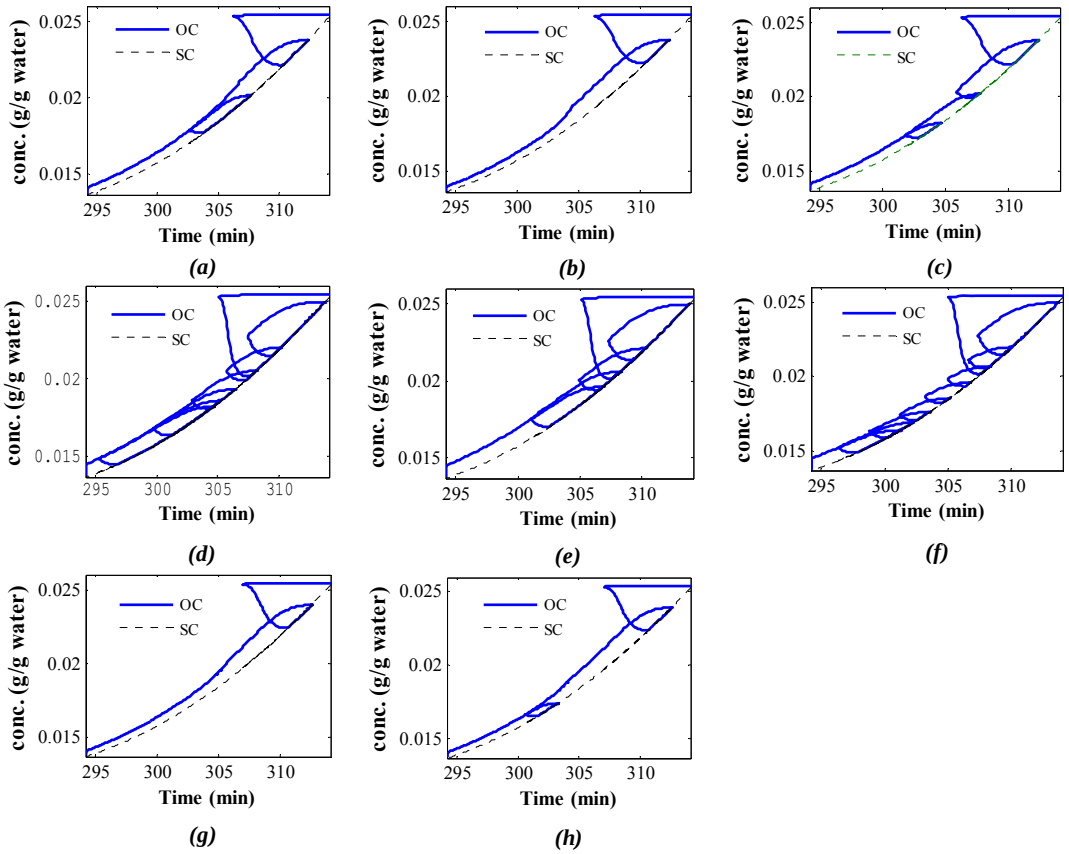


Figure 6.10: Cooling-heating cycles in Predictive DNC approach with target limits (a) optimal counts ±500 (b) optimal counts ±1000 (c) optimal counts ±100 (d) double of optimal counts ±500 (e) double of optimal counts ±1000 (f) double of optimal counts ±100 (g) half of optimal counts ±500 (h) half of optimal counts ±100.

Case 3: Applying the Reverse DNC Approach

The aim of this experiment was to investigate the effect of a different DNC structure on offset, batch time and temperature loops. Figure 6.11 (a-c) shows, how the set point target of counts/s was achieved along the temperature profile when optimal counts/s is the target. System's responses with different acceptable ranges were plotted in the same plot to compare their effects. It is shown clearly that, in this case the batch time reduces for TC±100 case (see Figure 6.11 and Figure 6.12). The inclusion of heating as the counts/s crosses the target limit made the system more unstable with many smaller cooling-heating cycles. The minimum offset was 100 for

TC±100 case and it was 35% larger than the predictive DNC. It was also observed that this structure has the tendency of oscillating either around the upper or lower acceptable limit. Batch times increased as compared to the conventional DNC cases by about 100 minutes and for the TC± 500 case, batch time was greater than the optimal batch time as well. Similar results were obtained for the case where the target was double the optimal counts/s. Figure 6.13 shows the temperature loops in phase diagram. As it is seen in the temperature profiles (please see Figure 6.11 (b) and Figure 6.12 (b)), there are many temperature loops created in this structure.

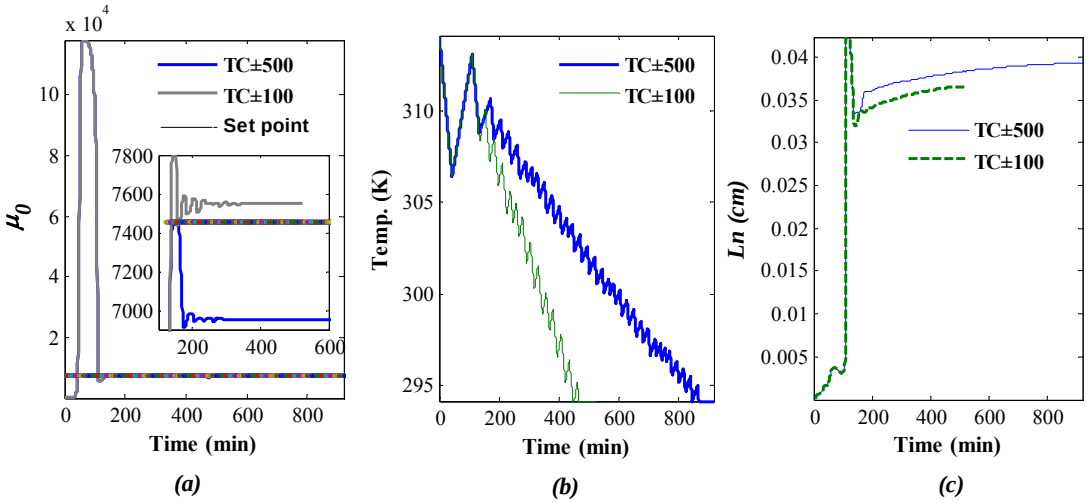


Figure 6.11: Reverse DNC (a) counts/s (b) mean length (c) temperature profile when optimal counts/s is the target.

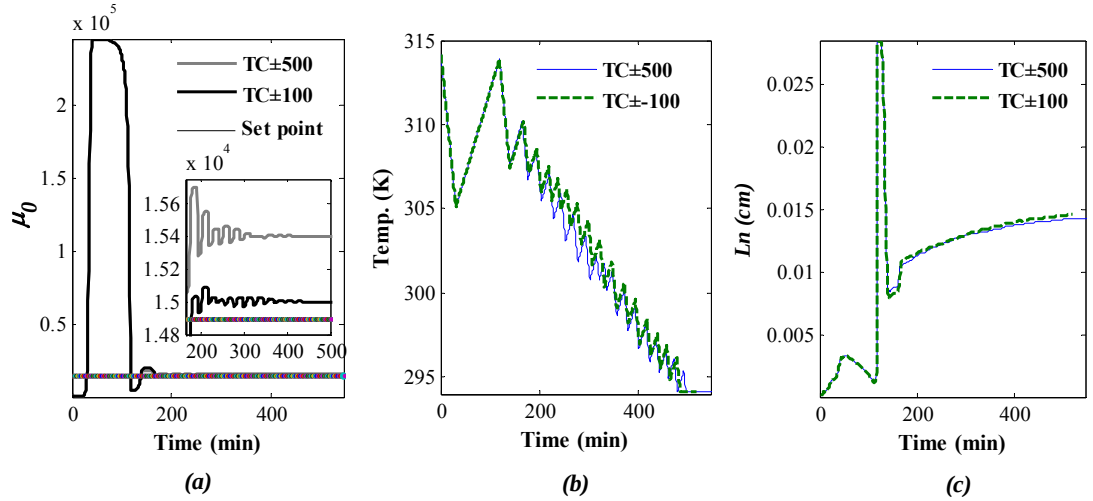


Figure 6.12: Reverse DNC (a) counts/s (b) mean length (c) temperature profile when optimal counts/s is doubled and set as the target.

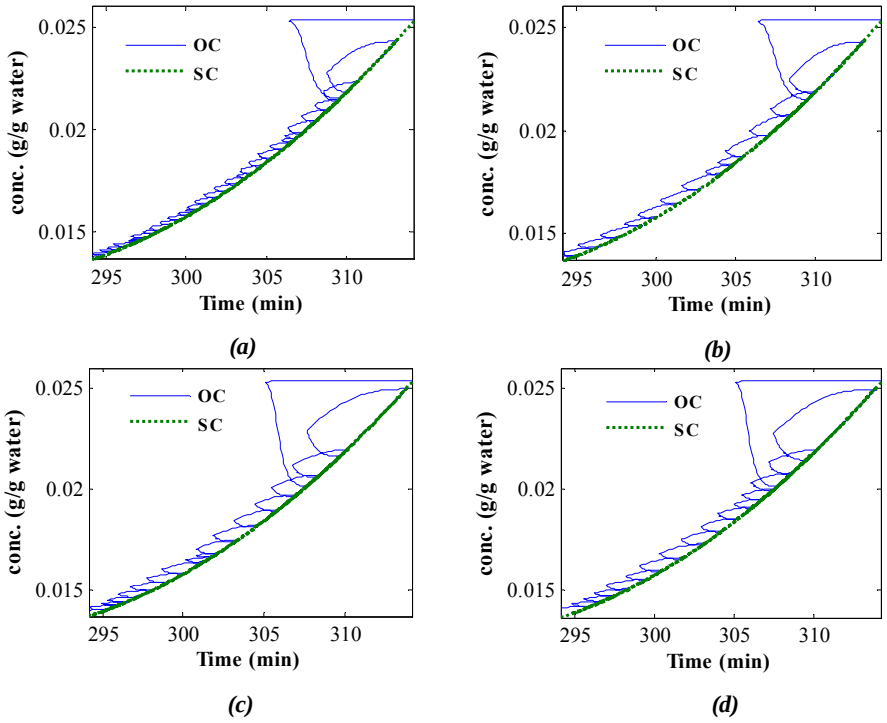


Figure 6.13: Cooling-heating cycles in Reverse DNC approach (a) optimal counts/s± 500 (b) optimal counts/s± 100 (c) doubled optimal counts/s± 500 (d) doubled optimal counts/s± 100.

Case 4: Applying the basic DNC approach

The aim of this experiment was to investigate the effect of eliminating the lower bound of target counts/s. The effects of introducing heating steps as well as its performance compared to model based optimal control was also examined. Figure 6.14 (a-c) shows, how the set point target of counts/s was achieved along with the mean length and temperature profile when optimal counts/s is the target. System's responses with different acceptable ranges were plotted in the same plot to compare their effects. As usual, with a smaller acceptable range of +100 counts/s, the target was achieved very closely (offset was 95) and for the largest range of +1000 counts/s, it was the maximum (offset was 490) from the target as expected. The initial overshoot was the same for all. For all cases, the mean length of crystals (Ln) were almost three times greater than the optimal mean length of 0.015 cm with the maximum achieved by TC+100 case of 0.0435 cm. This was because, in these studies the yield achieved was 3.5 % greater than the optimal case. All three simulations took 200 to 240 minutes to finish which was less than the time used in the optimal case study. Similar results were obtained for cases, when the target was double the optimal

counts/s and half the optimal counts/s as shown in Figures 6.15 (a-c) and Figure 6.16 (a-c) respectively. All the cases started from 314 K and ended at 294.15 K. The bottleneck of this approach is the rate of cooling. A higher cooling rate (for both fast and slow cooling) is required for large target and vice versa. The heating rates were almost the same for all the cases. Therefore, selection of an appropriate cooling rate is a challenge for this approach. Figure 6.17 shows the temperature loops created by the operating curve (OC) in the phase diagram.

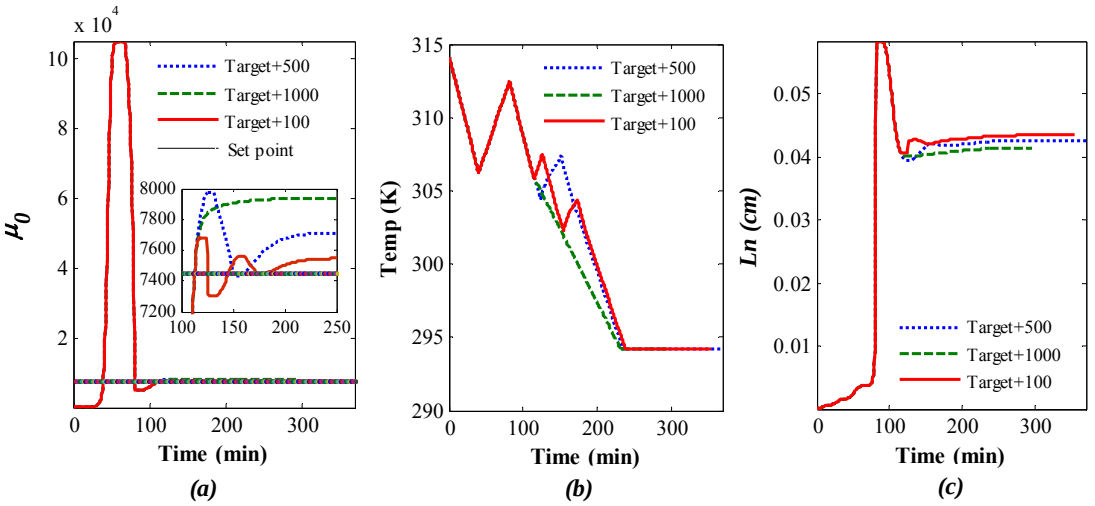


Figure 6.14: Basic DNC (a) counts/s (b) mean length (c) temperature profile when optimal counts/s is the target.

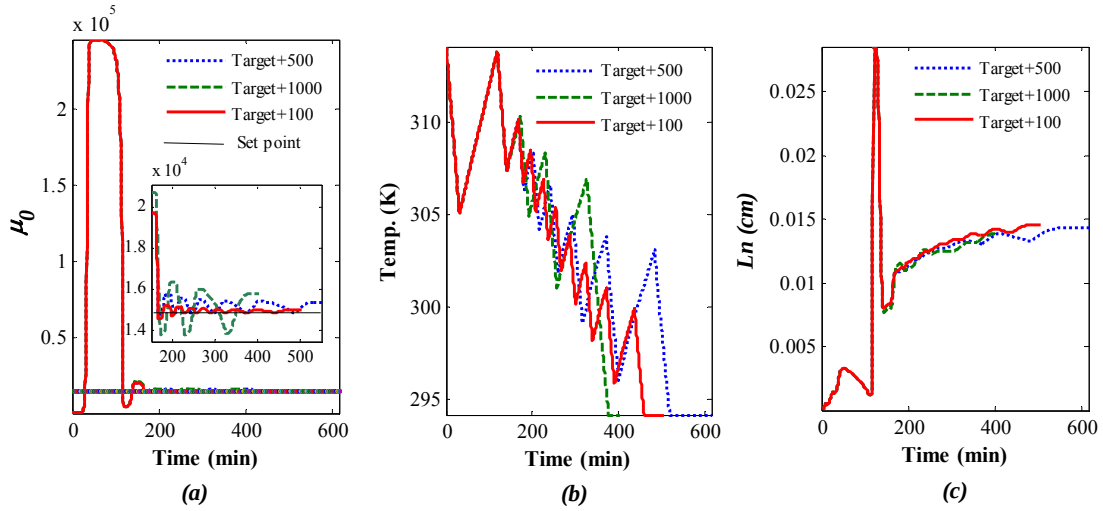


Figure 6.15: Basic DNC (a) counts/s (b) mean length (c) temperature profile when optimal counts/s is doubled and set as the target.

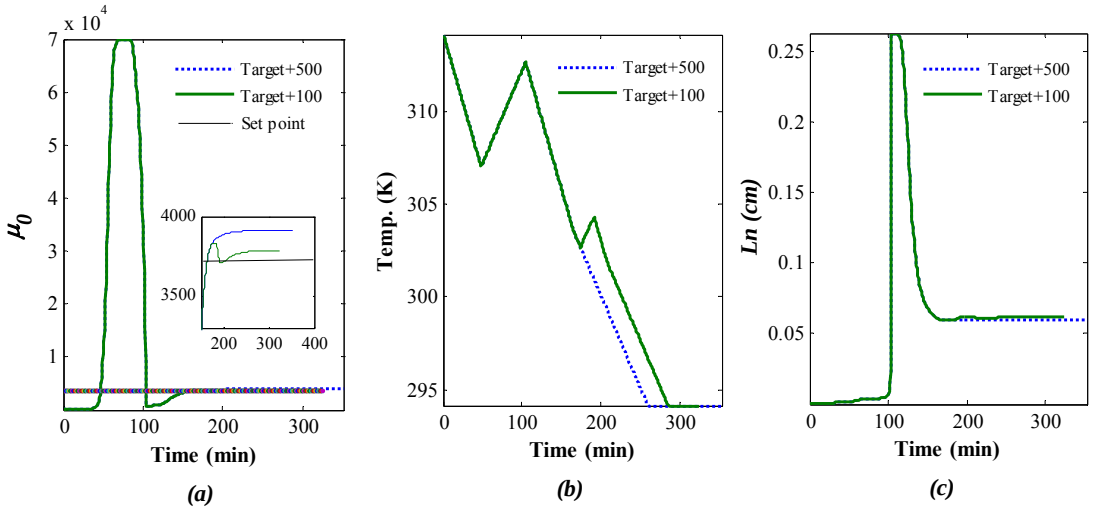


Figure 6.16: Basic DNC (a) counts/s (b) mean length (c) temperature profile when optimal counts/s is reduced by 50% and set as the target.

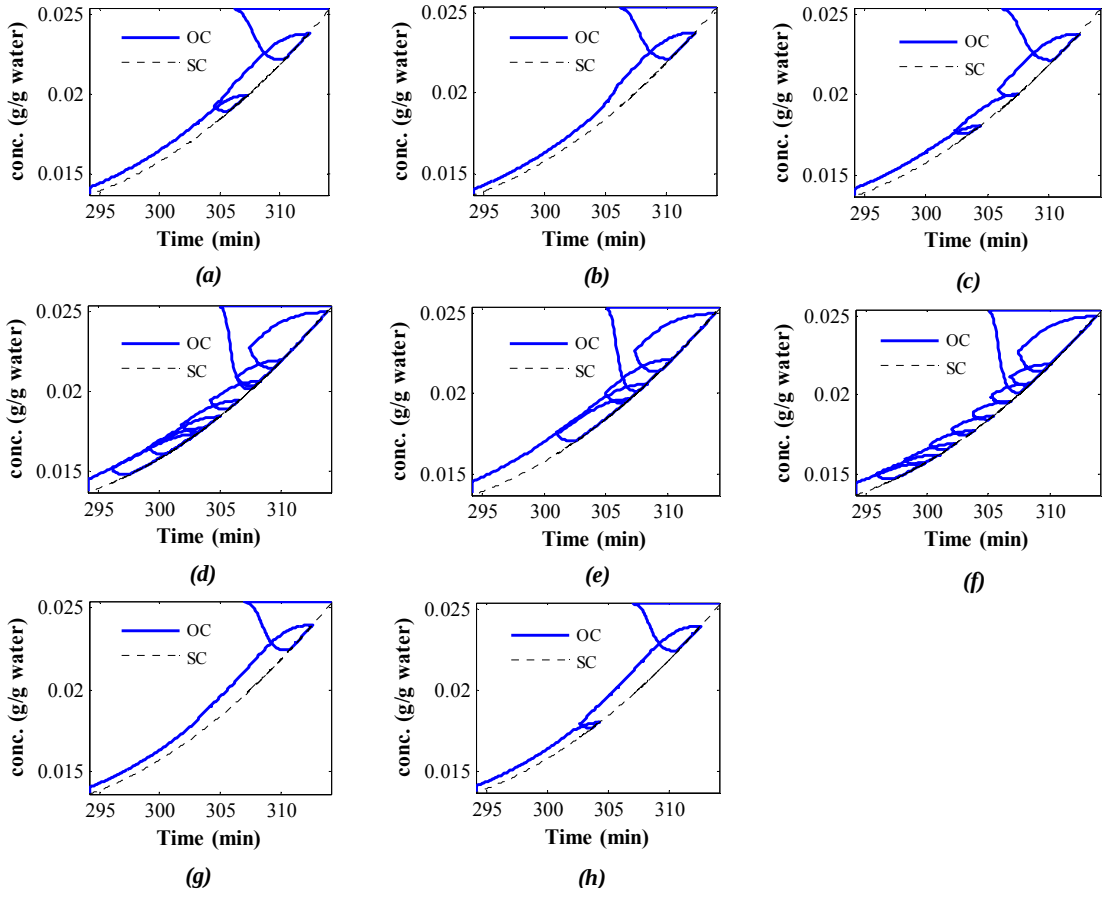


Figure 6.17: Cooling-heating cycles in Basic DNC approach with target limits (a) optimal counts ±500 (b) optimal counts ±1000 (c) optimal counts ±100 (d) double of optimal counts ±500 (e) double of optimal counts ±1000 (f) double of optimal counts ±100 (g) half of optimal counts ±500 (h) half of optimal counts ±100.

6.4.2 DNC Experiments

Figure 6.18 and Figure 6.19 shows the results of the Basic and Simple DNC respectively.

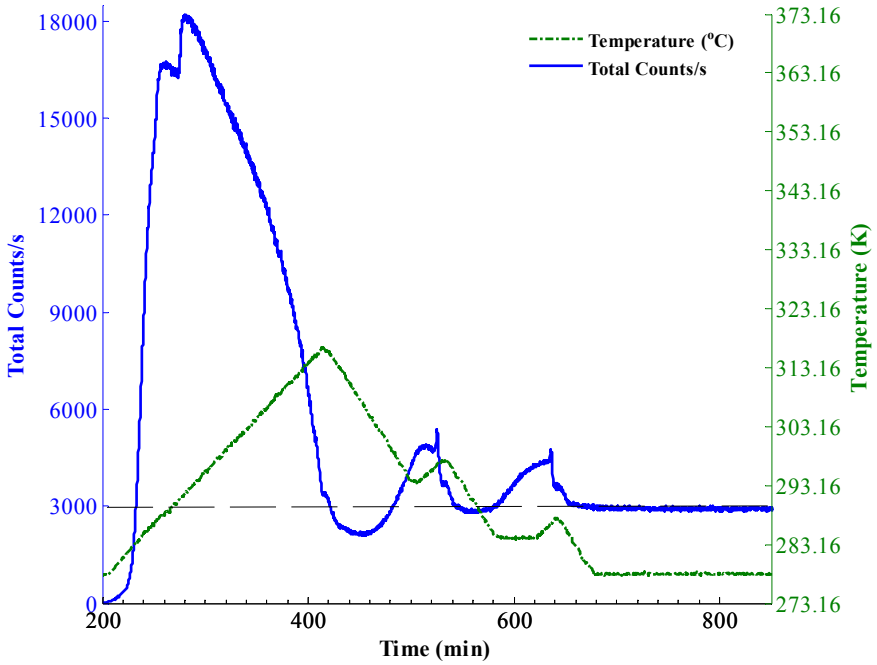


Figure 6.18: Temperature and counts/s profile for the Basic DNC.

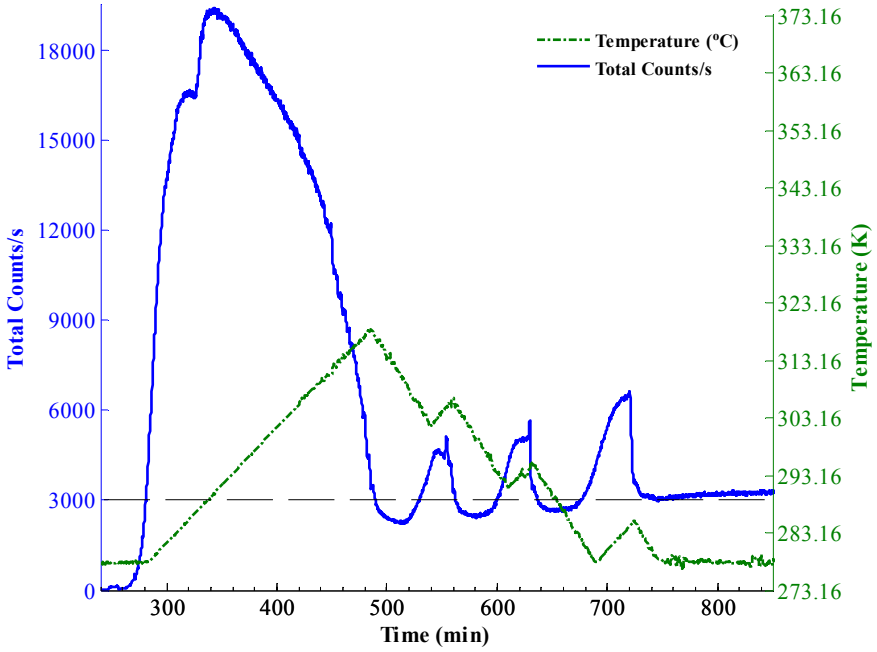


Figure 6.19: Temperature and counts/s profile for the Simple DNC.

In both cases, primary nucleation generated a significant overshoot in the FBRM counts/s which took place at about 278.16 K. The large primary nucleation zone generated very high initial supersaturation, leading to a very fast and significant nucleation. Due to the overshoot the DNC system switched to the heating stage automatically. Since, in the second and subsequent cooling cycles particles were already present, both the DNC automatically switches to the heating stage earlier as the increase in counts/s is detected leading to the smaller cycles. These results exhibit the core advantage of the DNC approach, that it can detect any variations in number of counts/s and can change the operating conditions (heating or cooling rates) accordingly.

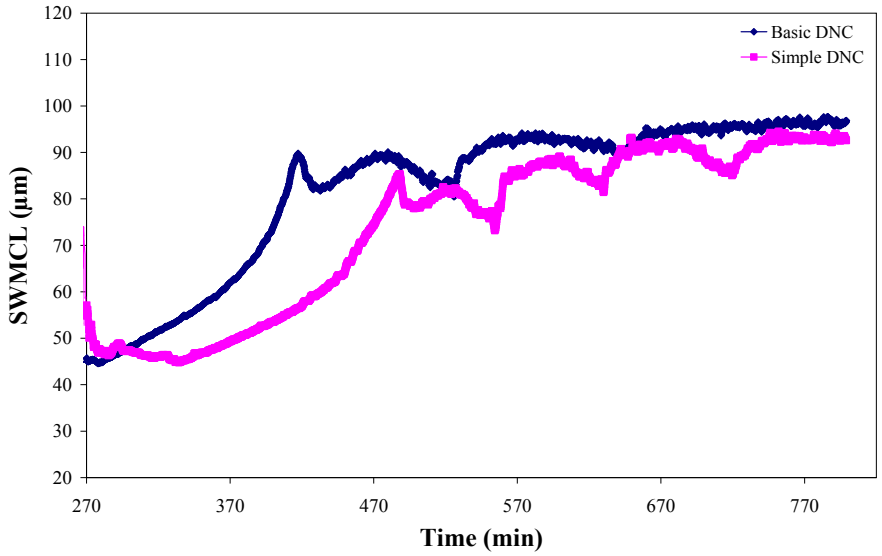


Figure 6.20: SWMCL over the entire batch time of the crystals produced by Basic DNC and Simple DNC experiments.

Figure 6.20 shows the comparative square weighted mean chord lengths (SWMCL) results and Figure 6.21 shows a comparison of the square weighted chord length distributions (SWCLD) for the two DNC experiments. After the systems stabilised, SWMCL for Basic DNC was 94.15 µm and for Simple DNC it as 93.88 µm and both the DNCs showed unimodal SWCLD at the end of the batch. The PVM images of Basic and Simple DNC have been shown in Figure 6.22 (a) and Figure 6.22 (b) respectively. These PVM figures also reveal that the crystals produced by different DNC approaches are of almost similar size and shapes.

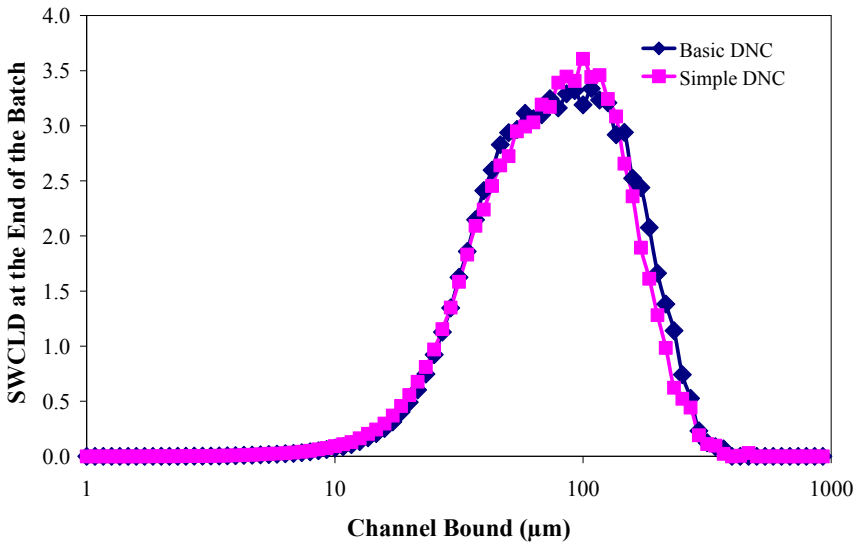
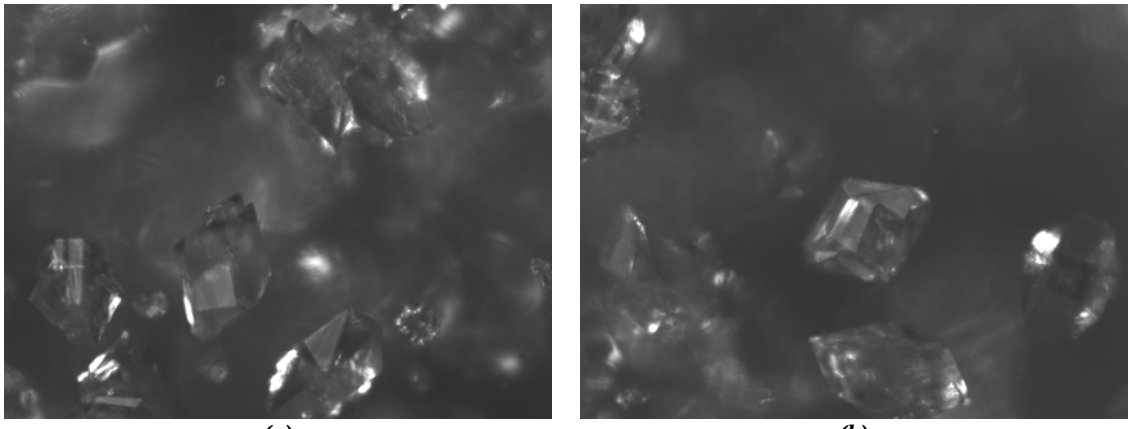


Figure 6.21: SWCLD at the end of the batches.



(a) *(b)*

Figure 6.22: PVM images of (a) Basic DNC (b) Simple DNC.

6.4.3 Comparative Analysis of Different Simulated and Experimental DNC Results

DNC works through a feedback control strategy, which reduces the solution temperature to create nuclei up to a desired number of counts/s and increases the temperature to dissolve excess nuclei. The results of simulation case studies, Case 1 to Case 4 reveal the performances of different DNC structures. The observations are listed below,

1. While comparing the results (i.e. yield, mean crystal length, batch time) with those obtained by model based optimal control, it was found that all the DNC structures provide better results in terms of increased yield (3.5%) and larger mean crystal length (215%) though some batches were unusually lengthy. In fact, all the results prove the robustness of DNC as a crystallisation control method.
2. It was observed that the mean crystal length mainly depends on the target counts/s; that is, a lower target counts/s resulted in larger crystals with the same yield produced as larger target counts/s produces.
3. In the cases of Reverse and Simple DNC, more heating/cooling cycles were generated resulting in longer batch times and it was more difficult to control the process at lower counts/s. These results indeed reflect the overprotective design of reverse and imperceptive design of Simple DNC structures.
4. While designing the Reverse DNC structure, it was expected to reduce the initial overshoot in counts/s as an early heating step was introduced. However, the results showed there is no improvement with this end.
5. Only the Simple DNC structure maintained zero offset with respect to target counts/s for all three conditions.
6. Although, the pattern and the number of temperature cycles were the same for both Basic and Predictive DNC structure whilst the later took a slightly longer batch time.
7. The main difference between basic and other DNC was that, in Basic DNC the final no. of counts/s always resided over the target as compared to other structures where the final counts/s tended to reside within the lower and upper bounds. As a result, sometimes there was reduced number of counts/s at the end of the batch.
8. It was found that the Basic DNC provided the best performance with respect to reduced batch time while maintaining the same yield as other structures.
9. As observed in the simulation case studies, the Basic DNC requires less number of heating-cooling loops than the Simple DNC. In addition, for the Simple DNC it was more difficult to maintain the counts without any acceptable range which led to relatively noisy temperature which kept

changing towards the end. As it was observed in simulations, the Simple DNC took longer batch time (600 min) to reach and stabilize at the desired # counts/sec than the Basic DNC (470 min).

Since, in batch crystallisation, the focus is to produce large uniform crystals within a given time (Nagy et al., 2008a); the performance of the Basic DNC is preferable over other DNC structures.

6.5 Conclusions

A strategic evaluation of different direct nucleation control (DNC) approaches were performed for the first time to compare its performance with model based optimal control of a batch cooling crystallisation system of paracetamol in water. In addition, different DNC structures were examined to understand the impact of different designs on batch length, mean crystal size and the number of cooling-heating cycles required to reach the target counts/s. Simulation case studies were performed to controls the amount of nuclei present in the system directly by imitating the performance of FBRM in real life. It was also shown that the laboratory DNC experimental results conform to the simulation findings successfully. The bottleneck of the proposed DNC approach is determination of the appropriate cooling and heating rates, which demands extensive trial and error experimentation to finalise these rates. The main advantage of this simple model free approach is continuous in situ fine removal during the heating stages without the installation of external heating loops leading to the growth of larger crystals even in the presence of unknown disturbances.

Chapter 7

Polynomial Chaos Expansion (PCE) Based Modelling and Optimisation of Batch Crystallisation Processes

7.1 Overview

In this chapter an operating data based surrogate modelling and optimisation technique has been developed for batch crystallisation processes. The proposed methodology is based on polynomial chaos expansion (PCE) containing orthogonal basis with respect to the Gaussian probability measure. The method was successfully applied for designing nonlinear surrogate model of a batch cooling crystallisation system of Paracetamol in water. Initially, a MatLab model of the system (see Chapter 3) was treated as the real process and used to generate historical data. The system was then re-identified under the nonlinear PCE scheme using those historical data. The developed model was then validated by using different inputs. Later the nonlinear model was used to optimise the temperature profile needed to obtain a desired mean length of crystals at the end of the batch. A brief introduction about the state of the art, development of the methodology and simulated results have been presented and discussed herein.

7.2 Introduction

There is a growing emphasis on the control of complex distributed parameter chemical systems due to the boost of computing power, significant evolution in sensor and actuator, and the development of modern optimisation and model reduction algorithms (Roman et al., 2009; Araujo et al., 2007; Skogestad, 2004). Typically batch processes are distributed in nature that are widely applied in many sectors of the chemical industries including many high value products such as pharmaceuticals, batteries, microelectronic devices, and artificial organs which are manufactured using

finite-time processing steps. These processes often throw up many challenging issues which engineers must endeavour to understand, model, and control (Ekpo, 2006). A few of these are time varying characteristics, strongly nonlinear behaviour, and the presence of disturbances. Because of this inherent nonlinearity of batch processes, the use of typical linear data-driven modelling approaches cannot yield models with acceptable accuracy and robustness. In addition, due to the limited availability of robust on-line sensors, often only off-line quality measurements are widely available. As a result, there is a growing demand for the development of relatively simple data-driven and computationally efficient nonlinear models that can be applied for robust model based optimisation or the robust optimal control of these processes.

One general trend is to state a system as a polynomial based on the assumption that a finite sum of polynomials can accurately approximate the function of interest. For polynomial approximations, orthogonal polynomials are often used. (Kim and Braatz, 2012) and different orthogonal functions are optimal for different parameter probability density functions (PDFs) (e.g. Gaussian, Gamma, Beta, Uniform, Poisson, Binomial). Table 7.1 summarises the correspondence between the choice of polynomials and the type of distribution of the random variables.

Table 7.1: Most Common Distributions of Random Parameters with Corresponding Polynomial Bases (Nagy and Braatz, 2010)

Random variable	Polynomials
Beta	Jacobi
Gamma	Laguerre
Gaussian	Hermite
Uniform	Legendre

Since PCE contains orthogonal basis with respect to the Gaussian probability measure, it is stated as an expansion of multidimensional Hermite polynomial functions of the uncertain parameters. PCE can be used to replace a nonlinear system with surrogate model that accurately describes the input-to-state and input-to-output behaviour within the trajectory bundle (Braatz, 2010).

After the introduction of PCE by Wiener in the late thirties for turbulence modeling (Wiener, 1938) only relatively recently PCE has been widely accepted and applied in different disciplines, e.g. climate modelling, hurricane prediction, computational fluid dynamics (CFD), and batch process control for uncertainty propagation (Nagy and Braatz, 2007; Huan and Marzouk, 2013). Researchers have also demonstrated that use of PCE promises to be a computationally efficient and cheap alternative to Monte Carlo (MC) approaches for analysis and controller design of uncertain systems (Kim and Braatz, 2012; Augustin et al., 2008). However, despite their potential to capture the systems nonlinear behavior until now only a few studies have been directed towards the application of PCE in the field of batch chemical processing. PCE is well suited to robust design and control when the objectives are strongly dependent on the shape or tails of the distributions of product quality or economic objectives. PCE is convergent in the mean-square sense (Ghanem and Spanos, 1991), so the coefficients in the PCE can be calculated using least-squares minimisation (LSM) considering sample input/output pairs from a complex model or directly from experiments.

In this work polynomial chaos expansion (PCE) is used to provide surrogate models for a batch crystallisation process. In addition, performance analysis was performed on the surrogate model to evaluate its accuracy. Later this model was used to optimise the temperature profile required to obtain a desired mean length of crystal at the end of the batch for analysing the robustness of the developed surrogate model.

7.3 Methodology Development

This work presents a computationally efficient approach to represent a data-driven input/output model between the finite-time control trajectories and the quality index at the end of the batch, based on the approximate representation of the full process model via PCE. The batch cooling crystallisation system of Paracetamol in water was used to estimate the dependence of output mean length of crystals at the end of the batch on the temperature trajectory used during the crystallisation. The methodology followed the PCE approach described by Nagy and Braatz (2007). If the input temperature trajectory described in terms of standard normal random variables, the polynomial chaos expansion (PCE) can describe the model output ψ as an expansion

of multidimensional Hermite polynomial functions of the input parameters θ (Nagy and Braatz, 2010). Using the Hermite bases in the PCE, the output can be expressed as shown in Equation 7.1, in terms of the standard random normal variables $\{\theta_i\}$ using an expansion of order d,

$$\psi^{(d)} = \underbrace{a_o^{(d)}\Gamma_o}_{\text{constant}} + \underbrace{\sum_{i_1=1}^{n_\theta} a_{i_1}^{(d)}\Gamma_1(\theta_{i_1})}_{\text{first-order terms}} + \underbrace{\sum_{i_1=1}^{n_\theta}\sum_{i_2=1}^{i_1} a_{i_1 i_2}^{(d)}\Gamma_2(\theta_{i_1},\theta_{i_2})}_{\text{second-order terms}} + \underbrace{\sum_{i_1=1}^{n_\theta}\sum_{i_2=1}^{i_1}\sum_{i_3=1}^{i_2} a_{i_1 i_2 i_3}^{(d)}\Gamma_3(\theta_{i_1},\theta_{i_2},\theta_{i_3})}_{\text{third-order terms}} + \ldots \tag{7.1}$$

where n_θ is the number of parameters, the $a_{i_1}^{(d)}, a_{i_1 i_2}^{(d)}$, and $a_{i_1 i_2 i_3}^{(d)}$ are the deterministic coefficients in $\mathbb{R}$ to be estimated, Γ_1, Γ_2, and Γ_3 are the successive polynomial chaoses of their arguments, the subscripts denote the order of the expansion which is convergent in the mean square. The Hermite polynomials of order greater than one have mean zero, and polynomials of different order are orthogonal to each other; so are polynomials of the same order with a different argument list. Up to the third order, the Hermite polynomials are given by the set of expressions given by Equation 7.2,

$$\Gamma_0 = 1,$$

$$\Gamma_1(\theta_{i_1}) = \theta_{i_1},$$

$$\Gamma_2(\theta_{i_1},\theta_{i_2}) = (\theta_{i_1}\theta_{i_1} - 1) + (\theta_{i_2}\theta_{i_2} - 1) + \theta_{i_1}\theta_{i_2}, \text{ and}$$

$$\begin{aligned}\Gamma_3(\theta_{i_1},\theta_{i_2},\theta_{i_3}) = {} & (\theta_{i_1}\theta_{i_1}\theta_{i_1} - 3\theta_{i_1}) + (\theta_{i_2}\theta_{i_2}\theta_{i_2} - 3\theta_{i_2}) + (\theta_{i_3}\theta_{i_3}\theta_{i_3} - 3\theta_{i_3}) + \\ & (\theta_{i_1}\theta_{i_1}\theta_{i_1} - \theta_{i_1}) + (\theta_{i_2}\theta_{i_2}\theta_{i_2} - \theta_{i_2}) + (\theta_{i_3}\theta_{i_3}\theta_{i_3} - \theta_{i_3}) + \theta_{i_1}({\theta_{i_2}}^2 - 1) + \theta_{i_2}({\theta_{i_3}}^2 - 1) + \\ & \theta_{i_2}({\theta_{i_3}}^2 - 1) + \theta_{i_2}({\theta_{i1}}^2 - 1) + \theta_{i_3}({\theta_{i_1}}^2 - 1) + \theta_{i_3}({\theta_{i_2}}^2 - 1) + \theta_{i_1}(\theta_{i_3}\theta_{i_1} - 1) + \theta_{i_1}\theta_{i_2}\theta_{i_3}\end{aligned} \tag{7.2}$$

A combined alternative expression for deriving the multi-dimensional Hermite polynomials of degree $m = i_1, i_2, \ldots, i_{n_\theta}, \Gamma_m(\theta_{i_1},\ldots,\theta_m)$ is shown in Equation 7.3,

$$\Gamma_m(\theta_{i_1},\ldots,\theta_m) = (-1)^m e^{(1/2)\theta^T\theta}\frac{\partial^m e^{-(1/2)\theta^T\theta}}{\partial\theta_1\ldots\partial\theta_m} \tag{7.3}$$

The parameter vector in the proposed approach represents the temperature values at the discretised batch times. The polynomial chaos terms are random variables, since they are functions of the random variables, and terms of different order are orthogonal to each other (with respect to an inner product defined in Gaussian measures as the

expected value of the product of the two random variable, i.e. $\varepsilon[\Gamma_i\Gamma_j]=0$ for $\Gamma_i \neq \Gamma_j$. In PCE any form of polynomial could be used but the properties of orthogonal polynomials make the uncertainty analysis more efficient (Nagy and Braatz, 2007). The number of coefficients (N) in the PCE depends on the number of uncertain parameters (n_θ) and the order of expansion (m), Equation 7.4 shows the general formula for the determination of number of coefficients,

$$N = 1 + \frac{n_\theta!}{(n_\theta-1)!1!} + \frac{(n_\theta+1)!}{(n_\theta-1)!2!} + \frac{(n_\theta+2)!}{(n_\theta-1)!3!} + \ldots + \frac{(n_\theta+m-1)}{(n_\theta-1)!m!} \tag{7.4}$$

Figure 7.1 shows the flowchart summarising the PCE based surrogate modelling and model optimisation steps.

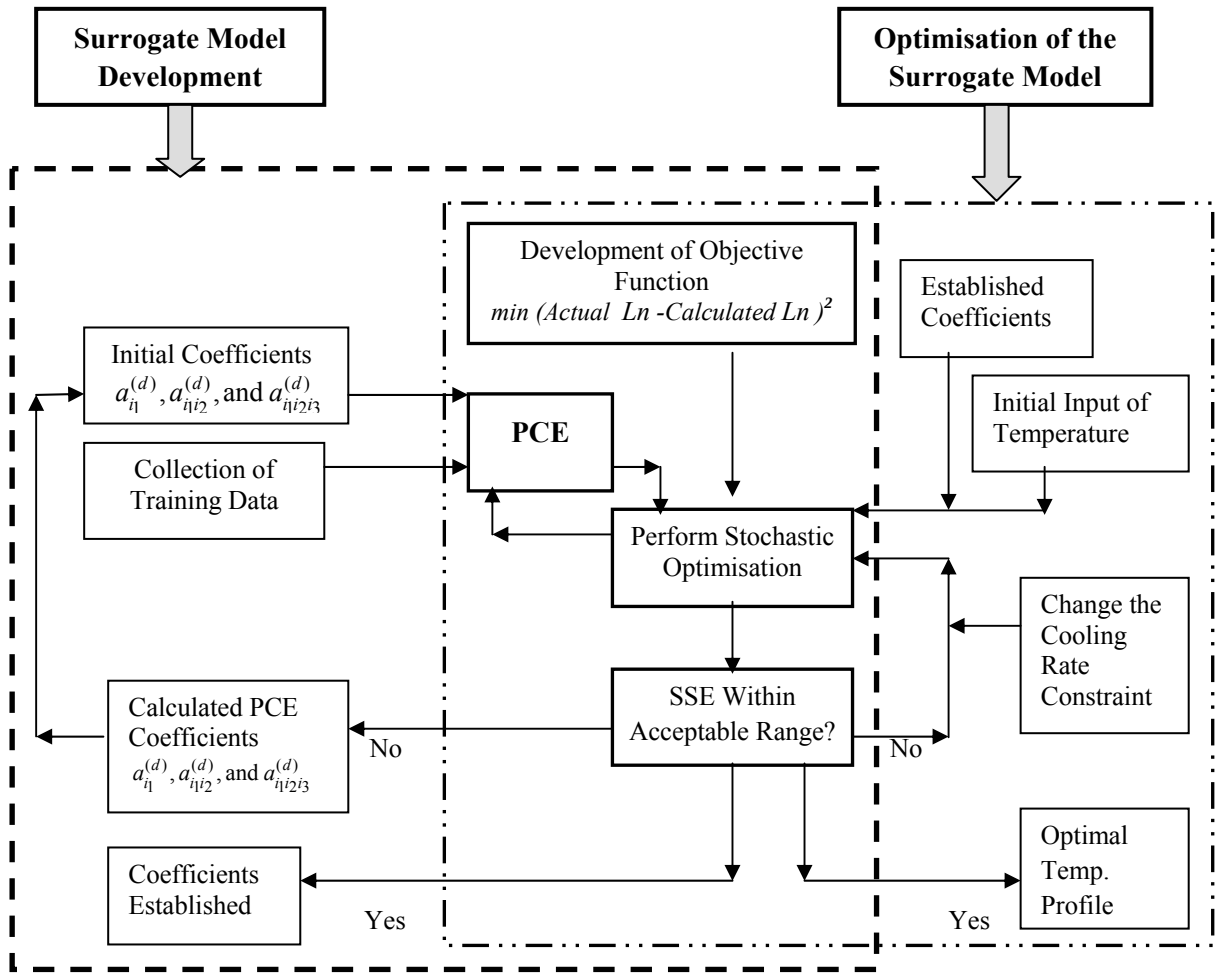


Figure 7.1: The flowchart summarising the PCE based surrogate modelling and model optimisation steps.

For most engineering applications, in order to adequately representing fairly large levels of random fluctuations the recommended order of expansion is not higher than four (Ghanem and Spanos, 1991). Since, the PCE is convergent in the mean-square sense it is beneficial to calculate the coefficients (e.g. $a_{i_1}^{(d)}, a_{i_1 i_2}^{(d)}$, and $a_{i_1 i_2 i_3}^{(d)}$) using least-square minimisation (LSM) considering sample input/output pairs from the model. During computer simulations, the LSM based determination of the PCE coefficients run the optimisation repeatedly from the previous solution to allow convergence to the best PCE parameters. In this way, the best fit is achieved between the surrogate PCE model and the nonlinear model (or experimental data).

7.4 Results and Discussions

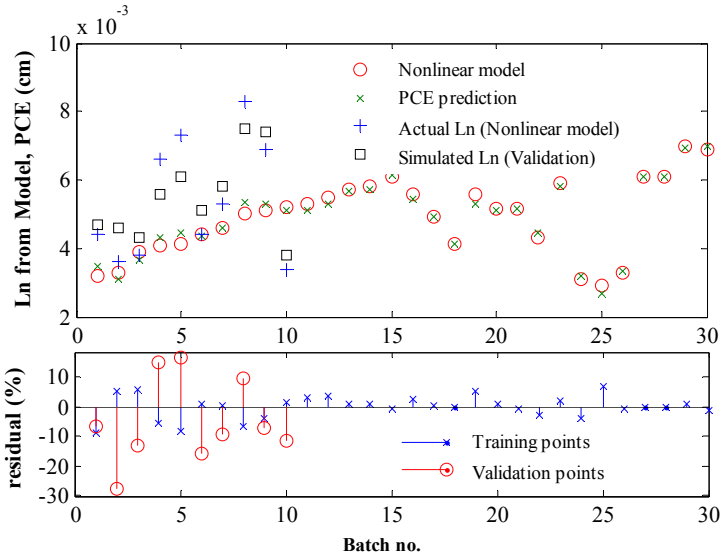
7.4.1 Surrogate Model Identification and Validation

The application of PCE for the surrogate modelling of the batch crystallisation process was evaluated first via simulations. In this case, a detailed mathematical model of the batch crystallisation system was developed and treated as the real processes to generate historical input output data. The details of the mathematical model development and historical data generation have been given in Chapter 3. For this particular study, thirty sets of historical data were used as training data. The criterion for generating the training data was to span the behaviour of the states as much as possible so that they can capture the system's response. The inputs were the temperature trajectories discretised in 9 points (hence 10 input parameters, θ_i) over the batch duration. The output was the corresponding mean length of crystal (Ln) at the end of the batch (i.e. a single parameter). The system was then re-identified under the nonlinear PCE scheme using these training data. Both second and third order PCE was tested. For second and third order PCE with 10 parameters, the numbers of coefficients are 66 and 286 respectively according to Equation 7.4. The Hermite polynomials for the second-order-ten-dimensional PCE have been shown in Table 7.2 and the Hermite polynomials for the third-order-ten-dimensional PCE have been given in Appendix E.

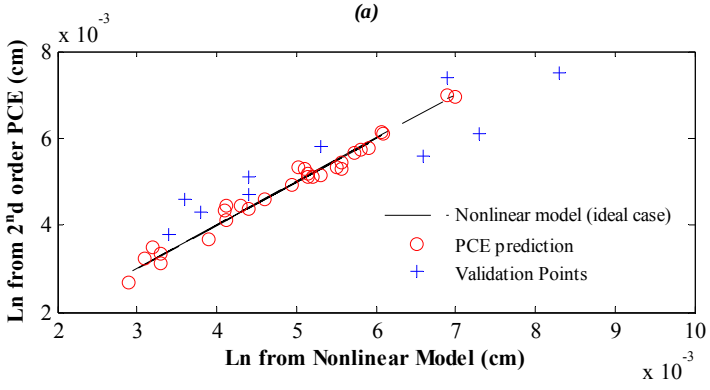
Table 7.2: Hermite Polynomials for the Second-Order-Ten-Dimensional PCE

i^{th} Polynomial Chaos	Γ_i	Order of Polynomial Chaos	i^{th} Polynomial Chaos	Γ_i	Order of Polynomial Chaos
0	1	1	33	$(\theta_3\theta_6)$	2
1	θ_1	1	34	$(\theta_3\theta_7)$	2
2	θ_2	1	35	$(\theta_3\theta_8)$	2
3	θ_3	1	36	$(\theta_3\theta_9)$	2
4	θ_4	1	37	$(\theta_3\theta_{10})$	2
5	θ_5	1	38	(θ_4^2-1)	2
6	θ_6	1	39	$(\theta_4\theta_5)$	2
7	θ_7	1	40	$(\theta_4\theta_6)$	2
8	θ_8	1	41	$(\theta_4\theta_7)$	2
9	θ_9	1	42	$(\theta_4\theta_8)$	2
10	θ_{10}	1	43	$(\theta_4\theta_9)$	2
11	(θ_1^2-1)	2	44	$(\theta_4\theta_{10})$	2
12	$(\theta_1\theta_2)$	2	45	(θ_5^2-1)	2
13	$(\theta_1\theta_3)$	2	46	$(\theta_5\theta_6)$	2
14	$(\theta_1\theta_4)$	2	47	$(\theta_5\theta_7)$	2
15	$(\theta_1\theta_5)$	2	48	$(\theta_5\theta_8)$	2
16	$(\theta_1\theta_6)$	2	49	$(\theta_5\theta_9)$	2
17	$(\theta_1\theta_7)$	2	50	$(\theta_5\theta_{10})$	2
18	$(\theta_1\theta_8)$	2	51	(θ_6^2-1)	2
19	$(\theta_1\theta_9)$	2	52	$(\theta_6\theta_7)$	2
20	$(\theta_1\theta_{10})$	2	53	$(\theta_6\theta_8)$	2
21	(θ_2^2-1)	2	54	$(\theta_6\theta_9)$	2
22	$(\theta_2\theta_3)$	2	55	$(\theta_6\theta_{10})$	2
23	$(\theta_2\theta_4)$	2	56	(θ_7^2-1)	2
24	$(\theta_2\theta_5)$	2	57	$(\theta_7\theta_8)$	2
25	$(\theta_2\theta_6)$	2	58	$(\theta_7\theta_9)$	2
26	$(\theta_2\theta_7)$	2	59	$(\theta_7\theta_{10})$	2
27	$(\theta_2\theta_8)$	2	60	(θ_8^2-1)	2
28	$(\theta_2\theta_9)$	2	61	$(\theta_8\theta_9)$	2
29	$(\theta_2\theta_{10})$	2	62	$(\theta_8\theta_{10})$	2
30	(θ_3^2-1)	2	63	(θ_9^2-1)	2
31	$(\theta_3\theta_4)$	2	64	$(\theta_9\theta_{10})$	2
32	$(\theta_3\theta_5)$	2	65	(θ_{10}^2-1)	2

In order to initiate the calculation of the PCE coefficients by the LSM method, a set of initial coefficients were assumed randomly. Selection of the initial coefficients is important since they affect the accuracy of the approximation. For this study, initial coefficients were selected through successive trials, i.e. the simulation were continued from one trial to another using the coefficients calculated by the previous trial as the initial guess for the next trial until there was no further improvement in prediction accuracy. Afterwards, the surrogate model was validated using other input profiles, which were not used in the training data. The validation data were selected as such that some input profiles lead to Ln within the range used for the PCE identification and some were outside the range to check extrapolation ability too. The results of the second order and third order PCE prediction have been shown in Figure 7.2 (a), 7.2(b) and Figure 7.3 (a), 7.3 (b) respectively along with the validation points.



(a)



(b)

Figure 7.2: Prediction of the second order PCE (a) for 30 training batches and 10 validation batches (b) comparison of PCE prediction with nonlinear model.

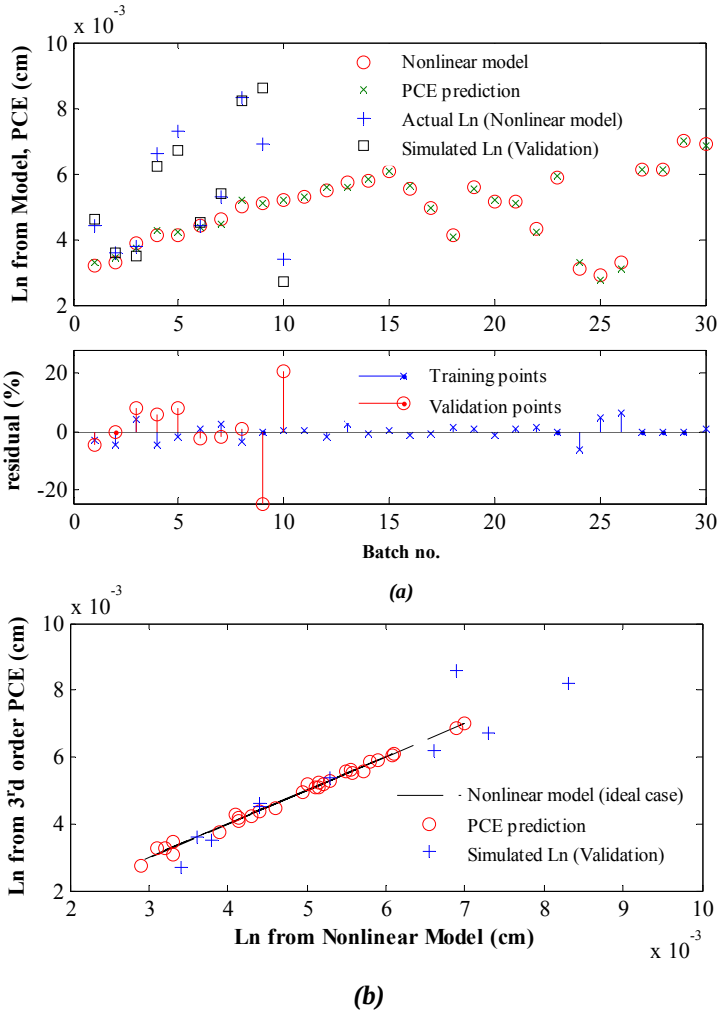


Figure 7.3: Prediction of the third order PCE (a) for 30 training batches and 10 validation batches (b) comparison of PCE prediction with nonlinear model.

It is evident from the figures that the third order PCE captured the system more closely as compared to the second order predictions. However, it took almost 8 hours to finish the third order computations whilst it took only 15 seconds for the second order computations. The computation time is based on a personal computer with Microsoft Windows XP Professional Version 2002 Service Pack 3 operating system and Intel Core 2 Duo processor with 2 GB of RAM. Table 7.3 gives the validation results for better understanding of the actual values. The sum squared error (SSE) was calculated as, SSE = ∑(actual Ln from the nonlinear model – calculated Ln by the surrogate model)^2. For the training and validation of the second order PCE the overall SSE was 2.5338×10^{-8} and 5.7943×10^{-7} respectively. On the other hand, for the

training and validation of the third order PCE the overall SSE was 9.8300×10^{-9} and 4.1397×10^{-7} respectively.

Table 7.3: Actual and Calculated Ln Values by Different Order PCE and the Corresponding SSEs.

Sl. No.	Actual *Ln*	Second order *Ln*	Third order *Ln*	Second Order SSE	Third Order SSE
Input trajectories within the limit of the training data.					
1	0.0044	0.0047	0.0046	9.0000×10^{-8}	4.0000×10^{-8}
2	0.0036	0.0046	0.0036	1.0000×10^{-6}	0
3	0.0038	0.0043	0.0035	2.5000×10^{-7}	9.0000×10^{-8}
4	0.0066	0.0056	0.0062	1.0000×10^{-6}	1.6000×10^{-8}
5	0.0043577	0.0051	0.0045	5.5101×10^{-7}	1.5426×10^{-8}
6	0.005261	0.0058	0.0054	2.9052×10^{-7}	2.4274×10^{-8}
7	0.0069	0.0074	0.0086	2.5000×10^{-7}	2.8900×10^{-8}
8	0.0034	0.0038	0.0027	1.6000×10^{-7}	4.9000×10^{-8}
Input trajectories outside the limit of the training data.					
9	0.0073294	0.0061	0.006689	1.5114×10^{-6}	4.1011×10^{-7}
10	0.0083315	0.0075	0.0081904	6.9139×10^{-7}	1.9909×10^{-8}

7.4.2 Optimisation of the Surrogate Model

After validation, the nonlinear surrogate model was then used to determine the optimal temperature profile needed to obtain a desired mean length (*Ln*) of crystals at the end of the batch. To compare the performance of the developed nonlinear surrogate model, the desired mean length (*Ln*) was set as the one obtained from the optimisation of the first principle nonlinear model of Paracetamol in water (please see subsection 7.4.1). The following sub-sections describe the procedure in detail.

7.4.2.1 First Principle Model Based Open Loop Optimal Control

The simulation model of Paracetamol in water (please see Chapter 3 for details of the kinetics and other parameters for model development) was subject to optimise its performance. The first principle model based optimisation followed the exact procedure as described in subsection 6.4.1.1 with the same optimal control problem. Figure 7.4 shows the optimal temperature trajectory and the corresponding mean length (Ln) trajectory. The mean length of crystals increased steadily with the maximum value at the end of the batch equal to 102 μm.

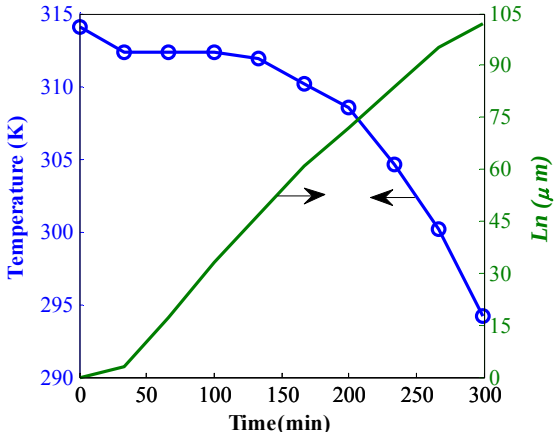


Figure 7.4: Optimum temperature profile and the corresponding Ln trajectory by first principle model based optimisation

7.4.2.2 Determination of the Optimal Temperature to Produce Crystals with Desired Mean Length

The nonlinear surrogate model was then used to determine the optimal temperature profile needed to obtain the crystals with the desired mean length (Ln) of 102 μm. The objective function is shown in Equation 7.8,

$$\min_{T(1),T(2),\ldots,T(N)} \left(\frac{\text{Desired } Ln \text{ - } Ln \text{ Calculated by the Surrogate Model}}{\text{Desired } Ln} \times 100 \right)^2 \tag{7.8}$$

The system was subjected to the following constraints of Equation 7.9.

$$\begin{aligned} &T_{\min} \le T(k) \le T_{\max}, \text{ and} \\ &R_{\min} \le dT/dt \le R_{\max} \end{aligned} \tag{7.9}$$

where, $T_{\min}$, $T_{\max}$, $R_{\min}$, and $R_{\max}$ were the same as those for the first principle model based optimisation. The minimum and maximum temperatures were 314.13 K

and 294.15 K. The temperature ramp rates were, $-1 < dt/dT \leq 0$ °K/min. This part was divided in four cases as described below.

Case 1a Optimisation of the Surrogate Model Using a Linear Initial Temperature Profile with Fixed Terminal Conditions on Temperatures

In this case, the initial profile was a linear cooling temperature profile that produced an Ln of 59 μm. During optimising the cooling temperature the initial and final temperature was kept constant at $T_0 = 314.087$K and $T_f = 294.15$K. These were the terminal temperatures determined by the first principle model based optimisation (please see sub-section 7.4.2.1). When applied to the theoretical nonlinear model, the optimum temperature calculated by the second order PCE produced an actual Ln of 67 μm at the end of the batch with the SSE of 1.225×10^{-5}. On the other hand, the optimum temperature calculated by the third order PCE produced an actual Ln of 71 μm at the end of the batch with the SSE of 9.61×10^{-6}. The results are shown in Figure 7.5 (a) to Figure 7.5 (d).

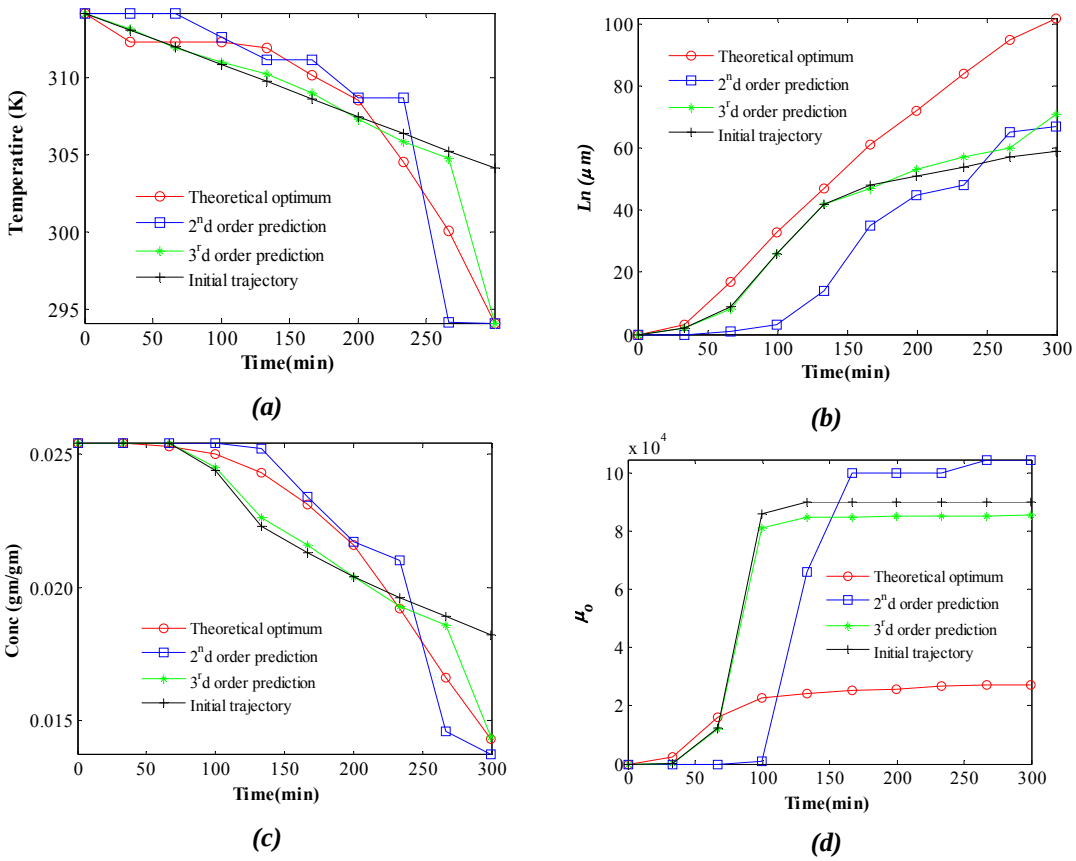


Figure 7.5: Optimum profiles for Case 1a (a) temperature (b) Ln (c) concentration (d) μ_o.

Case 1b Optimisation of the Surrogate Model Using a Nonlinear Initial Temperature Profile with Fixed Terminal Conditions on Temperatures

In this case, in an effort to further improve the performance of the surrogate model, the initial profile was changed to a nonlinear cooling temperature profile that produced an Ln of 73 μm. During optimising the cooling temperature the initial and final temperature was kept constant at $T_0 = 314.087\text{K}$ and $T_f = 294.15\text{K}$ as in Case 1a. As a result of this nonlinear temperature profile with improved initial Ln of 73 μm, the resultant optimal temperatures produced relatively better final Ln as compared to Case 1a. When applied to the theoretical nonlinear model, the optimum temperature calculated by the second order PCE produced an actual Ln of 70 μm at the end of the batch with the SSE of 1.024×10^{-5}. The optimum temperature calculated by the third order PCE produced an actual Ln of 78 μm at the end of the batch with the SSE of 5.76×10^{-6}, this was an improvement over the previous case. The results are shown in Figure 7.6 (a) to Figure 7.6 (d).

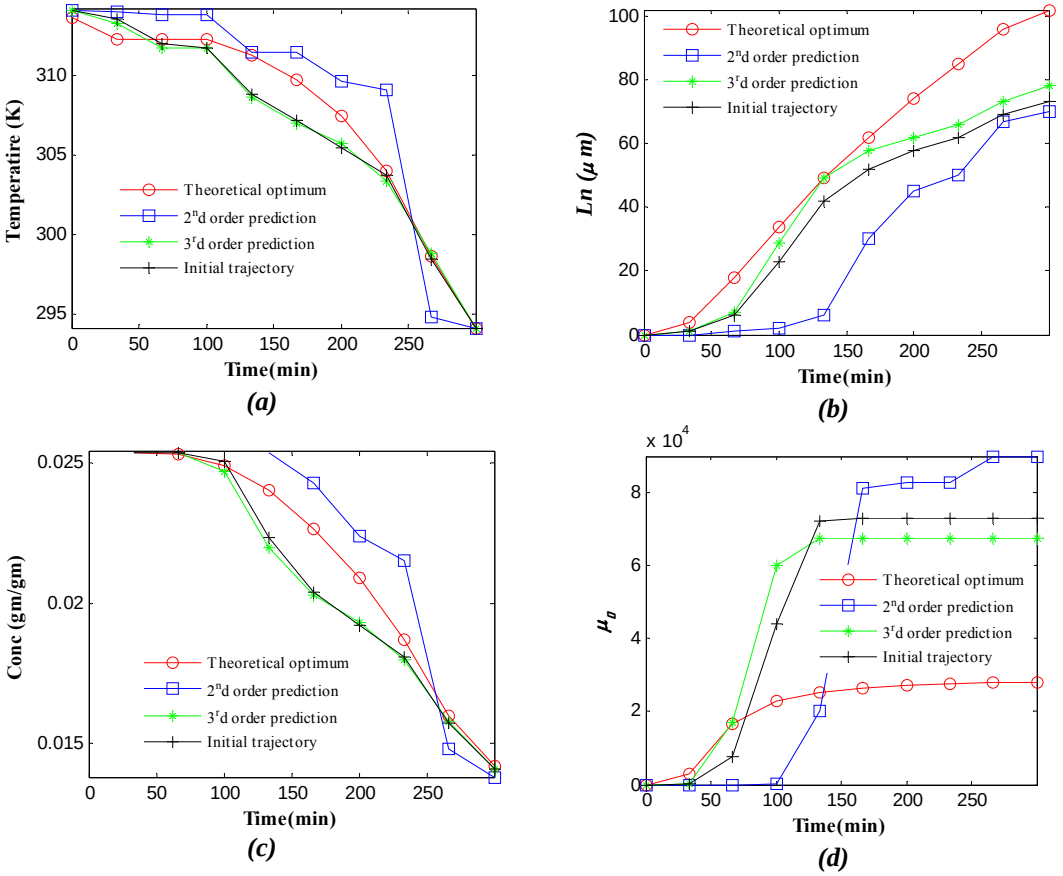


Figure 7.6: Optimum profiles for Case 1b (a) temperature (b) Ln (c) concentration (d) μo.

Case 2a Optimisation of the Surrogate Model Using a Linear Initial Temperature Profile without Fixing the Terminal Conditions on Temperatures

In this case, in an effort to improve the performance of the surrogate model, the constraints on the terminal temperatures, i.e. T_0 and T_f, were removed. As a result of this imposed flexibility, the optimal temperatures produced even better final Ln as compared to Case 1a and Case 1b. When applied to the theoretical nonlinear model, the optimum temperature calculated by the second order PCE produced an actual Ln of 67 μm at the end of the batch with the SSE of 1.225×10^{-5} which was the same as for Case 1a. However, the optimum temperature calculated by the third order PCE produced an actual Ln of 82 μm at the end of the batch with the SSE of 4×10^{-6}. The results are shown in Figure 7.7 (a) to Figure 7.7 (d).

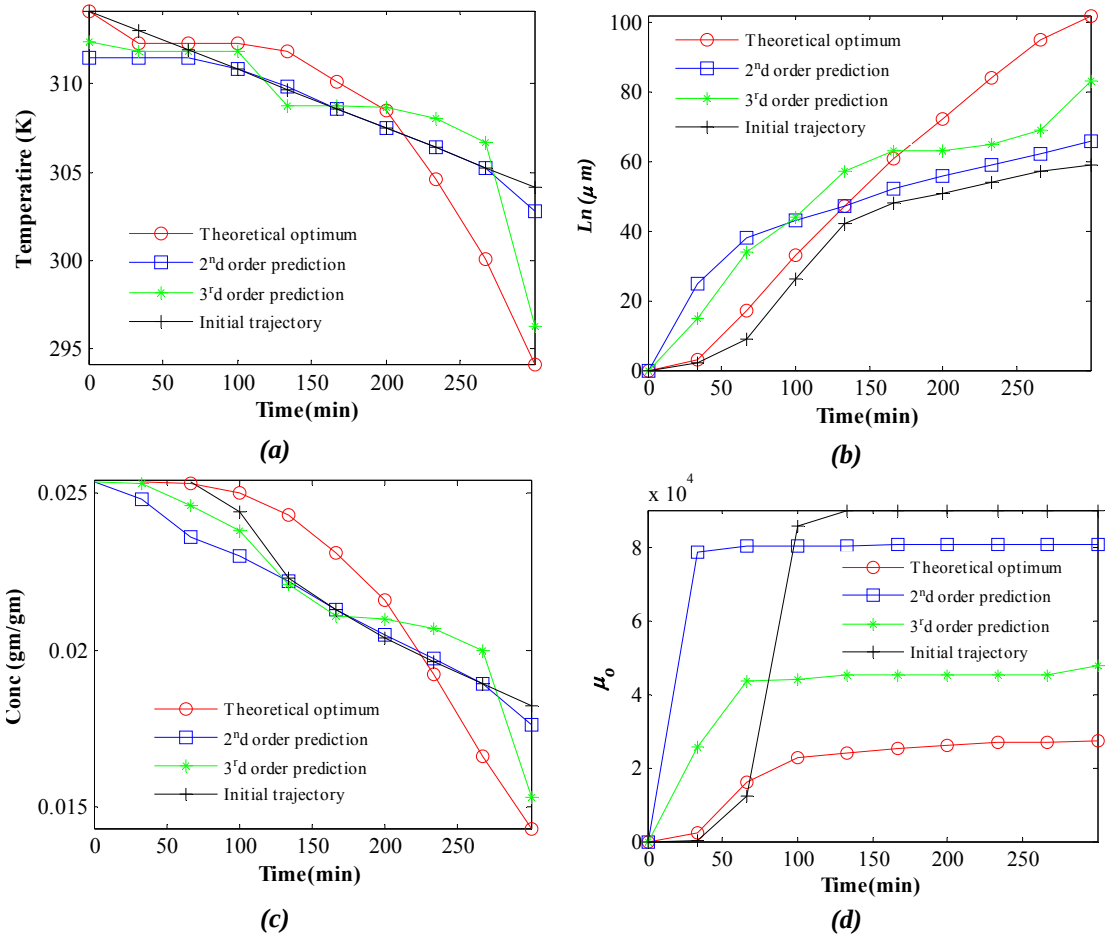


Figure 7.7: Optimum profiles for Case 2a (a) temperature (b) Ln (c) concentration (d) μ_o.

Case 2b Optimisation of the Surrogate Model Using a Nonlinear Initial Temperature Profile without Fixing the Terminal Conditions on Temperatures

In this case, again a nonlinear cooling temperature profile that produced an Ln of 73 μm was used. The constraints on the terminal temperatures were removed as well. As a result of this nonlinear temperature profile with improved initial Ln of 73 μm and imposed flexibility on optimal temperature calculation, the resultant optimal temperatures produced even better final Ln as compared to the previous cases. When applied to the theoretical nonlinear model, the optimum temperature calculated by the second order PCE produced an actual Ln of 89 μm at the end of the batch with the SSE of 1.69×10^{-6}. The optimum temperature calculated by the third order PCE produced an actual Ln of 96 μm at the end of the batch with the SSE of 3.6×10^{-7}, this was an improvement over the previous cases. The results are shown in Figure 7.8 (a) to Figure 7.8 (d).

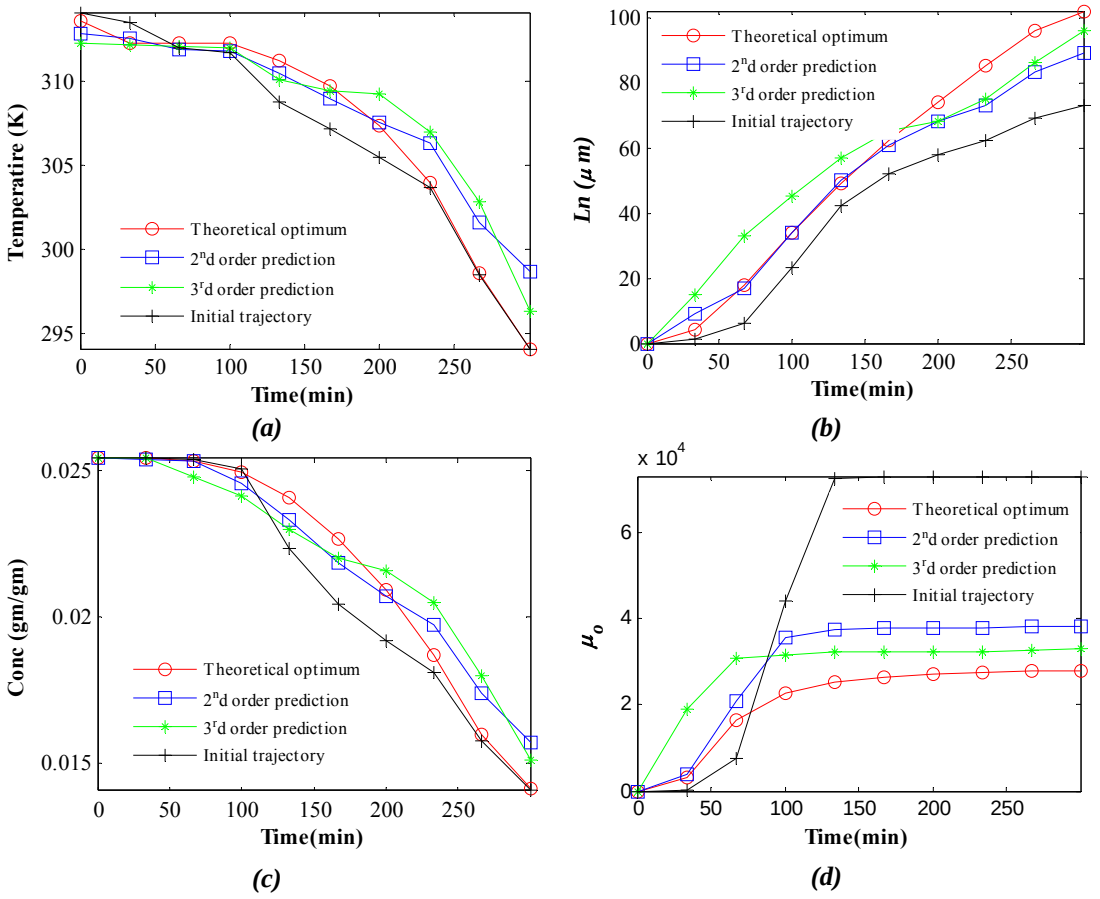


Figure 7.8: Optimum profiles for Case 2b (a) temperature (b) Ln (c) concentration (d) μ_o.

It was observed that the first principle optimal target of Ln = 102 μm was quite far from the maximum limit used in the training data (84 μm, please also see Table 7.3) while identifying the nonlinear surrogate model. As a result of this extrapolation, the Ln produced by the optimal temperature profiles by second and third order surrogate models were quite far from the desired 102 μm in Case 1a, Case 1b, and Case 2a. In addition, the linear initial profile used in these cases (Case 1a and Case 2a) was corresponding to a Ln of 59 μm. Since, this initial guess of 59 μm was very far from the desired 102 μm, the surrogate models suffered to capture the nonlinearity of the system properly. This inferior performance due to a large difference in the initial guess was proved when a nonlinear profile producing a closer initial guess, i.e. 73 μm was used in Case 1b and Case 2b (please see figure Figure 7.6 (b) and Figure 7.8 (b)). Although the second and third order surrogate models produced larger Ln, in both Case 1b and Case 2b as compared to Case 1a and Case 2a respectively, the corresponding temperature profiles were quite different for different initial temperatures under the same optimisation conditions. Theoretically, this study should have been produced two optimal temperature profiles, i.e. same optimal temperature profile for Case 1a and Case 1b and same optimal temperature profiles for Case 2a and Case 2b. This difference of resultant optimal temperature profiles under the same optimisation conditions can be identified as a limitation of the developed nonlinear surrogate model.

Another point to be noted that the second and third order optimal temperature profiles were not the same as the theoretical optimal profile. The reason behind this discrepancy can be the fact that, the first principle model based optimisation was subject to other nonlinear constraints (i.e. constraint on maximum concentration of solution after the batch). Moreover, since this study was aimed at the mean length at the end of the batch, it is possible to arrive at the same final Ln from multiple temperature trajectories. The SSE values for the optimisation test are in perfect harmony with the previous validation SSEs. Moreover, apart from the temperature and Ln profiles Figures 7.5 (c) - Figures 7.5 (d) to Figures 7.8 (c) - Figures 7.8 (d) shows the concentration and μ_o profiles. From these figures, it is evident that the performance of the third order surrogate model was better in terms of better yield and

nucleation point of view. This coherency indeed suggests the choice of third order PCE over second order PCE.

7.5 Conclusions

In this chapter a polynomial chaos expansion (PCE) based nonlinear surrogate modelling approach was developed for batch cooling crystallisation system. The approach used operating data to capture the system's response by representing the system as a sum of Hermite polynomials. The developed surrogate model was then validated and optimised to generate the required temperature profile to obtain a desired mean length (Ln) of crystals at the end of the batch. The PCE approach used least square minimisation (LSM) to calculate the coefficients. The initial assumption of the PCE coefficients played a vital role during all the simulations. So, the overall bottleneck of the PCE based nonlinear surrogate modelling can be identified to be the initial guess of coefficients (e.g. $a_{i_1}^{(d)}, a_{i_1 i_2}^{(d)}$, and $a_{i_1 i_2 i_3}^{(d)}$). Although, LSM is more likely to provide more robust PCE coefficients than the probabilistic collocation method (PCM) it requires many repeated optimisation iterations from previous solution. The LSM focuses mainly at the high probability region, which is good, but not always (e.g. worst case). Although LSM performs better off-line PCM would be required for robust optimisation for quick computation of the PCE coefficients. However, the findings conform to the fact that as the order of expansion was increased the nonlinear system can be identified more precisely. The validation and optimisation results prove that the experimental data based PCE can provide a very good approximation of the desired outputs, providing a generally applicable approach for rapid design, control, and optimisation of batch crystallisation systems based on experimental optimisation.

Chapter 8
Conclusions and Future Works

8.1 Conclusions

The main aim of this research work was to develop and apply different operating data based control strategies for batch chemical processes. As an example case of batch chemical process pharmaceutical batch cooling crystallisation system was chosen to evaluate the proposed data based control strategies. As a kernel of data based control the application of various PAT tools was also facilitated for monitoring and control of pharmaceutical crystallisation operations to ensure consistent production of the desired quality of APIs for efficient downstream operation and product effectiveness.

The work began with a review of the literary works pertaining to this research. The present state of various model based and data based control strategies for batch chemical processes were discussed along with an overview of the fundamentals and control of batch crystallisation processes. The various aspects of PAT tools and their applications in pharmaceutical crystallisation were discussed as well. This is a part of the objective to gain knowledge and understanding about batch processes so that these can be considered in the design of controllers for batch processes.

In this work an LTV perturbation model based ILC strategy was developed for controlling batch chemical processes. The initial concept was based on the work of Xiong and Zhang (2003). The linear perturbation model was obtained by linearizing the nonlinear model along the nominal trajectories to use in ILC scheme for tracking control of product quality. Since this is an operating data based methodology it is capable of controlling a process in the absence of a first principle model. The developed controller was evaluated through computer simulation studies using MATLAB® as platform for three cases. The results show that this approach can track the desired set points satisfactorily even in the present of model plant mismatch.

An industrial case study work has also been performed as a field evaluation of LTV perturbation model based ILC approach. The case studies were carried out in a pilot scale laboratory at GlaxoSmithKline Bangladesh Limited, Chittagong, Bangladesh. The objective was to determine the required drying temperature of Paracetamol granules to obtain desired moisture content at the end of the batch. The result conforms to the converging behaviors of ILC very well. Although the work was undertaken within a limited scope, it was a first hand experience of the researcher to work in an industrial environment.

A novel hierarchical ILC (HILC) scheme for the systematic design of the supersaturation control (SSC) of a seeded batch cooling crystalliser was developed. The proposed HILC can be a convenient tool to select the operating profile in phase diagram. This automated model free approach is implemented in a hierarchical structure. On the upper level, a data-driven supersaturation controller determines the extent of optimal supersaturation needed to produce the desired end-point property of crystals. On the lower level, the corresponding temperature trajectory is determined by time domain experiments to generate necessary supersaturation. The proposed method was evaluated using simulated batch cooling crystallisation process of Paracetamol in water and in a laboratory scale batch crystallisation system of Paracetamol in IPA. The results demonstrated that the approach is able to converge to the desired operating profiles even in the presence of kinetic parameter perturbations without the need of a detailed mechanistic process model. The experimental results also prove that defining the supersaturation trajectories in terms of temperature trajectories is a powerful technique to control the supersaturation throughout the batch. Not only that the temperature trajectories are easier to implement because of the availability of good quality temperature sensors but it also offers the flexibility for adjusting the batch time, which serves as an additional benefit for industrial scale usage.

A systematic evaluation strategy was designed and implemented for direct nucleation control (DNC) approaches of controlling batch cooling crystallisation systems. DNC, as named is aimed to control nucleation events to achieve the desired crystal size distribution (CSD) in a model free approach that requires no prior knowledge on

nucleation or growth kinetics of the system and responds immediately to any unexpected disturbances. For the first time the performance of DNC was compared to that of model based optimal control of a batch cooling crystallisation system of paracetamol in water. In addition, different DNC structures were examined to understand the impact of different designs on batch length, mean crystal size and the number of cooling-heating cycles required to reach the target counts/s. Simulation case studies were performed to controls the amount of nuclei present in the system directly by imitating the performance of FBRM in real life. It was also shown that the laboratory DNC experimental results conform to the simulation findings successfully. The main advantage of this simple model free approach is continuous in situ fine removal during the heating stages without the installation of external heating loops leading to the growth of larger crystals even in the presence of unknown disturbances.

A polynomial chaos expansion (PCE) based nonlinear surrogate modeling approach was developed for controlling batch cooling crystallisation system. The data based nonlinear surrogate model was validated first and then optimised to generate the required temperature profile to obtain a desired mean length (Ln) of crystals at the end of the batch. However, the validation and optimisation results prove that the experimental data based PCE can provide a very good approximation of the desired outputs, providing a generally applicable approach for rapid design, control, and optimisation of batch crystallisation systems based on experimental optimisation.

The research was aimed at developing data based control strategies for batch chemical processes. The developed approaches were then implemented and evaluated for their performance using a laboratory experimental setup built at Loughborough University, UK. The experiments presented in the thesis also illustrates the inclusive application of in situ PAT tools, such as focused beam reflectance measurement (FBRM) for nucleation detection, attenuated total reflection (ATR) UV/Vis spectroscopy for concentration monitoring, particle vision measurement (PVM) for in situ image observation. The experimental framework also satisfies the QbD concept, which accelerates process understanding, inspires incorporation of this process and product knowledge into the process design and ensures improved control of the pharmaceutical crystallisation processes. The key findings of this work can be used to

produce desired crystalline product consistently and commercially through minimal operation costs and reduced batch-to-batch variability.

8.2 Recommendations for Future Works

The following steps of works are recommended as future works:

a) The LTV perturbation model based ILC developed in this study can be applied to any batch process. As an example of field work, the drying temperature required to obtain desired moisture content in paracetamol granules was performed in GlaxoSmithKline, Bangladesh. The experimental evaluation field work was carried out under limited scope. It is recommended that other industrial case studies should be performed to evaluate the proposed approach under wider scope of work.

b) The HILC approach for systematic design of supersaturation control (SSC) of batch cooling crystallisation can also be applied to an industrial scale case study.

c) In this thesis, only computer simulations were performed for the validation and optimisation of the PCE based nonlinear surrogate modelling approach. However, application of this method in the real life laboratory experiments can be a more profound evaluation technique.

d) Both the DNC and PCE based nonlinear surrogate modelling needs to be put into ILC framework for better performance. In case of DNC it is challenging to establish the cooling and heating rates so that the system remains within the metastable limit. Initially for a new system, it requires some trial runs to tune the cooling and heating rates to their bests. It will be an extra benefit to the DNC if it can determine the required heating and cooling rate from the previous history of the systems response under an ILC scheme. In case of PCE based nonlinear surrogate modelling the overall bottleneck of the approach can be identified to be the initial guess of coefficients (e.g. $a_{i_1}^{(d)}, a_{i_1 i_2}^{(d)}$, and $a_{i_1 i_2 i_3}^{(d)}$). Therefore, it will also be helpful in PCE based surrogate modelling to finalise the initial coefficients using the ILC approach.

References

Aamir, E. (2010). *Population Balance Model-Based Optimal Control of Batch Crystallisation Processes for Systematic Crystal Size Distribution Design*. PhD Thesis. Loughborough University. Available online via https://dspace.lboro.ac.uk/2134/5679, accessed on 3/10/2013.

Aamir, E., Nagy, Z.K., & Rielly, C.D. (2008). Systematic design of supersaturation controlled crystallisation processes. *Annual Meeting of American Institute of Chemical Engineering (AIChE)*, Philadelphia, PA, USA.

Aamir, E., Nagy, Z.K., & Rielly, C.D. (2009). Population balance modelling of the dynamic evolution of the crystal size distribution under a size-dependent dissolution mechanism., in: Louhi-Kultanen, M., Hatakka, H. (Eds.), *Proc. of the 16th Int. Workshop on Industrial Crystallization*, Lappeenranta, Finland, pp. 61-68.

Abu Bakar, M.R., Nagy, Z.K., Saleemi, A.N., & Rielly, C.D. (2009). The impact of direct nucleation control on crystal size distribution in pharmaceutical crystallization processes, *Cryst. Growth Des.*, 9(3), pp. 1378-1384.

Adi, H., Larson, I., & Stewart, P. (2007). Use of milling and wet sieving to produce narrow particle size distributions of lactose monohyrate in the sub-sieve range. *Powder Technol.* 179, pp. 95-99.

Agachi, P.Ş., Nagy, Z.K., Cristea, M.V., & Imre-Lucaci, Á. (2006). *Model Predictive Control, in Model Based Control: Case Studies in Process Engineering*, Wiley-VCH Verlag GmbH & Co. KGaA, Weinheim, Germany. doi: 10.1002/9783527609475.ch2

Ahn, H.S., Chen, Y.Q., & Moore, K.L. (2007). Iterative learning control: brief survey and categorization. *IEEE transactions on systems, man, and cybernetics-part c: applications and reviews*, 37(6). pp. 1099-1121.

Allgower, F., Findeisen, R., & Nagy, Z.K. (2004). Nonlinear model predictive control: from theory to application. *Journal of the Chinese Institute of Chemical Engineers*, 35, pp. 299-315.

Anderson, J.E., Moore, S., Tarczynski, F., & Walker, D. (2001). Determination of the onset of crystallization of N1-2-(thiazolyl)sulfanilamide (sulfathiazole) by UV-Vis and calorimetry using an automated reaction platform; subsequent characterization of polymorphic forms using dispersive Raman spectroscopy. *Spectrochimica Acta Part A: Molecular and Biomolecular Spectroscopy,* 57(9), pp. 1793-1808.

Araujo, A.C.B., Govatsmark, M., & Skogestad, S. (2007). Application of plantwide control to the HAD process I-Steady-state optimization and self-optimizing control. *Control Engineering Practice*, 15(10), pp. 1222–1237.

Arimoto, S., Kawamura, S., & Miyazaki, F. (1984). Bettering operation of robots by learning, *J. Robotic Syst*., 1 (1). pp. 123-140.

Augustin, F., Gilg, A., Paffrath, M., Rentrop, P., & Wever, U. (2008). Polynomial chaos for the approximation of uncertainties: Chances and limits, *Euro. J. of Applied Mathematics*, 19, pp. 149-190.

Bakeev, K.A. (2005). *Process Analytical Technology*. Blackwell Publishing Ltd.

Barker, M. & Rawtani, J. (2004). *Practical Batch Process Management*. First Edition. Elsevier Science.

Barrett, M., McNamara, M., Hao, H.X., Barrett, P., & Glennon, B. (2010). Supersaturation tracking for the development, optimization and control of crystallisation processes. *Chem. Eng. Res. Des*., 88 (8A), pp. 1108-1119.

Barrett, P. & Glennon, B. (2002). Characterizing the Metastable Zone width and solubility curve using Lasentec FBRM and PVM. *Trans IChemE, Part A*, 80, pp. 799-805.

Barrett, P., Smith, B., Worlitschek, J., Bracken, V., O'Sullivan, B., & O'Grady, D. (2005). A review of the use of process analytical technology for the understanding and optimization of production batch crystallization processes. *Organic Process Research & Development*, 9, pp. 348-355.

Barthe, S.C., Grover, M.A., & Rousseau, R.W. (2008). Observation of Polymorphic Change through Analysis of FBRM Data: Transformation of Paracetamol from Form II to Form I. *Crystal Growth & Design*, 8(9), pp. 3316-3322.

Barton, A.D., Lewin, P.L., & Brown, D.J. (2000). Practical implementation of a real-time iterative learning position controller. *International Journal of Control*, 73 (10), pp. 992–999.

Bemporad, A. & Morari, M. (1999). Robust model predictive control: A survey. In Garulli, A., Tesi, A., and Vicino, A. (eds.), *Robustness in identification and control*, *Lecture Notes in Control and Information Sciences*, 245. Berlin: Springer, pp. 207-226.

Berber, R. (1996). Control of batch reactors: a review. *Trans IChemE*, 74, pp. 3-20.

Bhalani, K.P. (2010). Moisture Content Determination in Fluid Bed Dryer by Near Infrared Spectroscopy (NIRS). Available via http://pharma.financialexpress.com/20100831/pharmaally09.shtml, accessed 23-9-2013.

Bo, C.M., Li, J., Sun, C.Y., & Wang, Y.R. (2003). The application of neural network soft sensor technology to an advanced control system of distillation operation. *IJCNN*, 2, pp. 1054-1058.

Bonne, D. (2005). *Optimal and reproducible operation of batch processes*. PhD Thesis. Department of Chemical Engineering. Technical University of Denmark.

Bonvin, D. & Mellichamp, D.A. (1982). A unified derivation and critical review of modal approaches to model reduction. *International Journal of Control*, 35, pp. 829-839.

Bonvin, D. (2013). Control and Optimization of Batch Processes, available online via *http://infoscience.epfl.ch/record/188242/files/CObatch.pdf*, accessed on 30-09-2013.

Braatz, R.D. (2002). Advanced control of crystallisation processes. *Annual Reviews in Control*, 26, pp. 87-99.

Braatz, R.D. (2010). *Robust Optimal Control of Finite-time Distributed Parameter Systems*. Available via internet at http://sites.uclouvain.be/inma/reddot/slides/Braatz2009.pdf, accessed 18/10/2013.

Buzzard, G.T. (2011). Global sensitivity analysis using sparse grid interpolation and polynomial chaos. *Reliability Engineering and System Safety*, doi:10.1016/j.ress.2011.07.011.

Cameron, R.H. & Martin, W.T. (1947). The orthogonal development on non-linear functionals in series of Fourier- Hermite functionals. *The Annals of Mathematics*, 48(2), pp. 385-392.

Cazes, J. (2005). *Ewing's Analytical Instrumentation Handbook*. 3rd edition. Marcel Dekker.

Challa, S. & Potumarthi, R. (2013). Chemometrics-based process analytical technology (PAT) tools: applications and adaptation in pharmaceutical and biopharmaceutical industries. *Appl Biochem Biotechnol*, 169(1), pp. 66-76. doi: 10.1007/s12010-012-9950-y.

Chen, J., Sarma, B., Evans, J.M.B., & Myerson, A.S. (2011). Pharmaceutical crystallisation. *Cryst. Growth. Des*.,11, pp. 887-895.

Chen, Y.Q. & Moore, K.L. (2002). A practical iterative learning pathfollowing control of an omni-directional vehicle. *Asian J. Contr*., 4 (1), pp. 90-98.

Chew, J.W., Black, S.N., Chow, P.S., & Tan, R.B.H. (2007a). Comparison between open-loop temperature control and closed-loop supersaturation control for cooling crystallization of glycine. *Ind. Eng. Chem. Res*., 46, pp. 830-838.

Chew, J.W., Chow, P.S., & Tan, R.B.H. (2007b). Automated In-line Technique Using FBRM to Achieve Consistent Product Quality in Cooling Crystallization. *Cryst. Growth Des*., 7 (8), pp. 1416-1422.

Chiu, T. & Christofides, P. (1999). Nonlinear control of particulate processes. *American Institute of Chemical Engineering Journal*, Vol. 45, pp. 1279-1297.

Choong, K.L. & Smith, R., (2004). Optimization of batch cooling crystallization. *Chemical Engineering Science*, 59, pp. 313-327.

Christofides, P.D. (2001). Control of nonlinear distributed process systems: recent developments and challenges. *American Institute of Chemical Engineering Journal*, 47(3), pp. 514-518.

Cichy, B., Galkowski, K., Rogers, E., & Kummert, A. (2011). An approach to iterative learning control for spatio-temporal dynamics using nD discrete linear systems models. *Multidimensional Systems and Signal Processing*, 22, pp. 83-96.

Curtain, R.F. (2003). Model reduction for control design for distributed parameter systems. In R.C. Smith & M.A. Demetriou (eds.), *Research directions in distributed parameter systems*, pp. 95–118. Philadelphia: SIAM: Frontiers in Applied Mathematics.

Dawoodbahai, S. and Rhodes, C.T. (1989). The Effect of Moisture on Powder Flow and on Compaction and Physical Stability of Tablets. *Drug Dev. Ind. Pharm*., 15 (10), pp. 1577-1600.

de Roover, D. & Bosgra, O.H. (2000). Synthesis of robust multivariable iterative learning controllers with application to a wafer stage motion system. *Int. J. Contr*., 73 (10), pp. 968–979.

Diehl, M., Gerhard, J., Marquardt, W., & Mönnigmann, M. (2008). Numerical solution approaches for robust nonlinear optimal control problems. *Computers & Chemical Engineering*, 32 (6), pp. 1287-1292.

Doki, N., Kubota, N., Yokota, M., Kimura, S., & Sasaki, S. (2002). Production of sodium chloride crystals of uni-modal size distribution by batch dilution crystallization, J. Chem. Eng. Jpn., 35, pp. 1099-1104.

Ekpo, E.E. (2006). Dynamic optimisation and control of batch polymerisation process. *PhD thesis dissertation* (*unpublished*). University of Bradford, UK.

Fagiano, L. & Khammash, M. (2012). Simulation of stochastic systems via polynomial chaos expansions and convex optimization. To appear. Preliminary version available on arXiv - arXiv:1202.0753v1.

FDA, U.S. Food and Drug Administration. (2004). *Guidance for Industry: PAT – A Framework for Innovative Pharmaceutical Development, Manufacturing, and Quality Assurance*. Available via the Internet at *http://www.fda.gov/cder/guidance/6419fnl.pdf* (accessed 05.05.13).

Findeisen, R., Imsland, L., Allgöwer, F., & Foss, B. (2003). State and output feedback nonlinear model predictive control: an overview. *Eur. J. Contr*., 9(2-3), p. 190.

Fisher, J. & Bhattacharya, R. (2009). Linear quadratic regulation of systems with stochastic parameter uncertainties. *Automatica*, 45(12), pp. 2831 - 2841.

Forgione, M., Mesbah, A., Bombois, X., & Van den Hof, P.M.J. (2012). Iterative Learning Control of Supersaturation in Batch Cooling Crystallization. *Proceedings of the American Control Conference (ACC)*, Montreal, Canada, June 27-29, pp. 6455-6460.

Fujiwara, M., Chow, P.S., Ma, D.L., & Braatz, R.D. (2002). Paracetamol crystallization using laser backscattering and ATR–FTIR spectroscopy: metastability, agglomeration, and control. *Crystal Growth & Design*, 2, pp. 363-370.

Fujiwara, M., Nagy, Z.K., Chew, J.W., & Braatz, R.D. (2005). First principles and direct design approaches for the control of pharmaceutical crystallisation. *Journal of Process Control*, 15, pp. 493-504.

Gao, F., Yang, Y., & Shao, C. (2001). Robust iterative learning control with applications to injection molding process, *Chem. Eng. Sci.*, 56, (24), pp. 7025-7034.

Garimella, S. & Srinivasan, K. (1998). Application of iterative learning control to coil-to-coil control in rolling. *IEEE Trans. Contr. Syst. Technol.*, 6 (2), pp. 281-293.

Gay, D.H. & Ray, W.H. (1995). Identification and control of distributed parameter systems by means of the singular value decomposition. *Chemical Engineering Science*, 50 (10), pp. 1519-1539.

Ghanem, R. & Spanos, P. (1991). Spectral Stochastic Finite-Element Formulation for Reliability Analysis. *J. Eng. Mech.*, 117(10), pp. 2351-2372. http://dx.doi.org/10.1061/(ASCE)0733-9399(1991)117:10(2351).

Ghanem, R. & Spanos, P. (1993). A stochastic galerkin expansion for non-linear random vibration analysis. *Probabilistic Engineering Mechanics*, 8, pp. 255-264.

Giulietti, M., Seckler, M.M., Derenzo, S., Ré, M.I., & Cekinski, E. (2001). Industrial crystallisation and precipitation from solutions: state of the technique. *Braz. J. Chem. Eng.*, 18(4), available via Internet at http://dx.doi.org/10.1590/S0104-66322001000400007 (accessed 05.05.13).

Glennon, B. (2002). Characterising the metastable zone and solubility curve using Lasentec FBRM and PVM. *Chem. Eng. Res. Des.,* 80, pp. 799-805.

Hanczyc, E.M. & Palazoglu, A. (1995). Sliding Mode Control of Nonlinear Distributed Parameter Chemical Processes. *Ind. Eng. Chem. Res.*, Vol. 34. pp. 557-566.

Hangos, K.M. & Virág, T. (1986). The effect of point-like noise sources on chemical distributed parameter systems. *System Modelling and Optimization-Lecture Notes in Control and Information Sciences*, 84, pp. 298–303, DOI: 10.1007/BFb0043850.

Hardenberg, J.V., Kenning, D.B.R., Xing, H., & Smith, L.A. (2004). Identification of nucleation site interactions. International Journal of Heat and Fluid Flow 25, pp. 298-304.

Hastie, T., Tibshirani, R., & Friedman, J. (2001). *The elements of statistical learning: Data mining, inference, and prediction*. Springer.

Haykin, S. (1994). *Neural Networks - A Comprehensive Foundation*. Macmillan College

Hixson, A.W. & Knox, K.L. (1951). Effect of agitation on rate of growth of single crystals. *Ind. Eng. Chem*., 43, pp. 2144 - 2151.

Hoffmann, W., Peterson, K., & Stephanopoulos, A.G. (2003). Iterative learning control for soft landing of electromechanical valve actuator in camless engines. *IEEE Trans. Contr. Syst. Technol.*, 11(2), pp. 174-184.

Hojjati, H. & Rohani, S. (2006). Measurement and Prediction of Solubility of Paracetamol in Water−Isopropanol Solution. Part 1. Measurement and Data Analysis. *Organic Process Research & Development*, 10(6), pp. 1101-1109.

Hounslow, M.J. & Reynolds, G.K. (2006). Product engineering for crystal size distribution. *AIChE Journal*, 52, pp. 2507-2517.

Howard, K.S., Nagy, Z.K., Saha, B.,Roberston, A.L., Steele, G., & Martin, D. (2009). A process analytical technology based investigation of the polymorphic transformations during the antisolvent crystallization of sodium benzoate from IPA/water mixture. *Cryst. Growth Des.*, 9, pp. 3964-3975.

Huan, X. & Marzouk, Y.M. (2013). Simulation-based optimal Bayesian experimental design for nonlinear systems. *Journal of Computational Physics*, 232, pp. 288-317.

Huang, R., Patwardhan, S.C., & Biegler, L.T. (2009). Multi-scenario-based robust nonlinear model predictive control with first principle models. *10th International Symposium on Process Systems Engineering - PSE2009*, Bahia, Brazil.

Hukkanen, E.J. & Braatz, R.D. (2003). Measurement of particle size distribution in suspension polymerzation using in situ laser backscattering". *Sensors and Actuators*, B96, pp. 451-459.

Hussain, M.A. (1999). Review of the applications of neural networks in chemical process control- simulation and on-line implementation. Artificial Intelligence in Engineering, 13, pp. 55–68.

Isukapalli, S.S., Roy, A., & Georgopoulos, P.G. (1998). Stochastic Response Surface Methods (SRSMs) for uncertainty propagation: Application to environmental and biological systems. *Risk Analysis*, 18(3), pp. 351–363.

Jagadesh, D., Kubota, N., Yokota, M., Doki, N., Sato, A., & Tavare, N. (1996). Large and mono-size product crystals from natural cooling mode batch crystallization, *J. Chem. Eng. Jpn.*, 29, pp. 865– 873.

Jang, J.S.R., Sun, C.T., & Mizutani, E. (1997). Neuro-fuzzy and soft computing. Upper Saddle River, NJ: Prentice Hall.

Jolliffe, I.T. (2002). *Principal component analysis*. Springer.

Jones, A.G. (1974). Optimal operation of a batch crystallizer. *Chem. Eng. Sci*., 29, pp. 1075–1087.

Jones, A.G. (2002). *Crystallization Process Systems*. Butterworth-Heinemann.

Kadlec, P., Gabrys, B., & Stran dt, S. (2009). Data-driven soft sensors in the process industry. *Comput. Chem. Eng*., 33, pp. 795–814

Kano, M., & Nakagawa, Y. (2008). Data-based process monitoring, process control, and quality improvement: recent developments and applications in steel industry. Comput Chem Eng., 32, pp. 12–24.

Kayihan, F. (1997). A review of modeling and control in the pulp and paper industries. In Kantor, J.C., Garcıa, C.E., and Carnahan, B. (eds.). *Fifth international conference on chemical process control,* California, USA, pp. 117–132.

Kee, N.C.S., Tan, R.B.H. & Braatz, R.D. (2009). Selective Crystallization of the Metastable α-Form of L-Glutamic Acid using Concentration Feedback Control. *Crystal Growth & Design*, 9(7), pp. 3044- 3051.

Keese, A. & Matthies, H.G. (2003). Sparse quadrature as an alternative toMonte Carlo for stochastic finite element techniques. *Proc. Appl.Math. Mech*., 3, pp. 493-494. 0.1002/pamm.200310516.

Kim, D.I., & Kim, S. (1996). An iterative learning control method with application for CNC machine tools. *IEEE Trans. Ind. Applicat.*, 32 (1), pp. 66–72.

Kim, H., Bang, Y., Lee, K.S. & Yang, D.R. (2009). Use of calorimetry model and batch control technique for scale-up of unseeded batch cooling crystallization of Poly (Hydroxybenzophenone). *Ind. Eng. Chem. Res.*, 48, pp. 6776–6782.

Kim, K.K.K. & Braatz, R.D. (2012). Generalized polynomial chaos expansion approaches to approximate stochastic receding horizon control with applications to probabilistic collision checking and avoidance. *In Proc. of the IEEE Conference on Control Applications*, Dubrovnik, Croatia, pp. 350-355.

Lee, J.H. & Lee, K.S. (2007). Iterative learning control applied to batch processes: An Overview. *Control Engineering Practice*, 15, pp. 1306–1318.

Lee, J.H. (2008). Lecture 3-Dynamic Modeling Part II: writing balances for lumped and distributed parameter systems. From *http://www.coursehero.com/file/2111661/ Lecture3b2up/?v0=1*. Accessed on 2 June 2011.

Lee, J.H., Lee, K.S., & Kim, W.C. (2000). Model-based iterative learning control with a quadratic criterion for time-varying linear systems. *Automatica*, 36, pp. 641–657.

Lee, K.S. & Lee, J. H. (2003). Iterative learning control-based batch process control technique for integrated control of end product properties and transient profiles of process variables. *Journal of Process Control*, 13, pp. 607–621.

Lee, K.S. & Lee, J.H. (1999). Model based refinement of input trajectories for batch and other transient processes. AIChE Meeting, Chicago (1996). Also *Automatica*, in press, *http://procd.sogang.ac.kr/pub.html#jint*.

Lee, K.S., Bang, S.H., & Chang, K.S. (1994). Feedback-assisted iterative learning control based on an inverse process model. *J. Process Control*, 4 (2), pp. 77–89.

Lee, K.S., Kim, W.C., & Lee, J.H. (1996). Model-based iterative learning control with quadratic criterion for linear batch processes. *J. Cont. Autom. Sys. Engng*., 2, pp. 148–157.

Lee, K.S., Lee, J.H., Chin, I.S., & Lee, H.J. (1999). Model predictive control technique combined with iterative learning control for batch processes, *AIChE Journal*, 45, pp. 2175–2187.

Lepage. K.D. (2006). Estimation of acoustic propagation uncertainty through polynomial chaos expansions. *9th International Conference on Information Fusion*, Florence, Italy, pp. 1–5.

Li, H. & Zhang, D. (2009). Probabilistic collocation method for flow in porous media: Comparisons with other stochastic methods. *Water Resources Research*, 43, pp. 44–48.

Li, H.X. & Qi, C. (2010). Modeling of distributed parameter systems for applications-A synthesized review from time-space separation. *Journal of Process Control*, 20, pp. 891–901.

Limon, D., Alamo, T., Raimondo, D., Peña, D.M., Bravo, J., & Camacho, E. (2009). Input-to-state stability: a unifying framework for robust model predictive control. In: Thoma, M., Allgöwer, F. and Morari, M., (eds.). *Lecture Notes in Control and Information Sciences*, 384, NY: Springer-Verlag, pp. 1–26.

Lin, C. & Lee, C. (1996). *Neural fuzzy systems: A neuro-fuzzy synergism to intelligent systems.* Upper Saddle River, NJ, USA: Prentice-Hall, Inc.

Lin, G. & Tartakovsky, A.M. (2009). An efficient, high-order probabilistic collocation method on sparse gridsfor three-dimensional flow and solute transport in randomly heterogeneous porous media. Advances in Water Resources 32 (5):712-722. doi:10.1016/j.advwatres.2008.09.003.

Lin, G., Engel, D.W., & Eslinger, P.W. (2012). *Survey and Evaluate Uncertainty Quantification Methodologies*. Prepared for the U.S. Department of Energy under Contract DE-AC05-76RL01830, PNNL- 20914. Available online at http://www.pnnl.gov/main/publications/external/technical_reports/PNNL-20914.pdf, accessed on 7/10/2013.

Liotta, V. & Sabesan, V. (2004). Monitoring and Feedback Control of Supersaturation Using ATRFTIR to Produce an Active Pharmaceutical Ingredient of a Desired Crystal Size. *Organic Process Research & Development*, 8(3), pp. 488-494.

Liu, G., Yu, S., Mei, C., & Ding, Y. (2011). A Novel Soft Sensor Model Based on Artificial Neural Network in the Fermentation Process. *Afr. J. Biotechnol*., 10, pp. 19780–19787.

Loan, M., Parkinson, G., Newman, M., & Farrow, J. (2002). Iron oxy-hydroxide crystallization in a hydrometallurgical residue. *Journal of Crystal Growth*, 235(1-4), pp. 482-488.

Logsdon, J.S. & Biegler, L.T. (1989). Accurate Solution of Differential-Algebraic Optimization Problems. *Ind. Eng. Chem. Res*., 28, pp. 1628–1639.

Matthies, H.G. & Keese, A. (2005). Galerkin methods for linear and non-linear elliptic stochastic partial differential equations. *Comp. Meth. Appl. Mech. Engrg*., 194, pp. 1295–1331.

McCulloch, W.S. & Pitts, W. (1943). A logical calculus of ideas immanent in nervous activity. *Bull. Math. Biophys*., 5, pp. 115-133.

Mi, C., Lin, H., & Zhang, Y. (2005). Iterative learning control of antilock braking of electric and hybrid vehicles. *IEEE Trans. Veh. Technol*., 54 (2), pp. 486–494.

Miller, S.M. & Rawlings, J.B. (1994). Model identification and control strategies for batch cooling crystallizers. *AIChE Journal*, 40, pp. 1312–1327.

Modarresi, H., Conte, E., Abildskov, J., Gani, R. & Crafts, P. (2008). Model-Based Calculation of Solid Solubility for Solvent Selection – A Review. *Industrial & Engineering Chemistry Research*, 47(15), pp. 5234-5242.

Mohameed, H.A., Abdel-Jabbar, N., Takrouri, K., & Nasr, A. (2003). Model-based optimal cooling strategy for batch crystallization processes. *Chem. Eng. Res. Des*., 81, pp. 578–584.

Moore, K.L. (1998). Iterative learning control-an expository overview, in: B.S. Datta (ed.). *Applied & Computational Controls, Signal Processing, and Circuits*, Boston: Kluwer Academic, pp. 425–488.

Motz, S. & Gilles, E.D. (2008). State estimation in batch crystallisation using reduced population balance models. *J. Process Control*, 18, 361-337.

Mullin, J.W. & Gaska, C. (1969). The growth and dissolution of potassium sulphate crystals in a fluidized bed crystallizer. *Can. J. Chem. Engng*, 47, pp. 483-489.

Mullin, J.W. (2001). *Crystallization*. Fourth ed. Butterworth Heinemann: London, UK.

Myerson, A.S. (2002). *Handbook of Industrial Crystallization*. Butterworth-Heinemann Ltd: Oxford.

Nagy, Z.K, Aamir, E., & Rielly, C.D. (2011). Internal fines removal using population balance model based on control of crystal size distribution under dissolution, growth, and nucleation mechanisms. *Cryst. Growth. Des.*, 11, pp. 2205–2219.

Nagy, Z.K. & Allgower, F. (2004). Nonlinear model predictive control: from chemical industry to microelectronics. *43rd IEEE Conference on Decision and Control*, Atlantis, Bahamas.

Nagy, Z.K. & Braatz, R.D. (2003). Robust nonlinear model predictive control of batch processes. *AIChE Journal*, 49, pp. 1776–1786.

Nagy, Z.K. & Braatz, R.D. (2004). Open-loop and closed-loop robust optimal control of batch processes using distributional and worst-case analysis. *J. of Process Control*, 14, pp. 411-422.

Nagy, Z.K. & Braatz, R.D. (2007). Distributional uncertainty analysis using power series and polynomial chaos expansions. *Journal of Process Control*, 17, pp. 229–240, doi:10.1016/j.jprocont.2006.10.008.

Nagy, Z.K. & Braatz, R.D. (2010). Distributional Uncertainty Analysis Using Polynomial Chaos Expansions. In proceedings of the *IEEE International Symposium on Computer-Aided Control System Design*, Yokohama, Japan, pp. 1103-1108.

Nagy, Z.K. (2009). Model based robust control approach for batch crystallization product design. *Computers and Chemical Engineering*, 33, pp. 1685–1691.

Nagy, Z.K., Chew, J.W., Fujiwara, M., & Braatz, R.D. (2008a). Comparative performance of concentration and temperature controlled crystallizations. *Journal of Process Control,* 18 (3–4), pp. 399–407.

Nagy, Z.K., Fujiwara, M., & Braatz, R.D. (2006). Optimal control of combined cooling and anti-solvent pharmaceutical crystallization. *13th International Workshop on Industrial Crystallization (BIWIC 2006)*, Delft, The Netherlands.

Nagy, Z.K., Fujiwara, M., Woo, X.Y., & Braatz, R.D. (2008b). Determination of the kinetic parameters for the crystallization of paracetamol from water using metastable zone width experiments. *Ind. Eng. Chem. Res.*, 47, p. 1245.

Nikolaou, M. & Misra, P. (2003). Linear control of nonlinear processes: recent developments and future directions. *Computers and Chemical Engineering*, 27, pp. 1043–1059.

Nokhodchi, A. (2005). An Overview of the Effect of Moisture on Compaction and Compression. Pharmaceutical Technology, pp 46-66. Available via *http://www.pharmtech.com/pharmtech/data/articlestandard/pharmtech/022005/141826/article.pdf*, accessed on 18-9-2013.

Norrlof, M. (2002). An adaptive iterative learning control algorithm with experiments on an industrial robot. *IEEE Trans. Robot. Automat*., 18 (2), pp. 245–251.

Nyvlt, J., Karel, M., & Pisarik, S. (1994). Measurement of supersaturation. *Cryst. Res. Technol*., 29, pp. 409-415.

O'Grady, D. (2011). Supersaturation: Driving Force for Crystal Nucleation & Growth. Available via *http://blog.autochem.mt.com/2011/03/supersaturation-driving-force-for-crystal-nucleation-growth/*, accessed 23-9-2013.

Oladyshkin, S. & Nowak, W. (2012). Data–driven uncertainty quantification using the arbitrary polynomial chaos expansion. *Reliability Engineering and System Safety*, 106, pp. 179–190. Available from http://dx.doi.org/10.1016/j.ress.2012.05.002.

Oladyshkin, S., Class, H., Helmig, R., & Nowak, W. (2011). An integrative approach to robust design and probabilistic risk assessment for CO2 storage in geological formations. *Computational Geosciences*, 15(3), pp. 565–577.

Oladyshkin, S., de Barros, F.P.J., & Nowak, W. (2012). Global sensitivity analysis: a flexible and efficient framework with an example from stochastic hydrogeology. *Advances inWater Resources*, 37, pp. 1508- 1518.

Orukpe, P.E. (2005). Basics of model predictive control. *ICM*, *EEE-CAP*. Imperial College, London.

Padhi, R. and Ali, F. (2009). An account of chronological developments in control of distributed parameter systems. *Annual Reviews in Control*, 33. pp. 59-68.

Pons, M-N., Milferstedt, K., & Morgenroth, E. (2006). Modeling of chord length distributions. *Chem. Eng. Sci.*, 61, pp. 3962-3973.

Prempraneerach, P., Hover, F.S., Triantafyllou, M.S., & Karniadakis, G.E. (2010). Uncertainty quantification in simulations of power systems: Multielement polynomial chaos methods. *Reliability Engineering and System Safety*, 95, pp. 632-646.

Principe, J.C., Euliano, N.R., & Lefebvre, W.C. (2000). Neural and adaptive systems. New York: Wiley.

Qin, S.J. & Badgwell, T.A. (2003). A survey of industrial model predictive control technology. *Control Engineering Practice*, 11, pp. 733–764.

Qin, S.J. and Badgwell, T.A. (2000). An overview of nonlinear model predictive control applications. In: F. Allgower and A. Zheng (eds.), *Nonlinear model predictive control*, Switzerland: Birkhauser.

Qu, H. (2007). Towards desired crystalline product properties: in-situ monitoring of batch crystallization, Lappeenranta.

Rawlings, J.B., Miller, A.G., & Witkowaski, W.R. (1993). Model identification and control of solution crystallization processes: A review. *Ind. Eng. Chem. Res*., 32, pp.1275-1296.

Ray, W.H. (1981). *Advanced Process Control.* New York: McGraw-Hill.

Reutzel-Edens, S.M. (2006). Achieving polymorph selectivity in the crystallization of pharmaceutical solids: Basic considerations and recent advances*. Current Opinion in Drug Discovery & Development*, 9(6), pp. 806–815.

Rodriguez-Hornedo, N., & Murphy, D. (1999). Significance of controlling crystallization mechanisms and kinetics in pharmaceutical systems. *J. Pharm. Sci.*, 88 (7), pp. 651- 660.

Rogers, E., Gałkowski, K., & Owens, D.H. (2007). Control systems theory and applications for linear repetitive processes. *Lecture notes in control and information sciences*, 349. New York: Springer.

Rohani, S. (2010). Applications of the crystallization process in the pharmaceutical industry. *Front. Chem. Eng. China*, 4(1), pp. 2–9.

Roman, R., Nagy, Z.K., Cristea, M.V., & Agachi, P.S., (2009). Dynamic modelling and nonlinear model predictive control of a Fluid Catalytic Cracking Unit. *Computers and Chemical Engineering*, 33, pp. 605–617.

Russell, S.A., Kesavan, P., and Lee, J.H. (1998). Recursive data-based prediction and control of batch product quality. *AIChE Journal*, 44, pp. 2442–2458.

Saab, S.A. (2004). A stochastic iterative learning control algorithm with application to an induction motor. *Int. J. Contr*., 77 (2), pp. 144-163.

Saleemi, A., Rielly, C.D., & Nagy, Z.K. (2012a). Automated direct nucleation control for in situ dynamic fines removal in batch cooling crystallization. *Cryst. Eng. Comm*., 14, pp. 2196–2203.

Saleemi, A.N., Rielly, C.D., & Nagy, Z.K. (2012b). Comparative investigation of supersaturation and automated direct nucleation control of crystal size distributions using ATR-UV/Vis spectroscopy and FBRM. *Cryst. Growth Des*., available via the Internet at *http://pubs.acs.org/doi/ipdf/10.1021/cg201269c* (accessed 05.05.13).

Sandoval, E.H., Anstett-Collin, F., & Basset, M. (2012). Sensitivity study of dynamic systems using polynomial chaos. *Reliability Engineering and System Safety*, 104, pp. 15–26.

Seborg, D.E. 1999. A perspective on advanced strategies for process control (Revisited), In: P.M. Frank (ed.) *Advances in Control*, NY: Springer-Verlag, pp. 103-134.

Seborg, D.E., Edgar, T.F., & Mellichamp, D.A. (2004). Process Dynamics and Control, 2nd Edition., New York: Wiley.

Sepahvand, K., Marburg, S., & Hardtke, H.-J. (2010). Uncertainty quantification in stochastic systems using polynomial chaos expansion. *International Journal of Applied Mechanics*, 2 (2), pp. 305-353.

Shang, H., Forbes, J.F., & Guay, M. (2004). Model predictive control for quasilinear hyperbolic distributed parameter systems. *Ind. Eng. Chem. Res.*, 43, pp. 2140-2149.

Shang, H., Forbes, J.F., & Guay, M. (2005). Feedback control of hyperbolic distributed parameter systems. *Chemical Engineering Science*, 60, pp. 969-980.

Shen, J.X., Chiu, M.-S., & Wang, Q.G. (1999). A comparative study of model-based control techniques for batch crystallization process. *Journal of Chemical Engineering of Japan*, 32, 456–464.

Skogestad, S. (2004). Control structure design for complete chemical plants. *Computers & Chemical Engineering*, 28, pp. 219–234

Soos, M., Sefcik, J., & Morbidelli, M. (2006). Investigation of aggregation, breakage and restructuring kinetics of colloidal dispersions in turbulent flows by population balance modelling and static light scattering. *Chem. Eng. Sci*. 61, pp. 2349-2363.

Sudret, B. (2008). Global sensitivity analysis using polynomial chaos expansions. *Reliability Engineering and System Safety*, 93, pp. 964–979.

Svozil, D., Kvasnicka, V., & Posp´ıchal, J. (1997). Introduction to multi-layer feed-forward neural networks. *Chemom. Intell. Lab. Syst.*, 39, pp. 43-62.

Tavare, N.S. (1995). *Industrial Crystallization, Process Simulation, Analysis and Design*. Plenum Press, NY.

Templeton, B. (2009). *A Polynomial Chaos Approach to Control Design*. PhD thesis. Virginia Polytechnic Institute and State University.

Thomas, L. & C´edric, S. (2011). Analysis of saturated system with stochastic parameter uncertainties: a Polynomial Chaos approach. In *Preprints of the 18th IFAC World Congress*, Milano, Italy, pp. 11214- 11219.

Thompson, D.R., Kougoulos, E., Jones, A.G., & Wood-Kaczmar, M.W. (2005). Solute concentration measurement of an important organic compound using ATR-UV spectroscopy. *Journal of Crystal Growth*, 276(1-2), pp. 230-236.

Tian, S.P., Xie, S.L., & Xie, Z.D. (2004). Iterative learning control algorithms based on geometric analysis. *Control and Decision*, 19, pp. 1038-1041.

Tititz-Sargut, S. & Ulrich, J. (2002). Influence of additives on the width of the metastable zone. *Crystal Growth & Design*, 2, pp. 371-374.

Togkalidou, T., Fujiwara, M., Patel, S. & Braatz, R.D. (2001). Solute concentration prediction using chemometrics and ATR-FTIR spectroscopy. *Journal of Crystal Growth*, 231(4), pp. 534-543.

Tousey. M.D. (2002). The granulation process 101, basic technologies for tablet making. *Pharm. Tech. Tableting and Granulation*. 2002. Available via *http://www.techceuticals.com/The_Granulation_Process_101.pdf*, accessed on 18-9-2013.

United States Pharmacopeia (2002). United States Pharmacopeia/National Formulary (USP29/NF24)., Rockville, MD: United States Pharmacopeia Convention Inc. Available via http://www.pharmacopeia.cn/v29240/usp29nf24s0_c1151s87.html, accessed on 18-9-2013.

Valero, F. (2013). Bioprocess Engineering of Pichia pastoris, an Exciting Host Eukaryotic Cell Expression System, Protein Engineering - Technology and Application, Dr. Tomohisa Ogawa (Ed.), ISBN: 978-953-51-1138-2, InTech, DOI: 10.5772/56407. Available from: http://www.intechopen.com/books/protein-engineering-technology-and-application/bioprocess-engineering-of-pichia-pastoris-an-exciting-host-eukaryotic-cell-expression-system, accessed 1/10/2013.

Vergote, G.J., DE Beer, T.R.M., Vervaet, C., Remon, J.P., Baeyens, W.R.G., Diericx, N. & Verpoort, F. (2004). In-line monitoring of a pharmaceutical blending process using FT-Raman spectroscopy. *European Journal of Pharmaceutical Sciences*, 21(4), pp. 479-485.

Wan, X. & Karniadakis, G.E. (2006). Multi-element generalized polynomial chaos for arbitrary probability measures. *SIAM Journal of Scientific Computing*, 28(3), pp. 901-928.

Wang, F. & Berglund, K.A. (2000). Monitoring pH Swing Crystallization of Nicotinic Acid by the Use of Attenuated Total Reflection Fourier Transform Infrared Spectrometry. *Industrial & Engineering Chemistry Research*, 39(6), pp. 2101-2104.

Wang, H., Zhang, J.F., & Yue, H. (2005). Iterative learning control of output pdf shaping in stochastic systems. *Proceedings of the 2005 IEEE International Symposium on Intelligent Control*. Limassol, Cyprus, pp. 1225-1230.

Wang, M.L., Li, N., & Li, S.Y. (2010). Model-based predictive control for spatially-distributed systems using dimensional reduction models. *International Journal of Automation and Computing*: ISSN:1751-8520(Online) CN: 11-5350/TP [IJAC-2010-01-001].

Wang, Y., Shi, J., Zhou, D. & Gao, F. (2006). Iterative learning fault-tolerant control for batch processes. *Ind. Eng. Chem. Res*., 45, pp. 9050-9060.

Wiener, N. (1938). The homogeneous chaos. *Amer. J. Math*., 60, pp. 897-936.

Wold, S., Sjstrm, M., & Eriksson, L. (2001). PLS-regression: A basic tool of chemometrics. *Chemometrics and Intelligent Laboratory Systems*, 58(2), pp. 109-130.

Woo, X.Y., Nagy, Z.K., Tan, R.B.H., & Braatz, R.D. (2009). Adaptive concentration control of cooling and antisolvent crystallization with laser backscattering measurement. *Crystal Growth & Design*, 9, pp. 182-191.

Workman, J.Jr. (2005). Chemometrics and PAT: What Does it all Mean? *The Role of Spectroscopy in Process Analytical Technologies*, pp. 18-23.

World Health Organization (WHO) (2011). Revision of monograph on tablets-final text for addition to the international pharmacopoeia. Document QAS/09.324/Final. Available via *http://www.who.int/medicines/publications/pharmacopoeia/Tabs-GeneralMono-rev-FINAL_31032011.pdf,* accessed on 18-9-2013.

Worlitschek, J. & Mazzotti, M. (2004). Model-based optimization of particle size distribution in batch-cooling crystallization of paracetamol. *Crystal Growth & Design*, 4 (5), pp. 891-903.

Xie, S.L., Tian, S.P., & Xie, Z.D. (2004). New iterative learning control algorithms based on vector plots analysis. *Acta Automatica Sinica*, 30, pp. 161-168.

Xie, S.L., Tian, S.P., & Xie, Z.D. (2005). *Iterative learning control theory and application*. Beijing: Science Press.

Xie, S.L., Xie, Z.D., & Wei, G. (1999). Learning algorithm for tracking control of nonlinear distributed parameter systems. *Acta Automatica Sinica*, 25, pp. 627–632.

Xie, Z.D. & Liu, Y.Y. (1998). Two order P-type learning control algorithm of distributed parameter systems. *Journal of Jinan University*, 19, pp. 60-64.

Xiong, Z. & Zhang, J. (2003). Product quality trajectory tracking in batch processes using iterative learning control based on time-varying perturbation models. *Ind. Eng. Chem. Res.*, 42, pp. 6802-6814.

Xiong, Z. & Zhang, J. (2004). Batch-to-batch optimal control of nonlinear batch processes based on incrementally updated models. *IEE Proc.-Control Theory Appl*., 151(2), pp. 158-165.

Xiong, Z. & Zhang, J. (2005). A batch-to-batch iterative optimal control strategy based on recurrent neural network models. *Journal of Process Control*, 15, pp. 11-21.

Xiong, Z., Xu, Y., Dong, J., & Zhang, J. (2010). Neural network based iterative learning control for product qualities in batch processes. *International Journal of Modelling, Identification and Control*, 11(1-2), pp. 107-114.

Xiong, Z., Zhang, J., Wang, X., & Xu, Y. (2005). Tracking control for batch processes through integrating batch-to-batch iterative learning control and within-batch on-line control. *Ind. Eng. Chem. Res*., 44, pp. 3983-3992.

Xiu, D. & Hesthaven, J.S. (2005). High-order collocation methods for differential equations with random inputs. *SIAM Journal on Scientific Computing*, 27(3), pp. 1118-1139.

Xiu, D. & Karniadakis, G.E. (2002). The Wiener-Askey Polynomial Chaos for stochastic differential equations. *SIAM Journal of Scientific Computing*, 24 (2), pp. 619-644.

Xiu, D. (2010). *Numerical Methods for Stochastic Computations: A Spectral Method Approach*. Princeton University Press, Pinceton, New Jersey.

Xu, J.X. & Tan, Y. (2003). *Linear and nonlinear iterative learning control*. New York :Springer Berlin Heidelberg.

Yang, D.R., Lee, K.S., Ahn, H.J., & Lee, J.H. (2003). Experimental application of a quadratic optimal iterative learning control method for control of wafer temperature uniformity in rapid thermal processing. *IEEE Trans. Semiconduct. Manuf.*, 16(1), pp.36-44.

Yang, G. (2005). Control and simulation of batch crystallization, Lappeenranta, Finland.

Yu, L.X. (2008). Pharmaceutical quality by design: product and process development, understanding, and control. *Pharm. Res.,* 25, pp. 781-791.

Yu, L.X., Lionbergera, R.A., Rawa, A.S., D'Costa, R., Wub, H., & Hussain, A.S. (2003). Applications of process analytical technology to crystallization processes. *Adv. Drug Delivery Rev.*, 56, pp. 349-369.

Yu, Z.Q., Chew, J.W., Chow, P.S., & Tan, R.B.H. (2007). Recent advances in crystallization control: an industrial perspective. *Chem. Eng. Res. Des*., 85(A7), pp. 893-905.

Yu, Z.Q., Chow, P.S., & Tan, R.B.H. (2006). Application of Attenuated Total Reflectance Fourier Transform Infrared (ATR-FTIR) Technique in the Monitoring and Control of Anti-solvent Crystallization. *Industrial & Engineering Chemistry Research*, 45(1), pp. 438-444.

Yu, Z.Q., Tan, R.B.H., & Chow, P.S. (2005). Effects of operating conditions on agglomeration and habit of paracetamol crystals in anti-solvent crystallisation. *J Cryst. Growth*, 279, pp. 477- 488.

Zhang, G.P. & Rohani, S. (2003). On-line optimal control of a seeded batch cooling crystallizer. *Chem Eng Sci*, 58(9), pp. 1887-1896.

Zhang, J., Nguyan, J., Xiong, Z., & Morris, J. (2009a). Iterative learning control of a crystallisation process using batch wise updated linearised models identified using PLS. *19th European Symposium on Computer Aided Process Engineering (ESCAPE)*, Cracow, Poland, June 14-17.

Zhang, J., Nguyan, J., Xiong, Z., & Morris, J. (2009b). Iterative learning control of a crystallisation process using batch wise updated linearised models. *21st Chinese Control and Decision Conference (CCDC)*, Guilin, Peoples R China, June 17–19, pp. 1734-1739.

Zhao, L., Dou, Y., Mi, H., Ren, M., & Ren, Y. (2007). Non-destructive determination of metronidazole powder by using artificial neural networks on short-wavelength NIR spectroscopy. *Spectrochimica Acta Part A: Molecular and Biomolecular Spectroscopy*, 66(4-5), pp. 1327-1332.

Zheng, D. & Hoo, K.A. (2002). Low-order model identification for implementable control solutions of distributed parameter systems. *Computers and Chemical Engineering*, 26. pp. 1049-1076.

Zheng, L., Huiping, T., & Senping, T. (2009). Iterative learning control of distributed parameter systems based on geometric analysis. In *Proceedings of Fifth International Conference on Natural Computation*, Vol. 6, pp. 392-396.

Zhou, G.X., Fujiwara, M., Woo, X.Y., Rusli, E., Tung, H., Starbuck, C., Davidson, O., Ge, Z., & Braatz, R.D. (2006). Direct design of pharmaceutical antisolvent crystallization through concentration control. *Cryst. Growth Design*, 6 (4), pp. 892 - 898.

Zhou, T., Fujita, M., & Matsumura, F. (1992). Robust control of a two-axis, magnetic suspension, flexible-beam system based on H∞ optimization theory. *International Journal of Robust and Nonlinear Control*, 2 (3), pp. 165-182. DOI: 10.1002/rnc.4590020302.

Appendix A

Experimental setup

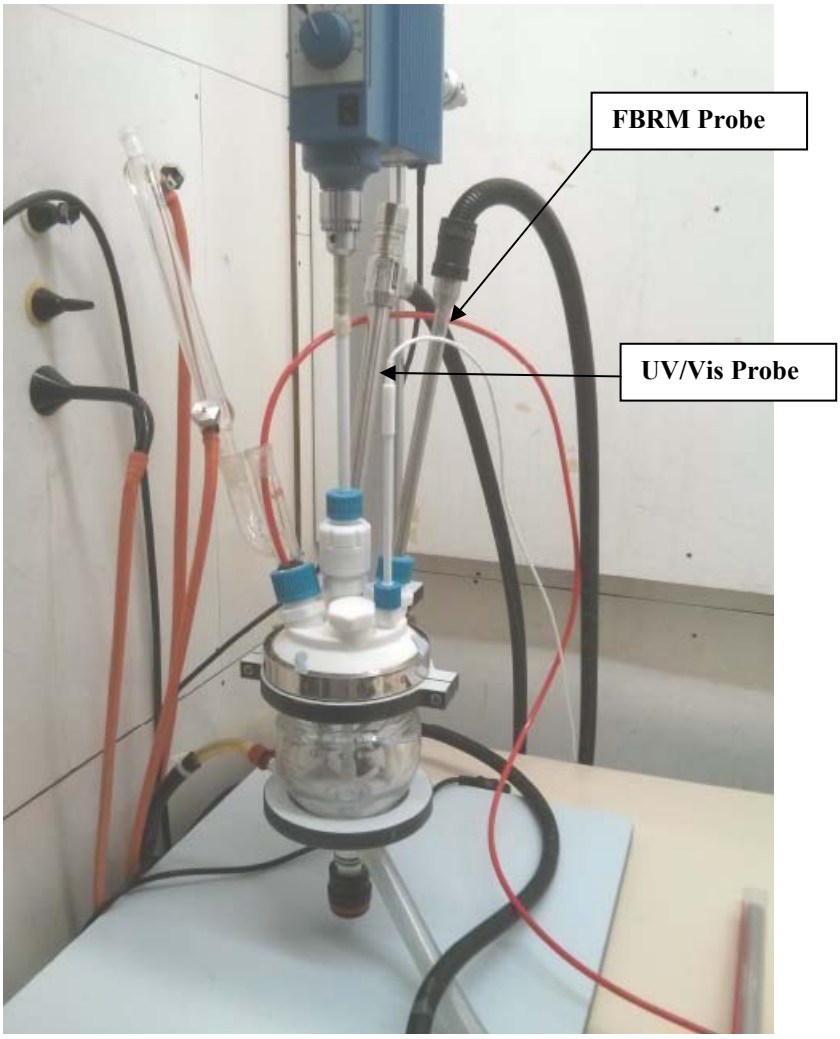


Figure D.1: Image of the experimental setup used to carry out the experiments for the Paracetamol in IPA system. In situ measurement for concentration and chord length distribution was obtained using ATR-UV/Vis and FBRM probes.

Appendix B

Crystallisation control interfaces used in the HILC and DNC experiments.

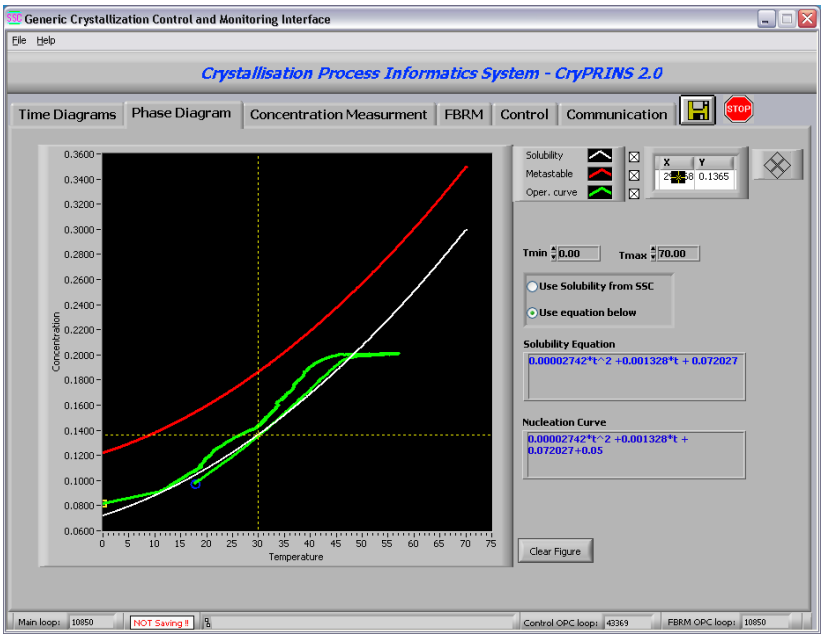


Figure B.1: CryPRINS Interface showing the phase diagram and operating line.

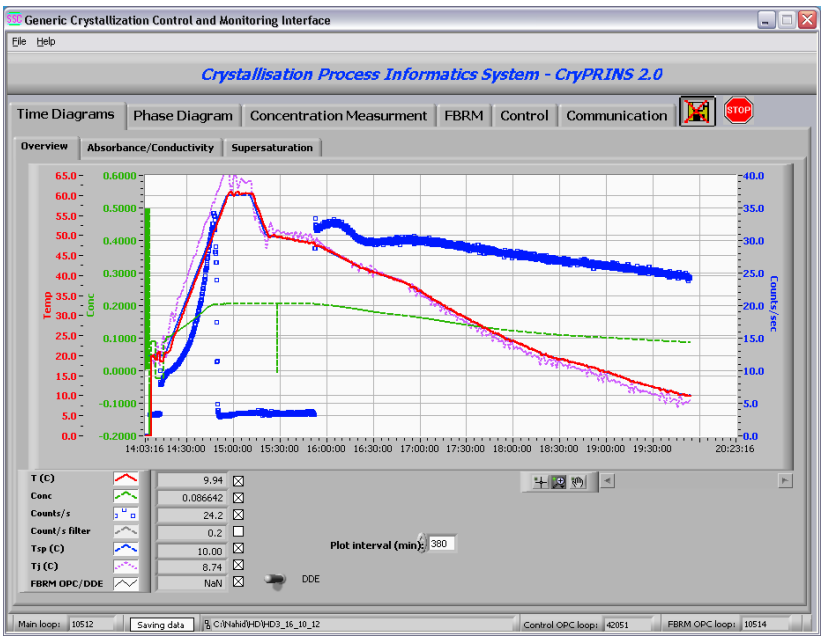


Figure B.2: CryPRINS Interface showing the operating lines of temperatures, concentration, # of counts/sec in time domain.

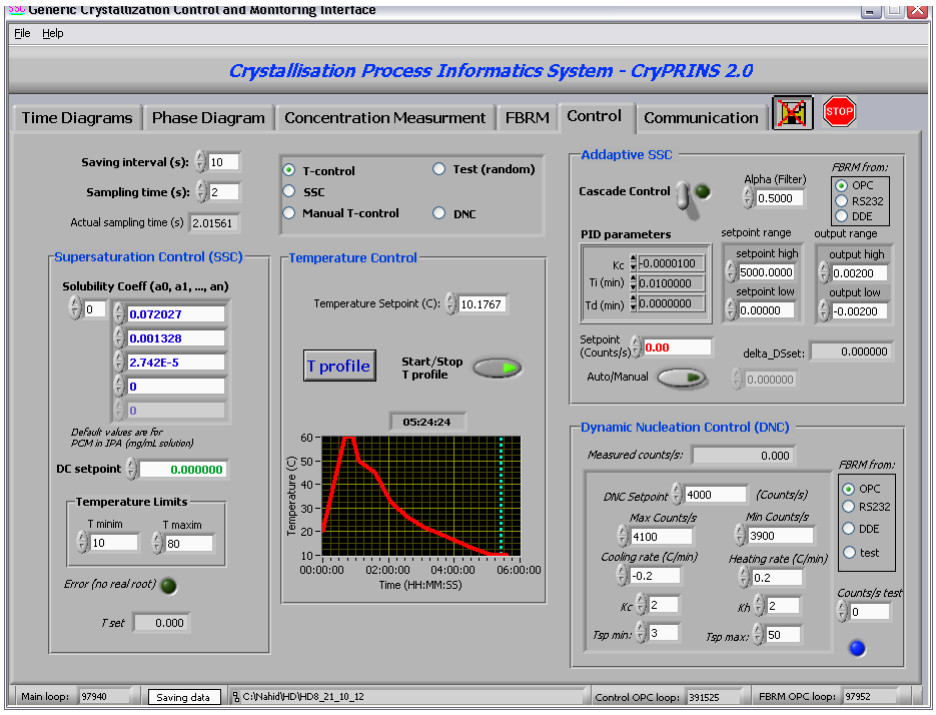


Figure B.3: CryPRINS Interface for selecting the type of control to be implemented.

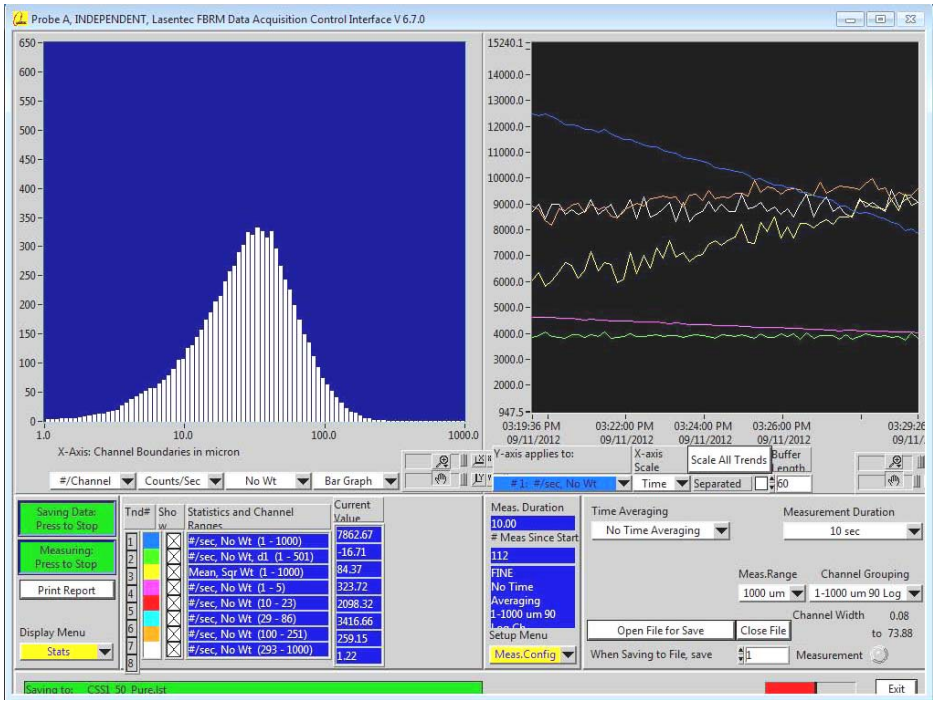


Figure B.4: Interface for Lasentec FBRM probe measurement observation.

Appendix C

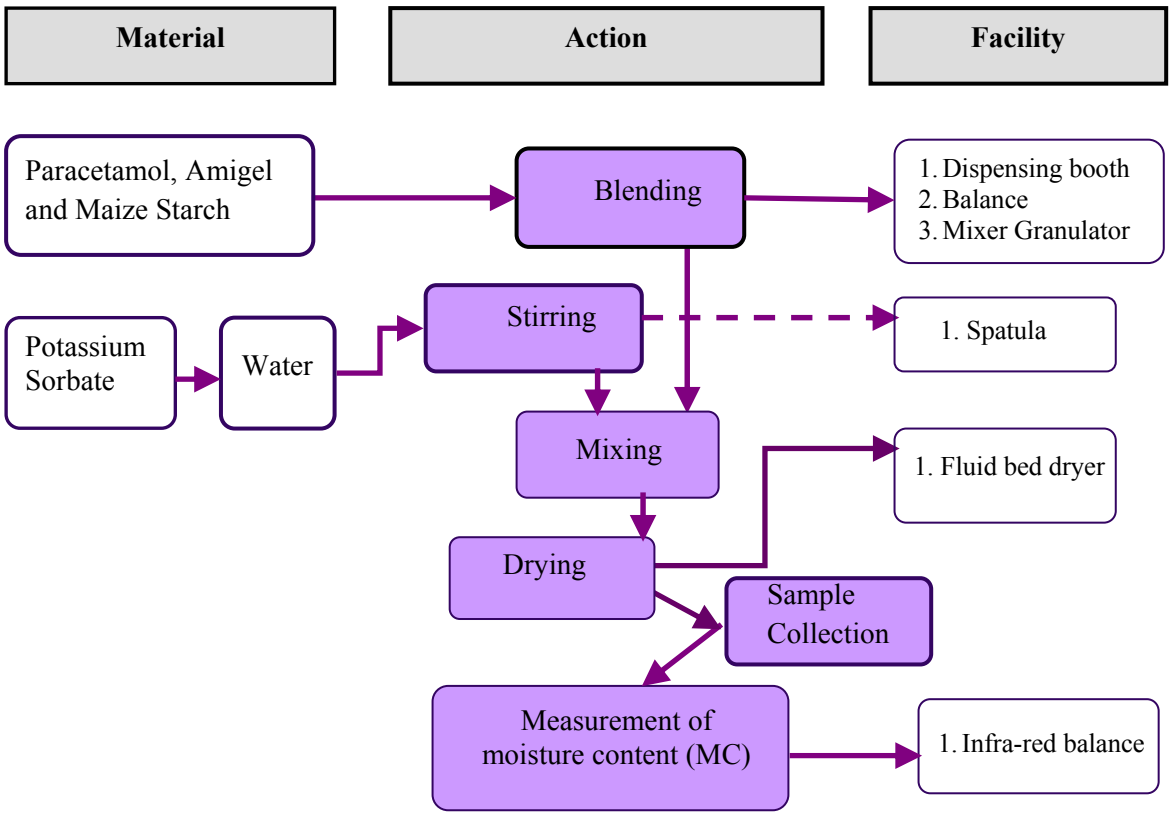


Figure 5: Process block diagram.

Figure C.1: Bock diagram of the drying process along with the materials and facilities required in GSK Limited, Bangladesh.

Appendix D

Materials used during the experimental works in GSK Limited, Bangladesh.

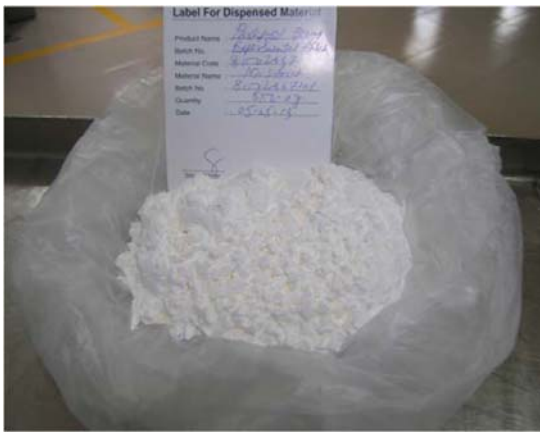


Figure D.1: Maize starch.

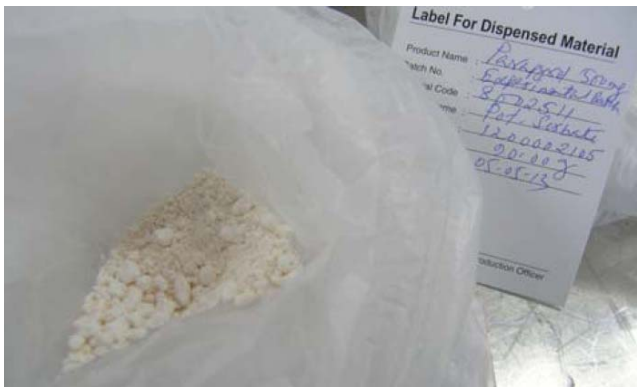


Figure D.2: Potassium Sorbate.

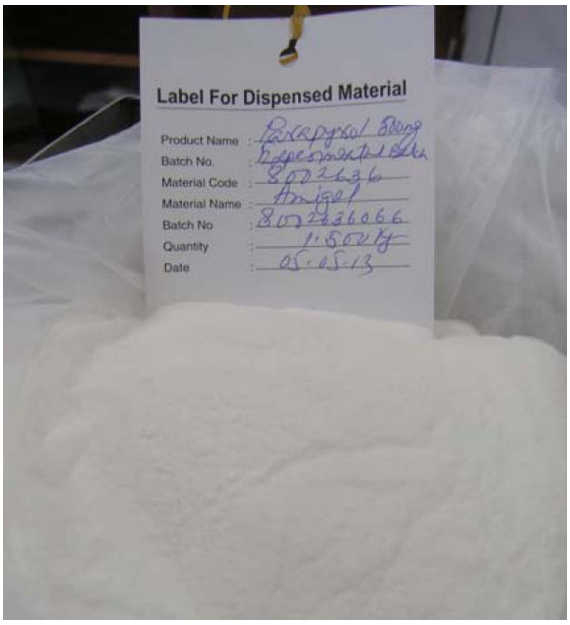


Figure D.3: Amigel.

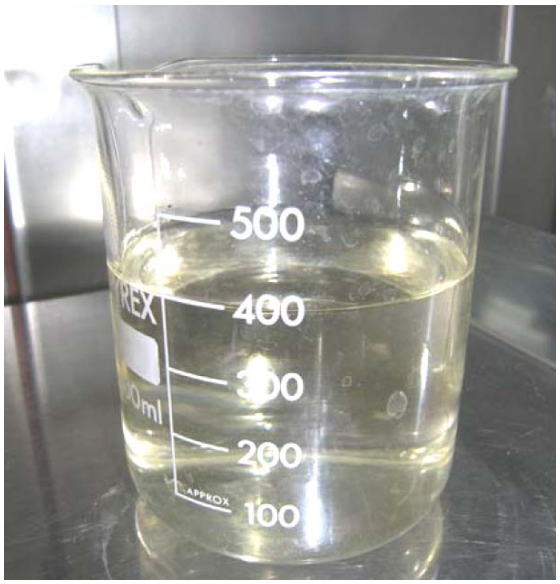


Figure D.4: Potassium Sorbate Solution.



Figure D.5: Dry granules of Paracetamol.



Figure D.6: Wet granules of Paracetamol.



Figure D.7: Granules on #20 Mesh.



Figure D.8: Sieved granules.

Appendix D

Table D.1: Hermite polynomials for the third-order-ten-dimensional PCE.

i^{th} Polynomial Chaos	Γ_i	Order of Polynomial Chaos	i^{th} Polynomial Chaos	Γ_i	Order of Polynomial Chaos
0	1	1	143	$(\theta_8\theta_7^2 - \theta_8)$	3
1	θ_1	1	144	$(\theta_8\theta_9^2 - \theta_8)$	3
2	θ_2	1	145	$(\theta_8\theta_{10}^2 - \theta_8)$	3
3	θ_3	1	146	$(\theta_9^3 - 3\theta_9)$	3
4	θ_4	1	147	$(\theta_9\theta_1^2 - \theta_9)$	3
5	θ_5	1	148	$(\theta_9\theta_2^2 - \theta_9)$	3
6	θ_6	1	149	$(\theta_9\theta_3^2 - \theta_9)$	3
7	θ_7	1	150	$(\theta_9\theta_4^2 - \theta_9)$	3
8	θ_8	1	151	$(\theta_9\theta_5^2 - \theta_9)$	3
9	θ_9	1	152	$(\theta_9\theta_6^2 - \theta_9)$	3
10	θ_{10}	1	153	$(\theta_9\theta_7^2 - \theta_9)$	3
11	$(\theta_1^2 - 1)$	2	154	$(\theta_9\theta_8^2 - \theta_9)$	3
12	$(\theta_1\theta_2)$	2	155	$(\theta_9\theta_{10}^2 - \theta_9)$	3
13	$(\theta_1\theta_3)$	2	156	$(\theta_{10}^3 - 3\theta_{10})$	3
14	$(\theta_1\theta_4)$	2	157	$(\theta_{10}\theta_1^2 - \theta_{10})$	3
15	$(\theta_1\theta_5)$	2	158	$(\theta_{10}\theta_2^2 - \theta_{10})$	3
16	$(\theta_1\theta_6)$	2	159	$(\theta_{10}\theta_3^2 - \theta_{10})$	3
17	$(\theta_1\theta_7)$	2	160	$(\theta_{10}\theta_4^2 - \theta_{10})$	3
18	$(\theta_1\theta_8)$	2	161	$(\theta_{10}\theta_5^2 - \theta_{10})$	3
19	$(\theta_1\theta_9)$	2	162	$(\theta_{10}\theta_6^2 - \theta_{10})$	3
20	$(\theta_1\theta_{10})$	2	163	$(\theta_{10}\theta_7^2 - \theta_{10})$	3
21	$(\theta_2^2 - 1)$	2	164	$(\theta_{10}\theta_8^2 - \theta_{10})$	3
22	$(\theta_2\theta_3)$	2	165	$(\theta_{10}\theta_9^2 - \theta_{10})$	3
23	$(\theta_2\theta_4)$	2	166	$\theta_1\theta_2\theta_3$	3
24	$(\theta_2\theta_5)$	2	167	$\theta_1\theta_2\theta_4$	3
25	$(\theta_2\theta_6)$	2	168	$\theta_1\theta_2\theta_5$	3
26	$(\theta_2\theta_7)$	2	169	$\theta_1\theta_2\theta_6$	3
27	$(\theta_2\theta_8)$	2	170	$\theta_1\theta_2\theta_7$	3
28	$(\theta_2\theta_9)$	2	171	$\theta_1\theta_2\theta_8$	3
29	$(\theta_2\theta_{10})$	2	172	$\theta_1\theta_2\theta_9$	3
30	$(\theta_3^2 - 1)$	2	173	$\theta_1\theta_2\theta_{10}$	3
31	$(\theta_3\theta_4)$	2	174	$\theta_1\theta_3\theta_4$	3
32	$(\theta_3\theta_5)$	2	175	$\theta_1\theta_3\theta_5$	3

i^{th} Polynomial Chaos	Γ_i	Order of polynomial chaos	i^{th} Polynomial Chaos	Γ_i	Order of polynomial chaos
33	$(\theta_3\theta_6)$	2	176	$\theta_1\theta_3\theta_6$	3
34	$(\theta_3\theta_7)$	2	177	$\theta_1\theta_3\theta_7$	3
35	$(\theta_3\theta_8)$	2	178	$\theta_1\theta_3\theta_8$	3
36	$(\theta_3\theta_9)$	2	179	$\theta_1\theta_3\theta_9$	3
37	$(\theta_3\theta_{10})$	2	180	$\theta_1\theta_3\theta_{10}$	3
38	(θ_4^2-1)	2	181	$\theta_1\theta_4\theta_5$	3
39	$(\theta_4\theta_5)$	2	182	$\theta_1\theta_4\theta_6$	3
40	$(\theta_4\theta_6)$	2	183	$\theta_1\theta_4\theta_7$	3
41	$(\theta_4\theta_7)$	2	184	$\theta_1\theta_4\theta_8$	3
42	$(\theta_4\theta_8)$	2	185	$\theta_1\theta_4\theta_9$	3
43	$(\theta_4\theta_9)$	2	186	$\theta_1\theta_4\theta_{10}$	3
44	$(\theta_4\theta_{10})$	2	187	$\theta_1\theta_5\theta_6$	3
45	(θ_5^2-1)	2	188	$\theta_1\theta_5\theta_7$	3
46	$(\theta_5\theta_6)$	2	189	$\theta_1\theta_5\theta_8$	3
47	$(\theta_5\theta_7)$	2	190	$\theta_1\theta_5\theta_9$	3
48	$(\theta_5\theta_8)$	2	191	$\theta_1\theta_5\theta_{10}$	3
49	$(\theta_5\theta_9)$	2	192	$\theta_1\theta_6\theta_7$	3
50	$(\theta_5\theta_{10})$	2	193	$\theta_1\theta_6\theta_8$	3
51	(θ_6^2-1)	2	194	$\theta_1\theta_6\theta_9$	3
52	$(\theta_6\theta_7)$	2	195	$\theta_1\theta_6\theta_{10}$	3
53	$(\theta_6\theta_8)$	2	196	$\theta_1\theta_7\theta_8$	3
54	$(\theta_6\theta_9)$	2	197	$\theta_1\theta_7\theta_9$	3
55	$(\theta_6\theta_{10})$	2	198	$\theta_1\theta_7\theta_{10}$	3
56	(θ_7^2-1)	2	199	$\theta_1\theta_8\theta_9$	3
57	$(\theta_7\theta_8)$	2	200	$\theta_1\theta_8\theta_{10}$	3
58	$(\theta_7\theta_9)$	2	201	$\theta_1\theta_9\theta_{10}$	3
59	$(\theta_7\theta_{10})$	2	202	$\theta_2\theta_3\theta_4$	3
60	(θ_8^2-1)	2	203	$\theta_2\theta_3\theta_5$	3
61	$(\theta_8\theta_9)$	2	204	$\theta_2\theta_3\theta_6$	3
62	$(\theta_8\theta_{10})$	2	205	$\theta_2\theta_3\theta_7$	3
63	(θ_9^2-1)	2	206	$\theta_2\theta_3\theta_8$	3
64	$(\theta_9\theta_{10})$	2	207	$\theta_2\theta_3\theta_9$	3
65	(θ_{10}^2-1)	2	208	$\theta_2\theta_3\theta_{10}$	3
66	$(\theta_1^3-3\theta_1)$	3	209	$\theta_2\theta_4\theta_5$	3
67	$(\theta_1\theta_2^2-\theta_1)$	3	210	$\theta_2\theta_4\theta_6$	3
68	$(\theta_1\theta_3^2-\theta_1)$	3	211	$\theta_2\theta_4\theta_7$	3
69	$(\theta_1\theta_4^2-\theta_1)$	3	212	$\theta_2\theta_4\theta_8$	3
70	$(\theta_1\theta_5^2-\theta_1)$	3	213	$\theta_2\theta_4\theta_9$	3
71	$(\theta_1\theta_6^2-\theta_1)$	3	214	$\theta_2\theta_4\theta_{10}$	3
72	$(\theta_1\theta_7^2-\theta_1)$	3	215	$\theta_2\theta_5\theta_6$	3

i^{th} Polynomial Chaos	Γ_i	Order of polynomial chaos	i^{th} Polynomial Chaos	Γ_i	Order of polynomial chaos
73	$(\theta_1\theta_8^2-\theta_1)$	3	216	$\theta_2\theta_5\theta_7$	3
74	$(\theta_1\theta_9^2-\theta_1)$	3	217	$\theta_2\theta_5\theta_8$	3
75	$(\theta_1\theta_{10}^2-\theta_1)$	3	218	$\theta_2\theta_5\theta_9$	3
76	$(\theta_2^3-3\theta_2)$	3	219	$\theta_2\theta_5\theta_{10}$	3
77	$(\theta_2\theta_1^2-\theta_2)$	3	220	$\theta_2\theta_6\theta_7$	3
78	$(\theta_2\theta_3^2-\theta_2)$	3	221	$\theta_2\theta_6\theta_8$	3
79	$(\theta_2\theta_4^2-\theta_2)$	3	222	$\theta_2\theta_6\theta_9$	3
80	$(\theta_2\theta_5^2-\theta_2)$	3	223	$\theta_2\theta_6\theta_{10}$	3
81	$(\theta_2\theta_6^2-\theta_2)$	3	224	$\theta_2\theta_7\theta_8$	3
82	$(\theta_2\theta_7^2-\theta_2)$	3	225	$\theta_2\theta_7\theta_9$	3
83	$(\theta_2\theta_8^2-\theta_2)$	3	226	$\theta_2\theta_7\theta_{10}$	3
84	$(\theta_2\theta_9^2-\theta_2)$	3	227	$\theta_2\theta_8\theta_9$	3
85	$(\theta_2\theta_{10}^2-\theta_2)$	3	228	$\theta_2\theta_8\theta_{10}$	3
86	$(\theta_3^3-3\theta_3)$	3	229	$\theta_2\theta_9\theta_{10}$	3
87	$(\theta_3\theta_1^2-\theta_3)$	3	230	$\theta_3\theta_4\theta_5$	3
88	$(\theta_3\theta_2^2-\theta_3)$	3	231	$\theta_3\theta_4\theta_6$	3
89	$(\theta_3\theta_4^2-\theta_3)$	3	232	$\theta_3\theta_4\theta_7$	3
90	$(\theta_3\theta_5^2-\theta_3)$	3	233	$\theta_3\theta_4\theta_8$	3
91	$(\theta_3\theta_6^2-\theta_3)$	3	234	$\theta_3\theta_4\theta_9$	3
92	$(\theta_3\theta_7^2-\theta_3)$	3	235	$\theta_3\theta_4\theta_{10}$	3
93	$(\theta_3\theta_8^2-\theta_3)$	3	236	$\theta_3\theta_5\theta_6$	3
94	$(\theta_3\theta_9^2-\theta_3)$	3	237	$\theta_3\theta_5\theta_7$	3
95	$(\theta_3\theta_{10}^2-\theta_3)$	3	238	$\theta_3\theta_5\theta_8$	3
96	$(\theta_4^3-3\theta_4)$	3	239	$\theta_3\theta_5\theta_9$	3
97	$(\theta_4\theta_1^2-\theta_4)$	3	240	$\theta_3\theta_5\theta_{10}$	3
98	$(\theta_4\theta_2^2-\theta_4)$	3	241	$\theta_3\theta_6\theta_7$	3
99	$(\theta_4\theta_3^2-\theta_4)$	3	242	$\theta_3\theta_6\theta_8$	3
100	$(\theta_4\theta_5^2-\theta_4)$	3	243	$\theta_3\theta_6\theta_9$	3
101	$(\theta_4\theta_6^2-\theta_4)$	3	244	$\theta_3\theta_6\theta_{10}$	3
102	$(\theta_4\theta_7^2-\theta_4)$	3	245	$\theta_3\theta_7\theta_8$	3
103	$(\theta_4\theta_8^2-\theta_4)$	3	246	$\theta_3\theta_7\theta_9$	3
104	$(\theta_4\theta_9^2-\theta_4)$	3	247	$\theta_3\theta_7\theta_{10}$	3
105	$(\theta_4\theta_{10}^2-\theta_4)$	3	248	$\theta_3\theta_8\theta_9$	3
106	$(\theta_5^3-3\theta_5)$	3	249	$\theta_3\theta_8\theta_{10}$	3
107	$(\theta_5\theta_1^2-\theta_5)$	3	250	$\theta_3\theta_9\theta_{10}$	3

i^{th} Polynomial Chaos	Γ_i	Order of polynomial chaos	i^{th} Polynomial Chaos	Γ_i	Order of polynomial chaos
108	$(\theta_5\theta_2^2-\theta_5)$	3	251	$\theta_4\theta_5\theta_6$	3
109	$(\theta_5\theta_3^2-\theta_5)$	3	252	$\theta_4\theta_5\theta_7$	3
110	$(\theta_5\theta_4^2-\theta_5)$	3	253	$\theta_4\theta_5\theta_8$	3
111	$(\theta_5\theta_6^2-\theta_5)$	3	254	$\theta_4\theta_5\theta_9$	3
112	$(\theta_5\theta_7^2-\theta_5)$	3	255	$\theta_4\theta_5\theta_{10}$	3
113	$(\theta_5\theta_8^2-\theta_5)$	3	256	$\theta_4\theta_6\theta_7$	3
114	$(\theta_5\theta_9^2-\theta_5)$	3	257	$\theta_4\theta_6\theta_8$	3
115	$(\theta_5\theta_{10}^2-\theta_5)$	3	258	$\theta_4\theta_6\theta_9$	3
116	$(\theta_6^3-3\theta_6)$	3	259	$\theta_4\theta_6\theta_{10}$	3
117	$(\theta_6\theta_1^2-\theta_6)$	3	260	$\theta_4\theta_7\theta_8$	3
118	$(\theta_6\theta_2^2-\theta_6)$	3	261	$\theta_4\theta_7\theta_9$	3
119	$(\theta_6\theta_3^2-\theta_6)$	3	262	$\theta_4\theta_7\theta_{10}$	3
120	$(\theta_6\theta_4^2-\theta_6)$	3	263	$\theta_4\theta_8\theta_9$	3
121	$(\theta_6\theta_5^2-\theta_6)$	3	264	$\theta_4\theta_8\theta_{10}$	3
122	$(\theta_6\theta_7^2-\theta_6)$	3	265	$\theta_4\theta_9\theta_{10}$	3
123	$(\theta_6\theta_8^2-\theta_6)$	3	266	$\theta_5\theta_6\theta_7$	3
124	$(\theta_6\theta_9^2-\theta_6)$	3	267	$\theta_5\theta_6\theta_8$	3
125	$(\theta_6\theta_{10}^2-\theta_6)$	3	268	$\theta_5\theta_6\theta_9$	3
126	$(\theta_7^3-3\theta_7)$	3	269	$\theta_5\theta_6\theta_{10}$	3
127	$(\theta_7\theta_1^2-\theta_7)$	3	270	$\theta_5\theta_7\theta_8$	3
128	$(\theta_7\theta_2^2-\theta_7)$	3	271	$\theta_5\theta_7\theta_9$	3
129	$(\theta_7\theta_3^2-\theta_7)$	3	272	$\theta_5\theta_7\theta_{10}$	3
130	$(\theta_7\theta_4^2-\theta_7)$	3	273	$\theta_5\theta_8\theta_9$	3
131	$(\theta_7\theta_5^2-\theta_7)$	3	274	$\theta_5\theta_8\theta_{10}$	3
132	$(\theta_7\theta_6^2-\theta_7)$	3	275	$\theta_5\theta_9\theta_{10}$	3
133	$(\theta_7\theta_8^2-\theta_7)$	3	276	$\theta_6\theta_7\theta_8$	3
134	$(\theta_7\theta_9^2-\theta_7)$	3	277	$\theta_6\theta_7\theta_9$	3
135	$(\theta_7\theta_{10}^2-\theta_7)$	3	278	$\theta_6\theta_7\theta_{10}$	3
136	$(\theta_8^3-3\theta_8)$	3	279	$\theta_6\theta_8\theta_9$	3
137	$(\theta_8\theta_1^2-\theta_8)$	3	280	$\theta_6\theta_8\theta_{10}$	3
138	$(\theta_8\theta_2^2-\theta_8)$	3	281	$\theta_6\theta_9\theta_{10}$	3
139	$(\theta_8\theta_3^2-\theta_8)$	3	282	$\theta_7\theta_8\theta_9$	3
140	$(\theta_8\theta_4^2-\theta_8)$	3	283	$\theta_7\theta_8\theta_{10}$	3
141	$(\theta_8\theta_5^2-\theta_8)$	3	284	$\theta_7\theta_9\theta_{10}$	3
142	$(\theta_8\theta_6^2-\theta_8)$	3	285	$\theta_8\theta_9\theta_{10}$	3

List of Publications

Journal Papers

1. N. Sanzida & Z.K. Nagy (2013). Iterative Learning Control for the Systematic Design of Supersaturation Controlled Batch Cooling Crystallisation Processes, Computers and Chemical Engineering, 59, pp. 111-121. http://dx.doi.org/10.1016/j.compchemeng.2013.05.027.

2. N. Sanzida & Z.K. Nagy, Strategic Evaluation of Different Direct Nucleation Control Approaches for Controlling Batch Cooling Crystallisation via Simulation and Experimental Case Studies, Chemical Engineering and Processing: Process Intensification. Submitted for review.

Proceeding Paper (Peer Reviewed)

1. N. Sanzida and Z.K. Nagy, Iterative Learning Control of a Batch Cooling Crystallisation Process based on Linear Time-Varying Perturbation Models, *in Proc. of the 22nd European Symposium on Computer Aided Process Engineering*, 17-20 June 2012, London.

2. N. Sanzida and Z.K. Nagy, Polynomial Chaos Expansion (PCE) Based Modelling and Optimisation of Batch Crystallization Processes, Abstract accepted for the 2*4th European Symposium on Computer Aided Process Engineering (ESCAPE 24)*, 15-18 June 2014, Hungary.

Papers (In Preperation)

1. N. Sanzida & Z.K. Nagy. Iterative Learning Control for the Systematic Design of Supersaturation Controlled Batch Cooling Crystallisation Processes - Experimental Case Studies.

Presentations

1. Iterative Learning Control of a Batch Cooling Crystalliation Process based on Linear Time-Varying Perturbation Models, oral presentation at *the 22nd European Symposium on Computer Aided Process Engineering*, 17-20 June 2012, London, UK.